VIBRATION CONTROL OF STRUCTURES WITH VISCOELASTIC DAMPERS

By

TAN XIAOMING

A Thesis for the Degree of Doctor of Philosophy

Department of Civil and Structural Engineering

The Hong Kong Polytechnic University

Hong Kong

June 1998

To my wife, *CAI SILAN*

DECLARATION

I hereby declare that the work presented in this thesis entitled "**Vibration Control of Structures with Viscoelastic Dampers**" is original unless otherwise acknowledged in the text, and has not been, either in whole or in part, previously submitted to any other institution for a degree or other qualification.

SIGNED

_____

Tan Xiaoming

ACKNOWLEDGEMENTS

First of all I wish to express my deepest gratitude to my supervisor, Professor J. M. Ko, for his continued guidance, patience, encouragement, and invaluable help during the entire duration of my research and the preparation of this thesis. I am also greatly indebted to my co-supervisor, Professor E. H. Fang. Although she is in Tsinghua University of P. R. C., she keeps on giving me advice and inspiration by electronic communication. Their confidence to me is especially appreciated.

My appreciation is also extended to Dr. Y. Q. Ni for helpful discussions and assistance. His collection of plentiful research material benefits me greatly. Gratitude also goes to Dr. Y. L. Xu for his suggestions and comments. I must thank Mr. S. Zhan, Mr. T. T. Wai and Mr. M. C. Ng for their supports of my laboratory work, and thank Mr. M. T. Ho for assistance in the use of computing facilities.

I would particularly thank to Research Committee of the Hong Kong Polytechnic University for awarding the studentship. Thanks are also due to Prof. X. L. Liu, Dr. K. G. Xin for their encouragement and support, and to all colleagues and friends who have given any support and help to me during my studies.

Finally special thanks are given to my wife, without her dedicated support and encouragement it would have been impossible for me to complete this thesis.

Abstract of thesis entitled:

VIBRATION CONTROL OF STRUCTURES WITH VISCOELASTIC DAMPERS

Submitted by Tan Xiaoming

for the degree of Doctor of Philosophy

at The Hong Kong Polytechnic University

June 1998

ABSTRACT

This dissertation is concerned with improvement and identification of the mathematical model for viscoelastic dampers, development of analytical methods for structures with such dampers, design of damping devices for horizontal and vertical vibration control and their application to building structures.

Experimental investigations on the selected viscoelastic dampers have been carried out. The hysteresis loops of such dampers under different excitation conditions have been found and their associated equivalent stiffness, damping ratio and energy dissipation ability have been determined.

Based on the review of the commonly used mathematical models for viscoelastic dampers and the dynamic characteristics obtained in the experimental studies, the fractional derivative model has been chosen and improved to describe the dynamic behaviours of viscoelastic dampers. To evaluate the parameters of the proposed model, two kinds of identification method which can facilitate the use of all test data simultaneously in the identification process have been developed. Parameter values of the proposed model for the two selected dampers have been obtained by the developed methods. By comparison between the hysteresis loops derived from the proposed model and the corresponding loops of the tested results, and also those derived from the commonly used Kelvin-Voigt model, it has been found that the proposed model can well describe the dynamic behaviours of various viscoelastic dampers, and is more versatile and can be used more widely for various kinds of viscoelastic damper than the Kelvin-Voigt model. Moreover, parametric studies on the proposed mathematical model have been carried out and the features of the model have been discussed in detail.

Two schemes for modelling viscoelastic dampers in the structural response analysis have been proposed. An analytical method in time domain in association with the modelling schemes has been developed. Since the proposed model has

simple expression in frequency domain, an analytical method in hybrid time-frequency domain has also been developed. This method can save more computing time than the method in time domain and can be used for structures subject to not only sinusoidal excitation, but also random excitation like seismic loading. In addition, the damping matrix of structures incorporated with viscoelastic dampers can be obtained by the proposed analytical methods, which is useful for carrying out dynamic analysis with other commercial software packages.

A practical damping device has been designed for horizontal vibration control of framed structures. It has been proved experimentally that such damping device is effective in attenuating horizontal vibration. By comparison of experimental and analytical results, the proposed analytical methods for predicting the dynamic responses of structures incorporated with such damping devices have been verified. A large amount of numerical simulation work with various parameters has been carried out on a multi-story building structure. Some useful guidelines for practical design of horizontal vibration control with such damping devices have been obtained.

To control vertical vibrations of long span structures, a beam-column connection incorporated with viscoelastic dampers has been proposed. Great effectiveness in control the vertical vibration of beam structures can be achieved, which has been demonstrated by the experimental tests carried out on a long span beam with such beam-column connections. Comparisons between the analytical results and the experimental results have been made with which the analytical methods have been verified. Numerical simulation has been carried out on a real long span beam with and without such beam-column connections. The effects of various parameters on vertical vibration control have been studied and useful design guidelines for the design of vibration control for long span structures with the proposed beam-column connections have been drawn.

LIST OF TABLES

LIST OF FIGURES

LIST OF PHOTOS

CONTENTS

CHAPTER 1
INTRODUCTION

1.1 Introduction

In recent years, along with the development of building materials and construction technology, a great number of contemporary slender structures, including television towers, high-rise buildings and long-span cable-stayed or suspension bridges, have been rapidly built in large cities. It is expected that more and more such structures with greater height or longer span will be erected in the near future. Because of their low natural frequencies, these flexible structures are vulnerable to dynamic loading such as wind load, seismic excitation, vehicles load and other environmental excitation (Ding W. J., 1988). Violent vibration of slender structures caused by such loading may induce damage to these structures, discomfort to occupants or malfunction of equipment housed in the structures. Therefore, it is of great significance to develop effective and practical measures to suppress structural vibrations induced by dynamic loading. Vibration control technology also plays an important role for continuing development of large-scale slender structures. It is because cost may be cut down greatly in building a structure satisfying the same requirements if vibration control techniques are applied. For seaside cities such as Hong Kong with high incidence of typhoons and for cities in seismic areas like Beijing with high incidence of earthquakes, vibration control of slender structures is in particular a special challenge to structural engineers. Recently, many researchers have been attracted to this area. A large amount of useful researches findings and meaningful practical

applications have been achieved. As one of the control method, viscoelastic dampers with proper installation can reduce dynamic response of a structure significantly. A lot of research work on vibration control with viscoelastic dampers has been done in past years by many researchers (Soong T. T. et al, 1990).

It is popularly known that viscoelastic material is good at dissipating energy. Upon cyclic displacement, the stress and strain of a damper made of such material are out of phase. This phenomenon which can be represented by a hysteresis loop with an enclosed area proportional to the energy dissipated in a complete damper displacement cycle is illustrated in Figure 1.1 (Lai Ming-Lai, 1993). Hysteresis loops depict generic nonlinear feature of such material under sinusoidal excitation, in which the restoring force depends not only on instantaneous deformation, but also on the exciting frequency and temperature of environment (Chang K. C. et al, 1992). Since different dampers would have different properties, in order to predict more accurately their behaviours for practical design purpose, properties of the selected viscoelastic dampers should be obtained based on experimental work.

To analyze a structure with viscoelastic dampers, a suitable mathematical model should be built to represent the dampers. In past years, various types of model such as Kelvin-Voigt model, Maxwell model, complex modulus model and fractional derivative models have been developed. Each model has its advantages and disadvantages. Some of them are too simple to be able to describe various kinds of viscoelastic dampers. And parameters of some other models are too difficult to be identified. To develop a suitable model which is versatile enough

to describe the dynamic behaviours of various dampers and can be handled conveniently in the identification and analysis processes is of great significance in vibration control with viscoelastic dampers.

Viscoelastic damper properties are dependent on excitation frequency. A proper mathematical model being able to describe the behaviours of a damper under different excitation conditions may be affected by several parameters. As the model with different sets of parameter value can describe the same behaviour of a damper in certain cases, to identify the parameters more accurately, all the test data obtained in different cases, especially those obtained at different excitation frequencies, should be considered at the same time. However, as a large amount of test data normally will be involved in the identification of parameters of a sophisticated model for viscoelastic dampers, it is in fact a rather difficult task. So far, very little work has been done to solve this problem in past years and further development work is required.

The dynamic responses of a structure incorporated with viscoelastic dampers should be determined to study their effectiveness in vibration control. Much work has been done on the analysis of structures with viscoelastic dampers in time domain or in frequency domain. Analysis of non-linear structures in time domain however costs much computing time and the time step is difficult to be determined for achieving solution convergence (Hsu Sheng-Yung, 1992, Tan X. M., 1995). Analysis in frequency domain on the other hand cannot predict response accurately for instantaneous state. Hybrid frequency-time-domain method has been used in dynamic analysis of soil-structure interaction. Darbre Georges R. et al applied this method in seismic analysis of non-linearly base-

isolated soil-structure interacting reactor building (1988) and derived a criterion of stability pertaining to this method (1990). For frequency dependent viscoelastic dampers, the hybrid time-frequency domain method should have more advantages than the methods in time domain and in frequency domain. The application of this method for structures incorporated with viscoelastic dampers is promising.

Viscoelastic dampers and the structure itself have their own damping ratios. The damping ratio of the whole system can embody the effectiveness in vibration control with viscoelastic dampers. Some researchers (Nashif Ahid D., 1985) have performed related research work already. Sause R. et al (1994) assumed the hysteretic behaviours of viscoelastic elements to be linear and modeled the viscoelastic elements with K_{ve} and loss factor η. Tong M. et al (1994) proposed an index of damping non-proportionality for a lumped-mass vibrating system. However the damping ratio obtained by such methods is inadequate for real analysis and design. If viscoelastic dampers are represented by proper models which are applied directly to determine the damping matrix of the hysteretic structure system, the result thus obtained should be more reliable in predicting the dynamic response of structures incorporated with viscoelastic dampers.

Many devices for vibration control with viscoelastic dampers have been designed by other researchers. It can be classified broadly into two groups, namely, horizontal vibration control and vertical vibration control. Vibration control devices should be designed according to the practical conditions and should be convenient for installation and maintenance. When a damping device is figured

out, its effectiveness in vibration control should be worked out analytically and if necessary, confirmed experimentally.

In practical design, damper type, damper sizes, damper number, damper location would be determined before proceeding to any structural analysis, which are mainly based on previous design and research experience. So far, most research work are concentrated on the effectiveness in vibration control of structures under special conditions, and not much work has been done for optimal design by former researchers. Effectiveness in vibration attenuation for structures with dampers under various conditions should be carried out by numerical simulation and comparison can thus be made, based on which design guidelines can be established.

1.2 Objectives of the Thesis

The main objectives to be achieved in this dissertation are as follows:

1. To select and improve if necessary a mathematical model suitable to describe the dynamic behaviours of various viscoelastic dampers and to develop identification methods to evaluate the model parameters based on test data obtained from dynamic tests on the dampers.

2. To develop methods of analysis both in time domain and hybrid time frequency domain with the proposed mathematical model for structures incorporated with viscoelastic dampers and to obtain the equivalent stiffness and damping matrix for the hysteretic structures based on the developed methods.

3. To design suitable viscoelastic damping devices for vertical and horizontal vibration control of two selected structures and to carry out experimental work on

these two selected structures for the verification of the proposed methods and also to investigate their effectiveness in vibration control. Based on parametric studies, to establish design guidelines for vibration control of structures with these devices.

1.3 Organization of the Thesis

According to the objectives of the research, organization of the thesis is presented as follows,

Firstly, literature reviews are presented in Chapter Two. As the research basis, vibration control history and its state of art with emphasis on vibration control with viscoelastic dampers, mathematical models for viscoelastic dampers, system identification methods and methods of analysis for structures with viscoelastic dampers have been introduced and discussed in detail.

Dynamic tests on viscoelastic dampers are introduced in Chapter Three. Viscoelastic dampers, test set-up, test methods and results are described. Conclusions on the damper properties have been drawn from the comparisons of different test cases.

Based on the comparisons of different mathematical model, the fractional derivative model has been selected and further developed to simulate the dynamic behaviours of viscoelastic dampers in Chapter Four. The parameters of the models have been identified by two developed methods. Verification of the model with test results and comparisons of the model with normally used Kelvin-Voigt model have been made. Studies of the characteristics of the model have been carried out by numerical simulation.

In Chapter Five, two schemes for modelling of viscoelastic dampers have been proposed for response analysis of structures. Analytical methods both in time domain and in hybrid time-frequency domain have been developed, where the fractional derivative model is used to represent the damper. Equivalent stiffness and damping matrix of the hysteretic structure system which can also be used by other analytical methods and commercial softwares have been derived. Based on the proposed method, the associated computer programs have been developed and the program structure is introduced.

A damping device has been designed for horizontal vibration control and dynamic tests have been done on a designed framed structure with and without viscoelastic dampers, which are presented in Chapter Six. Comparisons of the responses of the structure with and without dampers have been made. The tested structure has also been analyzed by the developed program both in time and hybrid time-frequency domain. Comparisons of analytical and experimental results have been done. Parametric studies on a multi-story building structure have been carried out and useful design guidelines have been obtained for structures with such damping devices.

A beam-column connection with viscoelastic dampers has been designed to reduce the vertical dynamic response of long span structures and dynamic tests on a long span beam with and without dampers under different conditions have been done, which are presented in Chapter Seven. Comparisons of responses of the beam with and without dampers and comparisons of experimental and analytical results have been made. Parametric studies on a long span beam have also been

carried out and some meaningful design guidelines have been drawn for long span structures with such beam-column connections.

Lastly, concluding remarks based on the research work have been made in Chapter Eight and further research and development work has also been suggested.

1.4 References

Chang K. C., Soong T. T., Oh S.T. and Lai M. L. (1992), Effect of Ambient Temperature on Viscoelastically Damped Structure, Journal of Structural Engineering, Vol. 118, No. 7, pp. 1955-1973, July.

Darbre Georges R. and Wolf John P. (1988), Criterion of Stability and Implementation Issues of Hybrid Frequency-Time-Domain Procedure for Non-Linear Dynamic Analysis, Earthquake Engineering and Structural Dynamics, Vol.16, pp.569-581.

Darbe Georges R. (1990), Seismic Analysis of Non-linearly Base-Isolated Soil-Structure Interacting Reactor Building by Way of The Hybrid Frequency-Time-Domain Procedure, Earthquake Engineering and Structural Dynamics, Vol.19, pp.725-738.

Ding W. J. (1988), Vibration Attenuation Theory, Tsinghua University Press, Beijing. (In Chinese)

Hsu Sheng-Yung and Fafitis Apostolos (1992), Seismic Analysis Design of Frames with Viscoelastic Connections, Journal of Structural Engineering, Vol.118, No.9.

Lai Ming-Lai (1995), Characteristics of Viscoelastic Materials and Dampers as Energy Dissipation Devices, A New Direction in Seismic Design, pp. 195-210, Tokyo.

Nashif Ahid D., Jones David I. G., Henderson John P. (1985), Vibration Damping, John Wiley &Sons, New York.

Sause R., Hemingway G. and Kasai K. (1994), Simplified Seismic Response Analysis of Viscoelastic-Damped Frame Structures, Fifth U.S. National Conference on Earthquake Engineering, Vol.1, pp.839-849, Chicago, Illinois.

Soong T. T. and Mahmoodi P. (1990), Seismic Behavior of Structures with Added Viscoelastic Dampers, Proceedings of Fourth U.S. National Conference on Earthquake Engineering, Vol.3, pp.499-506.

Tan X. M., Ko J. M., Fang E. H. (1995), Experimental and Analytical study on a Framed Structure Incorporated with Viscoelastic Dampers, Proceedings of SDVNC'95, pp.301-306, Hong Kong.

Tong M., Liang Z. and Lee G. C. (1994), An Index of Damping Non-Proportionality for Discrete Vibrating Systems, Journal of Sound and Vibration, Vol. 174, No. 1, pp.37-55.

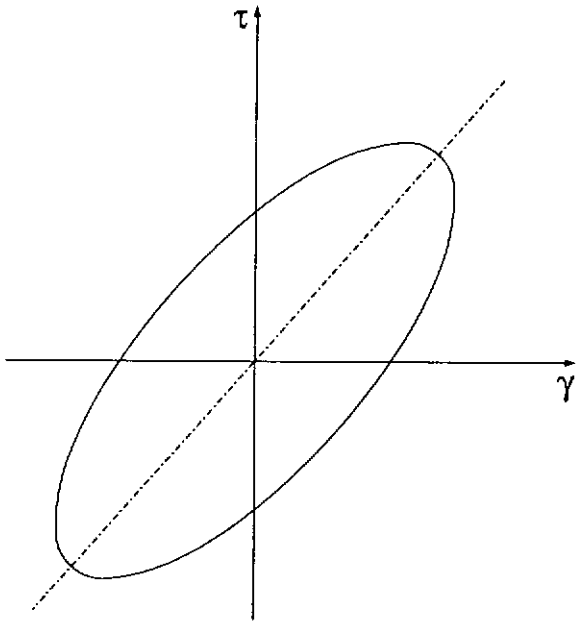

Figure 1.1 Hysteresis loop of a viscoelastic damper

CHAPTER 2
LITERATURE REVIEW

2.1 Vibration control with viscoelastic dampers

2.1.1 History of vibration control

Vibration control technology has been developed for nearly one century. The original idea of vibration control was base-isolation, this concept was given in early 1910's in U.S. (Way D. et al, 1992). In the following several decades, many base-isolation methods using different devices like springs, balls, ball bearings, steel plates with graphite between layers and plastic material, etc., were worked out and proposed to be applied in real structures. The techniques of seismic isolation have been widely used in many places of the world (Skinner et al, 1993). These methods have been proved to be very effective in vibration attenuation in the design for machinery foundation and low-story structures. But for large-scale structures such as high-rise buildings and long span bridges, base-isolation is not so practical.

Many types of devices have been designed and installed to control the vibration of structures, where dynamic energy is dissipated passively. Various of tuned mass damper (Hartog Den, 1956, Hunt J. B., 1979, Kaynia A. M. et al, 1981, Kwok K. C. S., 1984 and Yamaguchi H. et al, 1993) and tuned liquid damper (Kareem A. et al, 1987, Welt F. et al, 1989, Xu Y.L. et al, 1992, Koh C. G. et al, 1995 and Sun L. M. et al, 1995) methods have been studied and utilized for structures subjected to wind and seismic excitation since 1950's. The working mechanism of a multi-mass tuned damper system is shown in Figure 2.1.

Damping of the structures with such systems increases considerably and dynamic response decreases greatly. But to realize a successful practical application of such systems in a large scaled structure, a great mass need to be added and a special structure has to be designed for building up such a system which is very costly and also very spacious.

Recently, many hysteretic damping systems such as metallic dampers, friction dampers, sliding friction systems, semi-rigid or flexible joints, viscoelastic dampers and viscous fluid dampers have been proposed to be used to dissipate energy while vibration takes place in structures (Soong T. T., 1997). These energy-absorbing devices can be used for the design of buildings of any height including super high-rise buildings and can also be used for the disaster rehabilitation of existing buildings. There are two examples of devices based on dissipating energy through plastic deformation of mild steel or frictional loss in sliding joint as shown in Figure 2.2 and Figure 2.3 respectively, which have been proposed and used in real structures in recent years. However, these devices also have disadvantages, for mild steel devices with an initial elastic range of behaviour, it can only dissipate significant amount of energy when undergoing large plastic deformation. For friction devices, it can only take great effect until being loaded beyond the slip threshold. In other words, they are ineffective under small vibration.

Vibration control of structures with viscoelastic dampers has attracted considerable interest of researchers and has developed rapidly in recent several decades. As the background of this thesis, it will be described in more detail in the next section.

In order to improve the effectiveness and efficiency of vibration control, semi-active and active vibration control technology started to be developed in 1980's based on the passive vibration control methods (Sause R. et al, 1994). It is an area of structural protection in which the motion of a structure is controlled or modified by means of a control system through some external energy supply. Although considerable attention has been paid to active control research in recent years, with particular emphasis on the suppression of wind and seismic response, instruments of such system are very costly and a relative short service life is still a problem for these instruments.

2.1.2 Vibration control with viscoelastic dampers

Viscoelastic dampers installed in a structure can increase the structural damping, thereby reducing sway and oscillation of the structure. Such dampers are readily preferred in many slender structures where vibrations are likely to be noticeable and objectionable. No matter these are new structures to be designed (Ito Yoshio, 1995) or old structures to be retrofitted (Maison Bruce F., 1994), passive damping supplied by viscoelastic dampers may significantly improve their dynamic and acoustic performance. Viscoelastic dampers are not only used for vibration control of slender structures under wind loading or other environmental excitation, but also used for vibration control of those in earthquake areas to resist seismic loading (Aiken Ian D., 1990).

Viscoelastic dampers were studied experimentally and theoretically in past years. Hsu Sheng-Yung et al (1992) developed a kind of viscoelastic connection in framed structures and obtained satisfactory results. Kirekawa A. et al (1992)

carried out a study on a damper composed of lamination of steel plates and viscoelastic material and incorporated such dampers in diagonals of high-rise buildings. Bergman D. M. and Hanson R. D. (1990) installed devices made up of steel plates with added viscoelastic damping in a building frame so that story drift causes the steel plates moving relative to each other to shear the viscoelastic material.

Various types of viscoelastic damper have been found in many applications for vibration attenuation in real structures (P. Mahmoodi et al). Viscoelastic dampers were conceived and developed as a part of the structural design for the twin towers of the World Trade Center Towers in New York in 1969 and they were proved to be very effective. In 1982, a non-structural passive damping system was designed and installed in the Columbia Sea First Building in Seattle, Washington and a unique passive viscoelastic damping system was installed in the Two Union Square Building located in the same city in 1988. Recently, viscoelastic dampers were utilized for seismic retrofit in the 13 story San Jose GSA building in the United States. In Japan, dampers were installed in a 29 story steel moment frame building, the Chiba Portside Tower, to reduce vibration induced by wind and small to moderate earthquake in 1992 (Ito Yoshio et al, 1995). Some structures are also attempted to apply viscoelastic dampers as vibration control measure in recent years. It is a tendency that more and more building structures, especially high-rise buildings, will hire viscoelastic dampers to safeguard against being damaged by dynamic loading.

2.2 Mathematical Models for Viscoelastic Dampers and System Identification

For viscoelastic dampers, customary elementary and linear material models describing the time-dependent response of damping materials have certain difficulties, the predicted damping value by such a linear elastic model is zero, which shows that actual viscoelastic materials cannot be adequately described.

Dynamic characteristics of viscoelastic dampers have been described in many ways according to the experimental conditions and the methods for structural analysis. The basis of the mathematical approach to modelling the damping phenomena is rheology, the science of deformation and flow of matter. Dynamic properties are mainly embodied by the relation of restoring stress to strain. Generally, they can be expressed in mathematical form by five different types of models viz. standard linear model, generalized standard model, complex modulus model, integral model and generalized derivatives model.

Simplest linear viscoelastic relationships (standard linear models and generalized standard model) are widely used by researchers to analyze structures incorporated with viscoelastic dampers (Crandall S. H., 1970, Scanlan R. H., 1970). These models are often characterized as one spring and one dashpot (standard linear model) or a series of springs and dashpots (generalized standard model) connected in parallel. For example, one of the standard models, the Kelvin-Voigt model consists of two elements as shown in Figure 2.4. It is expressed as $\sigma = E\varepsilon + \eta\dot{\varepsilon}$, where E is the elastic modulus, η is the viscosity coefficient and overdot indicates time derivative. The energy dissipated per cycle by such models is proportional to, or inversely proportional to the frequency. It appears that such

models require a large number of constitutive terms such as springs and dashpots to cover a large frequency range of interest and the models are usually not good enough to describe accurately the viscoelastic material (Nashif Ahid D., 1985).

The complex model, wherein the elastic modulus is replaced by a complex constant, has been proposed as a means to describe material damping (Torvik P. J. et al, 1987). This device creates a component of stress out of phase with the strain, thereby leading to an energy dissipation per cycle which is proportional to the square of the strain amplitude and independent of frequency. The simplicity and relative effectiveness of this approach have made it popular and is now nearly a standard model for describing slightly inelastic materials. Viscoelastic material is often characterized by storage modulus (G') and loss modulus (G'') to represent the elastic and viscous properties respectively (Lai Ming-Lai, 1995, Kasai Kazuhiko et al, 1995). The ratio of the loss modulus to the storage modulus is the loss factor (η). It is convenient to use complex variables to describe the viscoelastic material as $G^* = G' + jG''$, where, $j = \sqrt{-1}$. Direct curve fitting techniques are also employed to obtain expressions for the real and imaginary parts of the complex modulus, which leads to the generalized complex modulus method. Such a modelling process works well in applications involving only a single and fixed frequency. But it is not suitable for viscoelastic dampers of which their properties change with the excitation frequency.

To describe the dynamic characteristics of viscoelastic material which are frequency and temperature dependent, Kirekawa A. et al (1992) proposed a Degrading Maxwell Model, where one of the three Maxwell elements connected in parallel is replaced by the spring element (5-element model) as shown in

Figure 2.5. It was also expressed by the complex modulus, which were functions of temperature and excitation frequency.

In addition to linear models, generalized standard models and complex models, integral equation based on the Boltzmann's superposition principle was also developed to describe the behaviours of viscoelastic dampers (Shen K. L. et al, 1995). It was expressed as $\sigma(t) = \int_0^t G(\tau)\dot{\varepsilon}(t-\tau)d\tau$, in which $G(\tau)$ was the stress relaxation modulus. Since the function $G(\tau)$ is always represented by empirical formulation and defined as the ratio of stress to strain at constant deformation, which is not easy to be determined accurately.

In the models mentioned above, linear viscous damping is usually assumed, which means that the loss factor is linearly proportional to the strain rate. It is not always true for the viscoelastic materials. In order to reduce the number of terms required by the generalized standard model to take adequate account of the slower rate of change of properties with frequency as observed from experimental results, a fractional derivative model for the elastomer damper was developed by Bagley in 1979. A theoretical basis drawn from the molecular theory for the new constitutional relationships was also established and generalized derivative models was built based on this relationships (Bagley 1983). A simplest form of the constitutional relationship has a fractional derivative form as $\sigma(t) = E_0\varepsilon(t) + E_1 D^{\alpha}[\varepsilon(t)]$, $0 < \alpha < 1$, where τ and γ are the shear stress and shear strain respectively, E_0 and E_1 represent the modulus corresponding to the storage energy and the loss energy, respectively. Limitation also exists in the original fractional derivative model. Since the model will be chosen to be developed in this thesis, it will be introduced in detail in Chapter Three.

Before mathematical models of dampers being applied for dynamic analysis, their parameters need to be determined first. Identification procedure for dynamic system has received wide attention in recent years because of the development in measurement and instrumentation technology facilitating the acquisition and the analysis of data with sufficient accuracy. Many common system identification methods were introduced by Ljun Lennart et al (1987). Recently, more and more attention has been paid to identification procedure of non-linear dynamic system. Parametric and non-parametric identification techniques have been studied intensively by many researchers. However, most of these procedures have problems of mathematical complexity, convergence rate, storage requirements and a large amount of computation time. For some simple mathematical models used for viscoelastic dampers, parameters of them can be measured directly from test results. And parameters of some other models are identified by the least square methods with sufficient number of special data points measured in time domain.

During past years, much work for system identification has been done in time domain, especially for nonlinear system (Julius S. Bendat et al, 1990, Koh Chan Ghee et al, 1991). Mottershead J. E. et al (1986) proposed a method to identify the two damping parameters associated with the non-linear nth-power velocity model from time series records of the displacement and velocity responses to sinusoidal excitation. Hollowell William T. et al (1988) developed a method to determine the mass and the nonlinear stiffness and damping characteristics of structures subjected to crash-loading environments using adaptive time domain and constrained minimization techniques. Mook D. Joseph (1989) presented a technique for processing noisy state-observable time domain measurements of a

nonlinear dynamic system to optimally estimate both the state vector trajectory and any model error that may be present. These methods proposed by the researchers were mostly improved for special objectives. And time consuming is a big problem for these methods.

A paper which accommodates the multi-harmonic solution of hysteretic system in frequency domain was reported by Capecchi D. et al (1990), where the GNR method (Galerkin procedure followed by a Newton-Raphson approach) was used in conjunction with FFT technique to solve steady-state response of a single-degree-of-freedom hysteretic system. With respect to the model developed in the thesis, the idea to identify parameters of a sophisticated model in frequency domain is of much value.

2.3 Dynamic Analysis of Structures with Viscoelastic Dampers

General dynamic analytical methods for structures have been introduced by Clough R.W. et al (1993). To analyze a structure with viscoelastic dampers is a different subject. Some methods for viscoelastic systems have been developed by former researchers. Linear viscoelastic approaches were applied in the past for the analysis of such structures by Johnson and Kienholz (1982), Sun et al (1987) and Hu and Dokainish (1993). The concept of a complex modulus in viscoelastic theory provides a basic and mathematically consistent approach. The modal Strain Energy method (MSE) was first suggested by Ungar and Kerwin in 1962, then it has been used in tackling viscoelastic damping problems of sandwich structures by Johnson and Kienholz (1982), Soni and Bogner (1982) and Rogers (1989). The MSE approach has the advantage that it allows one to compute

modal damping by a real, instead of a complex, eigenvalue solution. Consequently, the computational cost is greatly reduced. Based on MSE, modified MSE methods have been developed by Javeed Munshi A. et al (1994) and Hu B-G. et al (1995). Nevertheless, these methods did not pay much attention to the frequency factor of the damper.

Damping ratio of structures will increase greatly with viscoelastic dampers being incorporated in, which is the main reason why the damper can attenuate the dynamic response of a structure. Some researchers looked for an equivalent damping ratio and equivalent stiffness to represent the effect of dampers (Kasai Kazuhiko et al, 1995), and the dynamic analysis of a structure with viscoelastic dampers can be easily done as for the linear structures. But the problem is that it is difficult to determine accurately the equivalent damping ratio of a real structure with viscoelastic dampers, therefore the above-mentioned method cannot accurately predict the response of such a structure.

Some researchers have applied the Kelvin-Voigt mathematical model for the dampers throughout the complete dynamic analysis of a structure and solve the equilibrium equation by numerical methods in time domain (Tan X. M., et al, 1995). It is reasonable to do like this, but the analysis procedure is very complicated especially when the dampers are represented by sophisticated mathematical models and the calculation is very time consuming.

2.4 Discussions and Conclusions

The state of arts of vibration control of building structures is described briefly in this chapter briefly. From the work done in recent years, it can be found that

vibration control of structures with viscoelastic dampers has attracted more and more attentions. Achievements by other researchers and the practical applications of vibration control of structures with viscoelastic dampers have been discussed. It can be seen that there is still much work on material selection, damping device, mathematical modelling and structural analysis needed to be done.

Dampers can be of different materials, with different hardness and dimensions. Characteristics of different viscoelastic dampers are different, experimental work should be done to obtain the characteristics of a damper. For dampers like the ZJD-1 which will be introduced in the following Chapter, simple generalized derivative mathematical model such as Kelvin-Voigt model is accurate enough to simulate their dynamic behaviours. But for dampers like HD91 which has also been investigated in the present study, it is hard for generalized derivative models to describe their characteristics properly. That is to say, mathematical models should be chosen according to results of the dynamic tests on the dampers and the requirements of application. Although viscoelastic dampers always have high damping ratio, they are not purely viscous, and their properties change with excitation frequency. It can be seen that among those mathematical models described above, most of them can not describe the dynamic behaviours of viscoelastic dampers satisfactorily except the fractional derivative model. Application area of this model is more widely than other models, thus the fractional derivative model has been selected and developed to simulate the dynamic behaviours in the present study.

Vibration problems exist in various forms in real structures. In addition to the vibration caused by wind or seismic loading, vibrations caused by walk or dance

steps and machines in long span beam or floors of buildings are also required to be controlled. In order to fully utilize the energy dissipation ability of viscoelastic dampers, dampers are always installed at positions where relative displacement is comparatively large. For building structures, story drifts are considered as the movement to activate the dampers. Various types of damping devices are configured by many researchers. Dampers can be effective only if it is installed with proper device and located at suitable positions. Actually, for building structures, dampers can be installed at many places such as beam-column connections, area between neighbour stories and seismic resistance gaps, etc. In the present study, two kinds of damping devices have been designed to control vertical and horizontal vibration respectively.

To identify parameters of the models, the least square concept is usually adopted. Because of the complication of the fractional derivative model, it is difficult to get accurately the parameter values from many independent sets of experimental data in time domain, which are under different excitation frequency or with different shear displacement amplitude. If to accomplish this task in time domain, each set of data would provide a set of parameter values, which is different from each other. To average them to obtain the final results is surely not a good approach. Therefore, parameter identification methods in frequency domain have been developed, which can deal with all sets of experimental data simultaneously.

In the past research work, structures with viscoelastic dampers were mostly analyzed with constant complex stiffness or approximate damping ratio and carried out in time domain, which is of course very time consuming. And direct substitution of the complex modulus is only valid for steady state, time harmonic,

forced vibrations of a viscoelastic material (Hu B-G. et al, 1995). However, the improved fractional derivative model in this thesis have simple form in frequency domain, if an analytical method in hybrid time-frequency domain can be developed, a great amount of time will be saved in the calculation work and the accuracy of the analytical result can also be improved. In the present study, a method of analysis in hybrid-time-frequency domain for the dynamic response of structures with viscoelastic dampers has been proposed and has been verified by experimental tests.

2.5 References

Aiken Ian D., Kelly James M. and Mahmoodi Parviz (1990), The Application of Viscoelastic Dampers to Seismically Resistant Structures, Proceedings of Fourth U.S. National Conference on Earthquake Engineering, Vol.3, pp.459-468.

Bagley Ronald L. and Torvik Peter J. (1979), A Generalized Derivative Model for Elastomer Damper, Shock and Vibration Bulletin, Vol.49, pp135-143.

Bagley Ronald L. and Torvik Peter J. (1983), Fractional Calculus-A Different Approach to the Analysis of Viscoelastically Damped Structures, AIAA Journal, Vol.21, No.5, pp741-748.

Bendat Julius S. and Palo Paul A. (1990), Practical Techniques for Nonlinear System Analysis / Identification, Sound and Vibration, pp28-33.

Bergman D. M. and Hanson R. D. (1990), Viscoelastic versus Steel Plate Mechanical Damping Devices: An Experimental Comparison, Proceeding

of Fourth U.S. National Conference on Earthquake Engineering, pp. 469-477.

Capecchi, D., and Vestroni, F. (1990), Periodic response of a class of hysteretic oscillators, International Journal of Non-Linear Mechanics, Vol. 25, pp309-317.

Clough Ray W. and Penzien Joseph (1993), Dynamics of Structures, McGraw-Hill, Inc. London.

Crandall S. H. (1970), The Role of Damping in Vibration theory, Journal of Sound Vibration, Vol.11, No.1, pp3-18.

Hartog Den (1956), Mechanical Vibrations, 4th Edition, McGraw-Hill, New York .

Hollowell William T., Pilkey Walter D. and Sieveka Edwin M. (1988), System Identification of Dynamic Structures, Finite Elements in Analysis and Design, Vol. 4, pp65-77.

Hong Kyu-Seon and Yun Chung-Bang (1993), Improved Method for Frequency Domain Identifications of Structures, Engineering of Structure, Vol. 15, No.3, pp179-188.

Hsu Sheng-Yung and Fafitis Apotolos (1992), Seismic Analysis Design of Frames with Viscoelastic Connections, Journal of Structural Engineering, Vol. 118, No. 9.

Hu, B-G and Dokainish, M. A. (1993), Damped Vibrations of Laminated Composite Plates--Modeling and Finite Element Analysis, J. Finite Elements in Analysis and Design, in press.

Hu B-G, Dokainish M. A. and Mansour W. M. (1995), A Modified MSE Method for Viscoelastic Systems: A Weighted Stiffness Matrix Approach, J. Vibration and Acoustics, Vol. 117, no. 4, pp. 226-231.

Hunt J. B. (1979), Dynamic Vibration Absorbers, Mechanical Engineering Publications Ltd., London.

Ito Yoshio, Kirekawa Akio, Asano Kiyoaki (1995), Vibration Control Utilizing Viscoelastic Material -Chiba Portside Tower Building-, A New Direction in Seismic Design, pp. 319-312, Tokyo.

Johnson, C. D. and Kienholz, D. A. (1982), Finite Element Prediction of Damping in Structures with Constrained Viscoelastic Layer, AIAA J. Vol. 20, pp. 1248-1290.

Kareem A. and Sun W. J. (1987), Stochastic Response of Structures with Fluid-Containing Appendages, Journal of Sound and Vibration, Vol.119, pp.389-408.

Kasai Kazuhiko and Fu Yaomin (1995), Seismic Analysis and Design Using Viscoelastic Dampers, A New Direction in Seismic Design, Tokyo, pp113-140.

Kaynia A. M., Veneziano D. and Biggs J. M. (1981), Seismic Effectiveness of Tuned Mass Dampers, Journal of Structural Division, ASCE Vol.107, pp1465-1484.

Kirekawa A., Ito Y. and Asano K. (1992), A Study of Structural Control Using Viscoelastic Material, the Tenth World Conference on Earthquake Engineering, Vol. 4, pp.2047-2054.

Koh C. G., Mahatma S. and Wang C. M. (1995), Reduction of Structural Vibrations by Multiple-Mode Liquid Dampers, Engineering Structures, Vol.17, No. 2, pp122-128.

Koh Chan Ghee, See Lin Ming and Balendra Thambirajah (1991), Estimation of Structural Parameters in Time Domain: A Substructure Approach, Earthquake Engineering and Structural Dynamics, Vol. 20, pp787-801.

Kwok K. C. S. (1984), Damping Increase in Building with Tuned Mass Damper, Journal of Engineering Mechanics, ASCE, Vol. 110, No. 11, pp1645-1649.

Lai Ming-Lai (1995), Characteristics of Viscoelastic Materials and Dampers as Energy Dissipation Devices, New Products Department, The 3M Company, A New Direction in Seismic Design, pp. 195-210, Tokyo.

Ljun Lennart (1987), System Identification: Theory for the Use, Prentice-Hall, Inc., Englewood Cliffs, New Jersey 076.

Mahmoodi P., Roberston L. E., Yontar M., Moy C. and Feld L., Performance of Viscoelastic Structural Dampers in World Trade Center Towers, Vibration Control Systems Construction Market.

Maison Bruce F., Kasai Kazuhiko (1994), A Case Study of Building Retrofit using Viscoelastic Dampers, Chicago, Illinois, Fifth U.S. National Conference on Earthquake Engineering, Vol.3, pp597-606.

Mook D. Joseph (1989), Estimation and Identification of Nonlinear Dynamic Systems, AIAA Journal, Vol. 27, No. 7, pp968-974.

Mottershead J. E. and Stanway R. (1986), Identification of Nth-Power Velocity Damping, Journal of Sound and Vibration, Vol.105, No.2, pp309-319.

Munshi Javeed A. and Kasai Kazuhiko (1994), Modal Analysis Procedures for Viscoelastic Frames, 5th U.S. National Conference on Earthquake Engineering, Vol.1, pp. 1055-1064, Chicago, Illinois.

Nashif Ahid D., Jones David I. G. and Henderson John P. (1985), Vibration Damping, John Wiley & Sons, New York.

Rogers, L. ed. (1989), Proceedings of Damping'89, West Palm Beach, FL., Wiley Interscience Publication.

Sause R., Hemingway G. and Kasai K. (1994), Simplified Seismic Response Analysis of Viscoelastic-Damped Frame Structures, Fifth U.S. National Conference on Earthquake Engineering, pp939-848.

Shen K. L., Soong T. T. (1995), Modeling of Viscoelastic Dampers for Structural Applications, Journal of Engineering Mechanics, Vol.121, No. 6, pp694-701.

Scanlan R. H. (1970), Linear damping models and causality in vibrations, Journal of Sound Vibration, Vol.13, No.4.

Skinner R. L., Robinson W. H. and Mcverry G. H. (1993), An Introduction to Seismic Isolation, John Wiley & Sons.

Soni, M. L., and Bogner, F. K. (1982), Finite Element Vibration Analysis of Damping Structures, AIAA J., Vol. 20, pp. 700-707.

Soong T. T., Dargush G. F. (1997), Passive Energy Dissipation Systems in Structural Engineering, John Wiley & Sons.

Sun, C. T. et al. (1987), Prediction of Material Damping of Laminated Polymer Matrix Composites, J. Material Science, Vol.22, pp. 1006-1012.

Sun L. M., Fujino Y. and Koga K. (1995), A Model of Tuned Liquid Damper for Suppressing Pitching Motions of Structures, Earthquake Engineering Structural Dynamics, Vol. 24, pp.625-636.

Tan X. M., Ko J. M. and Fang E. H. (1995), Experimental and Analytical Study on A Framed Structure Incorporated with Viscoelastic Dampers, Conference of SDVNC'95, pp.301-306, Hong Kong.

Torvik P. J., Bagley R. L. (1987), Fractional derivatives in the description of damping materials and phenomena, the 1987 ASME design technology conferences-11th Biennial Conference on Mechanical Vibration and Noise, pp.125-135.

Ungar E. E. and Kerwin E. M. Jr. (1962), Loss Factors of Viscoelastic Systems in Terms of Energy Concepts, J. Acoustical Society of America, Vol. 34, pp. 954-957.

Way D. and Howard J. (1992), Rehabilitation of the Mackay School of Mines, Phase III: With Base Isolation, Proceedings of the Tenth World Conference on Earthquake Engineering, Vol. 4, Madrid, Spain.

Welt F. and Modi V. J. (1989), Vibration Damping Through Liquid Sloshing: Part I - A Nonlinear Analysis, Proceeding of Diagnostics, Vehicle

Dynamics and Special Topics, ASME, Design Engineering Division (DE), 18-5, pp149-156.

Welt F. and Modi V. J. (1989), Vibration Damping Through Liquid Sloshing: Part II - Experimental Results, Proceeding of Diagnostics, Vehicle Dynamics and Special Topics, ASME, Design Engineering Division (DE), 18-5, pp.157-165.

Xu Y. L., Samali B. and Kwok K. C. S. (1992), Control of Along Wind Response of Structures by Mass and Liquid Dampers, Journal of Engineering Mechanics, ASCE, Vol. 118, No. 1, pp. 20-39.

Yamaguchi H. and Harnpornchai N. (1993), Fundamental Characteristics of Multiple Tuned Mass Dampers for Suppressing Harmonically Forced Oscillations, Earthquake Engineering Structural Dynamics, Vol.22, pp51-62.

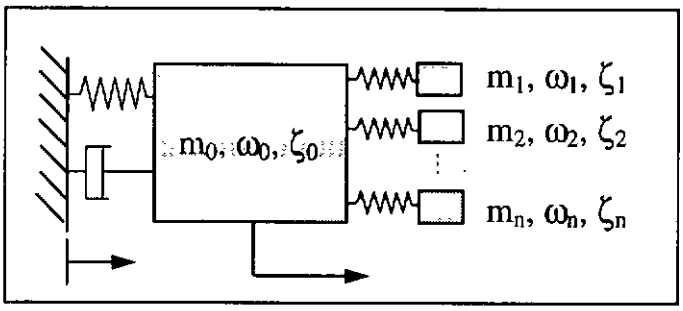

Figure 2.1 MTMDS system

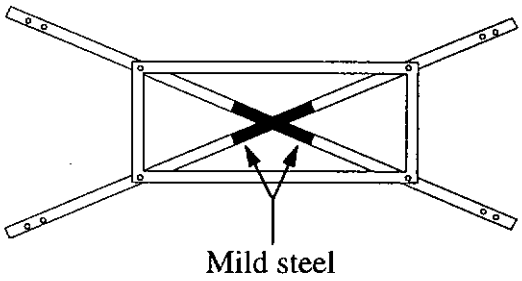

Figure 2.2 Friction energy dissipation brace with sliding slots

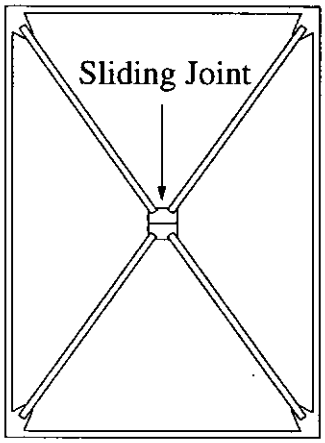

Figure 2.3 Shear energy dissipation brace

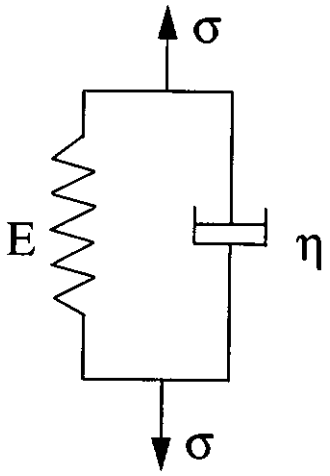

Figure 2.4 Kelvin-Voigt Model

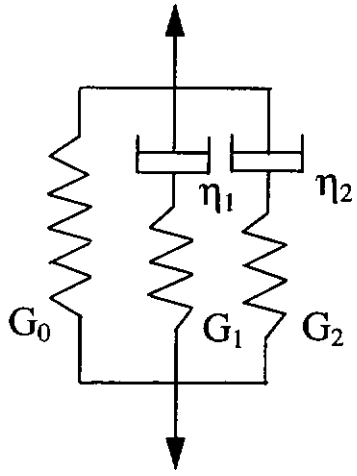

Figure 2.5 Degrading Maxwell Model

CHAPTER 3
DYNAMIC TESTS ON VISCOELASTIC DAMPERS

3.1 Introduction

Viscoelastic dampers are glassy substances or high polymer made of natural rubbers or synthetic rubbers, which have high damping. They can have different hardness, mass density, and can be produced by factories with different shapes. Properties of the dampers are determined by these factors. Before viscoelastic dampers are utilized in structures for vibration control, their dynamic behaviours under different conditions should be known. Although user guide and related data are usually supplied by the manufacturer, they cannot necessarily meet the need of every user. Data in the user guide are always not detail enough to provide all the properties that are required for the design of vibration control of a structure with viscoelastic dampers. If that is the case, dynamic tests should be performed on some specimens. Normally, damper properties can be obtained by the following experimental methods: Oberst beam vibration method, sinusoidal excitation method, phase-lag measurement method and free attenuation method (Sun Q. H. et al, 1993). For different experimental objectives, different kinds of method will be used with different test set-up.

Viscoelastic dampers always have good energy dissipation ability in their shear direction. Shear dynamic tests on various viscoelastic dampers have been carried out by many researchers with similar devices as shown in Figure 3.1. For instances, tests were carried out by using a standard MTS closed loop hydraulic test machine for material shear properties (Aiken Ian D. et al, 1990); dynamic

properties of a sheet of acrylic viscoelastic material with sizes of 4mm×5mm×2mm in its shear direction have been investigated at various temperature between 5°C and 35°C by Kirekawa A. et al (1992). Damper properties were obtained by both these two tests. Experimental results by the researchers mentioned above and the other researchers like Chang K. C. et al (1992, 1993) have shown that factors such as excitation frequencies, maximum shear strain and environmental temperature should be taken into account properly for practical design.

Dynamic test on viscoelastic dampers is also a way to know more about the damper material. From the tests, phenomena such as the behaviour of the dampers for vibration attenuation and energy dissipation can be observed clearly and this can also give us a better understanding how the dampers work when they are incorporated in real structures. Moreover, results from experimental work can help us to choose a proper model to describe the damper and the test data also forms the basis for the identification of model parameters.

Experimental investigations on the dynamic properties of two kinds of viscoelastic damper have been carried out and are presented in this chapter. Properties of these two kinds of damper, such as hysteresis loops, damping ratios, and equivalent stiffness have been studied based on the test results and difference between these two kinds of damper have been discussed. During the dynamic shear tests, shear displacement amplitude and excitation frequency are chosen as the variables.

Since the axial behaviour of dampers has to be considered in the analysis of structures with viscoelastic dampers in Chapter Five, the dynamic behaviours of

the dampers in axial direction which has been presented and referred to in this chapter is based on the experimental studies carried out by two former research students of this department.

3.2 Experimental Test

3.2.1 Test set-up

To obtain the dynamic properties of viscoelastic dampers in their shear direction, a double pendulum system is designed to conduct the shear tests under dynamic loading. Specimens are glued to two metal plates on both sides by Aradite glue, which has enough strength, and then installed between the two steel plates of the pendulum system by bolts. These two steel plates can move freely in parallel. The upper plate is connected to a rigid frame through a force transducer and three accelerometers, which are used to measure the shear displacement, velocity and acceleration, are fixed on the bottom plate and aligned in horizontal direction. The bottom plate is connected to an exciter, which is controlled by a signal generator via a signal amplifier. When the bottom plate being excited by the exciter, the specimen will undergo pure shear. Signals picked up by the transducer and accelerometers pass through the charge amplifiers with proper setting and then pass through the frequency filters to remove the disturbance of high frequency. When signals are observed to be stable from the digital oscilloscope, they are sent to the computer for analog to digital conversion by the A/C board. Restoring force, shear displacement, shear velocity and shear acceleration of the damper will be recorded in the computer simultaneously by

means of the software Global Lab. The set-up of the test system is shown in Figure 3.2. And the appearance of the test system can be seen from Photo 3.1.

When the test is performed, shear displacement is the control parameter. While setting the excitation frequency at a certain value, amplitude of acting force generated by the exciter is increased by tuning the buttons of the signal generator. The buttons should be tuned slowly to avoid the disturbance due to fast changing. When the shear displacement indicated on the oscilloscope reaches the required value and the hysteresis loop of the restoring force to shear displacement displayed on the oscilloscope is stable, data can be collected. Taking into account the need in data analysis by FFT, data collecting density is set to 128 points per cycle and at least 32 cycles of data are needed to be collected for each test case.

3.2.2 Dampers used for test

Viscoelastic dampers selected for tests are those which are used in the damping devices for the structures subjected to dynamic testing at a later stage in the present study. Two kinds of viscoelastic dampers, which are manufactured by Wuxi Vibration Isolator Company of the People's Republic of China, have been selected for tests. One is called ZJD-1, which is mounted on both sides in different directions as shown in Figure 3.3. It can be glued with other material firmly. Size of the damper ZJD-1 is 12cm×9cm×2cm. The other one, namely HD91, is 2mm thick only. A specimen with area of 7.5cm×7.5cm is cut from a big sheet.

3.2.3 Test cases

Damper specimens are installed in the test system and tested under sinusoidal forces at different excitation frequency with different shear displacement amplitude. With consideration of the excitation frequency range and maximum shear displacement in the dampers which are used at a later stage in the present study, the excitation frequencies are set to 3Hz, 6Hz, 9Hz, 12Hz, 15Hz, 18Hz, 20Hz, 25Hz, 30Hz, 35Hz, 40Hz and 45Hz. And the shear displacement amplitudes are chosen at the levels of 0.05mm, 0.10mm, 0.15mm, 0.20mm, 0.25mm, 0.30mm, 0.35mm and 0.40mm for both these two kinds of damper. During the test, it has been found that the hysteresis loops displayed on the oscilloscope may shift away from the original point of the cross axis. To guarantee the accuracy of the test results, no matter the loops shift or not, test data should be collected only when the hysteresis loop is stable enough.

3.3 Test Results

The hysteresis loop of restoring force with shear displacement, which is the most typical characteristic of viscoelastic dampers, has been studied. It is caused by phase-lag between the restoring force and the shear displacement of the damper. Energy dissipation ability, damping ratio and equivalent stiffness of a damper can be embodied by the hysteresis loop. The equivalent stiffness is taken as the slope of the line from center of the hysteresis loop to the point of the loop at the maximum displacement. During the tests, it can be found from the oscilloscope that a viscoelastic damper will give hysteresis loops with different shape and size under different conditions. Since the mathematical model to be adopted are based on the relationship between restoring force and shear displacement, relationship

between restoring force and shear velocity as well as that between restoring force and shear acceleration will not be discussed in this thesis.

The hysteresis loop should be in the same trail under the same conditions, however, it may shift with an acceptable error in reality, which can be seen from an example of damper ZJD-1 with shear displacement amplitude of 0.10mm at excitation frequency of 15Hz as shown in Figure 3.4. In order to compare the loops among different cases clearly, one-cycle loops taken from different cases have been drawn together in the following figures. Because the shear displacement amplitude of test results may have discrepancy with the predetermined value and the loop centre may shift away from zero point, raw test data has been adjusted to satisfy the predetermined displacement amplitude of the test case. For example, if the displacement of the test results is 0.99 of the predetermined value, all the test data in this case will be amplified by a factor $\frac{1}{0.99}$; if the maximum displacement is 0.11mm and the minimum displacement is 0.099mm, all the displacement values in this case will be added with -0.01mm while the restoring force values remain unchanged. To make the illustration distinct enough and keep figures clear, several test cases instead of all of them are listed in the following parts.

From the test results, it has been found that within the tested range, these two kinds of damper have some similar behaviors. No matter how the conditions change, the shape of hysteresis loop is elliptical with slanting major axis and the loop is nearly smooth with few mutations. If the shear displacement amplitude decreases while the excitation frequency is fixed, the loop size is reduced also. But the loop shape and equivalent stiffness do not change, which means the

damping ratio of the damper keeps at a constant value. Figure 3.5 and Figure 3.6 are examples of the test results with shear displacement amplitude changing from 0.05mm to 0.20mm for ZJD-1 and HD91 respectively, in which the exciting frequency is fixed at 9Hz.

When shear displacement amplitude is fixed, the hysteresis loop will swell if the excitation frequency increases. It means the energy dissipation ability of a damper is enhanced when the excitation frequency increases. The phenomena can be seen from Figure 3.7 for ZJD-1 and Figure 3.8 for HD91, in which the shear displacement amplitude is fixed at 0.10mm. It is not difficult to imagine that when the exciting frequency is reduced to a low enough value, the hysteresis loop would degenerate to a single line.

Difference between these two kinds of damper has also been found. When the excitation frequency changes, the equivalent stiffness of ZJD-1 changes little because the point at maximum displacement remains stationary as shown in Figure 3.7. However, the equivalent stiffness of HD91 increases with the excitation frequency. It can be seen from Figure 3.8 that the point at maximum displacement moves upward when the excitation frequency increases.

Damping ratios of the dampers have been calculated from test data by phase-lag method (Sun Q. H. et al, 1993), $\zeta = \frac{1}{2}\tan\varphi$, where φ is the phase-lag between the restoring force and the shear displacement. It has been found that the damping ratio of both these two kinds of damper does not change much with the shear displacement amplitude while the excitation frequency is fixed. But when the excitation frequency increases, the damping ratio will increase also. It can be seen from Figure 3.9 that damping ratio of damper ZJD-1 increases nearly linearly

with excitation frequency. However, the damping ratio of damper HD91 changes with the excitation frequency in a nonlinear curve, which can be seen from Figure 3.10. For both dampers, if linear relation is assumed as follows:

$$\zeta = c\omega + f \tag{3.1}$$

where, ω = frequency $\times 2\pi$, the parameters c and f have been determined to be 0.00261 and -0.0115 for damper ZJD-1, 0.00138 and 0.156 for damper HD91, respectively. Comparisons of the real damping curve with the linear damping curve have also been made in Figure 3.9 and Figure 3.10. It can be seen that the linear damping model can well simulate the damping ratio of damper ZJD-1, while it is poor for damper HD91.

Area of hysteresis loop indicates the capacity of energy being dissipated per cycle by the damper. The larger the area is, the higher the energy being dissipated will be. The Areas of loops in different cases are calculated by integration method. It is clear from Figure 3.11 and Figure 3.12 for damper ZJD-1 and damper HD91 respectively that energy dissipated per cycle increases with shear displacement with a nonlinear relation, which has been identified to be quadratic. Energy dissipated per cycle by damper ZJD-1 is nearly in linear relation with excitation frequency, which can be seen from Figure 3.13. But energy dissipated per cycle by damper HD91 is in a nonlinear relation with excitation frequency as Figure 3.14. Energy problem will be discussed again based on the mathematical model in Chapter Four.

Limited by the thesis page, test results of all test cases are not presented by figures. The equivalent stiffness, energy dissipated per cycle and damping ratio of

damper ZJD-1 and HD91 of all test cases have been calculated and shown in Appendix 1 and Appendix 2.

3.4 Dynamic Behaviours of the Dampers in Axial Direction

Dynamic tests on these two kinds of viscoelastic dampers in their axial direction have been done by the research students Mak M. F.(1991) and Lam J. Y. H. (1993) in the same department of the university. The test set-up is shown in Figure 3.15. During the tests, the axial displacement amplitudes were set from 0.05mm to 0.5mm and the excitation frequencies were set from 3Hz to 60Hz. Restoring force and axial displacement were recorded simultaneously for all test cases. From the test results, it has been found that the dynamic characteristics of the dampers in their axial direction have the similar behaviours as those in their shear direction. It can be seen from the hysteresis loops with different displacement amplitudes and at different excitation frequencies as reproduced in the figures from Figure 3.16 to Figure 3.19.

For the research work which was performed by Mak and Lam have been described in their thesis in detail. It will not be repeated here. Some of the test results (excitation frequency from 3Hz to 40Hz and shear displacement amplitude from 0.05mm to 0.40mm) are given in Appendix 3 and Appendix 4 for references.

3.5 Discussions and Conclusions

As the basis of model selection for viscoelastic dampers, dynamic characteristics of two kinds of viscoelastic dampers in their shear direction have been studied by

experimental work and discussed in detail in this chapter. The dynamic behaviours of these two kinds of dampers in their axial direction have been briefly described based on the research work carried out by others. Compared with the test results of other kinds of viscoelastic damper carried out under excitation of different shear displacement amplitudes and at different excitation frequencies by other researchers (Aiken Ian D. et al, 1990, Kirekawa A. et al, 1992, Chang K. C. et al, 1993), it can be found that those viscoelastic dampers also have the similar properties. It means that the properties of these two kinds of dampers carried out in the present study have covered those of the commonly used viscoelastic dampers. The properties of the dampers can be reflected accurately enough by the mathematical model proposed in the following chapter.

From the test results, it has been found that the hysteresis loops of restoring force against shear displacement change with shear displacement amplitude and excitation frequency. When the excitation frequency is fixed, area of the hysteresis loop, which presents the energy dissipation ability, increases with shear displacement amplitude while the loop shape remains unchanged. On the other hand, when the shear displacement amplitude is fixed, area of the loop increases with the excitation frequency and the loop shape changes also.

Differences in properties between different kinds of damper have been found. No matter under any shear displacement amplitude and at any excitation frequency, the equivalent stiffness of the damper ZJD-1 changes very little, however, that of the damper HD91 and other dampers investigated by other researchers increases noticeably with the excitation frequency. Damping ratio of damper ZJD-1 increases linearly with the excitation frequency, but that of the dampers like

HD91 changes nonlinearly with the excitation frequency. Furthermore, difference in energy dissipation ability between dampers like ZJD-1 and dampers like HD91 has also been found.

Figures shown in this chapter are only some examples of the experimental work which are considered to be clear enough to explain the properties of the dampers. Although test data of only a few cases are presented in the figures of this chapter, test data of other cases not presented have demonstrated similar behaviours. All the test data have been used for system identification of model parameters in Chapter Four.

When the tests were performed, environmental temperature was about 25°C. Limited by the laboratory facilities, temperature factor has not been considered in the experimental tests. However, since the property of viscoelastic dampers would vary with the change of temperature. The temperature effect is discussed in the formulation of mathematical model with reference to the results obtained by other researchers in the following chapter. For practical design in those cities like Hong Kong, where the temperature variation in a year is small, the dynamic behaviours of the viscoelastic dampers installed inside the buildings in particular those with air-condition, is not expected to have significant change due to temperature effect.

3.6 References

Aiken Ian D., Kelly James M. and Mahmoodi Parviz (1990), The Application of Viscoelastic Dampers to Seismically Resistant Structures, Proceedings of

Fourth U.S. National Conference on Earthquake Engineering, Vol.3, pp.459-468.

Chang K. C. (1993), Seismic Performance and Design of Steel Structures with Added Viscoelastic Dampers, the Fourth Ease Asia-Pacific Conference on Structural Engineering & Construction, Seoul, Korea.

Chang K. C., Lai M. L., Soong T. T., Hao D. S. and Yeh Y. C. (1993), Seismic Behaviour and Design Guidelines for Steel Frame Structures with Added Viscoelastic Dampers, NCEER 93-0009, National Center for Earthquake Engineering Research, Buffalo, NY.

Chang K. C., Soong T. T., Oh S. T. and Lai M. L. (1992), Effect of Ambient Temperature on Viscoelastically Damped Structure, Journal of Structure Engineering, Vol. 118, No. 7.

Kirekawa A., Ito Y. and Asano K. (1992), A Study of Structural Control Using Viscoelastic Material, Proceeding of the 10th World Conference, pp.2047-2054, Rotterdam.

Lam J. Y. H. (1993), Parameter Estimation of Viscoelastic Pad Isolator, A Thesis for the Degree of Master Philosophy, Department of Civil Engineering, the Hong Kong Polytechnic.

Mak M. F. (1991), Control of Beam Vibration with Dampers, Final Year Project (90/91), Department of Civil Engineering, the Hong Kong Polytechnic.

Sun Q. H., Zhang Q. J. and Yao H. Z. (1993), Damping Control of Vibration and Noise, Mechanical Industry Press. (In Chinese)

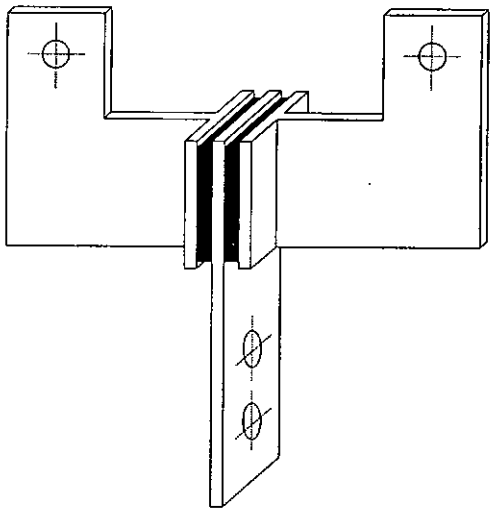

Figure 3.1 Shear test set-up for viscoelastic dampers

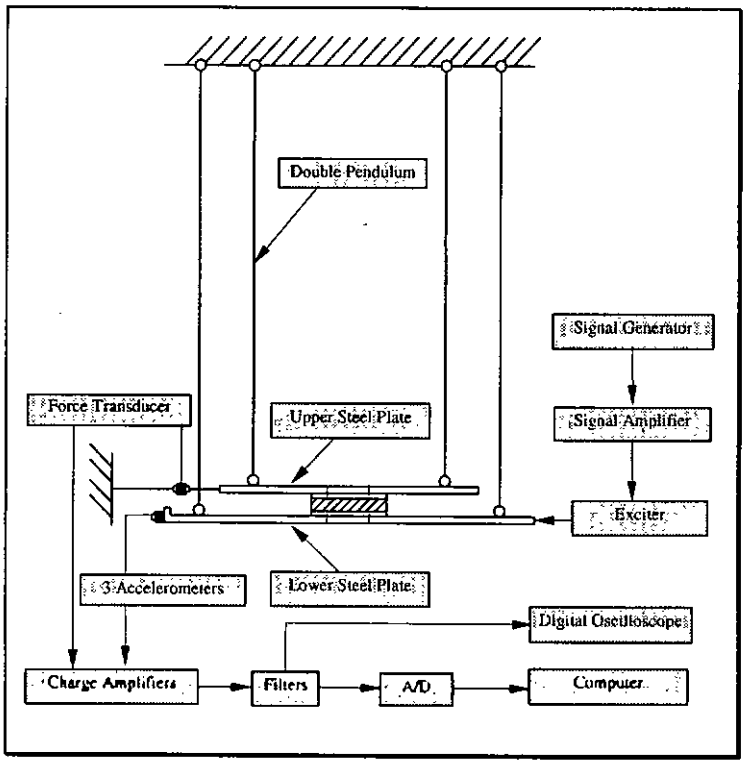

Figure 3.2 Set-up of the dynamic test system

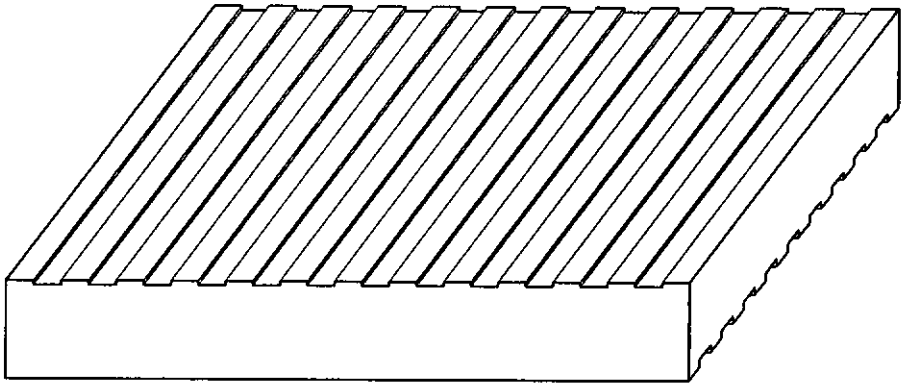

Figure 3.3 Appearance of damper ZJD-1

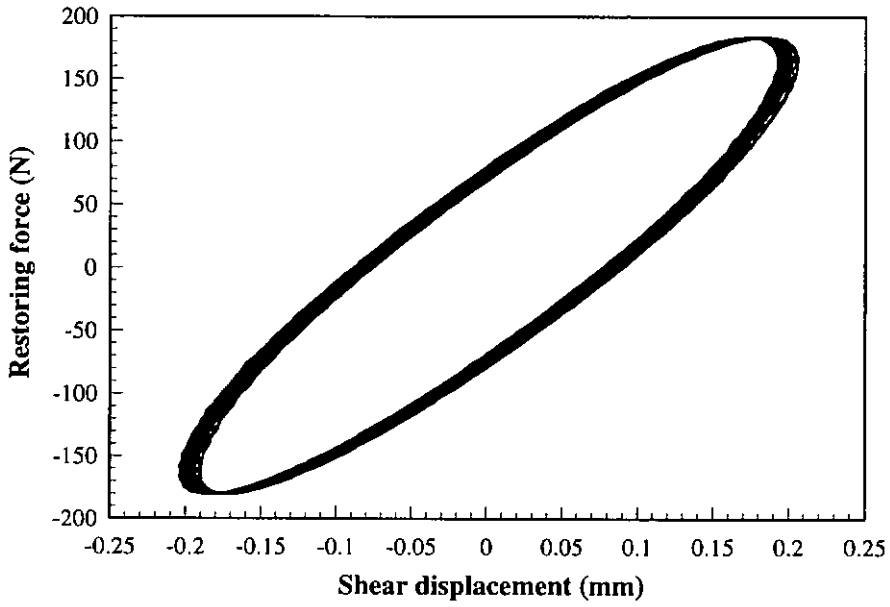

Figure 3.4 Hysteresis loops of damper ZJD-1 at excitation frequency of 15Hz

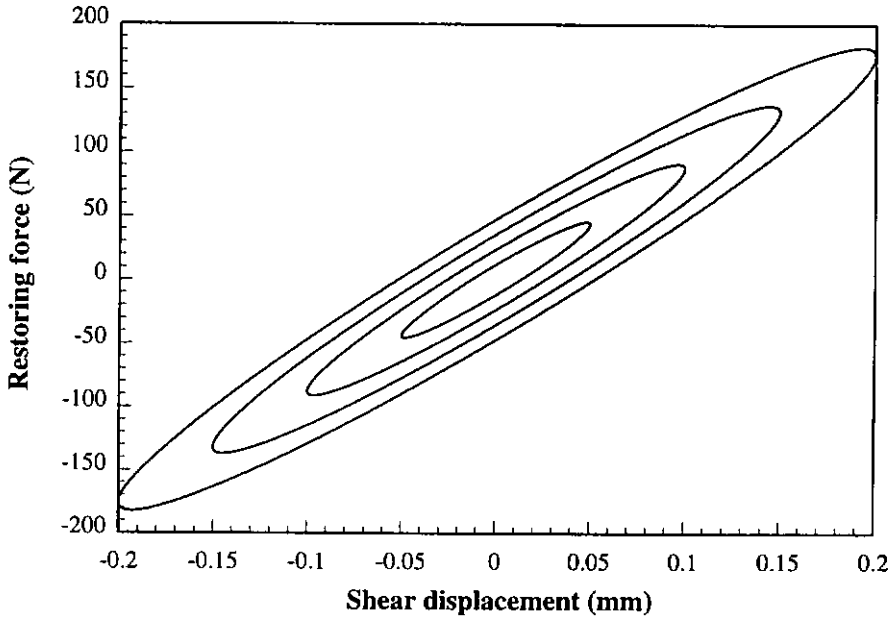

Figure 3.5 Hysteresis loops of damper ZJD-1 under shear displacement of different amplitudes with fixed excitation frequency of 9Hz

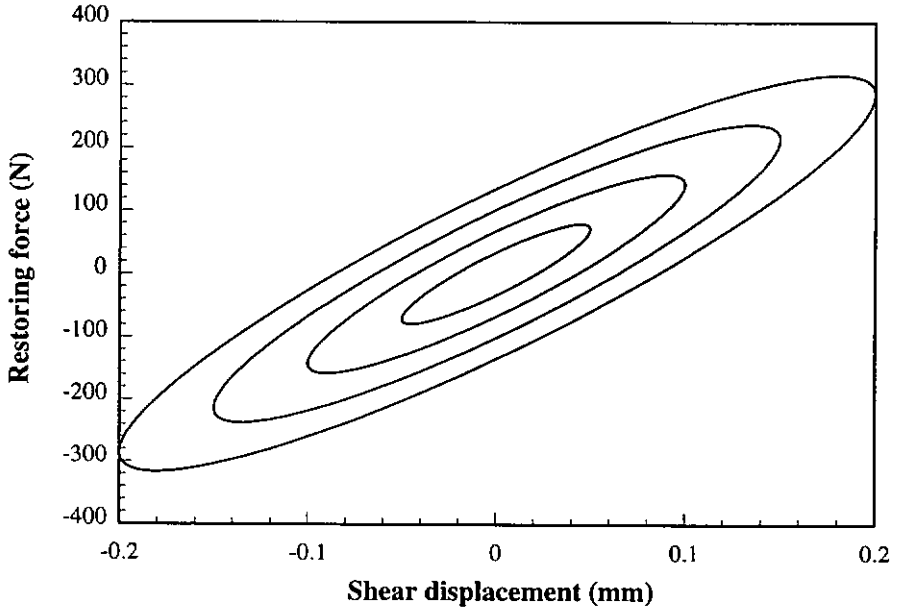

Figure 3.6 Hysteresis loops of damper HD91 under shear displacement of different amplitudes with fixed excitation frequency of 9Hz

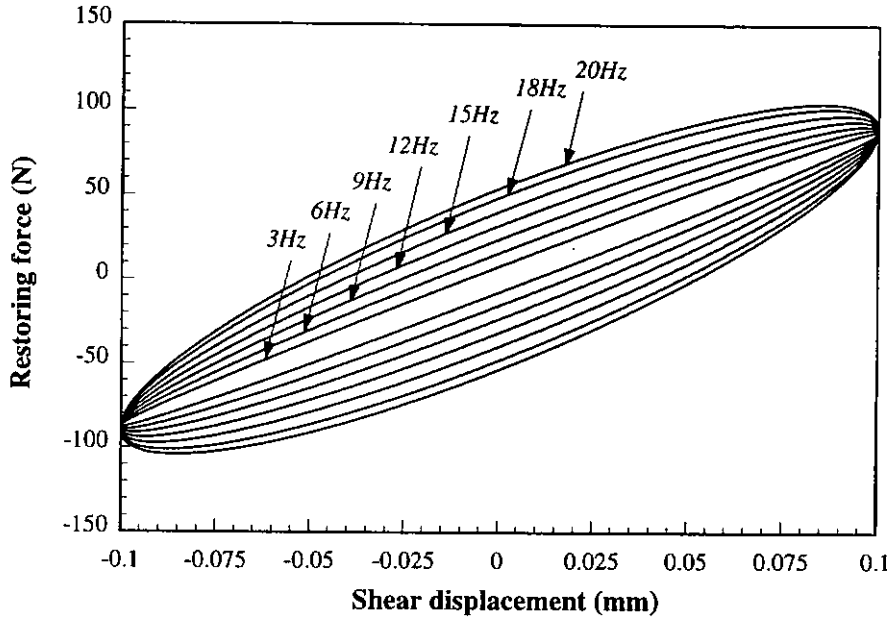

Figure 3.7 Hysteresis loops of damper ZJD-1 at different excitation frequencies

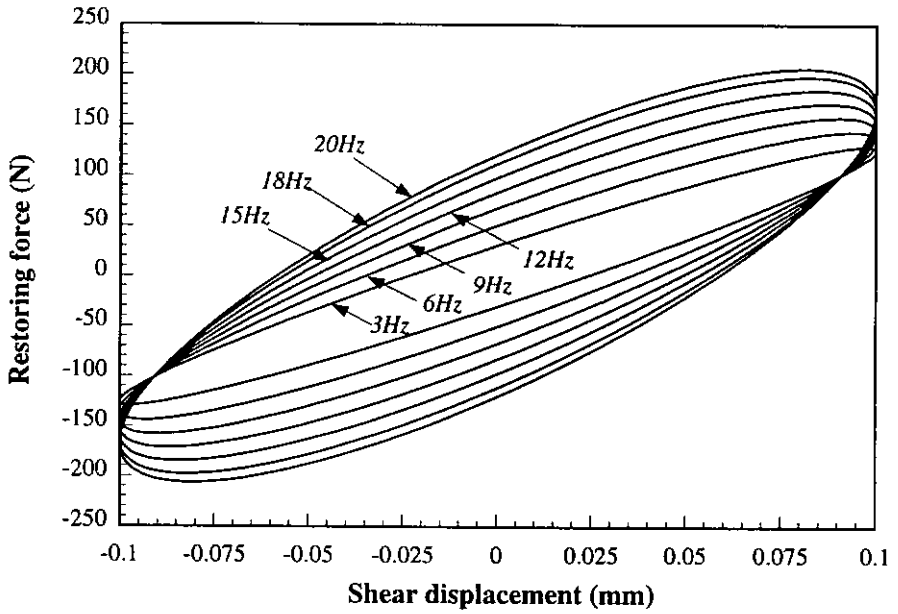

Figure 3.8 Hysteresis loops of damper HD91 at different excitation frequencies

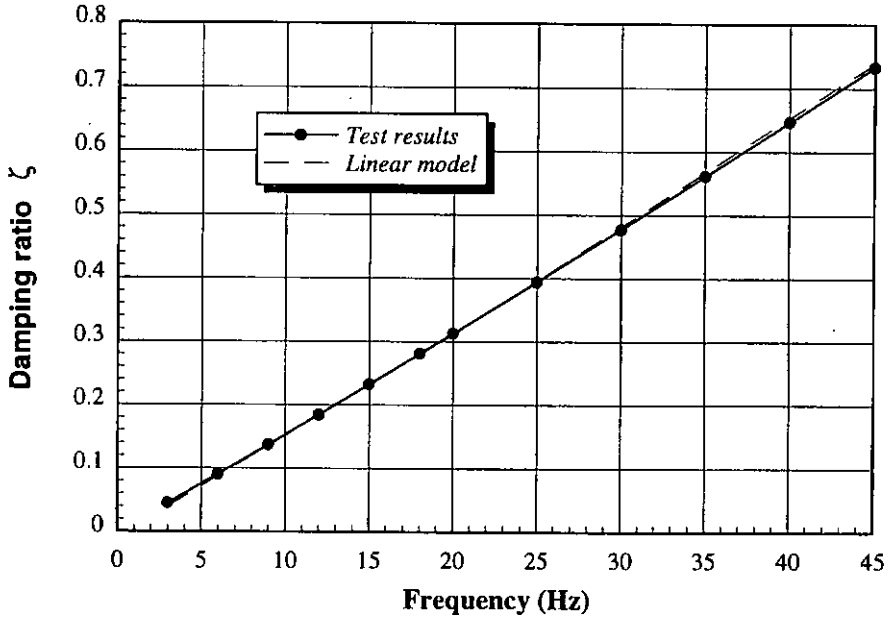

Figure 3.9 **Damping ratios of damper ZJD-1 at different excitation frequencies**

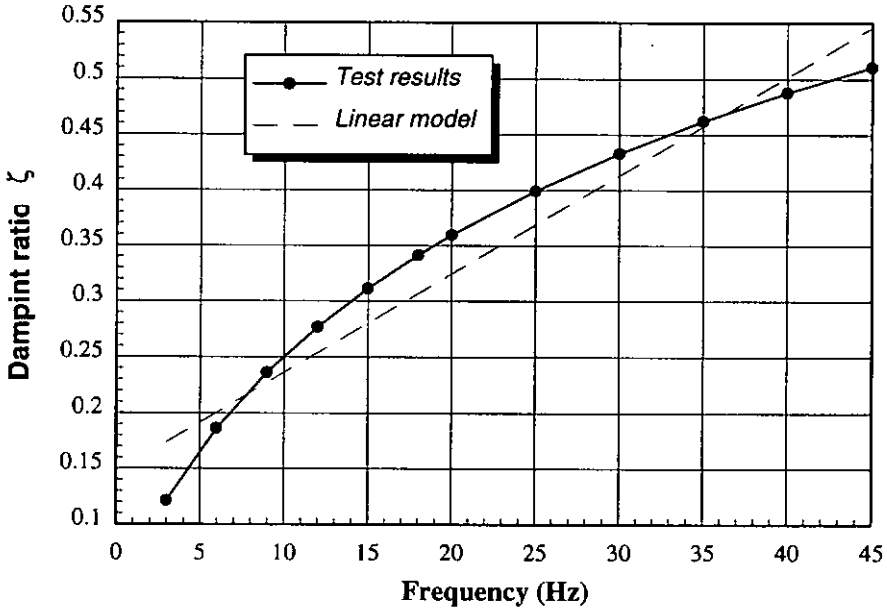

Figure 3.10 **Damping ratios of damper HD91 at different excitation frequencies**

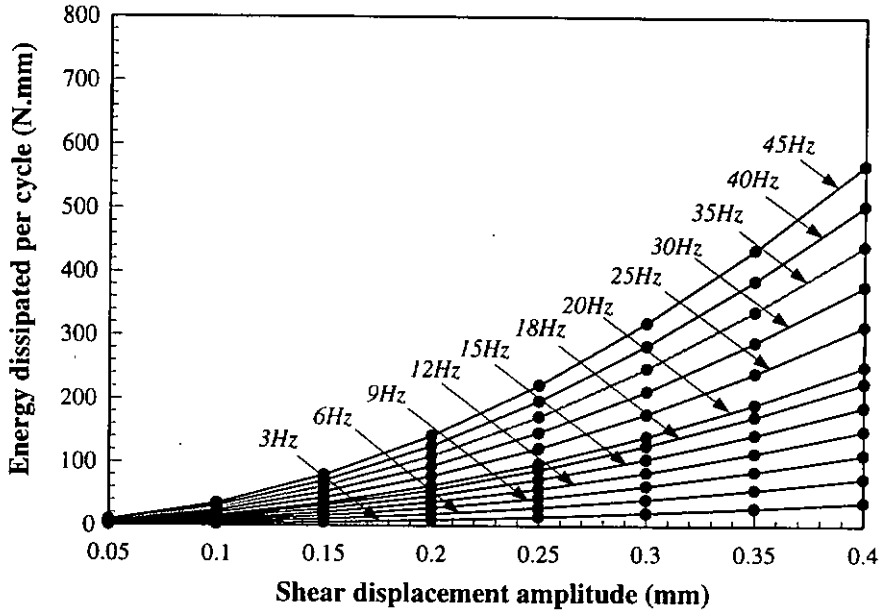

Figure 3.11 Energy dissipated per cycle by damper ZJD-1 (with amplitude of shear displacement)

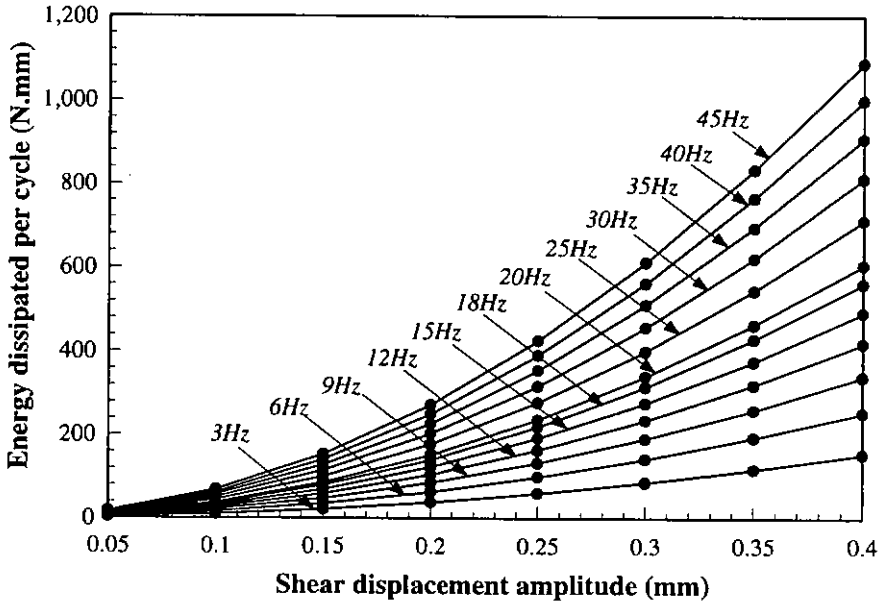

Figure 3.12 Energy dissipated per cycle by damper HD91 (with amplitude of shear displacement)

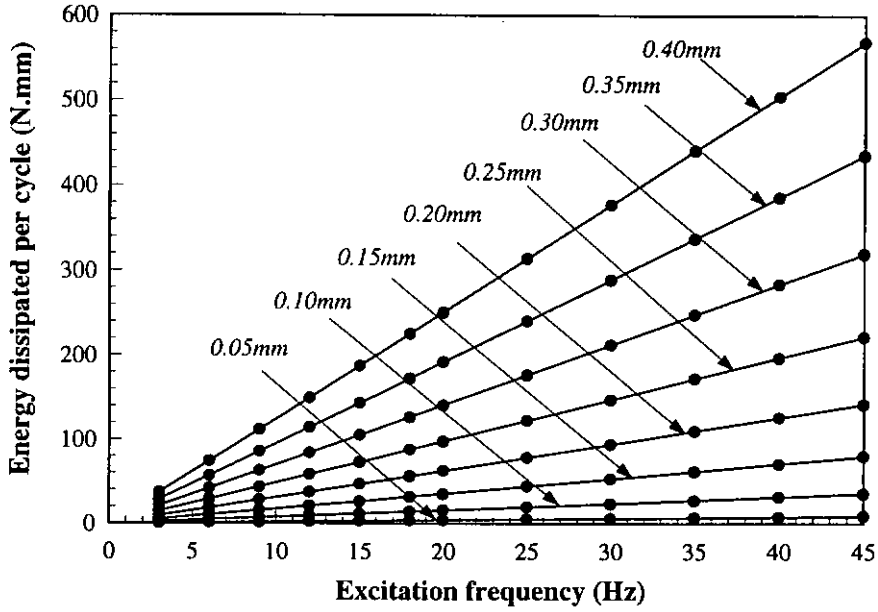

Figure 3.13 Energy dissipated per cycle by damper ZJD-1 (with excitation frequency)

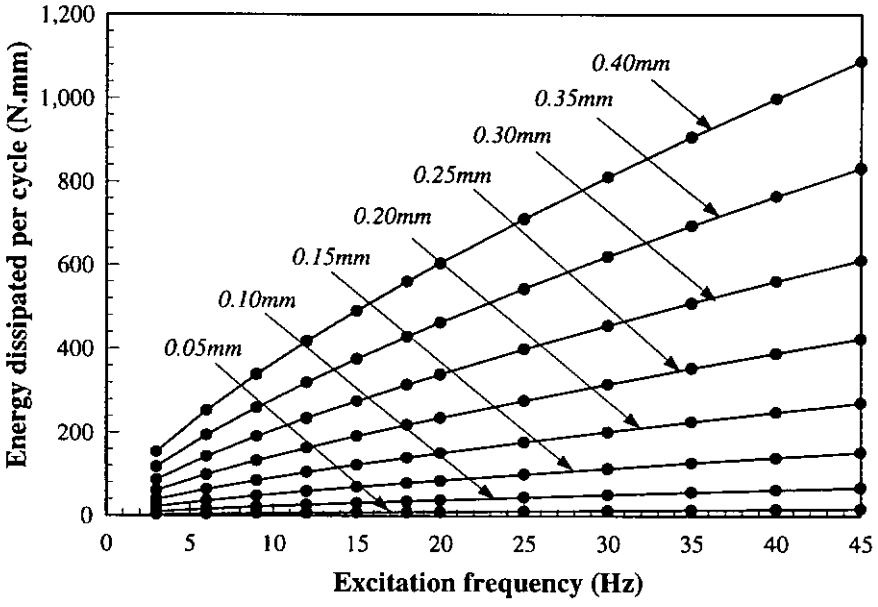

Figure 3.14 Energy dissipated per cycle by HD91 damper (with excitation frequency)

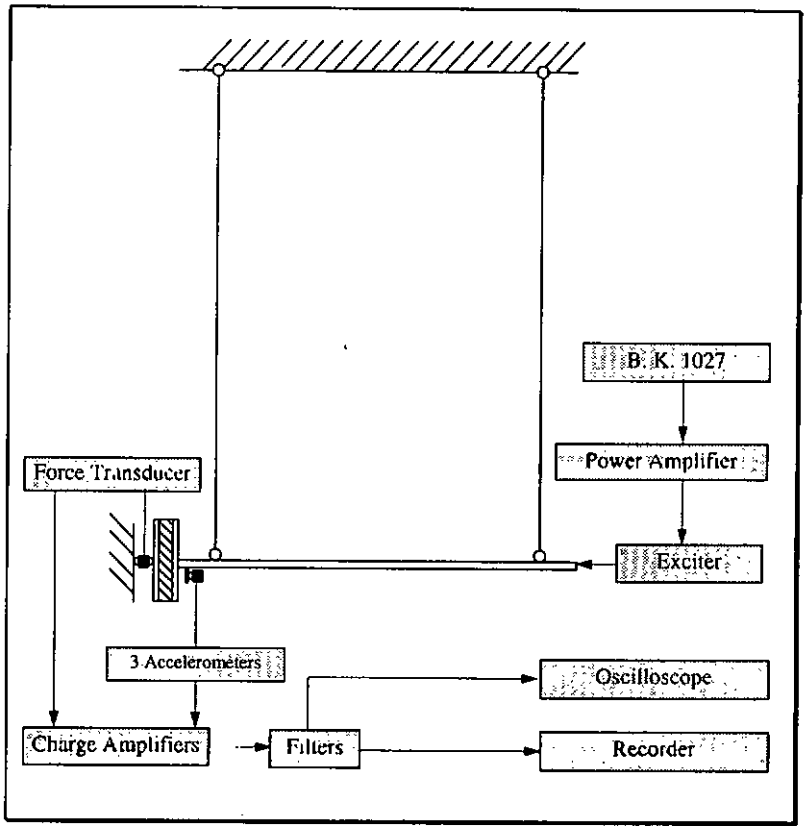

Figure 3.15 Set-up of the dynamic test in axial direction

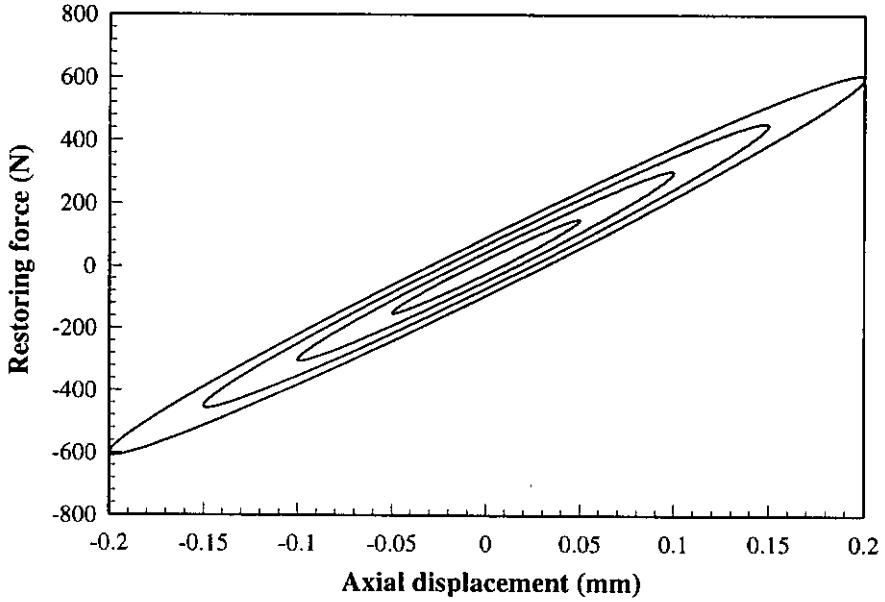

Figure 3.16 Hysteresis loops of damper ZJD-1 under axial displacement of different amplitudes with fixed excitation frequency of 9Hz

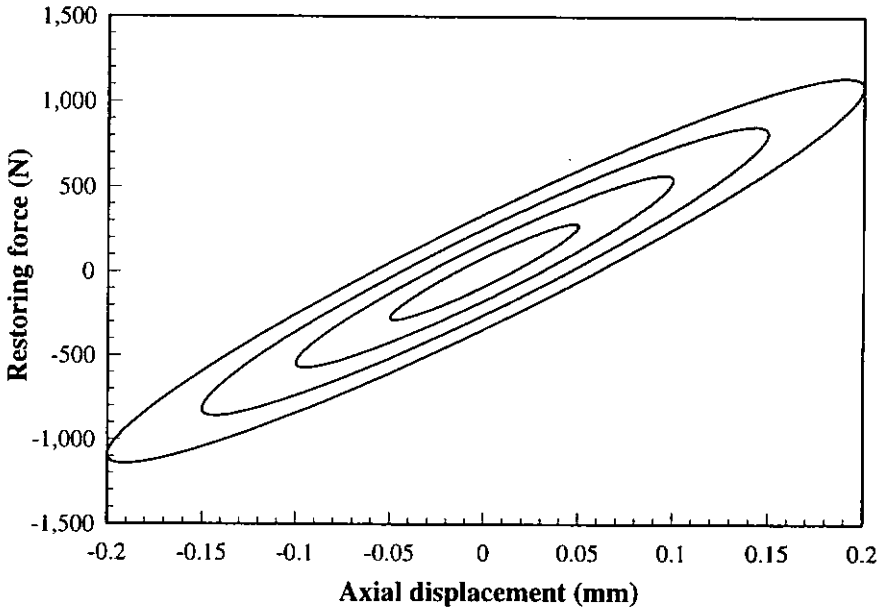

Figure 3.17 Hysteresis loops of damper HD91 under axial displacement of different amplitudes with fixed excitation frequency of 9Hz

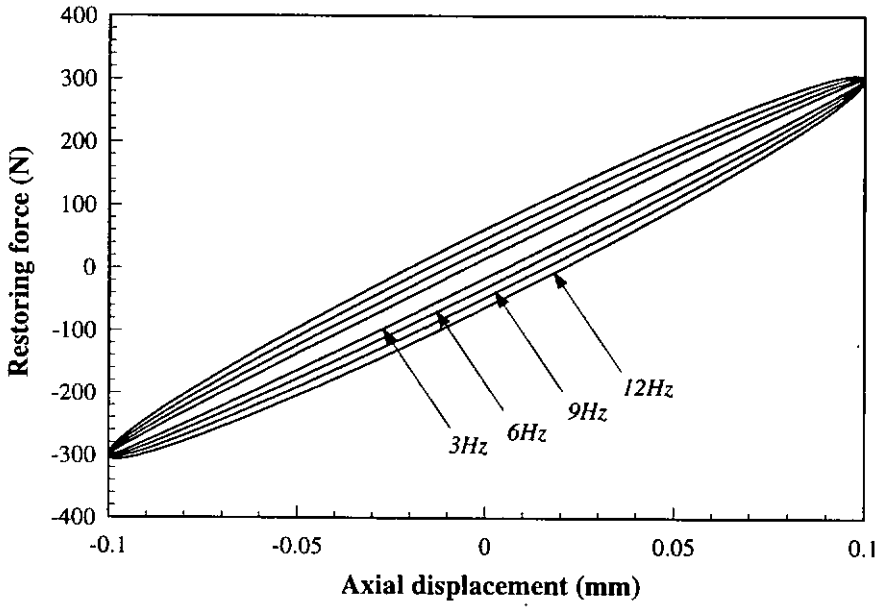

Figure 3.18 Hysteresis loops of damper ZJD-1 in axial direction at different excitation frequencies

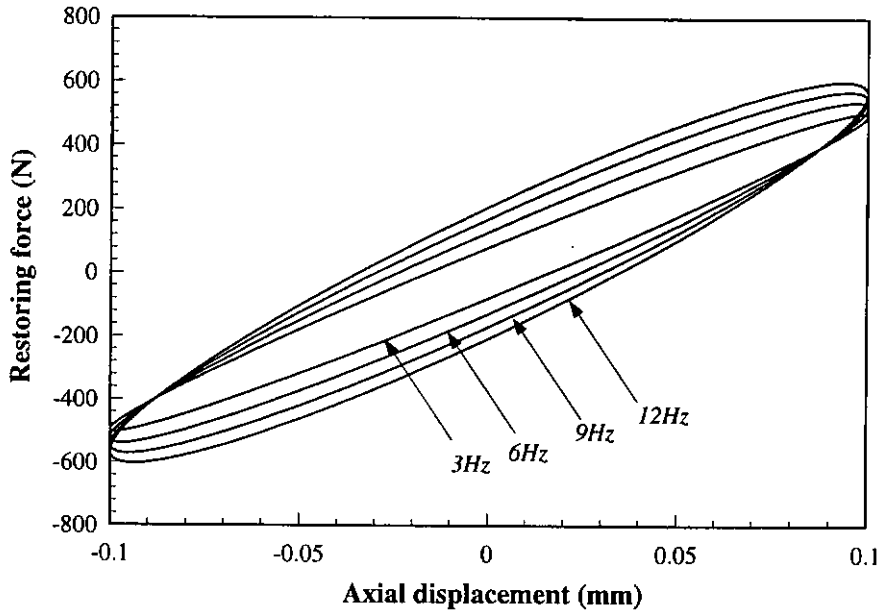

Figure 3.19 Hysteresis loops of damper HD91 in axial direction at different excitation frequencies

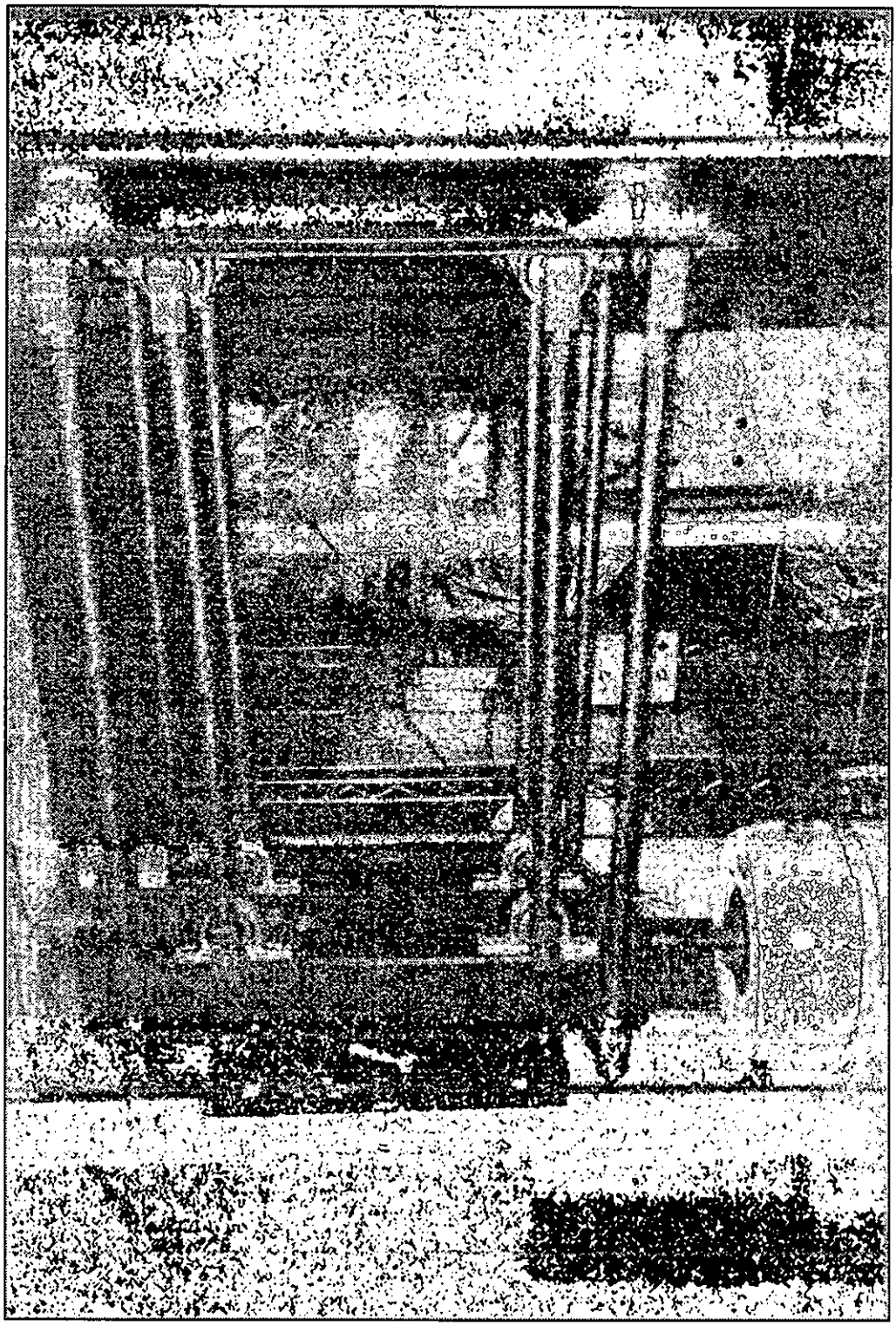

Photo 3.1 Setup of damper test

CHAPTER 4
MODELLING AND IDENTIFICATION

4.1 Introduction

In order to take the damper behaviour into account in vibration calculations such as to predict the response of a structure incorporated with viscoelastic dampers, the mathematical forms embodying the dynamic characteristics of the dampers have to be obtained. Commonly used mathematical models for viscoelastic dampers have been introduced and discussed in Chapter Two. From the experimental test of the two kinds of viscoelastic damper, it has been found that the dynamic properties such as storage modulus, loss modulus and damping ratio of viscoelastic dampers depend on the excitation frequency. Mathematical models like structural damping model with complex constants, or generalized derivative models which can be characteristiced by constant loss modulus and storage modulus are not accurate and versatile enough to describe the behaviour of various viscoelastic dampers. However, the fractional derivative model can predict the dynamic properties of dampers that vary with excitation frequency (Pritz T., 1996). Fractional derivative models can lead to well-posed equations of motion with causal solutions when used in modal analysis (Bagley R. L., 1983). Variety of materials employed in previous researches demonstrates that the fractional calculus model is a robust descriptor of the behavior of real materials (Bagley R. L. et al, 1986). In this thesis, by comparisons of commonly used mathematical models, the fractional derivative model has been selected and further developed to describe the dynamic behaviour of viscoelastic materials.

For frequency dependence of the damper, it is difficult to identify parameters of the model with accurate values by generally used least square method based on many groups of test data gathered in time domain. In the present study, to get the parameter value with sufficient accuracy, two kinds of identification methods for the fractional derivative model have been developed. By considering all the test data simultaneously, parameters of each damper have been obtained by the developed methods. Comparisons of the hysteresis loops of the improved model with those of the test results have been made to verify the reliability of the model as well as comparisons with the hysteresis loops of the widely used Kelvin-Voigt model to illustrate the advantage of the improved model. Moreover, characteristics of the model have been investigated in detail by numerical simulation.

4.2 Improved Fractional Derivative Model

4.2.1 Generalized Derivative Models

The characteristics of the hysteresis loops can be described by mathematical models which contain various factors affecting the relationship. Such models can be written in a very general form as

$$f\left[D_1(\sigma), D_2(\varepsilon), t, T, \cdots\right] = 0 \tag{4.1}$$

where, f represents a vector function of variables, σ is the stress tensor, ε is the strain tensor, t is the time, T is the temperature, D_1 and D_2 represent differential, integral, or combined operators, which are in general nonlinear (Nashif Ahid D., 1985). It is a general practice that experimental data of dynamic

tests on a specific damping material are used to build a mathematical model to describe the dynamic behaviour of dampers made of such material.

Frequency dependence of a viscoelastic damper can be realized by the material constitutive equations relating stress to strain. There are two types of constitutive equations as mentioned in Chapter Two both defining the stress-strain relationship in the time-domain. One is an integral equation based on the Boltzmann superposition principle; the other is a linear differential equation. The latter is most useful for finding frequency functions. The differential equation in its classical form contains time derivatives of integer order and can be written as

$$\sigma(t)+\sum_{i=1}^{n} b_i \frac{d^i\sigma(t)}{dt^i} = a_0\varepsilon(t)+\sum_{i=1}^{m} a_i \frac{d^i\varepsilon(t)}{dt^i} \tag{4.2}$$

where t is the time, a_0, a_i and b_i are parameters depending on the material.

The specific forms of the above equation are the mathematical basis of the widely used generalized standard models consisting of ideally elastic springs and viscous dashpots. If complex modulus models are used, the complex moduli for these models can easily be derived by taking the Fourier transform of both sides of the $\sigma-\varepsilon$ differential equation,

$$\sigma(\omega)+\sum_{i=1}^{n} b_i \frac{d^i\sigma(\omega)}{df^i} = a_0\varepsilon(\omega)+\sum_{i=1}^{m} a_i(j\omega)^i \frac{d^i\varepsilon(\omega)}{df^i} \tag{4.3}$$

The generalized standard models have been used for a long time (Harris Cyril M. and Crede Charles E., 1976; Lazan B. J., 1968), however, their qualitative behaviour is different from the real behaviour of viscoelastic dampers. This shortcoming of the generalized standard models can be immediately recognized from the hysteresis loops of HD91 damper under different excitation frequency.

The characteristic of frequency dependence could be similar, however, the experimental equivalent stiffness decreases with excitation frequency while the theoretical equivalent stiffness described by generalized standard models does not change. For viscoelastic materials, the complex modulus models have been developed and are widely used in structural dynamics, with an assumption that the loss modulus is constant for all frequencies. However, this assumption is found to be incorrect based on the experimental results and the complex modulus models are considered to be not accurate enough to represent various viscoelastic material.

4.2.2 Improved Fractional Derivative Model

4.2.2.1 Fractional Derivative Model

The qualitative behaviour of the generalized derivative model cannot be improved by increasing the number of terms. Therefore, it seems to be reasonable to assume that the source of inappropriateness of the generalized standard models is in the basic elements themselves. Moreover, it is reasonable to seek the source of inappropriateness in the viscous dashpot, instead of the elastic spring. When using the dashpot, it is implicitly assumed that the internal friction of the solid has a viscous nature like a fluid. Newton's viscosity law predicts that the stress in a fluid is proportional to the first time derivative of strain, that is

$$\sigma(t) \sim \frac{d\varepsilon(t)}{dt} \tag{4.4}$$

However, it is evident that pure viscous friction cannot describe the characteristics of a solid. For some solid materials, it is more realistic to assume that the stress due to the internal friction depends to a "lesser extent" on the time

variation of strain than in the case of a fluid. The "lesser extent" can be expressed mathematically by introducing a time derivative of order smaller than unity, called a fractional derivative, in the stress-strain relationship as

$$\sigma(t) \sim \frac{d^{\alpha}\varepsilon(t)}{dt^{\alpha}} \tag{4.5}$$

where, $0 < \alpha < 1$.

The αth order fractional derivative of a function $\varepsilon(t)$ is defined with the gamma function Γ as

$$\frac{d^{\alpha}}{dt^{\alpha}}\varepsilon(t) = \frac{1}{\Gamma(1-\alpha)}\frac{d}{dt}\int_0^t \frac{\varepsilon(t)}{(t-\tau)^{\alpha}}d\tau \tag{4.6}$$

where τ is an integral variable. Fortunately, the equation can be transformed easily to the frequency-domain,

$$\frac{d^{\alpha}}{dt^{\alpha}}\varepsilon(t) \rightarrow (j\omega)^{\alpha}\varepsilon(\omega) \tag{4.7}$$

The introduction of fractional derivatives into the differential type constitutive equations of materials results in the so-called fractional derivative models of materials. The general form of this model can be derived by replacing the integer order derivatives in equation (4.2) with fractional order ones,

$$\sigma(t) + \sum_{i=1}^{n} b_i D^{\beta_i}[\sigma(t)] = a_0\varepsilon(t) + \sum_{i=1}^{m} a_i D^{\alpha_i}[\varepsilon(t)] \quad (0 < \alpha_i < 1,\ 0 < \beta_i < 1) \tag{4.8}$$

where D denotes the operator of fractional differentiation, a_0, a_i, b_i, α_i and β_i are parameters dependent on the material.

It is clear from above equation that the introduction of fractional order time-derivatives results in power functions with powers smaller than unity in the

complex modulus frequency function. In this way, equivalent stiffness changing with frequency can be simulated, which is not possible with the generalized derivative models. Fractional derivative models of different behaviour can be developed, depending on the number of parameters which differ from zero in the above equation.

4.2.2.2 Improvement of the Fractional Derivative Model with parameter range

Parameter α of the normally used fractional derivative models is in the range of $0 < \alpha < 1.0$ for "lesser extent" solid materials. It is not suitable for pure spring and pure viscous materials. It has also been found from experimental work that the range is not suitable for "more extent" materials like ZJD-1. It is necessary to redefine the range. The gamma function is defined as (Writer Group of Mathematics Guide, 1979),

$$\frac{1}{\Gamma(z)} = \frac{1}{2\pi i}\int_{-\infty}^{0^+} e^t t^{-z} dt, \qquad (|\arg t| < \pi) \tag{4.9}$$

where, the integral trail starts from $t = -\infty$, after going around the original point in positive direction and it returns to the start point. The variable z can be any value.

It can be seen that the range is not constrained by the gamma function. The parameter α should be 0.0 for pure spring, 1.0 for pure viscous and larger than 1.0 for "more extent" materials. In order to make the original model more versatile, a new range of parameter α is defined as $\alpha \geq 0$. Therefore, the generalized derivative models can be improved as

$$\sigma(t) + \sum_{i=1}^{n} b_i D^{\beta_i}[\sigma(t)] = a_0 \varepsilon(t) + \sum_{i=1}^{m} a_i D^{\alpha_i}[\varepsilon(t)] \quad (\alpha_i \geq 0,\ \beta_i \geq 0) \tag{4.10}$$

Although the form is the same as equation (4.8), it covers more kinds of models than the original fractional derivative models and it still possesses all the advantages which equation (4.8) has. The nature of this equation is not different from the classical constitutive equations of viscoelasticity, since both the differential operator type equation with integer order derivatives and the Boltzmann-type integral equation (Shen K. L., 1995) are heuristic, the fractional derivative model with redefined parameter range is also heuristic. The improved fractional derivative model is capable of accurately describing quantitatively the dynamic behaviour of viscoelastic dampers. Furthermore, since only a few parameters are needed to describe the variations of dynamic properties in wide frequency ranges, the model is practical for vibration calculations. For viscoelastic dampers in applications, the frequency range is limited, a three-parameter model is sufficient to describe the dynamic behaviour of the dampers (Bagley R. L. et al, 1985). In the present study, the following simple form is chosen as the Improved Fractional Derivative Model (IFDM) to describe the relationship between the shear stress and the shear strain of a damper,

$$\tau = G_0\gamma(t) + G_1 D^{\alpha}[\gamma(t)] \quad (\alpha \geq 0) \tag{4.11.a}$$

And relationship between stress and strain in axial direction can be written as

$$\sigma = E_0\varepsilon(t) + E_1 D^{\alpha_a}[\varepsilon(t)] \quad (\alpha_a \geq 0) \tag{4.11.b}$$

When $\alpha = 0$ (or $\alpha_a = 0$), the model degrades to the pure linear model and when $\alpha = 1.0$ (or $\alpha_a = 1.0$), the model turns to be the Kelvin-Voigt model.

4.2.2.3 Development of the model with temperature consideration

For different kind of viscoelastic damper, the temperature effect is different. Tests should be performed at different temperatures to get the corresponding parameters G_0, G_1 and α. Thus, the temperature effect can be considered based on the curves of $G_0 \sim T$, $G_1 \sim T$ and $\alpha \sim T$.

The effect of temperature on some viscoelastic dampers is studied based on the test results carried out by other researchers (Kirekawa A. et al, 1992, Soong T. T. et al, 1997). It has been found that the storage modulus and loss modulus of the damper would decrease while temperature increases. From the figures presented by Soong T. T. et al (1997), the correlation between temperature and storage modulus and that between temperature and loss modulus of the dampers they have investigated are similar. And the correlation between modulus (storage modulus and loss modulus) and excitation frequency would not change with temperature, which means that temperature would not affect parameter α. If the IFDM is used to describe the dynamic behaviour of those viscoelastic dampers, the temperature effect could be considered with parameter G_0 and G_1 only.

From the above findings, the fractional derivative model for those dampers can be modified as follows,

$$\tau(t) = \psi_1(T) \cdot G_0 \gamma(t) + \psi_2(T) \cdot G_1 D^{\alpha} \gamma(t) \qquad (4.12)$$

where, $\psi_1(T)$ and $\psi_2(T)$ are functions of temperature T. Since parameters α, G_0 and G_1 are determined by test data obtained at a certain temperature T_0, $\psi_1(T)$ and $\psi_2(T)$ can be written as $\psi_1(T - T_0)$ and $\psi_2(T - T_0)$. If the correlation

with temperature for storage modulus and loss modulus are the same for a damper, one function can be used to represent the temperature effect and the final form of the IFDM with $\Delta T = T - T_0$ can be written as

$$\tau(t) = \psi(\Delta T)\left[G_0\gamma(t) + G_1 D^{\alpha}\gamma(t)\right] \tag{4.13}$$

Normally, the functions concerned with temperature effect should be expressed according to the test results and the related parameters should be identified by the test data. Based on the results obtained by some researchers (Soong T. T., 1997, Tsai C. S. et al, 1993), the temperature function of the materials they studied could be written in an exponential form as

$$\psi(\Delta T) = e^{-(\beta_1\Delta T+\beta_2\Delta T^2)} \tag{4.14}$$

4.3 Parameters Identification of the Improved Model

Restoring force $F(t)$ of a damper can be calculated from the shear displacement $X(t)$ based on the proposed model taking into consideration of the geometric dimensions of the damper. It can be written as

$$F(t) = \frac{A_r}{h}\psi(\Delta T)\left[G_0 X(t) + G_1 D^{\alpha} X(t)\right] \tag{4.15}$$

where A_r is the damper area, h is the damper thickness.

Since temperature does not change during tests on damper ZJD-1 and damper HD91, i.e., $\Delta T = 0$, the temperature function is omitted in this section as

$$F(t) = \frac{A_r}{h}\left[G_0 X(t) + G_1 D^{\alpha} X(t)\right] \tag{4.16}$$

From most of the past research work, it can be seen that the fractional derivative equations were solved in time domain with approximate methods (Tsai C. S., 1993, Makris Nicos et al, 1991, Koh Chan Ghee et al, 1990). It is difficult to calculate the fractional derivative part in time domain not only because the amount of calculation work is large, but also because the calculation is related to history of the damper deformation. In practice, a series of test data are obtained at arbitrary time, it is not suitable to use them without considering deformation history to identify the parameters of the model. And if the parameters are identified in time domain, different parameter values will be obtained from different data group, especially from data groups collected under different excitation frequencies. Although the average value of those parameter values identified from different data groups can be taken as the final result, the weightings for different data groups are hard to be determined. Therefore, the parameters obtained in this way are usually not accurate enough for analysis of structures incorporated with dampers.

However, as one of the advantages of the IFDM, the formulation form in frequency domain is very simple and it is not difficult to be solved. Moreover, different data groups can be applied simultaneously to identify the parameters. When the fractional derivative model is transformed to frequency domain by FFT, restoring force can be written as

$$F(\omega) = \frac{A_r}{h}\left[G_0 X(\omega) + G_1 (j\omega)^{\alpha} X(\omega)\right] \tag{4.17}$$

$F(\omega)$ and $X(\omega)$ can be obtained by FFT from each data group as $F(\omega_i)$ and $X(\omega_i)$, $i = 1, 2, \ldots, M$, where M is the number of data points applied for FFT.

Because signals have been filtered before data being collected, the super-harmonic factor of the experimental results is very small, it should be good enough to get one or two pairs of $[F(\omega), X(\omega)]$ for each data group.

4.3.1 Proposed system identification methods

4.3.1.1 Linear frequency-domain identification method for IFDM

An identification method, namely the linear frequency domain identification method (LFIM), is developed to identify values of the parameters of the IFDM, in which parameters G_0, G_1 and α can be obtained by finding the minimum difference of an Euclidean norm.

For all the test cases, assume that N pairs of $[F(\omega), X(\omega)]$ have been obtained for parameter identification. The restoring force of the i-th pair can be written as

$$F_i(\omega_i) = \frac{A_r}{h}\left[A_i G_0 + B_i G_1\right] \tag{4.18}$$

where,

$$A_i = X_i(\omega_i) = A_{iR} + jA_{iI} \tag{4.19}$$

$$B_i = X_i(\omega_i)(j\omega_i)^{\alpha} = B_{iR} + jB_{iI} \tag{4.20}$$

And the left term can be written as

$$F_i(\omega_i) = F_{iR} + jF_{iI} \tag{4.21}$$

Putting all test cases together, it can be written in a matrix form as

$$\mathbf{F} = \mathbf{CG} \tag{4.22}$$

where,

$$\mathbf{F} = \left(F_{1R}\ F_{1I} \cdots F_{iR}\ F_{iI} \cdots F_{NR}\ F_{NI}\right)^T \tag{4.23}$$

$$\mathbf{C} = \frac{A_r}{h}\begin{bmatrix} A_{1R}\ A_{1I} \cdots A_{iR}\ A_{iI} \cdots A_{NR}\ A_{NI} \\ B_{1R}\ B_{1I} \cdots B_{iR}\ B_{iI} \cdots B_{NR}\ B_{NI} \end{bmatrix}^T \tag{4.24}$$

$$\mathbf{G} = \left(g_1\ g_2\right)^T = \left(G_0\ G_1\right)^T \tag{4.25}$$

An approximate solution to this problem may be obtained by minimizing an Euclidean norm of the difference between the right and left sides of (4.22). The Euclidean norm of this difference is given by the following expression,

$$\left\|\varepsilon^2\right\| = (\mathbf{F} - \mathbf{CG})^T(\mathbf{F} - \mathbf{CG}) \tag{4.26}$$

The minimum of this norm can be calculated as a closed form solution, yielding the following expression,

$$\frac{\partial}{\partial g_i}\left\|\varepsilon^2\right\| = -2\mathbf{C}^T\mathbf{F} + 2\mathbf{C}^T\mathbf{CG} = 0 \quad (i = 1, 2) \tag{4.27}$$

The above equation can be solved for the coefficients $\mathbf{G}$ as

$$\mathbf{G} = \left(\mathbf{C}^T\mathbf{C}\right)^{-1}\mathbf{C}^T\mathbf{F} \tag{4.28}$$

Since matrix $\mathbf{C}$ changes with parameter α, for each α, a set of $\mathbf{G}$ can be obtained. Then the curves of $G_0 \sim \alpha$, $G_1 \sim \alpha$ and $\left\|\varepsilon^2\right\| \sim \alpha$ can be obtained. And the optimization point can be achieved at the point of $\left\|\varepsilon^2\right\|$ equal to the minimum value. Thus, corresponding to α, values of G_0 and G_1 can be determined from the curves.

4.3.1.2 Non-linear frequency-domain identification method for IFDM

The LFDM is a little bit complicated for operation. To check whether the parameter values identified by LFIM are reliable or not and make the identification procedure easier and more convenient, another identification method, namely the non-linear frequency-domain identification method (NFIM), is developed to identify values of the parameters of the IFDM. The parameters G_0, G_1 and α can be obtained by solving a nonlinear least squares problem using a modified Levenberg-Marquardt algorithm (IMSL, 1989, Ni Y. Q., 1997). The problem is stated as follows,

$$\min_{x \in IR^n} \frac{1}{2}\mathbf{F}(x)^T\mathbf{F}(x) = \frac{1}{2}\sum_{i=1}^{m} f_i(x)^2 \tag{4.29}$$

where, $m \geq n$, $\mathbf{F}: IR^n \rightarrow IR^m$, and $f_i(x)$ is the i-th component function of $\mathbf{F}(x)$.

From a current point, the algorithm uses the trust region approach,

$$\min_{x \in IR^n} \left\| \mathbf{F}(x_c) + \mathbf{J}(x_c)(x_n - x_c) \right\|_2 \tag{4.30}$$

subject to $\left\| x_n - x_c \right\|_2 \leq \delta_c$.

to get a new point x_n, which is computed as

$$x_n = x_c - \left[\mathbf{J}(x_c)^T\mathbf{J}(x_c) + \mu_c\mathbf{I}\right]^{-1}\mathbf{J}(x_c)^T\mathbf{F}(x_c) \tag{4.31}$$

where $\mu_c = 0$ if $\delta_c \geq \left\| \left[\mathbf{J}(x_c)^T\mathbf{J}(x_c) + \mu_c\mathbf{I}\right]^{-1}\mathbf{J}(x_c)^T\mathbf{F}(x_c)_2 \right\|$ and $\mu_c > 0$ otherwise.

$\mathbf{F}(x_c)$ and $\mathbf{J}(x_c)$ are the function values and the Jacobian evaluated at the current

point x_c, respectively. This procedure is repeated until the stopping criteria are satisfied.

For the IFDM, $\mathbf{x} = (G_0, G_1, \alpha)^T$, and the functions $f_i(x)$ are as follows,

for $i = 1,3 \cdots\cdots 2N-1$,

$$\begin{aligned} f_i(x) &= \mathrm{Re}\,al\big(F(\omega_i) - F_i(\omega_i)\big) \\ &= \mathrm{Re}\,al\left(\frac{A_r}{h}\Big[G_0 X_i(\omega_i) + G_1 (j\omega_i)^{\alpha} X_i(\omega_i)\Big] - F_i(\omega_i)\right) \end{aligned} \tag{4.32.a}$$

and for $i = 2,4 \cdots\cdots 2N$,

$$\begin{aligned} f_i(x) &= \mathrm{Im}\,ag\big(F(\omega_i) - F_i(\omega_i)\big) \\ &= \mathrm{Im}\,ag\left(\frac{A_r}{h}\Big[G_0 X_i(\omega_i) + G_1 (j\omega_i)^{\alpha} X_i(\omega_i)\Big] - F_i(\omega_i)\right) \end{aligned} \tag{4.32.b}$$

where, N is the number of pair of $[F(\omega_i), X(\omega_i)]$ applied for parameter identification.

The one-order derivations of parameters can be determined by the following equations,

$$\frac{\partial F(\omega)}{\partial G_0} = \frac{A_r}{h} X(\omega) \tag{4.33}$$

$$\frac{\partial F}{\partial G_1} = \frac{A_r}{h} (j\omega)^{\alpha} X(\omega) \tag{4.34}$$

$$\frac{\partial F(\omega)}{\partial \alpha} = \frac{A_r}{h} G_1 (j\omega)^{\alpha} \ln(j\omega) X(\omega) \tag{4.35}$$

And the Jacobian can be obtained from the following equations,

$$f_{Jac,G_0,i} = \mathrm{Re}\,al\left(\frac{A_r}{h} X_i(\omega_i)\right),\ i = 1,3 \cdots\cdots 2N-1 \tag{4.36.a}$$

$$f_{Jac,G_0,i} = \mathrm{Im}\,ag\left(\frac{A_r}{h} X_i(\omega_i)\right),\ i = 2,4 \cdots\cdots 2N \tag{4.36.b}$$

$$f_{Jac,G_1,i} = \mathrm{Re}\,al\left(\frac{A_r}{h}(j\omega_i)^{\alpha} X_i(\omega_i)\right),\ i = 1,3 \cdots\cdots 2N-1 \tag{4.37.a}$$

$$f_{Jac,G_1,i} = \mathrm{Im}\,ag\left(\frac{A_r}{h}(j\omega_i)^{\alpha} X_i(\omega_i)\right),\ i = 2,4 \cdots\cdots 2N \tag{4.37.b}$$

$$f_{Jac,\alpha,i} = \mathrm{Re}\,al\left(\frac{A_r}{h} G_1(j\omega_i)^{\alpha} \ln(j\omega_i) X_i(\omega_i)\right),\ i = 1,3 \cdots\cdots 2N-1 \tag{4.38.a}$$

$$f_{Jac,\alpha,i} = \mathrm{Im}\,ag\left(\frac{A_r}{h} G_1(j\omega_i)^{\alpha} \ln(j\omega_i) X_i(\omega_i)\right),\ i = 2,4 \cdots\cdots 2N \tag{4.38.b}$$

With the function $\mathbf{F(x)}$ and the Jacobian $\mathbf{J(x)}$ obtained by the above equations, the parameter values can be determined directly from $\mathbf{x}$ when the convergence criterion is satisfied.

4.3.2 Parameter identification for the dampers

4.3.2.1 Data preprocess before FFT to improve accuracy

Since test data recorded in computer is collected at arbitrary time, generally, the first point of a data group was not the one with maximum displacement or zero displacement. And difference exists between value of the first point and that of the last point of test data chosen for FFT. Leakage will occur during standard FFT if such test data is used directly. Locating the proper starting point and adjusting values of the test data properly for FFT is necessary.

Limited by the test condition or affected by test environment, the signal obtained from the instruments may contain data floating, for example, when shear displacement amplitude is set at 0.1mm for a damper, data recorded from test

may have the peak values of maximum 0.11mm and minimum -0.099mm. Error in FFT will also occur if such situation exists.

For test data from cyclic excitation, if the number of data points collected in one period is not 2^N, it is hard for FFT to work accurately. Even when the sampling velocity is set to 2^N per cycle while test is performed, error still exists due to system precision. When data points per cycle is not satisfied to the requirement, interpolating points for the whole test data before FFT are necessary.

According to the above considerations, all test data are pre-processed before being transformed by FFT. The procedures are as follows,

1. Find the positive maximum value of shear displacement in the first period and set it as the first point;

2. Find the positive peaks and negative peaks for the remainder test data, if the positive peak number is equal to the negative peak number, then calculate the average value of whole peaks and adjust all the test data. This step should be done for shear displacement and restoring force simultaneously;

3. Check the points between peaks, if it is not satisfying 2^N, then adjust all the points of each period, each point value can be determined by the values of neighbouring points by two-point interpolation or three-point interpolation.

After the test data being pre-processed, it will be transformed by FFT. From the results of FFT, large difference can be found between the test data before (case i) and after (case ii) being processed from some examples shown in Table 4.1. Values of $[F(\omega_i), X(\omega_i)]$ for several groups of test data under shear displacement of 0.1mm are compared here. All values in the table are obtained by

FFT with 4096 points (32 periods). It can be seen that the values are more regular after being pre-processed.

Table 4.1 FFT results of the test data before and after preprocess

Term	Excitation frequency		$F_R(\omega_i)$	$F_I(\omega_i)$	$X_R(\omega_i)$	$X_I(\omega_i)$
1	3Hz	i	37.327	103.891	-0.00304	0.09847
		ii	109.952	9.849	0.09818	0.00057
2	6Hz	i	40.006	104.212	0.00265	-0.10026
		ii	109.621	19.993	0.09861	0.00283
3	9Hz	i	47.919	103.848	-0.00598	0.09723
		ii	109.482	30.255	0.09863	-0.00108

4.3.2.2 Parameter values for the dampers and Comparison of identification methods

Parameters of the IFDM for the damper ZJD-1 and damper HD91 are identified here by both LFIM and NFIM. With preprocess of all the test data collected under different conditions, these data are transformed to frequency domain by FFT and then used to identify the parameters of IFDM for the damper simultaneously.

For damper ZJD-1 with LFIM, when parameter α changes from 0 to 2.0, the corresponding values of G_0, G_1 and $\|\varepsilon^2\|$ have been calculated for each damper and relations of $G_0, G_1 \sim \alpha$ and $\|\varepsilon^2\| \sim \alpha$ are shown in Figure 4.1 and Figure 4.2, respectively. Value of α corresponding to the lowest point of the curve in Figure 4.2 is determined to be 1.02 with the corresponding $\|\varepsilon^2\|$ equal to 2222.68. Thus G_0 and G_1 are determined from Figure 4.1 as $G_0 = 1.618$ and $G_1 = 0.0072$. For

damper HD91 with LFIM, relations of $G_0, G_1 \sim \alpha$ and $\|\varepsilon^2\| \sim \alpha$ are shown in Figure 4.3 and Figure 4.4, respectively. Parameter values are worked out in the same way as above-mentioned and are determined as $\alpha = 0.72404$, $G_0 = 0.79459$ and $G_1 = 0.0285$ while $\|\varepsilon^2\| = 3430.98$.

Parameter values for both dampers are also identified by NFIM. They are compared with those identified by LFIM as shown in Table 4.2 and Table 4.3 for damper ZJD-1 and HD91, respectively. It is obvious from these tables that the parameters identified by two methods are nearly the same. However, the parameter identification by NFIM only costs about several seconds while much more time is needed to find the parameter values by LFIM.

Table 4.2 Parameter values for ZJD-1 by the two identification methods

Method	G_0	G_1	α
LFIM	1.61689	0.00712	1.02135
NFIM	1.61674	0.00708	1.02117

Table 4.3 Parameter values for HD91 by the two identification methods

Method	G_0	G_1	α
LFIM	0.79459	0.02853	0.72404
NFIM	0.79451	0.02847	0.72388

Since the characteristics of the dampers in axial direction are similar to those in shear direction, the IFDM is also used for these dampers in axial direction. Parameters of the model for both dampers in axial direction have also been identified by NFIM and the values are found to be $\alpha = 1.011$, $E_0 = 5.577$, $E_1 = 0.01464$ for ZJD-1 and $\alpha = 0.684$, $E_0 = 3.225$, $E_1 = 0.087$ for HD91.

Parameters can also be identified in time domain with solution of the derivative parts obtained by approximate method. The calculation is very time consuming and because the solution is worked out approximately, error will be accumulated during the calculation. Even if only typical points of each case are used to identify the parameters, at least eight points should be chosen for each test case. If the chosen point is not suitable or only a few points are chosen for each data group, the identification will be inaccurate. Moreover, if data of all test cases are considered simultaneously, number of equations to be solved by the non-linear least square method will be very large.

4.4 Verification of the Improved Model with Test Results

After the parameter values being obtained, the IFDM can be verified by test data. For each case, displacement in time domain generated by $x = A\sin\omega t$ can be transformed to frequency domain by FFT, then the corresponding restoring force in frequency domain can be calculated by the model with the identified parameters. Then the restoring force in time domain can be obtained by inverse FFT. The procedure can be written as

$$X(t) \overset{\text{FFT}}{\rightarrow} X(\omega) \overset{\text{FDM}}{\rightarrow} F(\omega) \overset{\text{IFFT}}{\rightarrow} F(t) \tag{4.39}$$

Hysteresis loops of both damper ZJD-1 and damper HD91 at different shear displacement amplitude under different excitation frequency are obtained by the IFDM. No matter how many cycles are calculated, the loop of the model is in the same path, while the loops of test results shift with time. Figure 4.5 and Figure 4.6 are two examples of the comparison of hysteresis loops obtained from tests with the loops calculated by the model. The symbols on these two figures are data

points of 16 cycles. And the white curve in each figure is the loop of the model. The thickness of the model loop is enlarged to show the figures clearly. In order to make the comparisons convenient, one cycle loop of test results with adjustment of position and size as mentioned in Chapter Three is used for each case.

From examples shown in Figure 4.7 to Figure 4.11, it can be seen that the hysteresis loops calculated by the IFDM are in good agreement with the test results of damper ZJD-1 at different excitation frequency and the loops calculated by the model are also nearly the same as those of test results with different shear displacement amplitudes as shown in Figure 4.12. The same conclusions can be drawn for damper HD91 from Figure 4.13 to Figure 4.18. The maximum error of the hysteresis loop area between the loop of model and that of test results is less than 4% for all cases. From the above comparisons, conclusion can be drawn that the IFDM can well describe the dynamic behaviour of various viscoelastic dampers such as ZJD-1 and HD91.

4.5 Comparison of the Improved Model with Popularly Used Kelvin-Voigt Model

The advantages of the IFDM can be found by the comparisons of the loops with those calculated by other popularly used models such as Kelvin-Voigt Model. The relationship between restoring force and shear displacement of a damper with area A_r and thickness h can be expressed by Kelvin-Voigt model as

$$F = \frac{A_r}{h}\left[Gx(t) + \eta\dot{x}(t)\right] \tag{4.40}$$

where, G is the shear modulus and η is the viscosity coefficient.

When a damper is excited with a shear displacement of $x(t) = A\sin\omega t$, the restoring force can be written as

$$F(t) = \frac{A_r}{h}[GA\sin\omega t + \eta A\omega\cos\omega t] = B\sin(\omega t + \varphi) \tag{4.41}$$

in which,

$$B = \frac{A_r A}{h}\sqrt{G^2 + \eta^2\omega^2} \tag{4.42.a}$$

$$\varphi = \frac{\eta\omega}{G} \tag{4.42.b}$$

Damping ratio ζ can be calculated by the phase-lag method and can be written as

$$\zeta = \frac{1}{2}\tan\varphi = \frac{1}{2}\tan(\frac{\eta\omega}{G}) \tag{4.43}$$

According to equation (3.1),

$$\eta = \frac{G}{\omega}\arctan(2c\omega + 2f) \tag{4.44}$$

For different test cases, the parameter G can be obtained directly from the hysteresis loops and η can be calculated by (4.44). With these two parameters averaged for all cases, parameters G and η have been identified to be 1.6201 and 0.0072 for ZJD-1, 1.2238 and 0.0075 for HD91, respectively. Comparisons of the loops calculated by the Kelvin-Voigt model under shear displacement amplitude of 0.1mm at different excitation frequencies from 3Hz to 15Hz for damper ZJD-1 with those of test results are made as shown in Figure 4.19 to Figure 4.23. It can be seen that loops calculated by the model are in good

agreement with those of the test results. Comparisons of hysteresis loops calculated by the Kelvin-Voigt model under shear displacement amplitude of 0.1mm at different excitation frequencies from 3Hz to 15Hz for damper HD91 with those of the test results have also been made and shown in Figure 4.24 to Figure 4.28. It can be seen that under some conditions such as the damper being excited at excitation frequency of 15Hz, there is only little difference between hysteresis loops of model and those of test results. But under the other conditions, the discrepancy between them is quite large.

That is to say, although the Kelvin-Voigt model can be used for some kinds of viscoelastic damper like ZJD-1, it is not suitable for describing the behaviour of other kinds of damper like HD91. Therefore, Kelvin-Voigt model is not good enough to describe the behaviour of various viscoelastic dampers under dynamic loading.

From the above comparisons, it can be seen that the IFDM is more versatile than the Kelvin-Voigt model. Actually, as mentioned in section 4.2.3, the Kelvin-Voigt model is a special case of the IFDM with $\alpha = 1.0$, because parameter α of the IFDM is nearly equal to 1.0 for damper ZJD-1, the Kelvin-Voigt model can thus well describe the behaviour of damper ZJD-1 at any cases. However, α is only 0.724 for damper HD91, so it is hard for the Kelvin-Vogit Model to describe the behaviour of HD91 under various frequencies and shear displacements.

4.6 Characteristics of the Improved Model

From the above study, it can be seen that the IFDM can well describe the dynamic behaviour of different kinds of viscoelastic damper under different

excitation conditions. For a damper, what we care about most is its damping ratio, storage modulus and loss modulus. The first term $G_0\gamma(t)$ of the IFDM is a linear term synchronous with shear displacement and gives contribution to the storage modulus only. The second term $G_1 D^{\alpha}[\gamma(t)]$, which has a phase-lag with shear displacement, embodies the nonlinearity of the model. It contains two components, one is in linear with shear displacement and the other is in linear with shear velocity. In fact, the nonlinear term can be written in frequency domain to be $G_1(j\omega)^{\alpha}\gamma(\omega)$. The real part of the term contributes to storage modulus and the imaginary part contributes to loss modulus. Thus, the storage modulus is $G_0 + [G_1(\omega j)^{\alpha}]_{real}$ and the loss modulus is $[G_1(\omega j)^{\alpha}]_{imag}$. The phase-lag of the restoring stress to the shear strain can be obtained by

$$\varphi = \arctan\frac{[G_1(\omega j)^{\alpha}]_{imag}}{G_0 + [G_1(\omega j)^{\alpha}]_{real}} = \arctan\frac{G_1\omega^{\alpha}\sin\frac{\pi\alpha}{2}}{G_0 + G_1\omega^{\alpha}\cos\frac{\pi\alpha}{2}} \tag{4.45}$$

Damping ratio of a damper is half of the tangent of the phase lag. It is concerned with α, G_0, G_1 and excitation frequency. It does not have relation with displacement amplitude. Therefore, damping ratio of a damper under different shear displacement but at the same excitation frequency will be the same. Large amount of energy dissipated per cycle by a damper does not mean that the damper has high damping value. The energy can be calculated from the area of hysteresis loop as

$$E_d = \pi A_{disp}\left[\frac{A_r}{h}A_{disp}G_1(\omega j)^{\alpha}\right]_{imag} = \frac{\pi A_r A_{disp}^2 G_1\omega^{\alpha}}{h}\sin\frac{\pi\alpha}{2} \tag{4.46}$$

where E_d is the energy dissipated by the damper for each cycle; A_{disp} is the shear displacement amplitude. The energy is in quadric relation with A_{disp} which conforms to the test results. It is in linear with parameter G_1. The storage modulus does not give any contribution to energy dissipation at all.

It can also be known from the model that when $\alpha = 0$, the model degrades to a pure linear model, $E_d = 0$ and when $\alpha = 1.0$, the model degrades to the Kelvin-Voigt model and the energy dissipated per cycle is in linear with excitation frequency,

$$E_d = \frac{\pi A_r A_{disp}^2 G_1 \omega}{h}. \tag{4.47}$$

Thus, when the energy curve changing with excitation frequency is obtained, value of parameter α can be estimated approximately. For example, when tests on the two kinds of damper are finished, it can be determined that α for damper ZJD-1 is close to 1.0 and that for HD91 is less than 1.0 as indicated from Figure 3.13 and Figure 3.14.

The hysteresis loop of the model can be considered as the superposition of two parts, one part is an inclined line which is contributed by the storage modulus expressed as $G_0 + G_1\omega^\alpha \cos\frac{\alpha\pi}{2}$ and the other part is an ellipse with major and minor axis in the direction of X-axis and Y-axis, which is the effect of the loss modulus $G_1\omega^\alpha \sin\frac{\alpha\pi}{2}$. It can be illustrated by Figure 4.29.

To know more about the model, characteristics of model have been studied based on numerical simulation in the following sections.

4.6.1 Effect of parameter α

Parameter α plays an important role in the IFDM. Characteristics such as damping ratio, loss modulus and storage modulus are all concerned with parameter α. With different value of α, the fractional derivative model can degrades to different kind of model like linear model and generalized derivative models. Special frequency dependence of some viscoelastic dampers, like storage modulus changes with excitation frequency, which can not be embodied by commonly used models, can be represented by the IFDM.

To study the nonlinear term clearly, parameter G_0 is set to zero, a damper with area of 10800mm^2 and height of 20mm is assumed to be excited under shear displacement of $x(t) = 0.1\cos(\omega t)$. The period of the shear displacement is $T = 1/2\pi$, while parameter $G_1 = 0.007$. The hysteresis loops with different α are shown in Figure 4.30.

It is clear that when $\alpha = 0.0$, the loop is an inclined line with area equal to zero, the nonlinear term degrades to $G_1\gamma(t)$ like a spring, it is a pure storage term, phase-lag of the restoring force to shear displacement is zero and the storage modulus is G_1. When $\alpha = 1.0$, the loop is an ellipse, the major and the minor axis of which are along with X and Y axis, the nonlinear term becomes $G_1\dot{\gamma}(t)$, it is a pure loss term, phase-lag of the restoring force to the shear displacement is $\pi/2$ and the loss modulus is G_1. When $\alpha = 2.0$, the nonlinear term is expressed as $G_1\ddot{\gamma}(t)$, the hysteresis loop is also a slanting line with loop area equal to zero, the phase-lag is π and the storage modulus is $-G_1$. When α changes from 0 to 1.0, the storage modulus changes from G_1 to zero, damping changes from zero to

pure viscous damping and phase-lag is between zero and $\pi/2$, and when α changes from 1.0 to 2.0, the storage modulus changes from zero to $-G_1$, damping changes from pure viscous damping to zero and phase lag is between $\pi/2$ and π.

The variation of storage and loss modulus along with α can be seen from Figure 4.31. It is obvious that under the current parameter assumption, when $\alpha = 1.0$, loss modulus reaches its largest value.

The above study is based on $\omega = 1.0$, when ω is of other values, the characteristics will change. The behaviour of the nonlinear term under $\omega = 1.5$ has been investigated and the hysteresis loops are shown in Figure 4.32. It can be seen that the storage modulus is related to the excitation frequency. When the frequency is getting large, the influence to the storage modulus will be greater. The variation of storage modulus and loss modulus along with α can be seen in Figure 4.33.

For real materials, normally the linear term is not zero and it gives the main contribution to the storage modulus in a low frequency range. In another word, parameter G_0 is much larger than the real part of $G_1(\omega j)^{\alpha}$. The hysteresis loops of the model with different α at $G_0 = 0.01$ and $G_0 = 0.02$ are also calculated and shown in Figure 4.34 and Figure 4.35, respectively, where $\omega = 1.5$. It can be seen that when G_0 increases, the shape of hysteresis loops become thinner, while loss modulus still reaches its largest value when $\alpha = 1.0$.

The energy dissipated per cycle is also related to α. The curves of energy dissipated per cycle by the damper represented by the model with different parameter α under excitation frequency of 0.5, 1.0, and 1.5 are shown in Figure 4.36. It can be seen when the excitation frequency is less than 1.0, the maximum

energy dissipation occurs with α less than 1.0, and when the frequency is larger than 1.0, the maximum energy dissipation occurs with α larger than 1.0.

4.6.2 Effect of parameter G_1

Since the real part of the model determines the equivalent stiffness of a damper represented by the model and the imaginary part determines its hysteresis loop area, when parameter G_1 increases, both the imaginary part and the real part increase and therefore both the storage modulus and the energy dissipation ability increase. It can be seen clearly from the hysteresis loops in Figure 4.37 and Figure 4.38, where, $\omega = 1.5$ and $\alpha = 0.8$.

When $G_0 = 0$, the restoring force at time t can be written as $F(t) = A_{nonlinear}\cos(\omega t + \theta_{nonlinear})$, where $A_{nonlinear} = G_1\omega^{\alpha}$ and $\theta_{nonlinear} = \pi\alpha/2$, when G_1 changes, $\theta_{nonlinear}$ will not change and when $\cos(\omega t_i + \theta_{nonlinear}) = 0$, the restoring force is zero, so all hysteresis loops with different parameter G_1 pass through the same point at time t_i. When parameter G_0 is not equal to zero, $F(t) = G_0\cos(\omega t) + A_{nonlinear}\cos(\omega t + \theta_{nonlinear})$. Since the first term of right side does not change with G_1, when $\cos(\omega t_i + \theta_{nonlinear}) = 0$, $F(t) = G_0\cos(\omega t_i)$ is of the same value, thus all hysteresis loops also pass through the same point at time t_i. This property can explain the phenomena in Figure 3.7 that the restoring force at a certain displacement is the same for different excitation frequency.

4.6.3 Effect of parameter G_0

Parameter G_0 is the main part of the storage stiffness, when it becomes larger, the equivalent stiffness of the damper will increase also. Since it does not have relation with the imaginary part, area of the loop will not change with G_0. The hysteresis loops of the model with different value of G_0 are drawn in Figure 4.39, where $\omega = 1.5$ and $\alpha = 0.8$. However, when G_0 increases, the storage modulus of the model will increase while the loss modulus keeps unchanged, the hysteresis loop shape will become thinner and the tangent of phase-lag will decrease. It is obvious from Figure 4.40 that when G_0 is small, the phase lag changes greatly with G_0, however when G_0 is large enough, the phase lag changes slightly with G_0. It is because when G_0 is small, the phase-lag is mainly determined by the ratio of the imaginary part to the real part of the nonlinear term however when G_0 is large, the phase lag is mainly determined by the ratio of the imaginary part of the nonlinear term to G_0.

4.6.4 Model behaviour for different excitation frequency

For the model with constant parameters, the amplitude of the nonlinear term $G_1(\omega j)^\alpha$ increases with the excitation frequency. When G_0 value is much larger than the real part of $G_1(\omega j)^\alpha$, tangent of the phase-lag will increase which means the damping ratio increases. In fact, the characteristics of the model subject to different excitation frequency are similar to those of the model with different values of G_1 when the excitation frequency remains unchanged. The hysteresis loops of the model with the excitation frequency changing from 0.1Hz to 0.5Hz

while other parameters are kept constants are shown in Figure 4.41. From Figure 4.42, it can be seen that the phase-lag increases with the excitation frequency. When the excitation is large enough, no matter what value G_0 is, the phase-lag will be $\pi\alpha/2$.

For the model with constant parameters, the energy dissipation ability increases with the excitation frequency. The energy dissipated per cycle under different excitation frequencies is illustrated with an example as indicated in Figure 4.43 in which $\alpha = 0.6$, 0.8, 1.0 and 1.2, $G_1 = 0.007$ and frequency changes from 0 to 0.5Hz.

4.6.5 Model behaviour for different shear displacement

For different shear displacement amplitudes, the shape of hysteresis loop of the model keeps unchanged, which means the damping ratio will not change. The restoring force however is in linear relation with the displacement amplitude. Therefore when the amplitude changes, the hysteresis loop will amplify correspondingly and the area of the hysteresis loop will change in quadric relation with the amplitude. It can be seen obviously from Figure 4.44, in which the shear displacement changes from 0.10 to 0.30 while other parameters are kept the same.

4.6.6 Model behaviour for different temperature

An example for temperature effect on the IFDM is illustrated as follows. It is assumed that the IFDM can be used for a damper which has the characteristics given in figures (5.8, 5.9 and 5.10) of the book written by Soong T. T. et al

(1997). Parameters of the model have been identified by the developed methods based on the data groups calculated from the modulus supplied by the figures. The model can be written as

$$\tau(t) = e^{-(0.056T-1.218)}\left[0.0717\gamma(t) + 0.1186D^{0.575}\gamma(t)\right] \qquad (4.48)$$

Storage modulus and loss modulus of the damper have been calculated with the model and compared with the data provided in T. T. Soong's book as shown in Figure 4.45 and Figure 4.46. It can be seen that the model can well describe the storage modulus and loss modulus varying with excitation frequency and temperature.

Let damper area $A_r = 18\,in^2$ and damper thickness $h = 0.2\,in$. The hysteresis loops of the damper under excitation frequency of 3Hz and shear displacement of $x(t) = 0.1\sin\omega t\ (in)$ at different temperature have been calculated and drawn in the Figure 4.47. It can be seen that both the equivalent stiffness and the loop area decrease greatly when the temperature increases. From test results of some dampers by some other researchers, it can be seen that damping ratio does not change too much with temperature. Damping ratios of the damper at different temperatures under excitation frequency of 3Hz have been calculated and all of them are equal to 0.74. Since the loss stiffness of the damper will decrease when the temperature increases, the energy dissipated per cycle by the damper will reduce greatly also which can be seen from the Figure 4.48.

4.7 Discussions and Conclusions

In this chapter, the Fractional Derivative Model has been chosen and developed to simulate the dynamic behaviour of viscoelastic dampers. With redefined range

of parameter α and temperature consideration, the IFDM can be used much more widely for different materials or mediums and under various conditions other than the commonly used model.

To make use of all the test data simultaneously and more conveniently for the identification of parameters of the sophisticated model, two kinds of system identification methods, namely LFIM and NFIM, have been developed in frequency domain for the IFDM. In order to eliminate the experimental errors during data collection, data pre-processed method has been proposed and all the experimental data has been pre-processed before identification. The parameters of the model for the two kinds of damper used in the present studies have both been identified.

Hysteresis loops calculated by the IFDM under different conditions have been compared with those obtained from experiments. It has been found that the IFDM can well describe the dynamic behaviour of both damper ZJD-1 and damper HD91 at different excitation frequencies and subject to different shear displacements. Hysteresis loops calculated by the Kelvin-Voigt model with identified parameters for various cases have also been compared with those of test results. Although this model can well simulate the dynamic behaviour of ZJD-1 damper, it is not able to describe the behaviour of HD91. Conclusion can be drawn based on the comparison that the IFDM is a more versatile model for viscoelastic dampers than the other commonly used models which have been established in the past.

Characteristics of the model have been studied in detail. Storage modulus, loss modulus, phase-lag of stress to strain and energy dissipation ability of the IFDM

have been discussed based on numerical simulation. It can be seen that the parameter α plays the most important role in the IFDM and the model can simulate the real behaviour of viscoelastic dampers under different excitation and temperature conditions.

4.8 References

Bagley R. L. and Torvik P. J. (1986), On the Fractional Calculus Model of Viscoelastic Behavior, Journal of Rheology, Vol. 30, No. 1, pp133-155.

Bagley R. L. and Torvik P. J. (1985), Fractional Calculus in the Transient Analysis of Viscoelastically Damped Structures, AIAA Journal, Vol.23, No. 3, pp. 201-210.

Bagley Ronald L. and Torvik Peter J. (1983), Fractional Calculus-A Different Approach to the Analysis of Viscoelastically Damped Structures, AIAA Journal, Vol.21, No.5, pp741-748.

Harris Cyril M. and Crede Charles E. (1976), Shock and Vibration Handbook, the Second Edition, New York : McGraw-Hill.

IMSL (1989), IMSL (Problem-Solving Software Systems) MATH/LIBRARY user's Manual, version 1.1.

Kirekawa A., Ito Y. and Asano K. (1992), A study of structural control using viscoelastic material, Earthquake Engineering, Tenth World Conference, pp2047~2054.

Koh Chan Ghee and Kelly James M. (1990), Application of Fractional Derivatives to Seismic Analysis of Base-Isolated Models, Earthquake Engineering and Structural Dynamics, Vol.19, pp229-241.

Lazan B. J. (1968), Damping of Materials and Members in Structural Mechanics. Pergamon Press.

Makris Nicos and Constantinou M. C. (1991), Fractional-Derivative Maxwell Model for Viscous Dampers, Journal of Structural Engineering, Vol. 117, No. 9, pp2708-2724.

Nashif Ahid D., Jones David I. G. and Henderson John P. (1985), Vibration Damping, A Wiley-Interscience Publication, John Wiley @ Sons.

Ni Y. Q. (1997), Dynamic Response and System Identification of Nonlinear Hysteretic System, Ph.D. Thesis Dissertation of the Hong Kong Polytechnic University.

Pritz T. (1996), Analysis of Four-parameter Fractional Derivative Model of Real Solid Materials, Journal of Sound and Vibration, Vol.195, No.1, pp103-115.

Shen K. L. and Soong T. T. (1995), Modeling of Viscoelastic Dampers for Structural Applications, Journal of Engineering Mechanics, Vol.121, No. 6, pp694-701.

Soong T. T. and Dargush G. F. (1997), Passive Energy Dissipation Systems in Structural Engineering, John Wiley & Sons.

Tsai C. S. and Lee H. H. (1993), Applications of Viscoelastic Dampers to High-rise Buildings, Journal of Structural Engineering, Vol. 119, No. 4, pp1222-1233.

Tsai C. S. (1993), Innovative Design of Viscoelastic Dampers for Seismic Mitigation, Nuclear Engineering and Design, Vol. 139, pp165-182.

Writer Group of Mathematics Guide (1979), High Education Press, Beijing. (In Chinese)

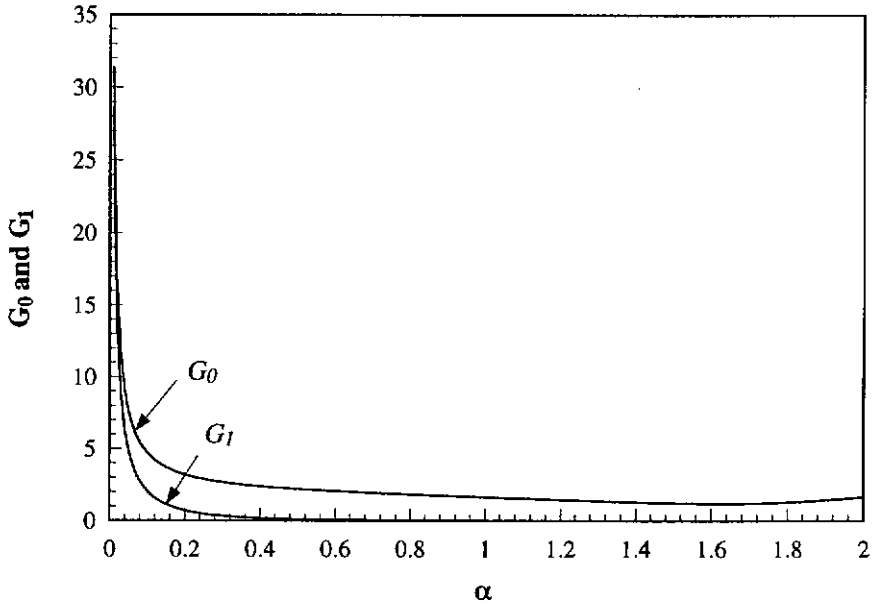

Figure 4.1 $G_0, G_1 \sim \alpha$ **of damper ZJD-1**

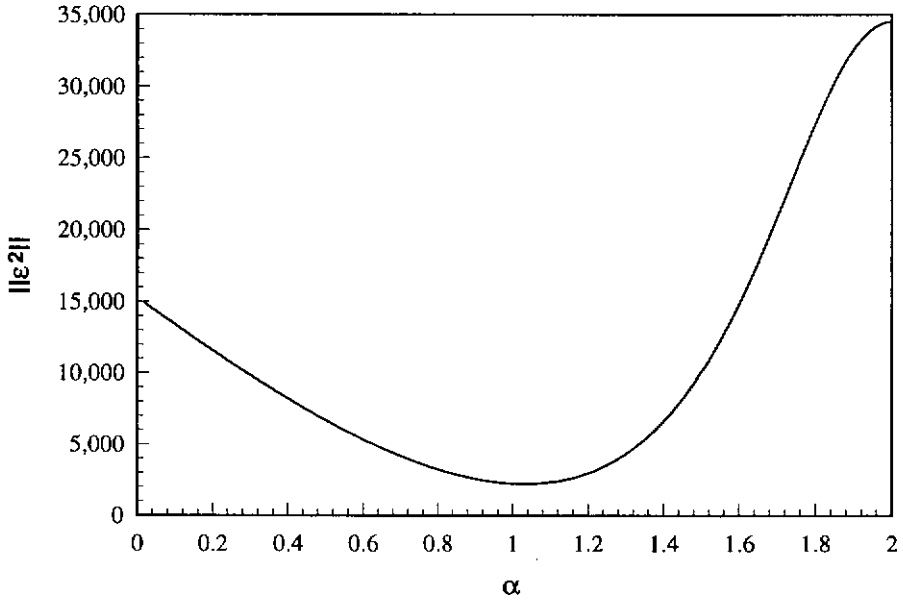

Figure 4.2 $\|\varepsilon^2\| \sim \alpha$ **of damper ZJD-1**

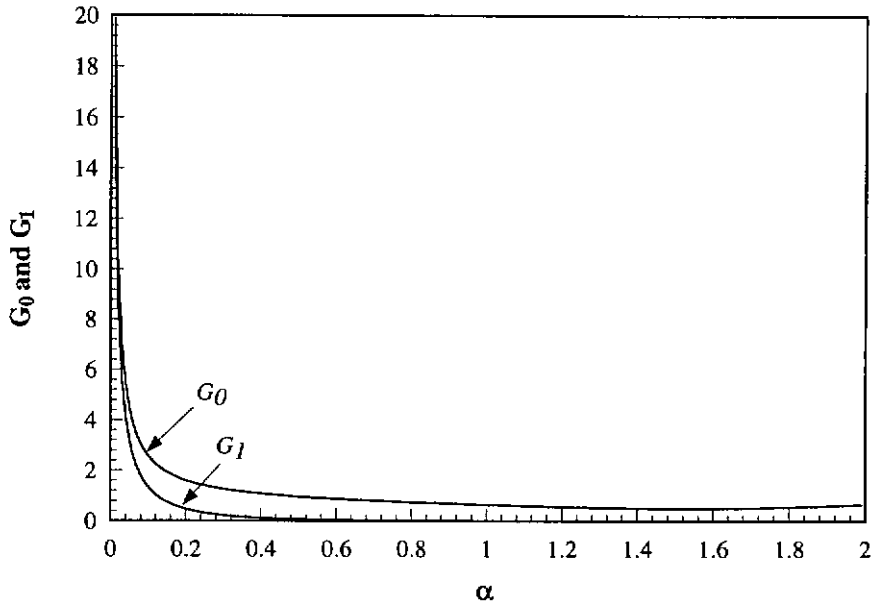

Figure 4.3 $G_0, G_1 \sim \alpha$ **of damper HD91**

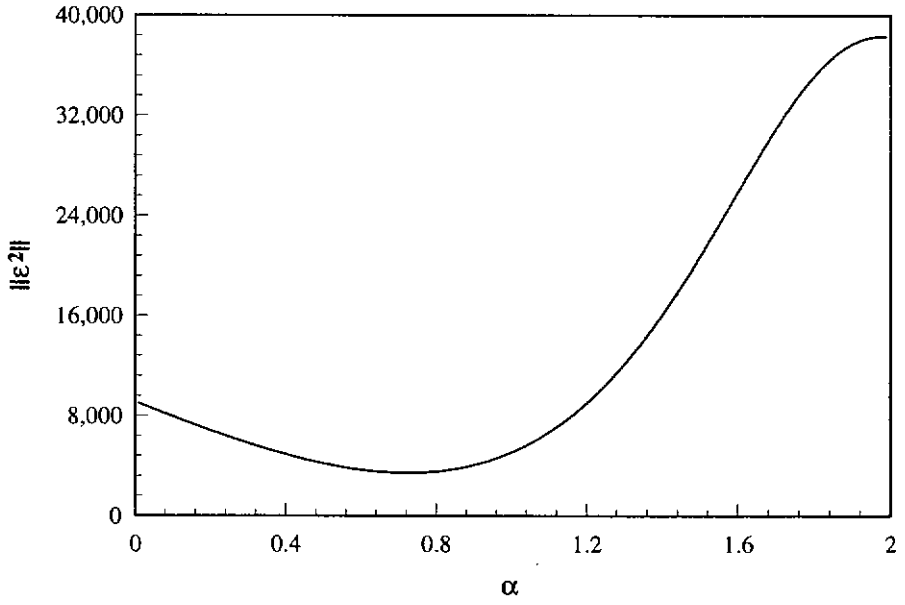

Figure 4.4 $\|\varepsilon^2\| \sim \alpha$ **of damper HD91**

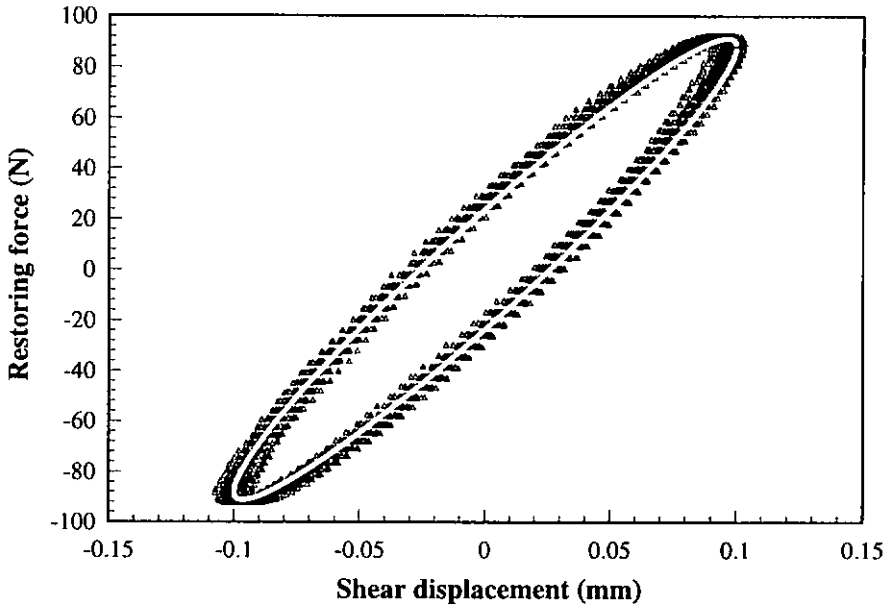

Figure 4.5 Comparison between the IFDM and the test results for damper ZJD-1 (9Hz)

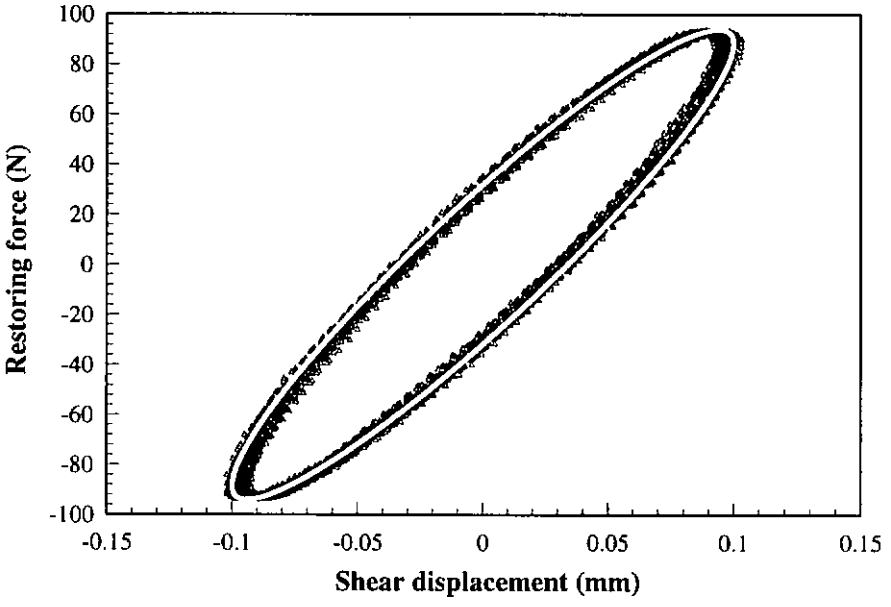

Figure 4.6 Comparison between the IFDM and the test results for damper ZJD-1 (12Hz)

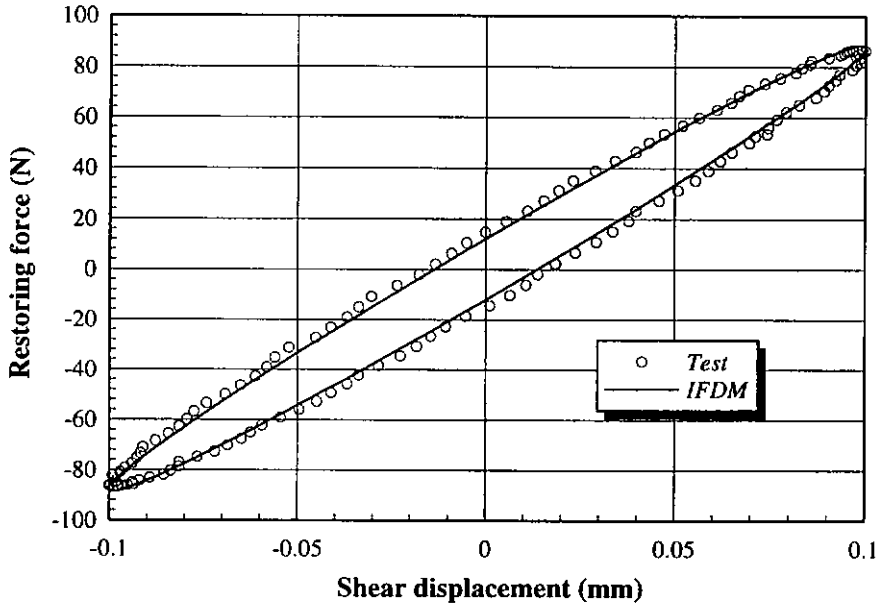

Figure 4.7 Comparison between the IFDM and the test results for damper ZJD-1 (3Hz)

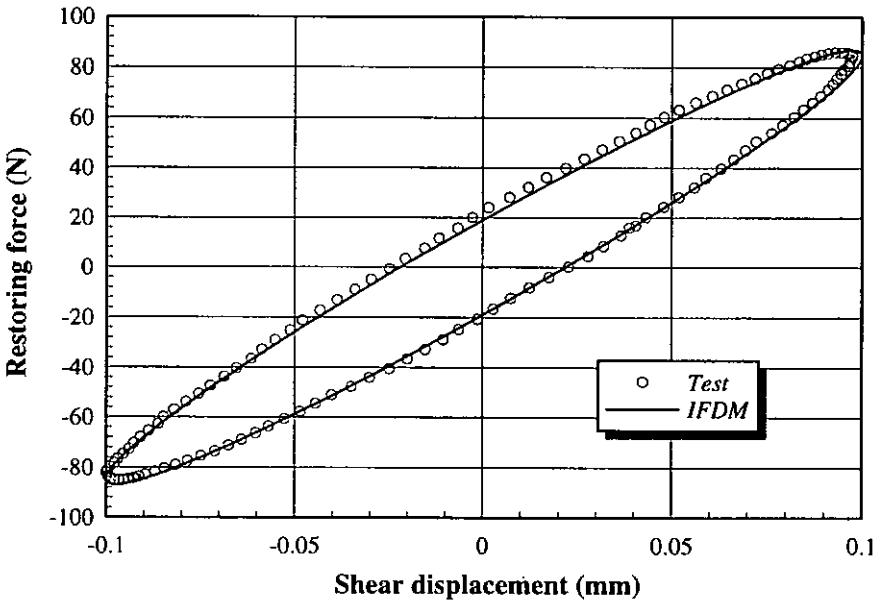

Figure 4.8 Comparison between the IFDM and the test results for damper ZJD-1 (6Hz)

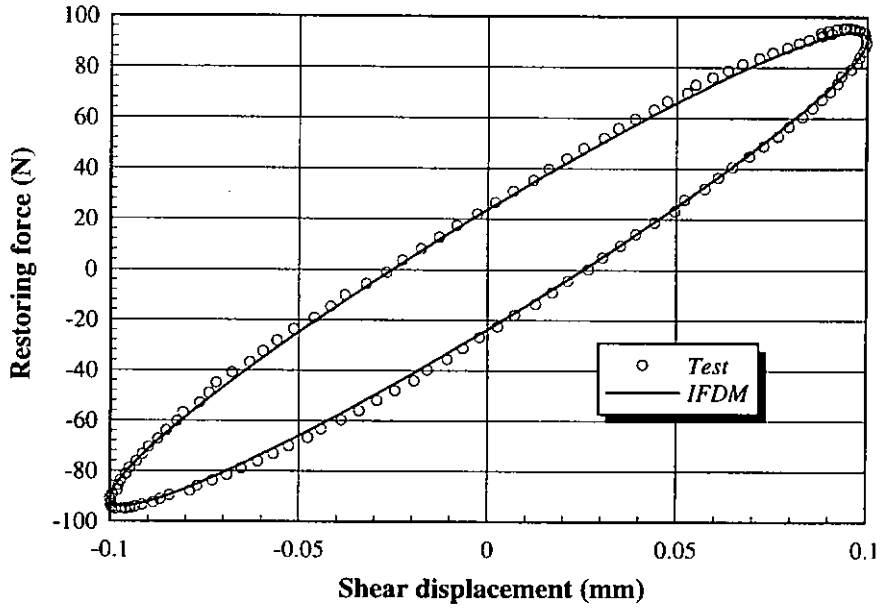

Figure 4.9 Comparison between the IFDM and the test results for damper ZJD-1 (9Hz)

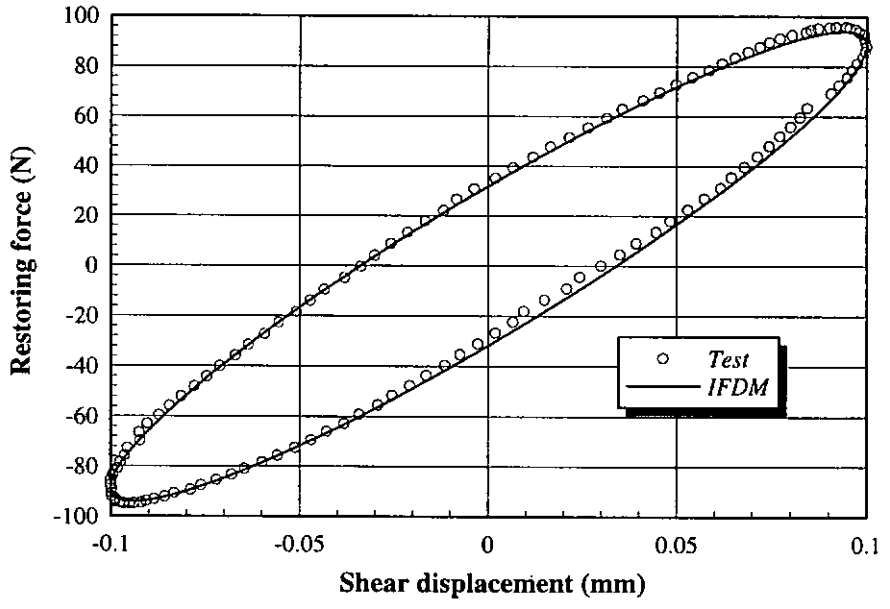

Figure 4.10 Comparison between the IFDM and the test results for damper ZJD-1 (12Hz)

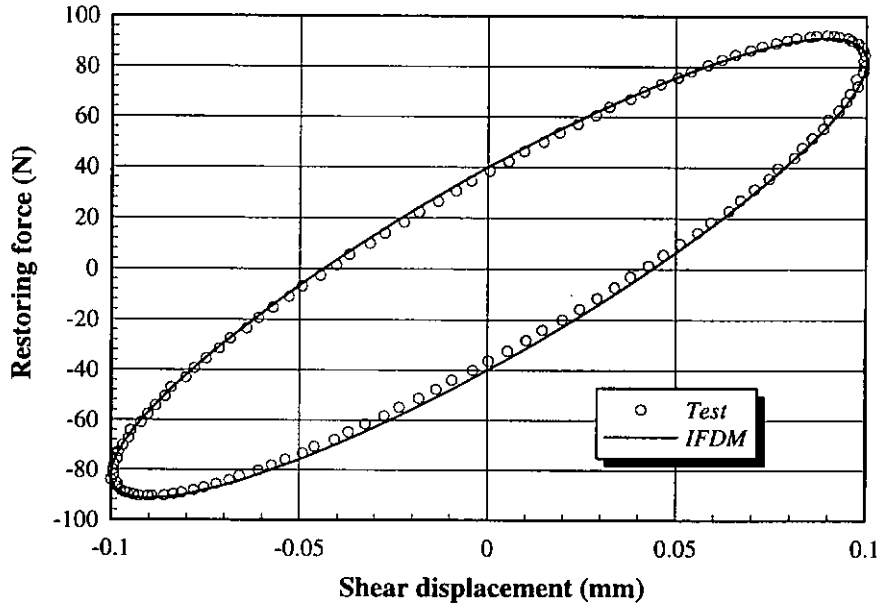

Figure 4.11 Comparison between the IFDM and the test results for damper ZJD-1 (15Hz)

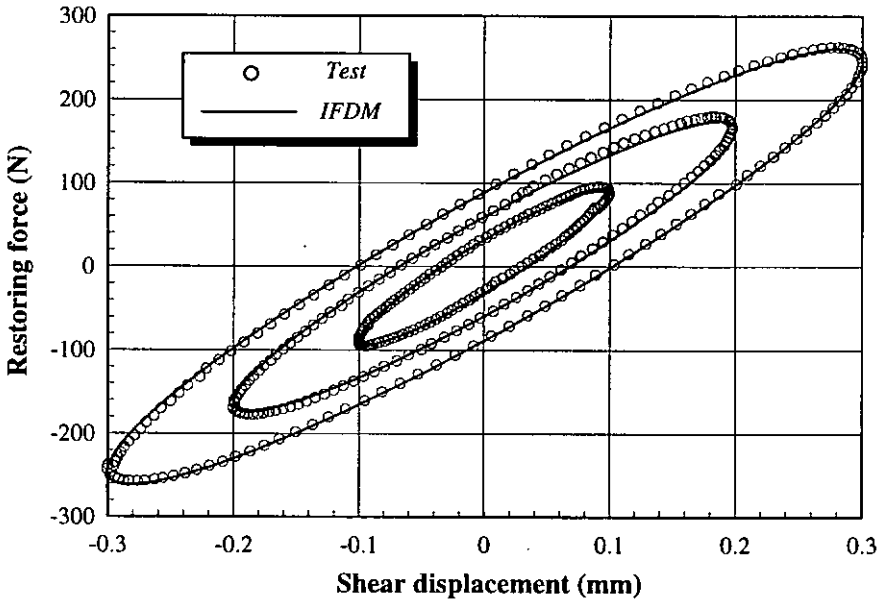

Figure 4.12 Comparison between the IFDM and the test results for damper ZJD-1 (12Hz)

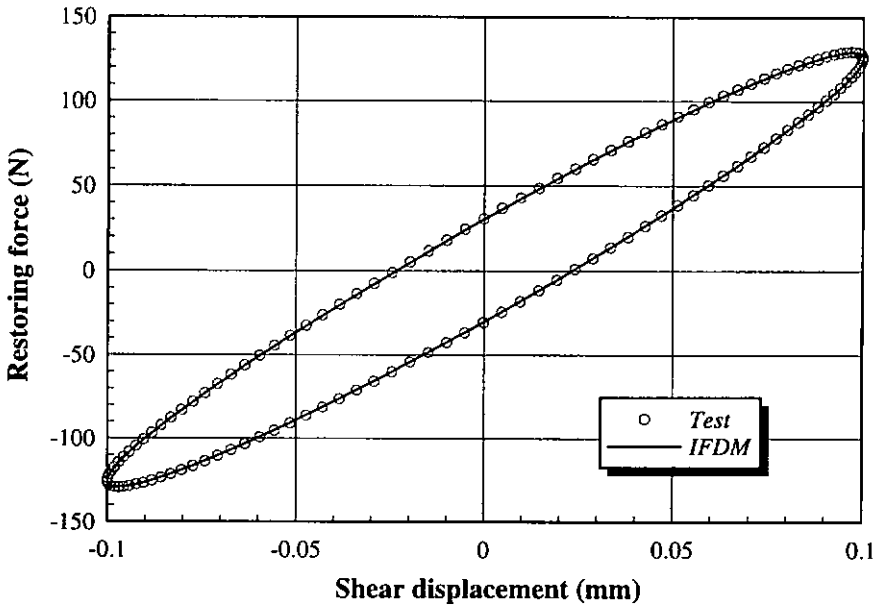

Figure 4.13 Comparison between the IFDM and the test results for damper HD91 (3Hz)

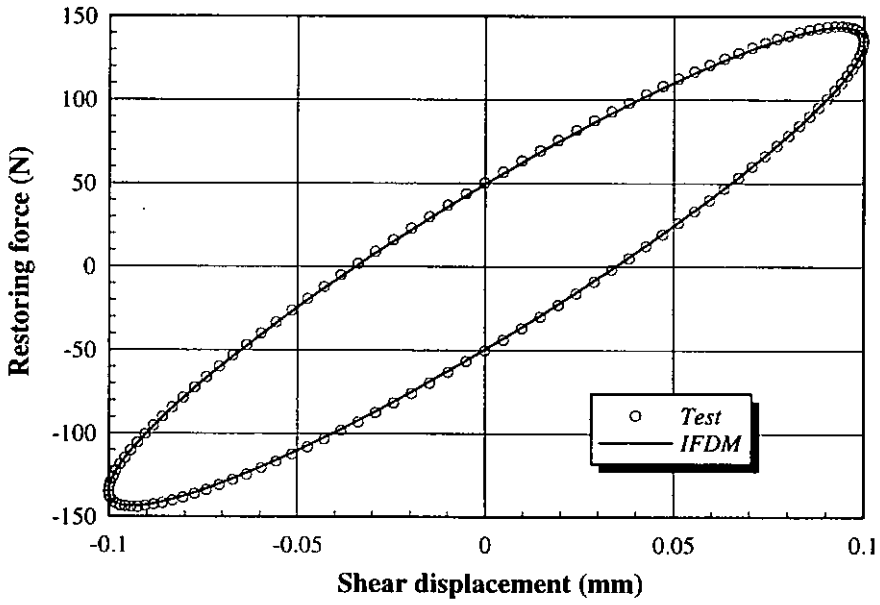

Figure 4.14 Comparison between the IFDM and the test results for damper HD91 (6Hz)

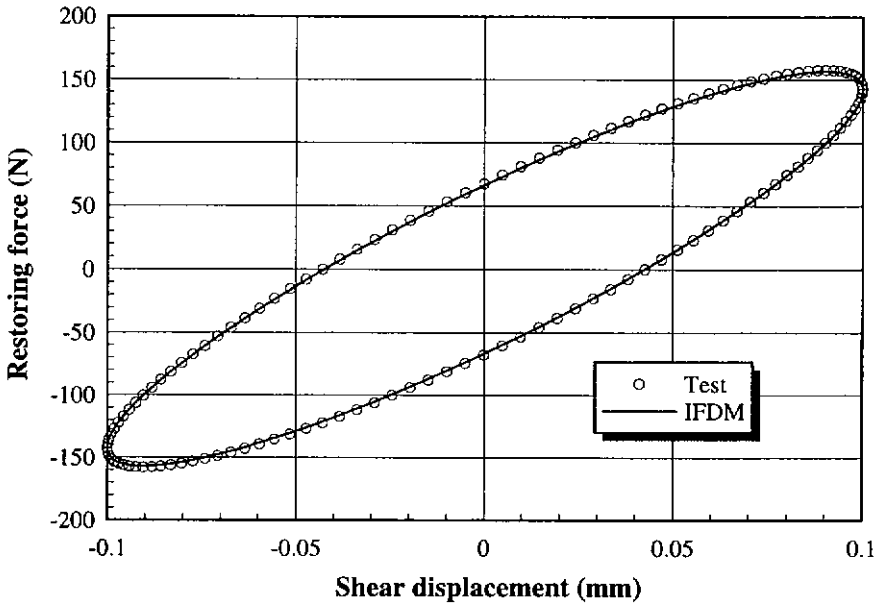

Figure 4.15 Comparison between the IFDM and the test results for damper HD91 (9Hz)

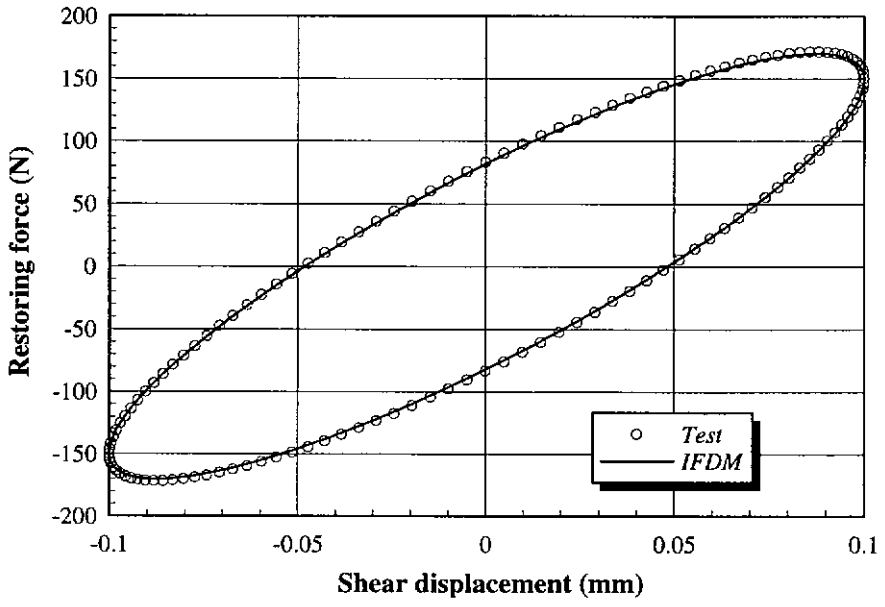

Figure 4.16 Comparison between the IFDM and the test results for damper HD91 (12Hz)

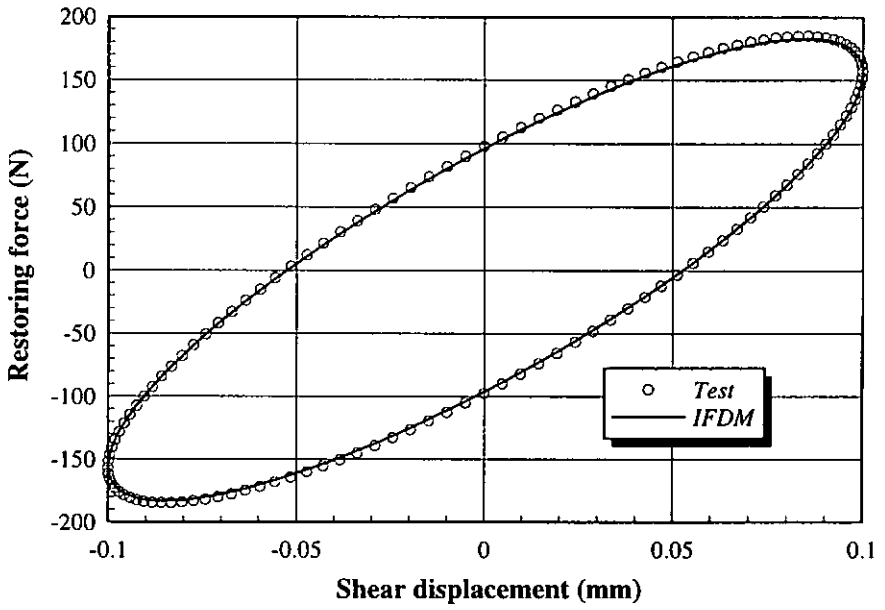

Figure 4.17 Comparison between the IFDM and the test results for damper HD91 (15Hz)

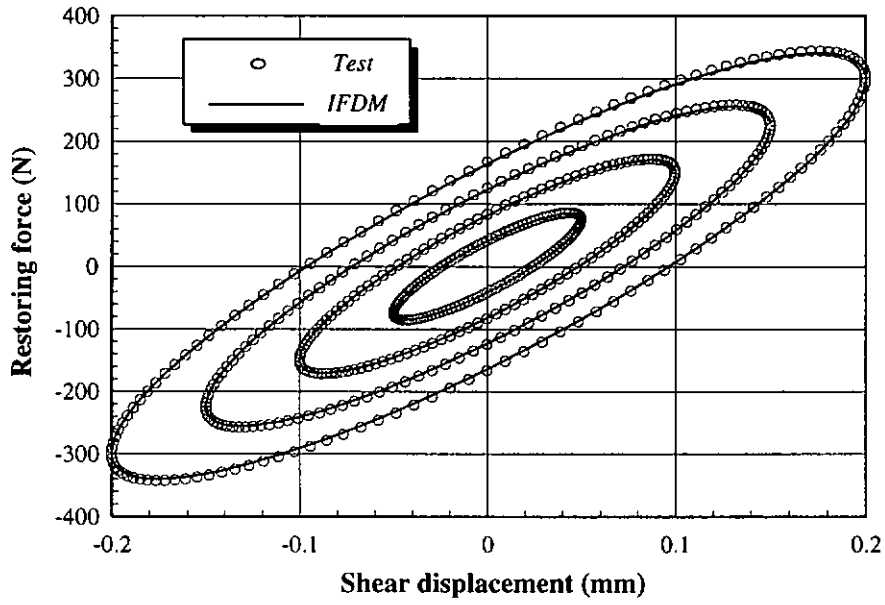

Figure 4.18 Comparison between the IFDM and the test results for damper HD91 (12Hz)

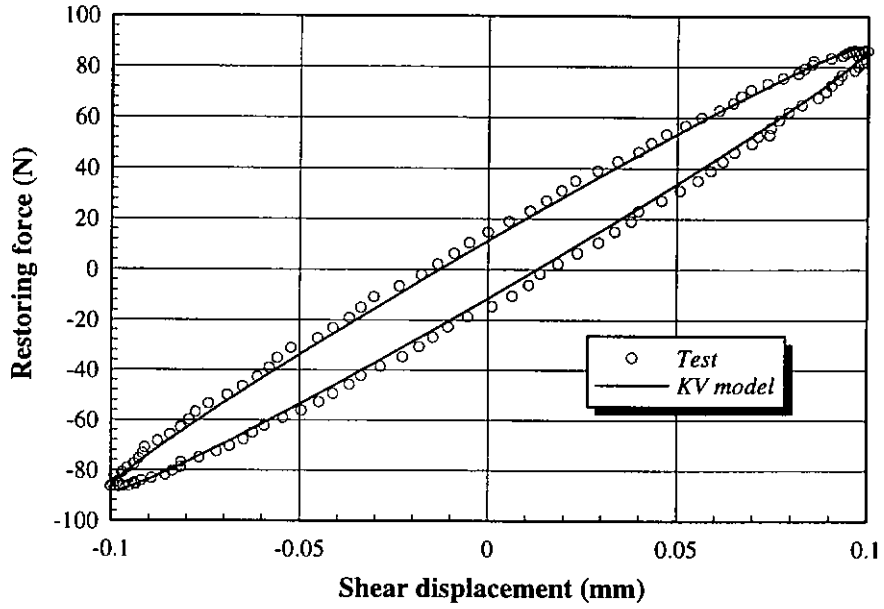

Figure 4.19 Comparison between the KV model and the test results for damper ZJD-1 (3Hz)

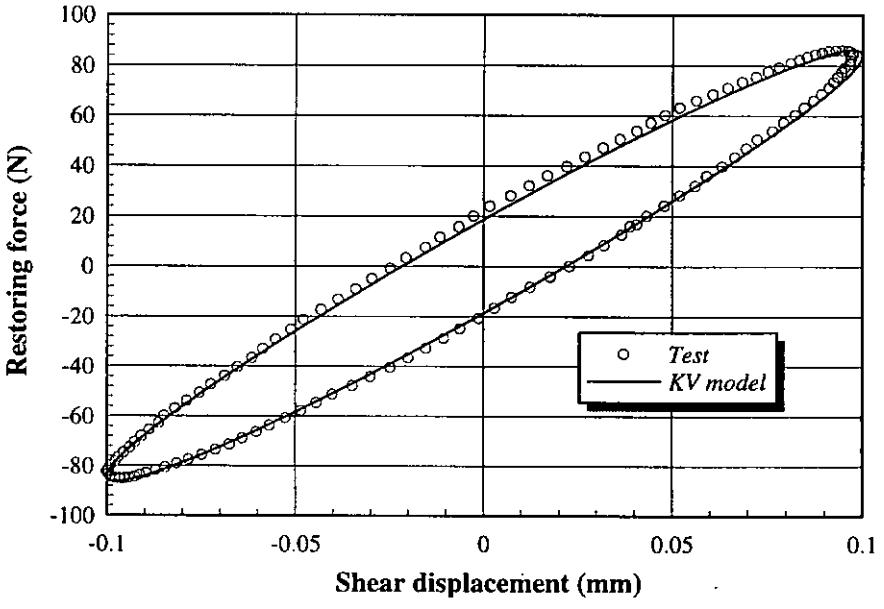

Figure 4.20 Comparison between the KV model and the test results for damper ZJD-1 (6Hz)

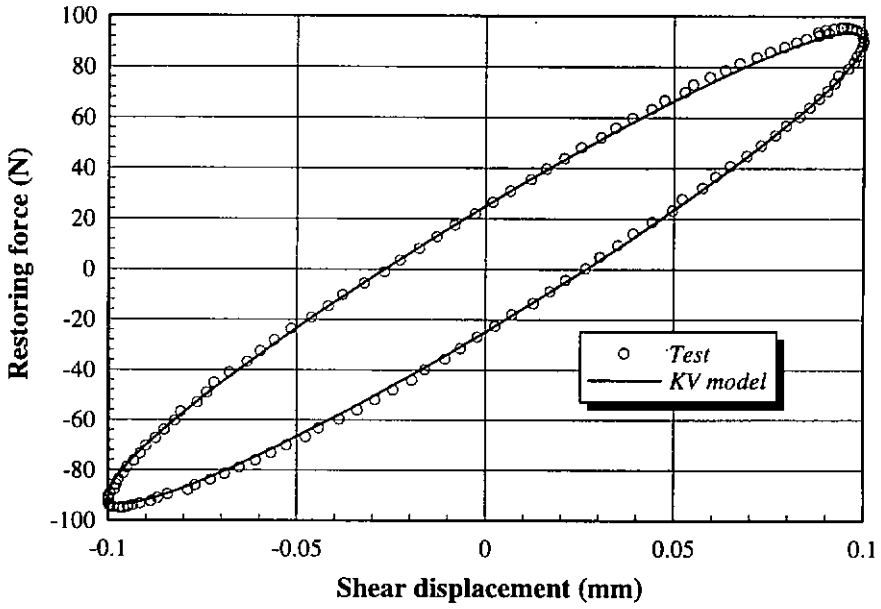

Figure 4.21 Comparison between the KV model and the test results for damper ZJD-1 (9Hz)

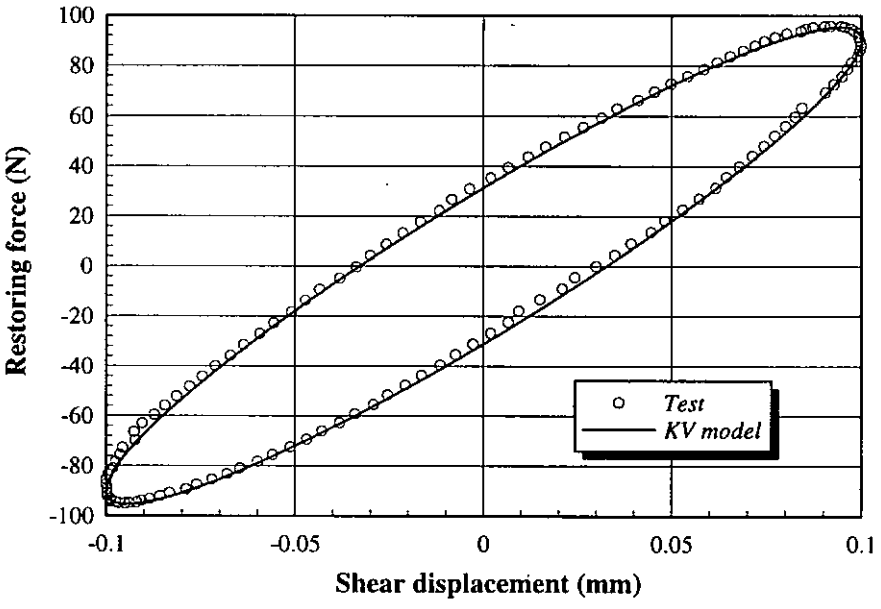

Figure 4.22 Comparison between the KV model and the test results for damper ZJD-1 (12Hz)

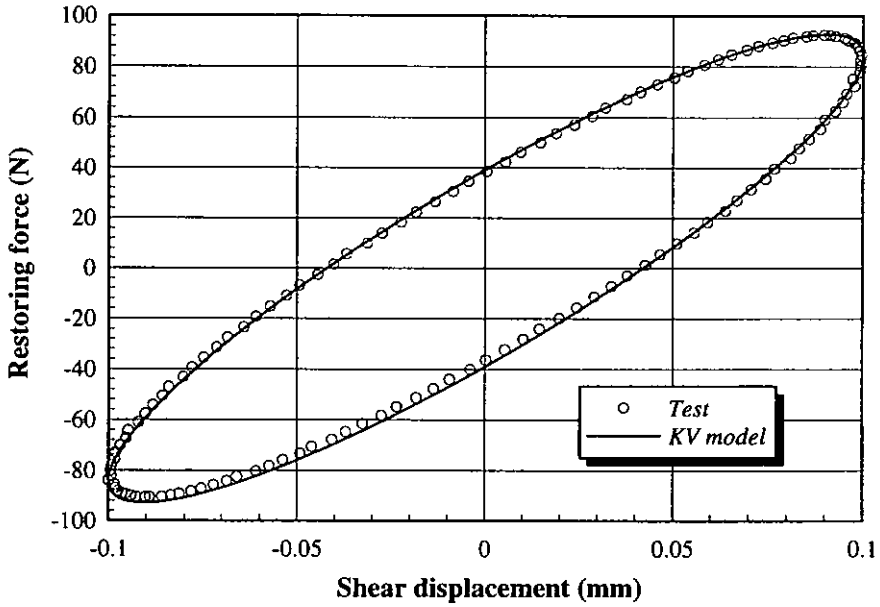

Figure 4.23 Comparison between the KV model and the test results for damper ZJD-1 (15Hz)

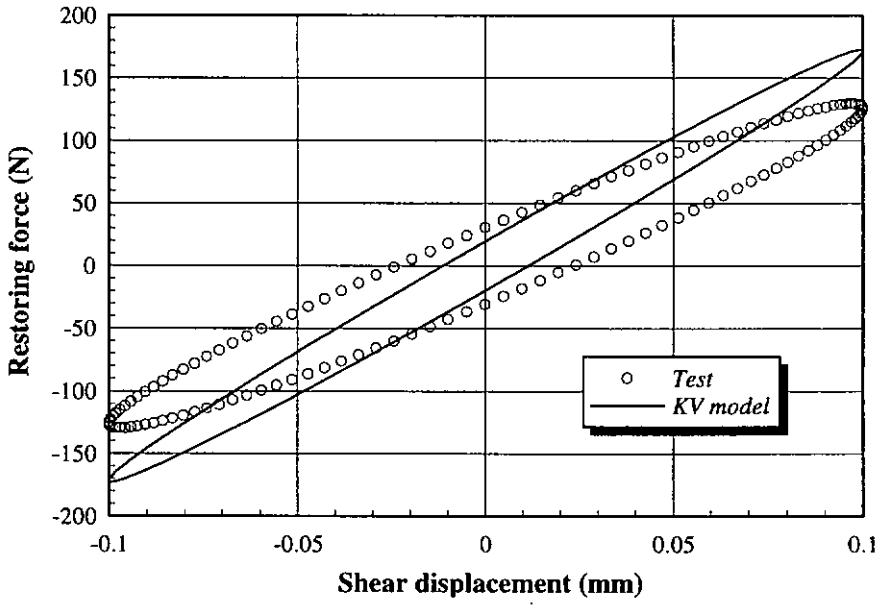

Figure 4.24 Comparison between the KV model and the test results for damper HD91 (3Hz)

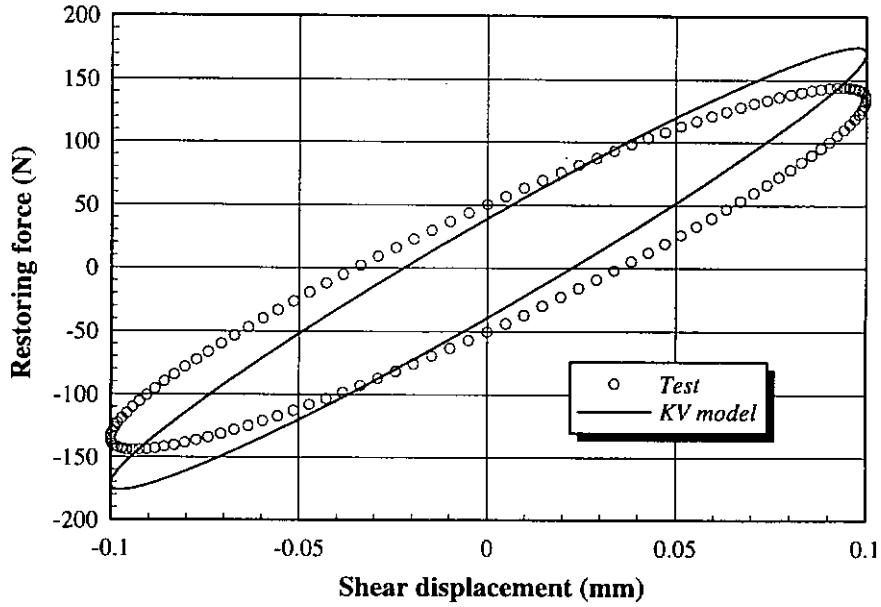

Figure 4.25 Comparison between the KV model and the test results for damper HD91 (6Hz)

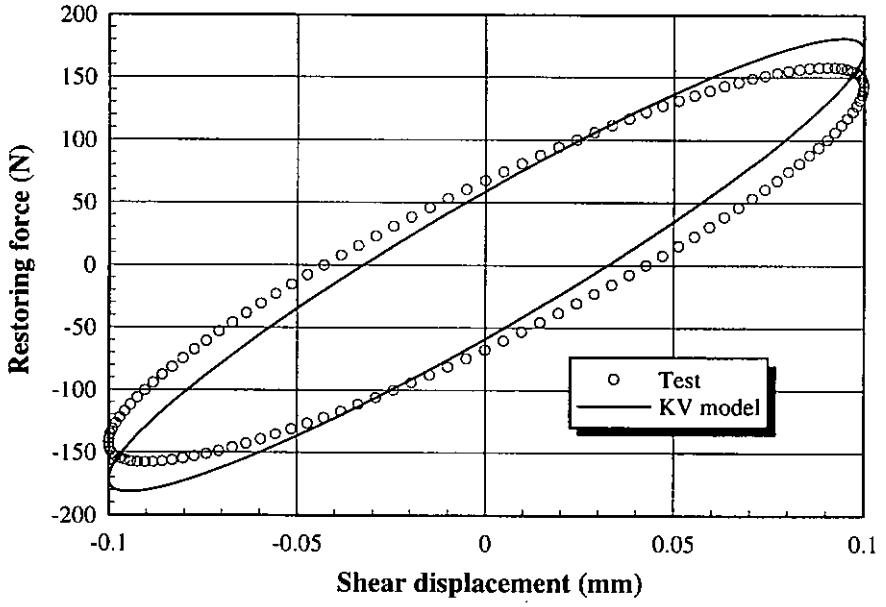

Figure 4.26 Comparison between the KV model and the test results for damper HD91 (9Hz)

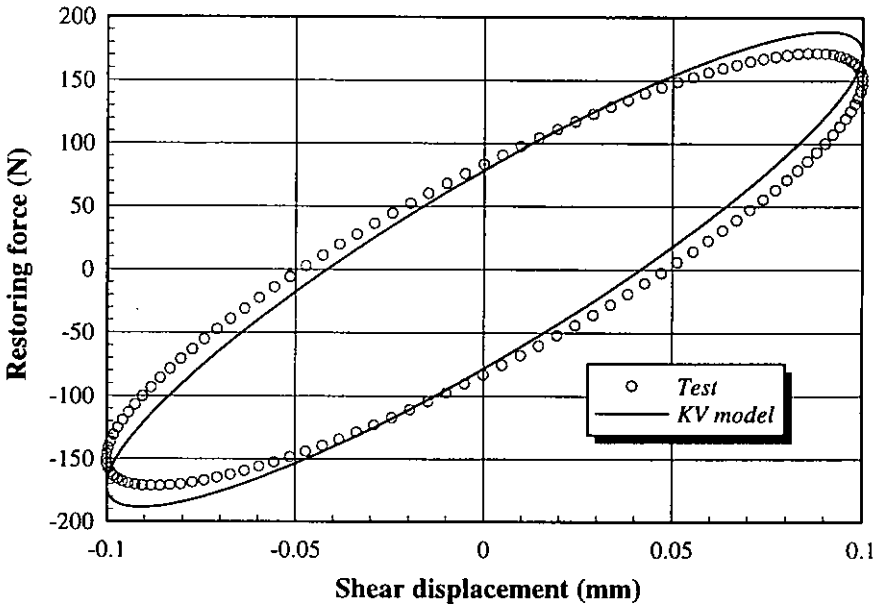

Figure 4.27 Comparison between the KV model and the test results for damper HD91 (12Hz)

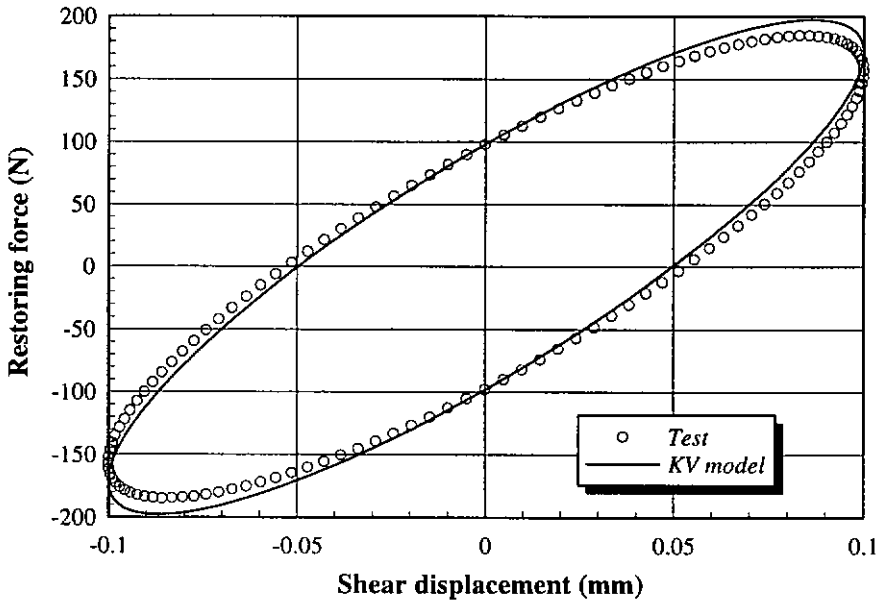

Figure 4.28 Comparison between the KV model and the test results for damper HD91 (15Hz)

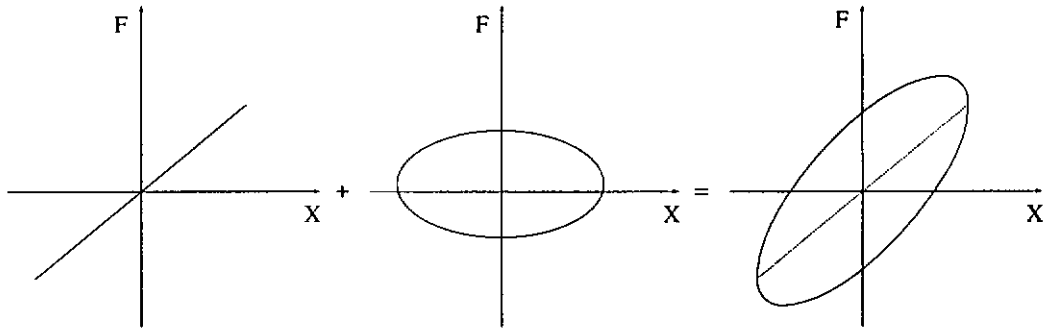

Figure 4.29 Hysteresis loop constitution of the IFDM

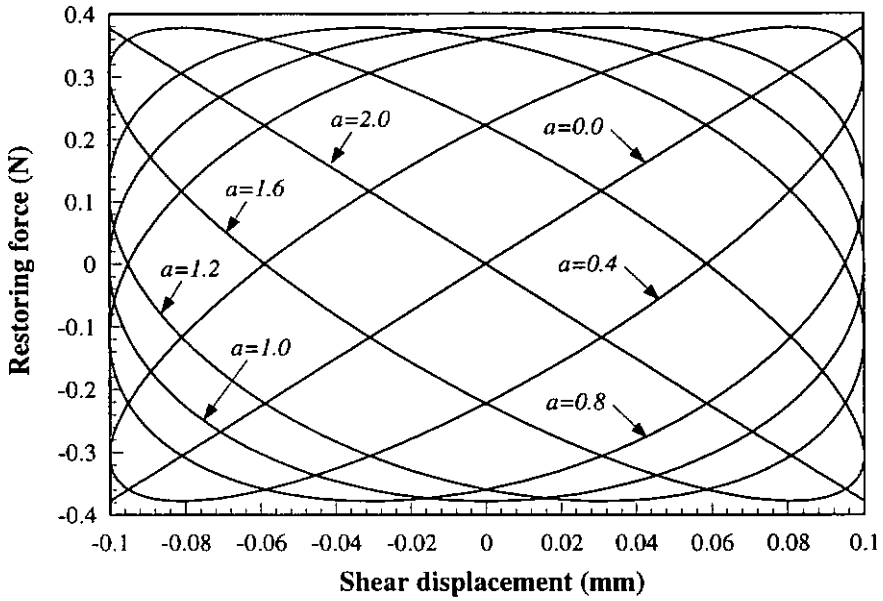

Figure 4.30 Hysteresis loops of the model with different parameter α

($G_0 = 0$ and $\omega = 1.0$)

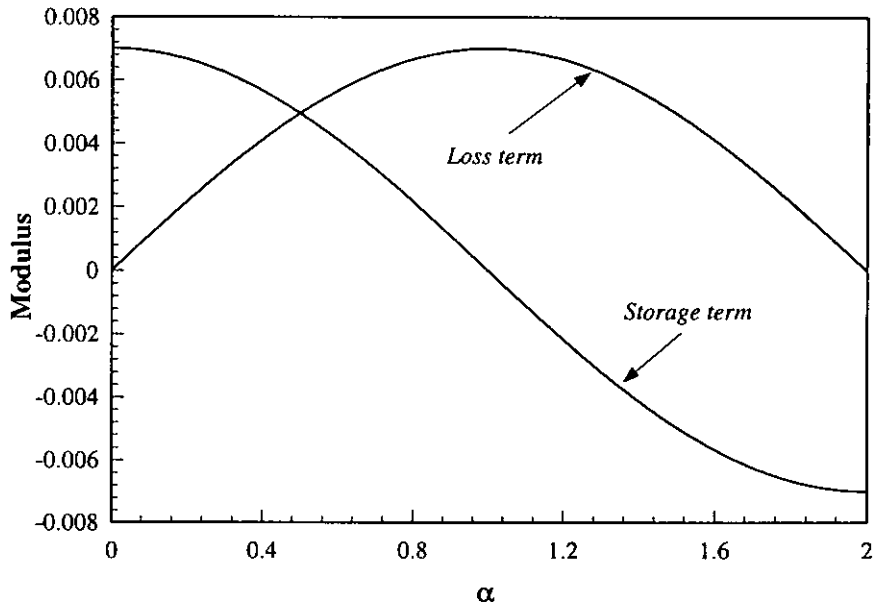

Figure 4.31 Relation between the modulus and parameter α ($G_0 = 0$ and $\omega = 1.0$)

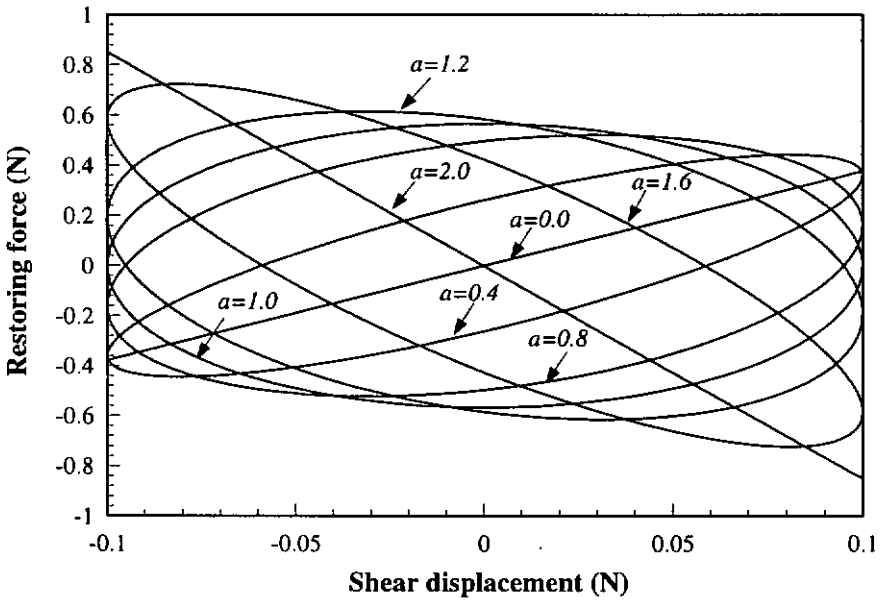

Figure 4.32 Hysteresis loops of the model with different parameter α ($G_0 = 0$ and $\omega = 1.5$)

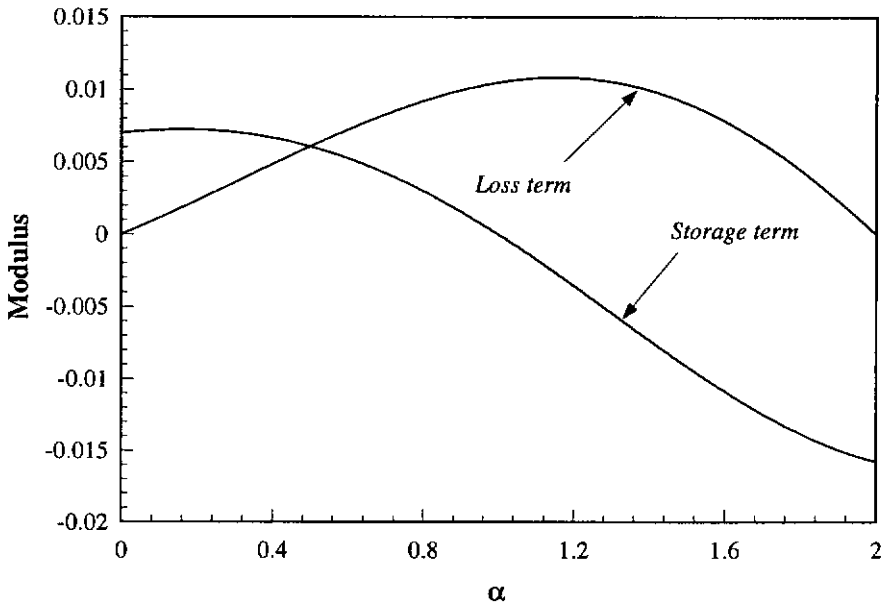

Figure 4.33 Relation between the modulus and parameter α ($G_0 = 0$ and $\omega = 1.5$)

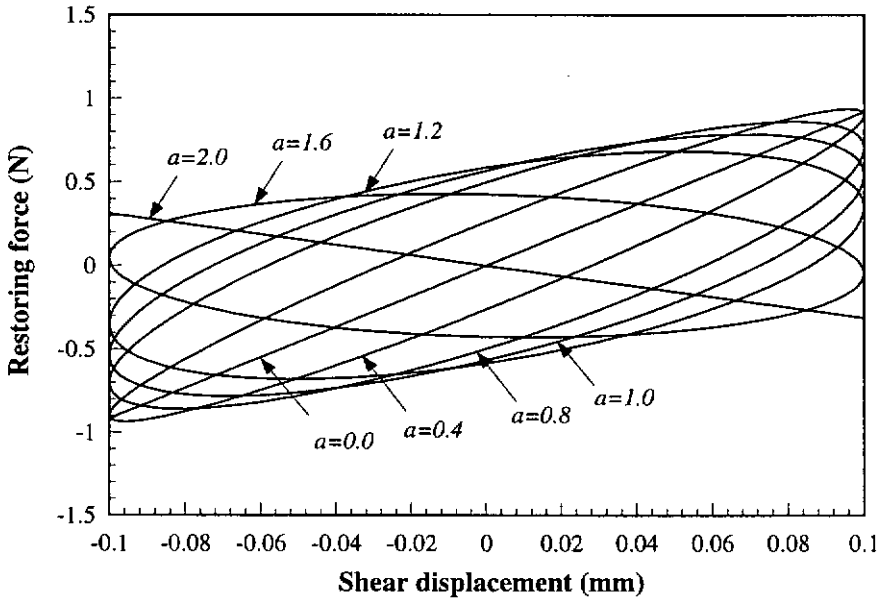

Figure 4.34 Hysteresis loops of the model with different parameter α ($G_0 = 0.01$)

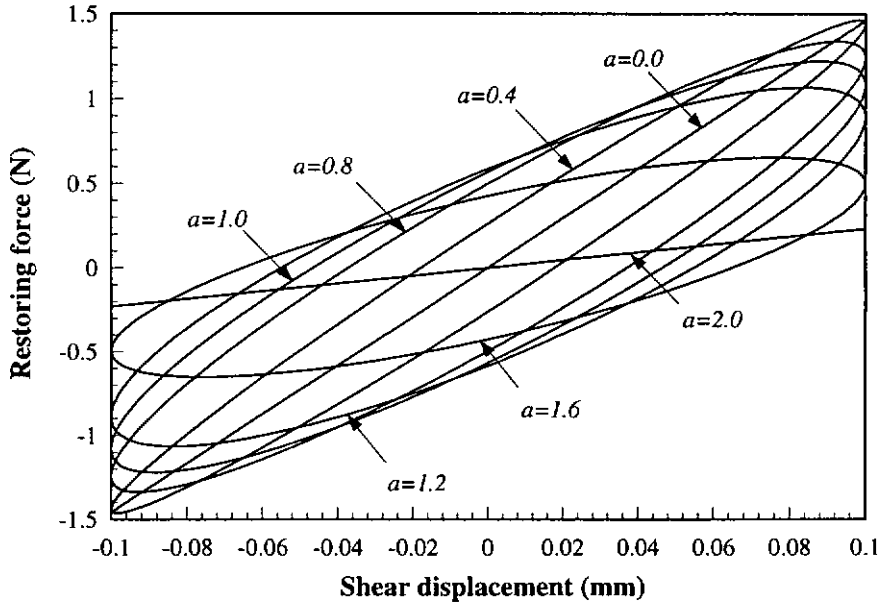

Figure 4.35 Hysteresis loops of the model with different parameter α ($G_0 = 0.02$)

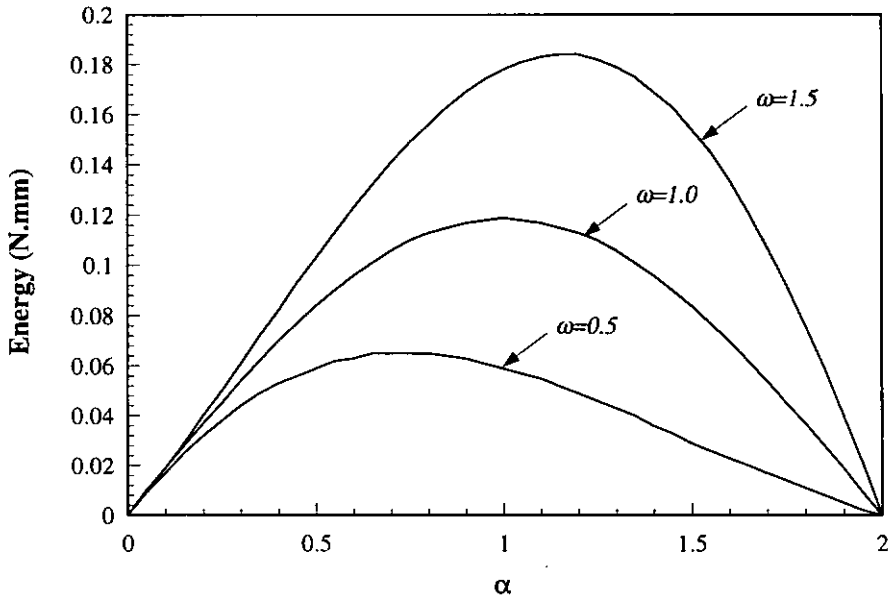

Figure 4.36 Relation between energy dissipated per cycle and parameter α

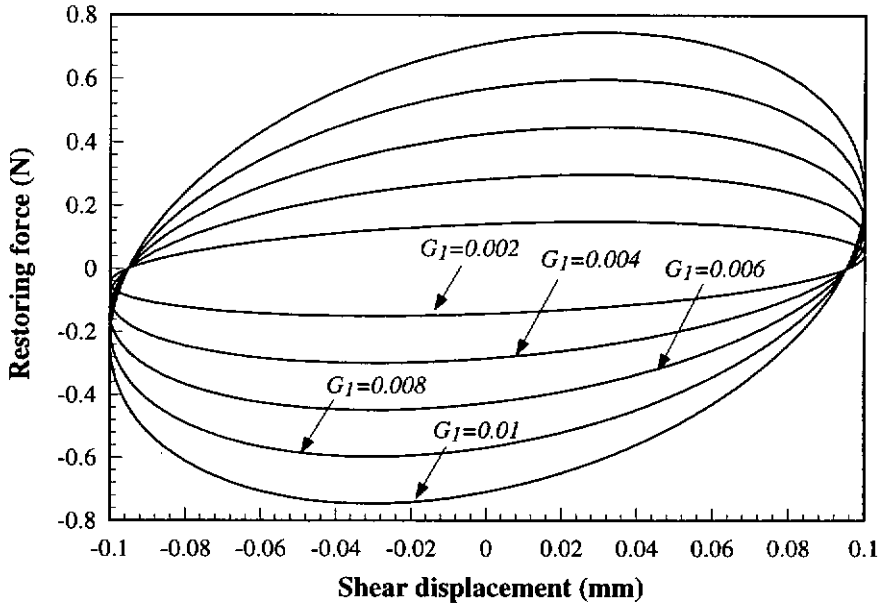

Figure 4.37 Hysteresis loops of the model with different parameter G_1 ($G_0 = 0.0$)

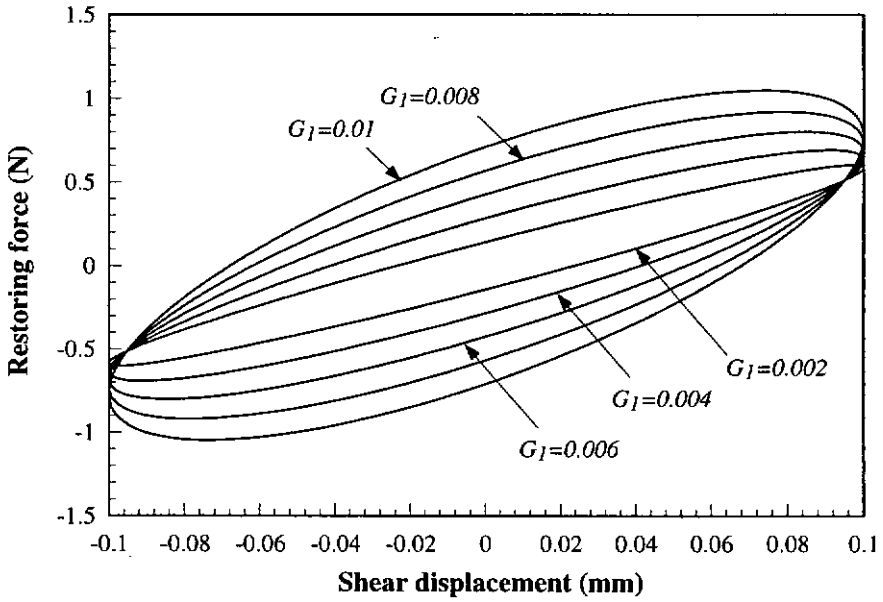

Figure 4.38 Hysteresis loops of the model with different parameter G_1 ($G_0 = 0.01$)

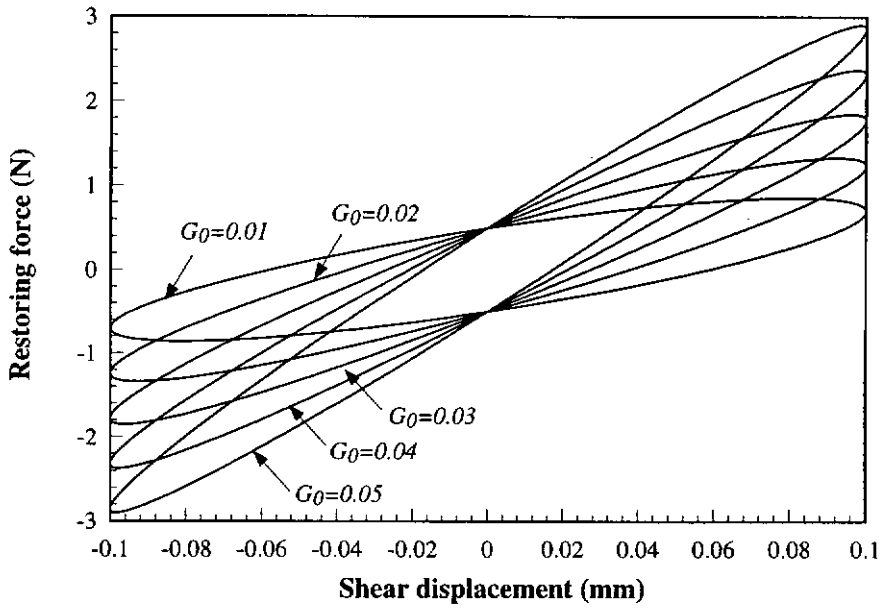

Figure 4.39 Hysteresis loops of the model with different parameter G_0

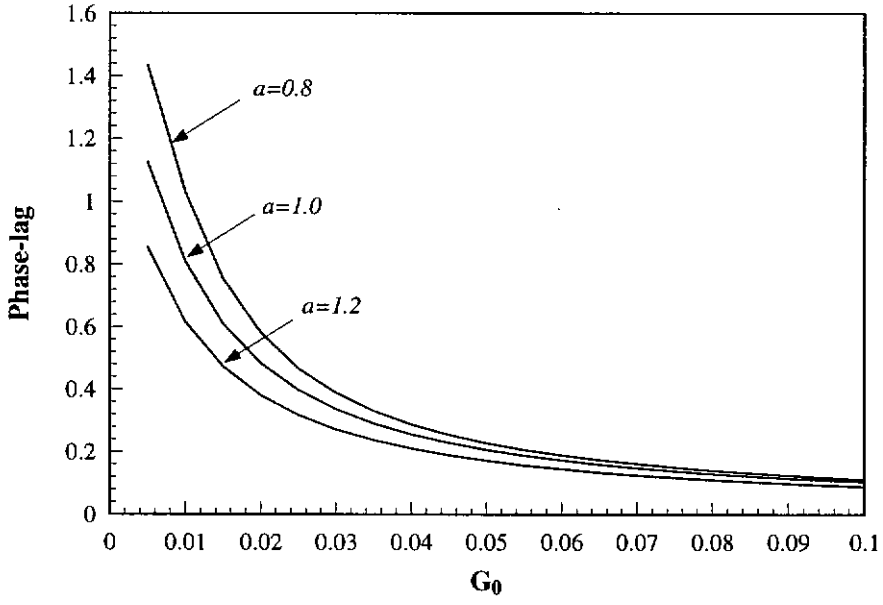

Figure 4.40 Relation between the phase-lag and parameter G_0

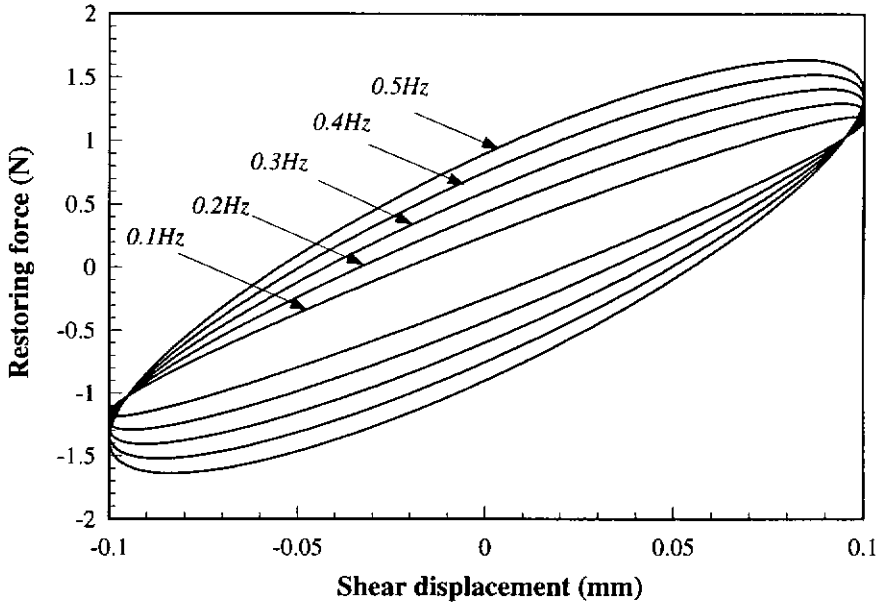

Figure 4.41 Hysteresis loops of a damper represented by the IFDM at different excitation frequencies

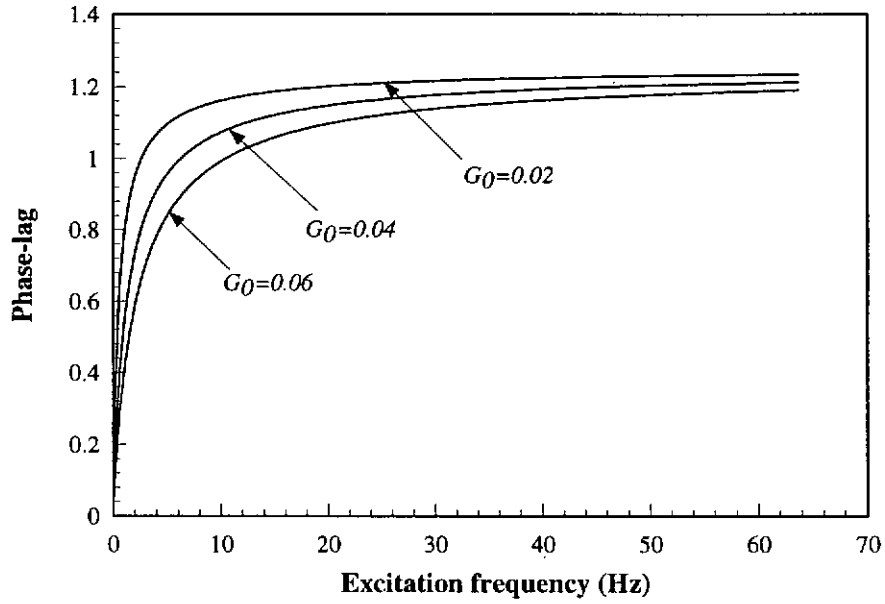

Figure 4.42 Phase-lag of a damper represented by the IFDM at different excitation frequencies

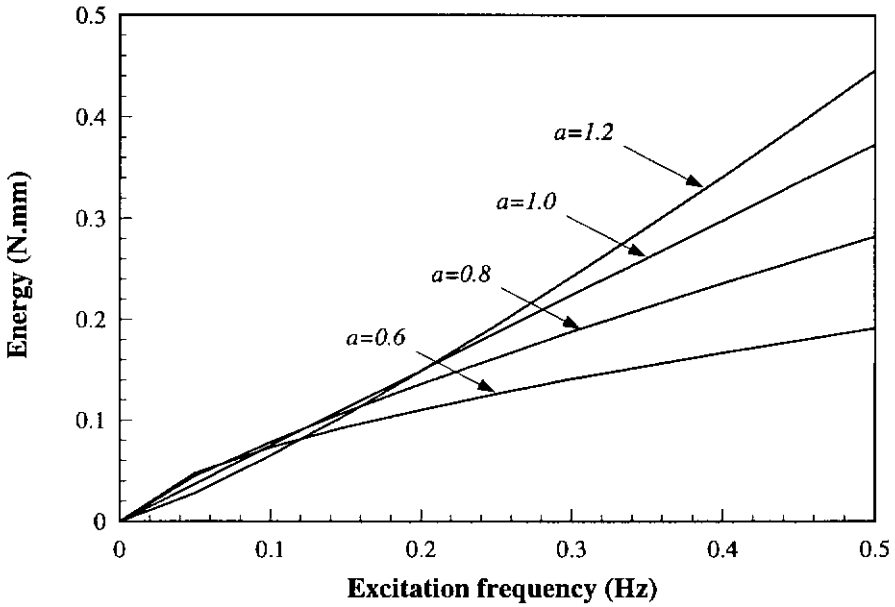

Figure 4.43 Energy dissipated per cycle by a damper represented by the IFDM under excitation of different frequencies

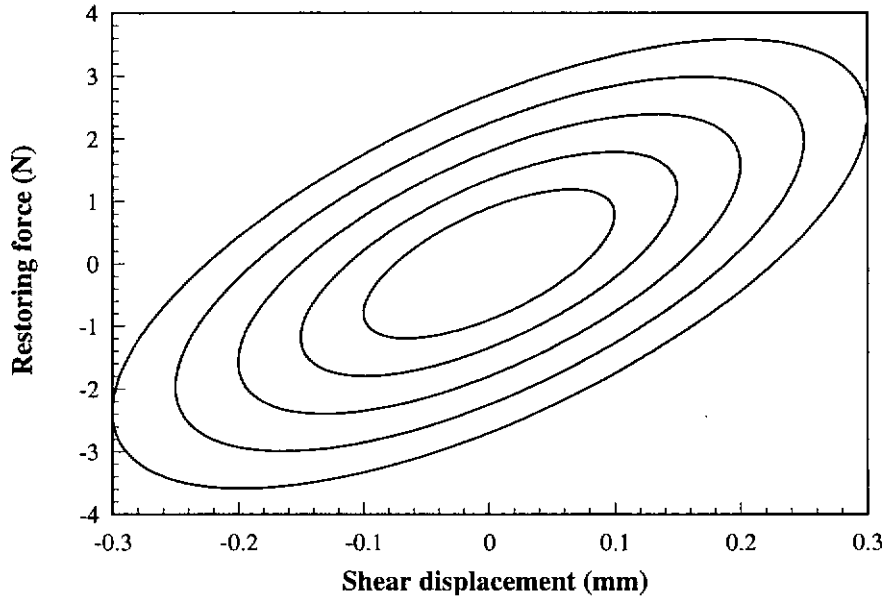

Figure 4.44 Hysteresis loops of a damper represented by the IFDM under excitation with shear displacement of different amplitudes

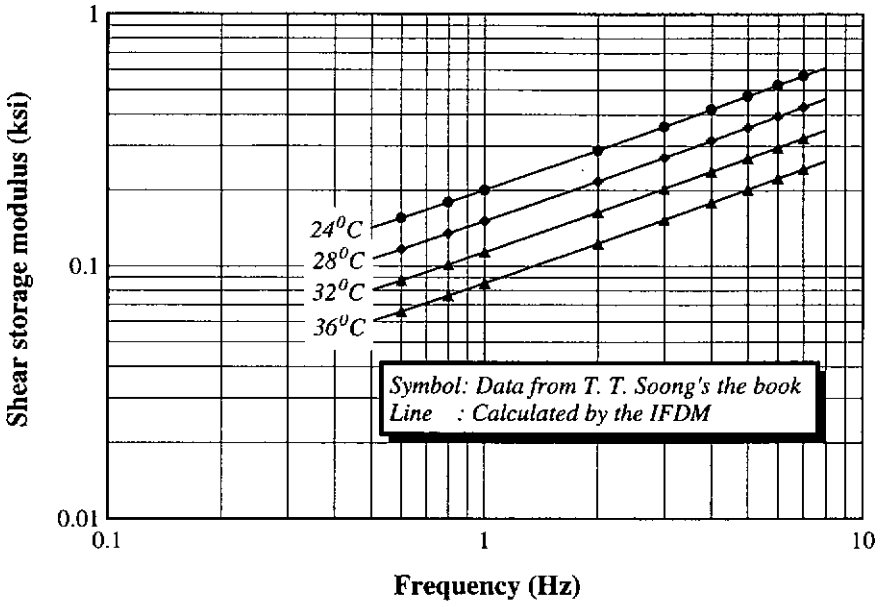

Figure 4. 45 Comparison of the shear storage modulus

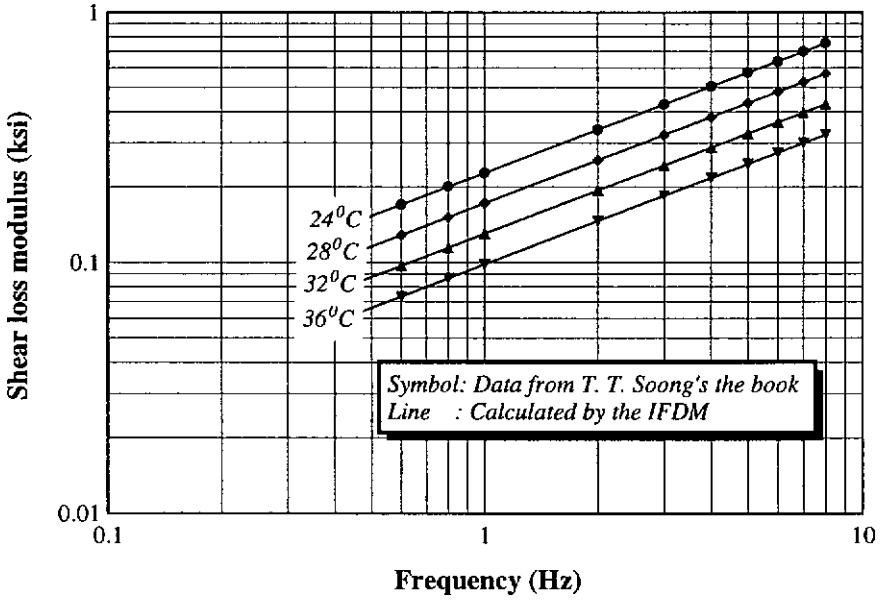

Figure 4. 46 Comparison of the shear loss modulus

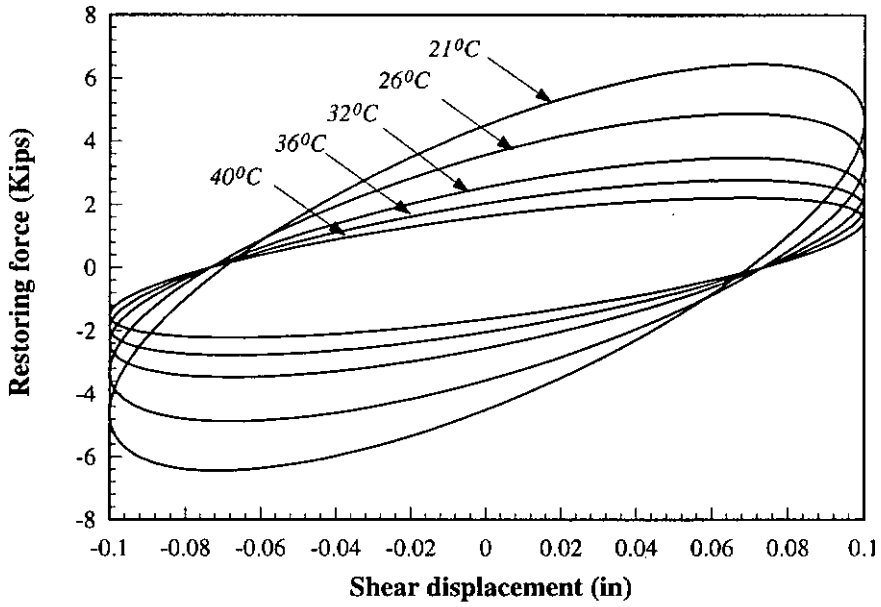

Figure 4.47 Hysteresis loops of the damper represented by the IFDM at different temperatures with excitation frequency of 3Hz

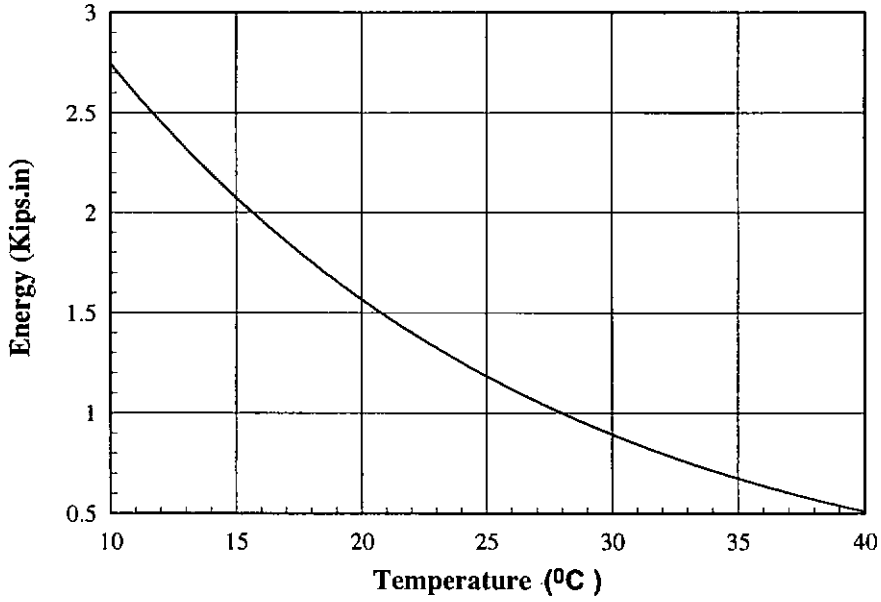

Figure 4.48 Energy dissipated per cycle by the damper represented by the IFDM at different temperatures

CHAPTER 5

MODELLING AND ANALYTICAL METHODS FOR STRUCTURES WITH VISCOELASTIC DAMPERS

5.1 Introduction

A necessary prerequisite to vibration control of structures with viscoelastic dampers is an understanding of the detailed dynamic behaviour of the system under excitation. Many approaches toward this task have been taken, including mathematical modelling and exact solution of the resulting partial differential equation(s) of motion (Chen Q. et al, 1989), discrete finite element modelling and solution of the large array of second-order differential equations (Tan X. M. et al, 1995, Tan X. M. et al, 1996), energy methods like Modal Strain Energy Method (MSE) (Chang K. C., 1993, Hu B-G., 1995), and combination of solutions corresponding to the subsets of the entire system (Kasai Kazuhiko et al, 1995). As discussed in Chapter Two, all these approaches have advantages and disadvantages.

Viscoelastic dampers can be designed to control vibration of structures in different directions. As discussed in Chapter Six and Chapter Seven, dampers have been utilized to attenuate horizontal vibration of framed structures and to suppress vertical vibration of long span beams with specially designed damping devices. In the present study, based on the IFDM and the installation conditions, two schemes dealing with viscoelastic dampers have been developed for response analysis of structures. An analytical method in time domain for structures with viscoelastic dampers has been proposed making use of the IFDM. Since the dynamic behaviours of viscoelastic dampers change with excitation frequency,

enlightened by the frequency domain idea used in other research areas (Cameron Timonthy M., 1988), response analysis of structures with viscoelastic dampers by hybrid time-frequency domain method has been developed together with an associated computer program.

5.2 Modelling Schemes for Viscoelastic Dampers in FEM

For a structure without viscoelastic dampers, the complete set of dynamic equilibrium equations can be given by,

$$\mathbf{M}\ddot{\mathbf{X}}(t)+\mathbf{C}\dot{\mathbf{X}}(t)+\mathbf{K}\mathbf{X}(t)=\mathbf{P}(t) \tag{5.1}$$

where $\mathbf{M}$ is the mass matrix of the structure, $\mathbf{C}$ is the damping matrix, $\mathbf{K}$ is the stiffness matrix, $\mathbf{X}(t)$ is the vector of the displacement and $\mathbf{P}(t)$ is the vector of the external force. In general, structures are analyzed by Finite Element Method (FEM) with normal structural elements like beam element. Contributions of these elements to structure stiffness consist of terms for shear, bending and tension or compression. For example, the stiffness matrix of normal beam element is,

$$\left[\bar{k}\right]^e=\begin{bmatrix} \frac{EA}{l} & 0 & 0 & -\frac{EA}{l} & 0 & 0 \\ 0 & \frac{12EI}{l^3} & -\frac{6EI}{l^2} & 0 & -\frac{12EI}{l^3} & -\frac{6EI}{l^2} \\ 0 & -\frac{6EI}{l^2} & \frac{4EI}{l} & 0 & \frac{6EI}{l^2} & \frac{2EI}{l} \\ -\frac{EA}{l} & 0 & 0 & \frac{EA}{l} & 0 & 0 \\ 0 & -\frac{12EI}{l^3} & \frac{6EI}{l^2} & 0 & \frac{12EI}{l^3} & \frac{6EI}{l^2} \\ 0 & -\frac{6EI}{l^2} & \frac{2EI}{l} & 0 & \frac{6EI}{l^2} & \frac{4EI}{l} \end{bmatrix} \tag{5.2}$$

The normal frame elements are mostly assumed to be of linear behaviour and their stiffness remain unchanged during vibration. The damping ratio of the structure without dampers is assumed to be proportional, which can be written as $[c]=\alpha[M]+\beta[K]$, where, $\alpha = \frac{2(\omega_2\zeta_1 - \omega_1\zeta_2)}{\omega_2^2 - \omega_1^2}\omega_1\omega_2$, $\beta = \frac{2(\omega_2\zeta_2 - \omega_1\zeta_1)}{\omega_2^2 - \omega_1^2}$, in which parameters ω_1 and ω_2 are the first two natural frequencies of the structure, ζ_1 and ζ_2 are the damping ratios corresponding to the first and second natural frequency respectively. The direct integration methods namely Wilson-θ and Newmark-β (Clough Ray W., 1993) can be used for the dynamic analysis of normal structures.

However, for a structure with viscoelastic dampers, the dynamic behaviour of the structure is different from that of a structure without dampers. To consider the effect of dampers on the structure properly, two schemes for modelling of viscoelastic dampers have been proposed for the response analysis of structures. When a structure is incorporated with viscoelastic dampers, the complete set of dynamic equilibrium equations can be written in two ways as follows,

$$\mathbf{M}\ddot{\mathbf{X}}(t) + \mathbf{C}\dot{\mathbf{X}}(t) + [\mathbf{K}^S + \mathbf{K}^D(t)]\mathbf{X}(t) = \mathbf{P}(t) \qquad (5.3.a)$$

$$\mathbf{M}\ddot{\mathbf{X}}(t) + \mathbf{C}\dot{\mathbf{X}}(t) + \mathbf{K}^S\mathbf{X}(t) + \mathbf{R}(t) = \mathbf{P}(t) \qquad (5.3.b)$$

where $\mathbf{K}^S$ is the stiffness matrix of the structure without damper, $\mathbf{K}^D$ is the additional stiffness matrix caused by viscoelastic dampers and $\mathbf{R}(t)$ is the restoring force vector induced by viscoelastic dampers.

Equation (5.3.a) or (5.3.b) can be chosen for response analysis according to different contribution of the viscoelastic dampers. If the restoring force of the

damper in shear direction (or axial direction) gives the FEM node, with which the damper connects, a contribution of a force and the shear displacement (or axial displacement) of the damper has direct relation with the FEM node, then the damper can be considered as a special element namely viscoelastic element or considered as a support namely viscoelastic support, either equation (5.3.a) or (5.3.b) can be applied. However, if the restoring force of the damper in shear direction (or axial direction) gives the FEM node another kind of contribution such as bending moment and the shear displacement (or axial displacement) of the damper does not have direct relation with the FEM node, the damper should be considered as a support, thus only equation (5.3.b) can be adopted. These two different schemes are described in detail in the following two sections respectively.

5.2.1 Viscoelastic elements

When viscoelastic dampers are considered as elements, stiffness of each viscoelastic element changes with time during vibration of the structure. The stiffness matrix of a viscoelastic element with displacement coordinates shown as Figure 5.1 can be modified as

$$\left[\bar{k}\right] = \begin{bmatrix} k_{11} & 0 & 0 & k_{14} & 0 & 0 \\ 0 & k_{22} & 0 & 0 & k_{25} & 0 \\ 0 & 0 & 0 & 0 & 0 & 0 \\ k_{41} & 0 & 0 & k_{44} & 0 & 0 \\ 0 & k_{52} & 0 & 0 & k_{55} & 0 \\ 0 & 0 & 0 & 0 & 0 & 0 \end{bmatrix} \tag{5.4}$$

Since viscoelastic dampers always undergo mainly shear deformation in practical application, only those terms concerned with shear restoring force are considered

to be effective and other terms are set to zero. As shown in Figure 5.2, assuming a damper is connected with node i and node j, displacement of which at time t are v_i and v_j, then shear displacement of the damper is $v_i - v_j$. By applying the mathematical model IFDM, the forces induced by the damper at node i and node j can be written as,

$$\begin{cases} k_{22}v_i + k_{25}v_j = f_i = \dfrac{A_r}{h}\psi(\Delta T)[G_0(v_i - v_j) + G_1 D^{\alpha}(v_i - v_j)] \\ k_{52}v_i + k_{55}v_j = f_j = -\dfrac{A_r}{h}\psi(\Delta T)[G_0(v_i - v_j) + G_1 D^{\alpha}(v_i - v_j)] \end{cases} \tag{5.5}$$

where A_r is the shear area of the damper and h is the thickness of the damper.

By considering the symmetry of the viscoelastic damper,

$$\begin{cases} k_{22} = k_{55} = k_1 \\ k_{25} = k_{52} = k_2 \end{cases} \tag{5.6}$$

k_1 and k_2 can be obtained by solving Equation (5.5) and can be written as,

$$k_1 = \frac{A_r}{h}\psi(\Delta T)\left[G_0 + \frac{G_1}{v_i - v_j}D^{\alpha}(v_i - v_j)\right] \tag{5.7.a}$$

$$k_2 = -\frac{A_r}{h}\psi(\Delta T)\left[G_0 + \frac{G_1}{v_i - v_j}D^{\alpha}(v_i - v_j)\right] \tag{5.7.b}$$

In some applications, dampers undergo axial deformation in addition to shear deformation. As mentioned in Chapter Three, it has been found from tests performed in axial direction by the other researchers on the same dampers ZJD-1 and HD91 that the dampers have similar characteristics in axial direction as those in shear direction. Therefore, the IFDM has also been used to simulate the behaviour of these dampers in axial direction and the corresponding parameters

of the IFDM for these dampers have been identified in Chapter Four. If the axial terms are needed to be considered, they can be obtained in the same way as those for shear terms and they have the similar expressions as equation (5.7),

$$k_{11} = k_{44} = \frac{A_r}{h}\psi(\Delta T)\left[E_0 + \frac{E_1}{u_i - u_j} D^{\alpha_a}(u_i - u_j)\right] \tag{5.8.a}$$

$$k_{14} = k_{41} = -\frac{A_r}{h}\psi(\Delta T)\left[E_0 + \frac{E_1}{u_i - u_j} D^{\alpha_a}(u_i - u_j)\right] \tag{5.8.b}$$

where u_i and u_j are the displacement of the nodes in the axial direction of the damper.

If the bending moment effect has to be included, more elements should be included for one damper and discretization of the structure should be modified. Thus effect of the bending moment can be embodied by the axial restoring forces of the elements acting at different positions of the structure.

Since the mass of the damper is much less than those of other members, terms of the element mass matrix can be omitted or simplified as follows,

$$m_{11} = m_{22} = m_{44} = m_{55} = \frac{1}{2} m_d \tag{5.9}$$

where m_d is mass of the damper. Other terms of the element mass matrix are set to zero.

All the nonlinearity and damping increment caused by dampers have been considered in the stiffness matrix of the viscoelastic element, the damping matrix of the structure should remain the same as that of the structure without dampers.

5.2.2 Viscoelastic supports

When the restoring force of a damper installed between two neighbouring normal FEM elements provides a bending moment to the node where the two normal elements are connected, it is difficult to treat the viscoelastic damper as a viscoelastic element without disturbing the original element discretization of the whole structure. Therefore, it is necessary to propose the following scheme.

If a damper is considered as a viscoelastic support, it will be separated from the linear structure during analysis. There is no need to modify the damping matrix and the stiffness matrix of the structure because the restoring forces have already coped with all the effects of the damper. Therefore, the structure can be analyzed easily without any special treatment and the study is then concentrated on the restoring force.

Viscoelastic dampers HD91 installed in the beam-column connections of a long span beam to suppress vertical vibration of the beam in Chapter Seven is a typical example that the dampers should be treated as supports. Dampers with dimensions shown in Figure 5.3 are glued between the beam flange and the angle bolted onto the column. When the beam is excited by dynamic loading, relative rotation of the beam around the beam-column connection will occur and the viscoelastic damper will mainly undergo shear deformation as shown in Figure 5.4. As a basis for the analysis discussed in Chapter Seven, the following derivation is carried out with reference to the setup of the dampers in the beam-column connection

When the beam is excited by dynamic loading, the relative rotation angle θ in Figure 5.4(a) is very small, shear displacement of the damper at the beam flange can be approximated as

$$v = \frac{H}{2} \cdot \theta \tag{5.10}$$

where, H is the height of the beam section.

Then the shear restoring force of each viscoelastic damper is

$$F_s = \frac{A_r}{h} \psi(\Delta T) \left[G_0 v + G_1 D^{\alpha}(v) \right] \tag{5.11}$$

With consideration of Equation (5.10), the restoring force can be written as

$$F_s = \frac{A_r H \psi(\Delta T)}{2h} \left[G_0 \theta + G_1 D^{\alpha}(\theta) \right] \tag{5.12}$$

Herewith, the moment about the centroidal axis produced by one damper can be obtained easily by,

$$M_s = F_s \frac{H}{2} = \frac{H^2 A_r \psi(\Delta T)}{4h} \left[G_0 \theta + G_1 D^{\alpha}(\theta) \right] \tag{5.13}$$

For most conditions, the damper installed at the beam-column connection subject to axial force as well as shear force. When a rotation angle occurs at one end of the beam as shown in Figure 5.5, the damper will undergo axial deformation in addition to shear deformation. And the axial deformation is not uniform across the length of the damper. It changes along the longitudinal direction of the damper. As shown in Figure 5.6(a), left side of the damper on the upper flange is in tension and the right side is in compression. The damper on the lower flange is

wholly in tension, which can be seen in Figure 5.6(b). The deformation in axial direction of the dampers can be expressed as follows,

$$\text{for the upper damper, } \Delta h_x = \theta x - \frac{H}{2}(1-\cos\theta) \quad (0 \le x \le a) \tag{5.14.a}$$

$$\text{for the lower damper, } \Delta h_x = \theta x + \frac{H}{2}(1-\cos\theta) \quad (0 \le x \le a) \tag{5.14.b}$$

where the damper edge is set as the origin of the X axis.

The restoring force in axial direction of a damper can be written as

$$F_a = \int_0^a \sigma_x b dx \tag{5.15}$$

where,

$$\sigma_x = \psi_a(\Delta T)\left[E_0\varepsilon_x + E_1 D^{\alpha_a}(\varepsilon_x)\right] \tag{5.16}$$

in which, E_0, E_1 and α_a are the parameters of the fractional derivative model for viscoelastic dampers in axial direction, $\psi_a(\Delta T)$ is the temperature factor in axial direction.

Substitution of the axial strain $\varepsilon_x = \frac{\Delta h_x}{h}$ into (5.16), it yields

$$\sigma_x = \frac{\psi_a(\Delta T)}{h}\left[E_0\Delta h_x + E_1 D^{\alpha_a}(\Delta h_x)\right] \tag{5.17}$$

Then, by applying (5.14) and (5.17), the restoring forces of the upper damper and the lower damper can be calculated by the following equation,

for the upper damper,

$$F_a = \psi_a(\Delta T)\left\{\frac{a^2 b}{2h}\left[E_0\theta + E_1 D^{\alpha_a}(\theta)\right] - \frac{abH}{2h}\left[E_0(1-\cos\theta) + E_1 D^{\alpha_a}(\cos\theta)\right]\right\} \tag{5.18.a}$$

and for the lower damper,

$$F_a = \psi_a(\Delta T)\left\{\frac{a^2 b}{2h}\left[E_0\theta + E_1 D^{\alpha_a}(\theta)\right] + \frac{abH}{2h}\left[E_0(1-\cos\theta) + E_1 D^{\alpha_a}(\cos\theta)\right]\right\} \tag{5.18.b}$$

And the additional moment around the centroidal axis of the beam end section is in the same direction as M_s and can be obtained in the same way for the upper and lower damper respectively as,

$$\begin{aligned} M_a &= \int_0^a \sigma_x b(x - \frac{H}{2}\theta)dx \\ &= \frac{b}{h}\psi_a(\Delta T)\int_0^a \left[E_0(\theta x - \frac{H}{2} + \frac{H}{2}\cos\theta) + E_1 D^{\alpha_a}(\theta x - \frac{H}{2} + \frac{H}{2}\cos\theta)\right](x - \frac{H}{2}\theta)dx \\ &= \frac{a^2 b}{h}\psi_a(\Delta T)\left\{E_0\left[\frac{a\theta}{3} - \frac{H}{4}(1-\cos\theta)\right] + E_1\left[\frac{a}{3}D^{\alpha_a}(\theta) + \frac{H}{4}D^{\alpha_a}(\cos\theta)\right]\right\} \\ &\quad - \frac{Hab\theta}{4h}\psi_a(\Delta T)\left\{E_0[a\theta - H(1-\cos\theta)] + E_1\left[aD^{\alpha_a}(\theta) + HD^{\alpha_a}(\cos\theta)\right]\right\} \end{aligned} \tag{5.19.a}$$

$$\begin{aligned} M_a &= \int_0^a \sigma_x b(x + \frac{H}{2}\theta)dx \\ &= \frac{b}{h}\psi_a(\Delta T)\int_0^a \left[E_0(\theta x + \frac{H}{2} - \frac{H}{2}\cos\theta) + E_1 D^{\alpha_a}(\theta x + \frac{H}{2} - \frac{H}{2}\cos\theta)\right](x + \frac{H}{2}\theta)dx \\ &= \frac{a^2 b}{h}\psi_a(\Delta T)\left\{E_0\left[\frac{a\theta}{3} + \frac{H}{4}(1-\cos\theta)\right] + E_1\left[\frac{a}{3}D^{\alpha_a}(\theta) - \frac{H}{4}D^{\alpha_a}(\cos\theta)\right]\right\} \\ &\quad + \frac{Hab\theta}{4h}\psi_a(\Delta T)\left\{E_0[a\theta + H(1-\cos\theta)] + E_1\left[aD^{\alpha_a}(\theta) - HD^{\alpha_a}(\cos\theta)\right]\right\} \end{aligned} \tag{5.19.b}$$

For the beam-column connection, two FEM nodes, i at the beam side and j at the column side, are set as shown in Figure 5.7. Relative rotation of the beam to the column around the joint is $\theta_i - \theta_j$. The restoring force vector $\mathbf{R}(t)$ caused by the dampers at this connection can be written as,

$$\mathbf{R}(t) = \begin{Bmatrix} \cdots \\ F_{x_i} \\ F_{y_i} \\ M_{\theta_i} \\ \cdots \\ F_{x_j} \\ F_{y_j} \\ M_{\theta_j} \\ \cdots \end{Bmatrix} = \begin{Bmatrix} \cdots \\ \sum_{ii=1}^{nn} F_{s_{ii}} \\ \sum_{ii=1}^{nn} F_{a_{ii}} \\ \sum_{ii=1}^{nn} (M_{s_{ii}} + M_{a_{ii}}) \\ \cdots \\ -\sum_{ii=1}^{nn} F_{s_{ii}} \\ -\sum_{ii=1}^{nn} F_{a_{ii}} \\ -\sum_{ii=1}^{nn} (M_{s_{ii}} + M_{ac_{ii}}) \\ \cdots \end{Bmatrix} \qquad nn = \begin{cases} 1 & (one\ damper) \\ or & \\ 2 & (two\ dampers) \end{cases} \tag{5.20}$$

in which, $F_{s_{ii}}$ and $F_{a_{ii}}$ are the forces in horizontal direction and vertical direction respectively induced by the ii-th damper at the joint i, $M_{s_{ii}}$ is the moment around the joint i induced by the shear restoring force of the ii-th damper, $M_{a_{ii}}$ is the moment around joint i induced by the axial restoring force of the ii-th damper and $M_{ac_{ii}}$ is the moment around node j induced by the axial restoring force of the ii-th damper. The term M_{ac} caused by the ii-th damper can be obtained by the following equations,

for the upper damper,

$$M_{ac} = \int_0^a \sigma_x b(\frac{H_2}{2} + x - \frac{H}{2}\theta)dx$$
$$= \frac{a^2 b}{h}\psi_a(\Delta T)\left\{E_0\left[\frac{a\theta}{3} - \frac{H}{4}(1-\cos\theta)\right] + E_1\left[\frac{a}{3}D^{\alpha_a}(\theta) + \frac{H}{4}D^{\alpha_a}(\cos\theta)\right]\right\}$$
$$+ \frac{Hab(H_2 - \theta)}{4h}\psi_a(\Delta T)\left\{E_0[a\theta - H(1-\cos\theta)] + E_1\left[aD^{\alpha_a}(\theta) + HD^{\alpha_a}(\cos\theta)\right]\right\}$$

(5.21.a)

and for the lower damper,

$$M_{ac} = \int_0^a \sigma_x b(\frac{H_2}{2} + x + \frac{H}{2}\theta)dx$$
$$= \frac{a^2 b}{h}\psi_a(\Delta T)\left\{E_0\left[\frac{a\theta}{3} - \frac{H}{4}(1-\cos\theta)\right] + E_1\left[\frac{a}{3}D^{\alpha_a}(\theta) + \frac{H}{4}D^{\alpha_a}(\cos\theta)\right]\right\}$$
$$+ \frac{Hab(H_2 + \theta)}{4h}\psi_a(\Delta T)\left\{E_0[a\theta - H(1-\cos\theta)] + E_1\left[aD^{\alpha_a}(\theta) + HD^{\alpha_a}(\cos\theta)\right]\right\}$$

(5.21.b)

5.3 Response Analysis by Time Domain Method (TDM)

After the viscoelastic damper is treated with one of the above mentioned schemes, the structure can be analyzed with step-by-step integration methods in time domain, which is called in this thesis as time domain method (TDM). The stiffness of damper elements or the restoring force induced by dampers are calculated based on the displacement (u, v, θ) of the nodes, with which the damper is connected, at the end of last time step. The problem here is how to calculate the fractional derivative part in the equations. An approximate method has been derived in the present study and each fractional derivative term can be solved in time domain as follows.

For a derivative term $D^{\alpha}v(t)$, which is written as

$$D^{\alpha}v(t) = \frac{1}{\Gamma(1-\alpha)}\frac{d}{dt}\int_0^t \frac{v(t)}{(t-\tau)^{\alpha}}d\tau \tag{5.22.a}$$

and its equivalent form is

$$D^{\alpha}v(t) = \frac{1}{\Gamma(1-\alpha)}\left[\frac{v(0)}{t^{\alpha}} + \int_0^t \frac{\dot{v}(\tau)}{(t-\tau)^{\alpha}}d\tau\right] \tag{5.22.b}$$

Change of variables in the above integral gives

$$D^{\alpha}v(t) = \frac{1}{\Gamma(1-q)}\left[\frac{v(0)}{t^{\alpha}} + \int_0^t \frac{\dot{v}(t-\tau)}{\tau^{\alpha}}d\tau\right] \tag{5.23}$$

It is noted that the first term is a singular term. However, the system is always assumed to be initially at rest, i.e. $v(0)=0$, so this term vanishes. Since $t=0$ is used as the initial time to determine the responses that follow, rather than a time at which the solution is to be determined, this term will be retained for convenience in the derivation of the linear numerical algorithm.

The integral in Equation (5.23) at $t = n\Delta t$ can be written as

$$\int_0^t \frac{\dot{v}(t-\tau)}{\tau^{\alpha}}d\tau = \sum_{j=0}^{n-1}\int_{j\Delta t}^{(j+1)\Delta t}\frac{\dot{v}(t-\tau)}{\tau^{\alpha}}d\tau \tag{5.24}$$

If $v(t)$ is assumed to be piecewise linear in each subinterval $[j\Delta t, (j+1)\Delta t]$, the velocity term in the subinterval can be approximated by

$$\dot{v}(t-\tau) \approx \frac{v_{n-j} - v_{n-j-1}}{\Delta t} \tag{5.25}$$

where, $j\Delta t \le \tau \le (j+1)\Delta t$.

Hence the linear algorithm for Equation (5.23) is

$$D^{\alpha}v_n = \frac{1}{\Delta t^{\alpha}\Gamma(1-\alpha)}\left\{\frac{v_0}{n^{\alpha}} + \frac{1}{1-\alpha}\sum_{j=0}^{n-1}(v_{n-j} - v_{n-j-1})[(j+1)^{1-\alpha} - j^{1-\alpha}]\right\} \tag{5.26}$$

where, $1 \le j \le n-1$.

For some fractional derivative parts like $D^{\alpha}(v_i - v_j)$ in former equations, it can be separated and written as $D^{\alpha}(v_i - v_j) = D^{\alpha}v_i - D^{\alpha}v_j$. With the fractional derivative parts obtained, response of the structure with viscoelastic dampers can be calculated by the direct integration method at each time step.

5.4 Response Analysis by Hybrid Time-frequency Domain Method

When the equation of motion contains parameters, which might be frequency dependent, such as the stiffness matrix or damping matrix, analysis of the structure by approaches in frequency domain should be much superior to approaches in time domain. For analysis of structures incorporated with viscoelastic dampers, an approach namely hybrid time-frequency domain method (HTFDM) has been developed with the application of the FFT technique and numerical procedures have been established for evaluating the response of structures subject to arbitrary loading in this section.

The HTFDM involves superposition of the effects on coordinate j of a load acting at coordinate i and in this case both the load and the response are harmonic. Assuming the loading is a force vector $p(t)$ having all zero components except the i-th term which is a harmonic loading, $p_i(t) = A\exp(j\omega t)$, where j in the bracket is imaginary unit, $j = \sqrt{-1}$. The steady-state response of the i-th

component of the displacement vector $x(t)$ will be $AH_{ij}(\omega)\exp(j\omega t)$, in which $H_{ij}(\omega)$ is defined as the frequency response transfer function.

If the loading in coordinate i is a general time varying load $p_i(t)$ like wind, earthquake or other stochastic loading rather than a harmonic loading, the forced vibration response in coordinate j can be obtained by superposing the effects of all the harmonics contained in $p_i(t)$. For this purpose, the time domain expression of the loading can be obtained by Fourier transformation,

$$p_i(\omega) = \int_{-\infty}^{\infty} p_i(t)\exp(-j\omega t)dt \tag{5.27}$$

and then by inverse Fourier transformation, the responses to all of these harmonics can be combined to obtain the total structural response by the force in coordinate j as follows,

$$x_{ij}(t) = \frac{1}{2\pi}\int_{-\infty}^{\infty} H_{ij}(\omega)p_i(\omega)\exp(j\omega t)d\omega \tag{5.28}$$

Then the total response in coordinate j produced by a general loading involving all components of the load vector $\mathbf{P}(t)$ can be obtained by superposing the contributions from all the load components,

$$x_j(t) = \frac{1}{2\pi}\sum_{i=1}^{N}\left[\int_{-\infty}^{\infty} H_{ij}(\omega)P_i(\omega)\exp(j\omega t)d\omega\right] \quad j = 1, 2, \ldots, N \tag{5.29}$$

With all transfer functions $H_{ij}(\omega)$ being obtained, the response vector $\mathbf{X}(\omega)$ can be easily obtained by

$$\mathbf{X}(\omega) = \mathbf{H}(\omega)\mathbf{P}(\omega) \tag{5.30}$$

where, $\mathbf{H}(\omega)$ is the N×N frequency response transfer matrix.

$$\mathbf{H}(\omega)=\begin{bmatrix} H_{11}(\omega) & H_{12}(\omega) & \cdots & H_{1N}(\omega) \\ H_{21}(\omega) & H_{22}(\omega) & \cdots & H_{2N}(\omega) \\ \vdots & \vdots & \vdots & \vdots \\ H_{N1}(\omega) & H_{N2}(\omega) & \cdots & H_{NN}(\omega) \end{bmatrix} \tag{5.31}$$

obtained for each frequency required in the response analysis. Once this frequency response transfer matrix has been obtained, the responses of the system under multiple sets of loading can be obtained. When vector $X(\omega)$ for each set is determined, inverse FFT procedure can be applied to obtain the corresponding set of displacement vector X(t).

Fourier transformation of the equation (5.3) for a general multi-degree-of-freedom system with viscoelastic dampers can be written as:

$$-\omega^2\mathbf{M}\mathbf{X}(\omega)+j\omega\mathbf{C}\mathbf{X}(\omega)+\mathbf{K}^S\mathbf{X}(\omega)+\mathbf{K}^D(\omega)\mathbf{X}(\omega)=\mathbf{P}(\omega) \tag{5.32.a}$$

$$-\omega^2\mathbf{M}\mathbf{X}(\omega)+j\omega\mathbf{C}\mathbf{X}(\omega)+\mathbf{K}^S\mathbf{X}(\omega)+\mathbf{R}(\omega)=\mathbf{P}(\omega) \tag{5.32.b}$$

When a damper supplies restoring force to the FEM node directly, $\mathbf{K}^D(\omega)\mathbf{X}(\omega)=\mathbf{R}(\omega)$, the above two equations for different damper modelling schemes are basically the same. The following procedures are based on (5.32.b).

Assuming a damper is incorporated between coordinate i and coordinate j, the shear restoring force vector can be written as,

$$\mathbf{R}(\omega)=\left[0,0,\cdots,0,r_i(\omega),0,\cdots,0,r_j(\omega),0,0\right]^T \tag{5.33}$$

in which,

$$r_i(\omega)=\frac{A_r}{h}\psi(\Delta T)\left[G_0+G_1(j\omega)^{\alpha}\right]\left[x_i(\omega)-x_j(\omega)\right] \tag{5.34.a}$$

$$r_j(\omega) = \frac{A_r}{h}\psi(\Delta T)\left[G_0 + G_1(j\omega)^{\alpha}\right]\left[x_j(\omega) - x_i(\omega)\right] \tag{5.34.b}$$

With consideration of the damper positions, the restoring force vector can be written as,

$$\mathbf{R}(\omega) = \frac{A_r}{h}\psi(\Delta T)\left[G_0 + G_1(j\omega)^{\alpha}\right]\mathbf{I}_v\mathbf{X}(\omega) \tag{5.35}$$

where, $\mathbf{I}_v$ is damper position matrix, it can be denoted as

$$\mathbf{I}_v = \begin{bmatrix} 0 & \cdots & 0 & \cdots & 0 & \cdots & 0 \\ \cdots & \cdots & \cdots & \cdots & \cdots & \cdots & \cdots \\ 0 & \cdots & 1 & \cdots & -1 & \cdots & 0 \\ \cdots & \cdots & \cdots & \cdots & \cdots & \cdots & \cdots \\ 0 & \cdots & -1 & \cdots & 1 & \cdots & 0 \\ \cdots & \cdots & \cdots & \cdots & \cdots & \cdots & \cdots \\ 0 & \cdots & 0 & \cdots & 0 & \cdots & 0 \end{bmatrix}_{n\times n} \begin{matrix} \\ \\ i \\ \\ j \\ \\ \end{matrix} \tag{5.36}$$

$$\begin{matrix} & & i & & j & & \end{matrix}$$

Therefore, the matrix equation of the motion can be given by

$$\left[-\omega^2\mathbf{M} + (j\omega)\mathbf{C} + \mathbf{K}^S + \frac{A_r\psi(\Delta T)}{h}(G_0 + G_1 j^{\alpha}\omega^{\alpha})\mathbf{I}_v\right]\mathbf{X}(\omega) = \mathbf{P}(\omega) \tag{5.37}$$

Symbolically, it may be written as

$$\bar{\mathbf{I}}(\omega)\mathbf{X}(\omega) = \mathbf{F}(\omega) \tag{5.38}$$

where,

$$\bar{\mathbf{I}}(\omega) = \left[-\omega^2\mathbf{M} + (j\omega)\mathbf{C} + \mathbf{K}^S + \frac{A_r\psi(\Delta T)}{h}(G_0 + G_1 j^{\alpha}\omega^{\alpha})\mathbf{I}_v\right] \tag{5.39}$$

If different kinds of dampers are installed in a structure with different installation methods, the last term of equation (5.39) should be obtained by superposition of the contribution of each damper.

Hence, the response vector $\mathbf{X}(\omega)$ can be obtained by

$$\mathbf{X}(\omega) = \bar{\mathbf{I}}(\omega)^{-1}\mathbf{F}(\omega) \tag{5.40}$$

which is the same as Equation (5.30). In the associated program, to get the transfer matrix $\bar{\mathbf{I}}(\omega)^{-1}$, a complex inverse matrix sub-program, which satisfies $\bar{\mathbf{I}}(\omega)\bar{\mathbf{I}}(\omega)^{-1} = \mathbf{I}_0$, has been developed, where $\mathbf{I}_0$ is a unit N×N matrix.

With the obtained $\mathbf{X}(\omega)$, response $\mathbf{X}(t)$ in time domain can be calculated by inverse FFT. Consequently, $\dot{\mathbf{X}}(t)$ and $\ddot{\mathbf{X}}(t)$ can be determined as well.

This method is a general method not only suitable for structures with viscoelastic dampers, but also for normal structures or structures with other additional components if the mathematical model for the components is provided. For normal structures without damper, the damper position matrix $\mathbf{I}_v$ is zero and $\bar{\mathbf{I}}(\omega)$ is only needed to be calculated by the first three terms on the right side of Equation (5.39). If this method is used for structures with other components, only the restoring force term in $\bar{\mathbf{I}}(\omega)$ should be modified.

5.5 Comparison of TDM and HTFDM for Response Analysis

Both analytical methods have their advantages and disadvantages. The response analysis by the TDM can give the response of the structure step by step during calculation. By the TDM, the whole set of equilibrium equations should be solved in each time step. However, the set of equations is only needed to be solved once for the whole calculation process if the HTFDM is applied. Therefore it is obvious that much greater efficiency can be achieved in terms of computational effort if the HTFDM is applied for structures with viscoelastic dampers which are

represented by sophisticated mathematical models like the IFDM. Time consumption comparison will be made between the TDM and the HTFDM in Chapter Six and Chapter Seven.

Depending on the nonlinearity of the structure system and the excitation condition, the HTFDM may also achieve better accuracy than the TDM. For solving the problem with the IFDM, Equation (5.26) is an approximate method and the accumulated errors will affect the accuracy of the results greatly. Moreover, analysis results by the TDM are concerned with the original conditions, and the actual value of which is hard to be determined, so normally the original shear displacement of the dampers are assumed to be zero. This difficulty can also be overcome by the HTFDM.

5.6 Equivalent Stiffness and Damping Matrix

Equivalent stiffness and damping of a structure with viscoelastic dampers have been used for analysis by many researchers. Normally it is hard to determine the values of them. As an additional result of the analytical method developed above, equivalent stiffness and damping matrices can be derived. For the equilibrium equations of a structure with viscoelastic dampers, effect of the dampers can be represented by an additional damping term and an additional stiffness term if the mathematical model for viscoelastic dampers is related to displacement and velocity, which can be written as,

$$\mathbf{M}\ddot{\mathbf{X}}(t)+\mathbf{C}\dot{\mathbf{X}}(t)+\mathbf{K}\mathbf{X}(t)+\tilde{\mathbf{C}}\dot{\mathbf{X}}(t)+\tilde{\mathbf{K}}\mathbf{X}(t)=\mathbf{P}(t) \tag{5.41}$$

For example, if the damper is described by Kelvin-Voigt model, the restoring forces of a damper connected with coordinate i and j are,

$$R_i(t) = GA_r \frac{x_i(t) - x_j(t)}{h} + \eta A_r \frac{\dot{x}_i(t) - \dot{x}_j(t)}{h} \tag{5.42.a}$$

$$R_j(t) = GA_r \frac{x_j(t) - x_i(t)}{h} + \eta A_r \frac{\dot{x}_j(t) - \dot{x}_i(t)}{h} \tag{5.42.b}$$

Then the additional stiffness and damping matrix can be written as

$$\tilde{\mathbf{K}} = \frac{GA_r}{h}\mathbf{I_p} \tag{5.43}$$

$$\tilde{\mathbf{C}} = \frac{\eta A_r}{h}\mathbf{I_p} \tag{5.44}$$

where, $\mathbf{I_p}$ is the matrix of damper positions.

They are constant matrices when the damper positions are defined.

Then the equilibrium equation can be re-written as,

$$\mathbf{M}\ddot{\mathbf{X}}(t) + \hat{\mathbf{C}}\dot{\mathbf{X}}(t) + \hat{\mathbf{K}}\mathbf{X}(t) = \mathbf{P}(t) \tag{5.45}$$

where,

$$\hat{\mathbf{C}} = \mathbf{C} + \tilde{\mathbf{C}} \text{ and } \hat{\mathbf{K}} = \mathbf{K} + \tilde{\mathbf{K}} \tag{5.46}$$

The revised stiffness matrix $\hat{\mathbf{K}}$ and damping matrix $\hat{\mathbf{C}}$ can be called as equivalent stiffness matrix and equivalent damping matrix of the structure. When the equivalent matrices of stiffness and damping are obtained, for a structure incorporated with viscoelastic dampers, it can be analyzed as a normal structure without any difficulties.

But when the IFDM is used to represent the viscoelastic dampers, the restoring force vector can not be separated directly into two parts of which one is related to shear displacement and the other is related to shear velocity in time domain. If the

equivalent stiffness matrix and damping matrix are needed to be obtained here, the additional stiffness matrix of a structure with a damper can be written as

$$\tilde{\mathbf{K}} = \frac{A_r \psi(\Delta T)}{h}[G_0 + G_1 S_k(t)]\mathbf{I_p} \tag{5.47}$$

And the additional damping matrix is

$$\tilde{\mathbf{C}} = \frac{G_1 A_r \psi(\Delta T)}{h} S_c(t)\mathbf{I_p} \tag{5.48}$$

where, $S_k(t)$ and $S_c(t)$ are functions which have relation with shear displacement and shear velocity. They are more complicated than those obtained with the Kelvin-Voigt model. From equation (5.26), it can be seen that they are not only related to the shear displacement of the damper, but also to the damper's past history, the working history of the damper.

However, if considering this problem in frequency domain, the additional equivalent stiffness matrix and damping matrix at different frequencies can be obtained conveniently as

$$\tilde{\mathbf{K}} = \frac{A_r \psi(\Delta T)(G_0 + G_1 \omega^{\alpha} \cos\frac{\pi\alpha}{2})}{h}\mathbf{I_p} \tag{5.49}$$

$$\tilde{\mathbf{C}} = \frac{A_r \psi(\Delta T) G_1 \omega^{\alpha} \sin\frac{\pi\alpha}{2}}{h}\mathbf{I_p} \tag{5.50}$$

If more than one damper is used in the structure, the equivalent matrices can be obtained in the same way by superposition of the additional matrices for each damper.

5.7 Discussions and Conclusions

Viscoelastic dampers can be installed in a structure by different measures and at different locations. Two kinds of modelling schemes for viscoelastic dampers incorporated in structures have been proposed according to their methods of installation. To determine the structural response, analytical methods in time domain (TDM) and in hybrid time-frequency domain (HTFDM) have been developed. The advantages and disadvantages of these two methods have been discussed. And a powerful associated program based on the proposed methods has been developed. Different damper schemes for modelling viscoelastic dampers and different analytical methods are all covered by the program. The structure of the program is shown in Figure 5.8, in which, the dot line is the running path when the dampers are treated as elements. The main program and some important sub-programs are illustrated by diagrams as shown in Figure 5.9, Figure 5.10, Figure 5.11 and Figure 5.12. The sub-program HTFDM and some other related sub-programs are listed in Appendix 5.

Although both modelling schemes are suitable for most applications, computing time is different in response analysis by linear acceleration method in time domain. For dampers being treated as elements, number of FEM nodes of a structure does not change when dampers are installed, the dimension of the stiffness matrix always keeps the same. But since the stiffness matrix varies at each time step, the inverse matrix of the effective stiffness should be calculated at each time step for the solution of the equations. However, for dampers being treated as supports, stiffness matrix of the structure with dampers is the same as that of the structure without damper, and the effective stiffness does not change

with time, its inverse matrix only need to be calculated once. The calculation time for the remainder work is nearly the same for both methods. Therefore, it is better to consider a damper as a support whenever it is appropriate.

The equivalent stiffness matrix and damping matrix of structures with viscoelastic dampers, which are commonly used by normal structural analysis software, have been derived by the proposed analytical method for those cases with sophisticated mathematical model for viscoelastic dampers. It is of much value to all those commercial software packages commonly used to carry out dynamic analysis.

5.8 References

Cameron Timonthy M. (1988), A New Method for Calculating the Steady-state Response of Nonlinear Dynamic Systems with Application to Design Optimization of Friction Dampers, Pittsburgh, Pennsylvania.

Chan Q. and Zhu D. M. (1989), Dynamic Analysis of Viscoelastic Structures, Journal of Vibration Engineering, Vol.2, No.3, pp.42-52. (In Chinese)

Chang K. C. (1993), Seismic Performance and Design of Steel Structures with Added Viscoelastic Dampers, The Fourth East-Pacific Conference on Structural Engineering & Construction, pp.1919-1924, Seoul, Korea.

Clough Ray W., Penzien Joseph (1993), Dynamics of Structures, McGraw-Hill, Inc., London.

Hu B-G, Dokainish M. A. and Mansour W. M. (1995), A Modified MSE Method for Viscoelastic Systems: A Weighted Stiffness Matrix Approach, J. Vibration and Acoustics, Vol. 117, no. 4, pp. 226-231.

Kasai Kazuhiko and Fu Yaomin (1995), Seismic Analysis and Design Using Viscoelastic Dampers, A New Direction in Seismic Design, Tokyo, pp113-140.

Tan X. M., Ko J. M. and Fang E. H. (1995), Experimental and Analytical Study on A Framed Structure Incorporated with Viscoelastic Dampers, Conference of SDVNC'95, pp.301~306, Hong Kong.

Tan X. M., Ko J. M. and Fang E. H. (1996), Dynamic Analysis of a Beam-Column Connection Incorporated with Viscoelastic Dampers, Asia-Pacific Conference on Shell and Spatial Structures, Beijing.

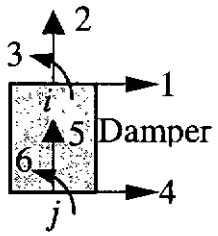

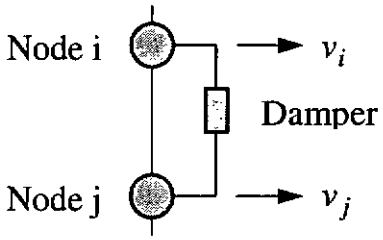

Figure 5.1 Displacement coordinates **Figure 5.2 A damper between two nodes**

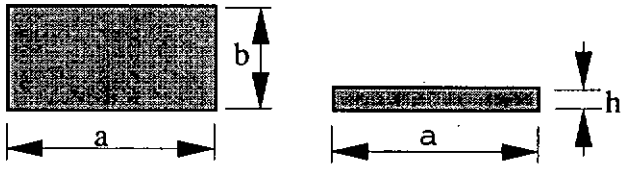

Figure 5.3 Dimensions of the damper

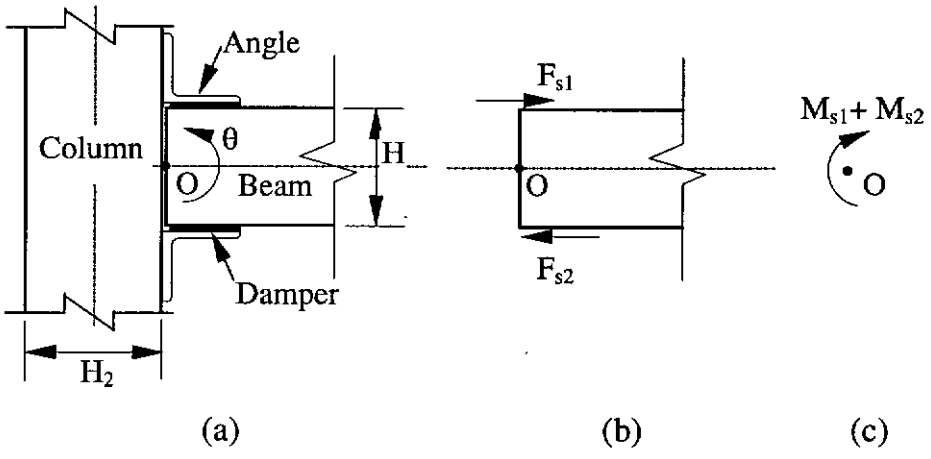

Figure 5.4 Effect of the shear restoring force of viscoelastic dampers

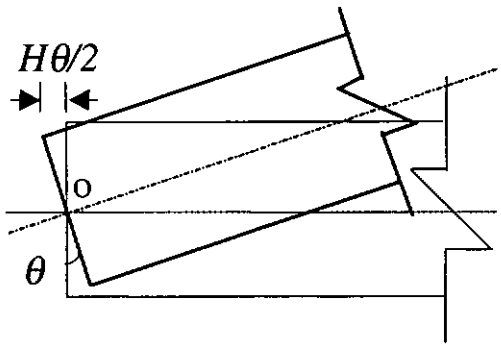

Figure 5.5 Illustration of beam rotation around point o

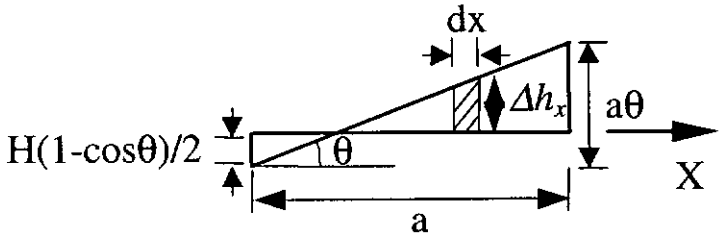

(a) Axial deformation of the damper on the upper flange

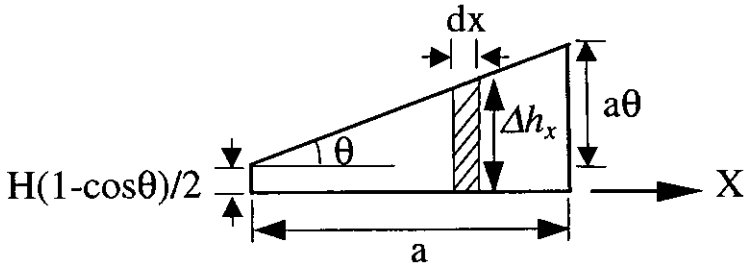

(b) Axial deformation of the damper on the lower flange

Figure 5.6 Distribution of axial deformation of the damper

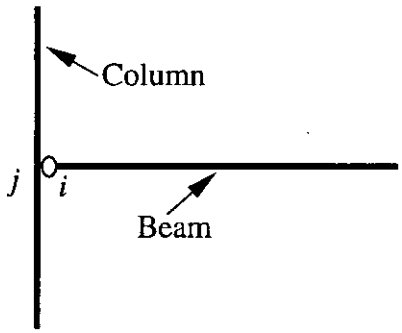

Figure 5.7 Node codes at the joint for FEM

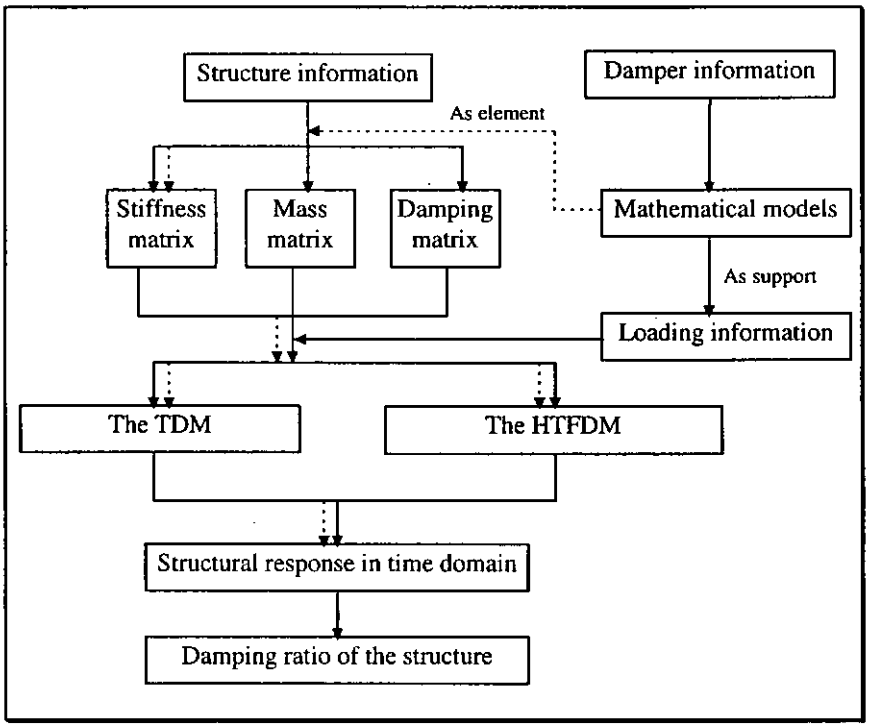

Figure 5.8 Structure of the computing program

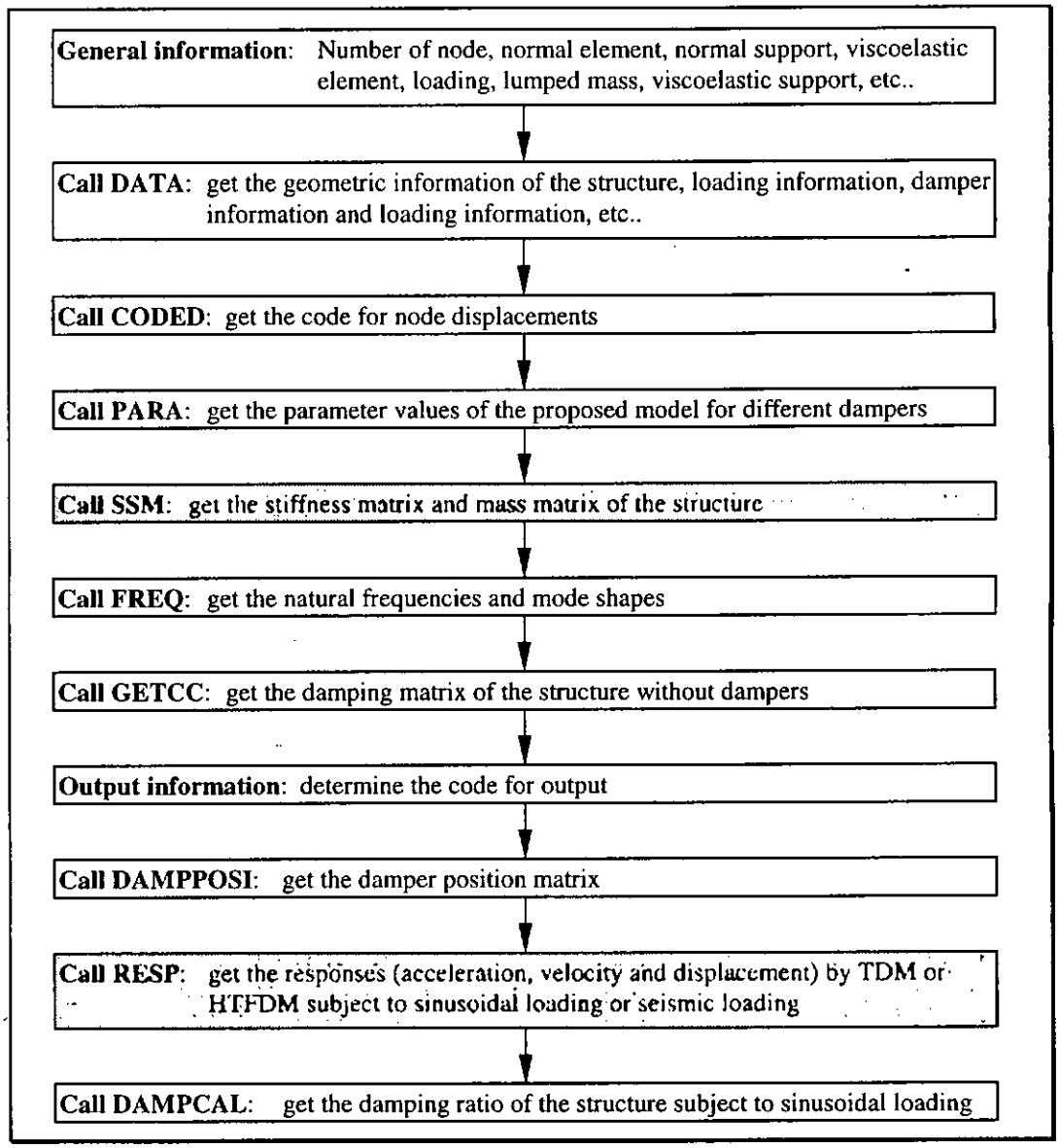

Figure 5.9 Diagram of the main program

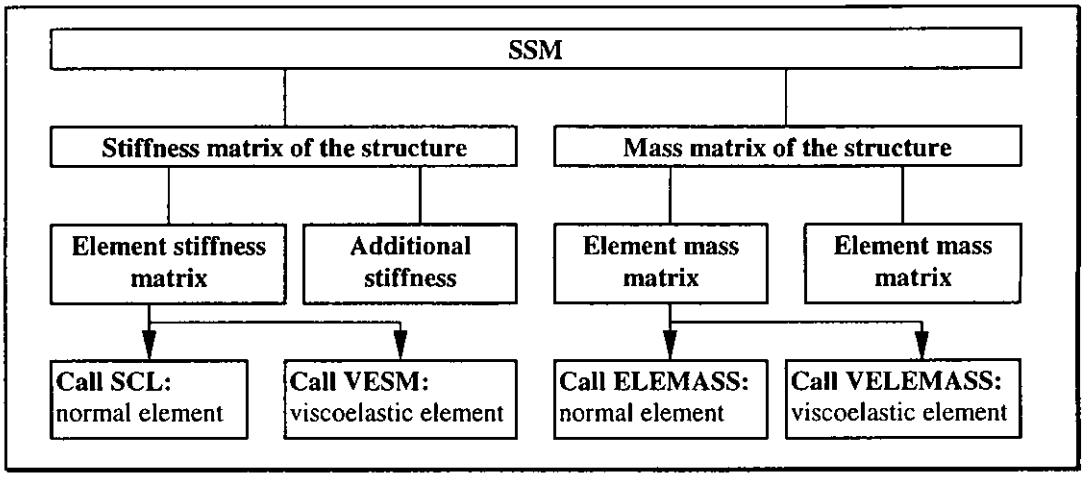

Figure 5.10 Diagram of the sub-program SSM

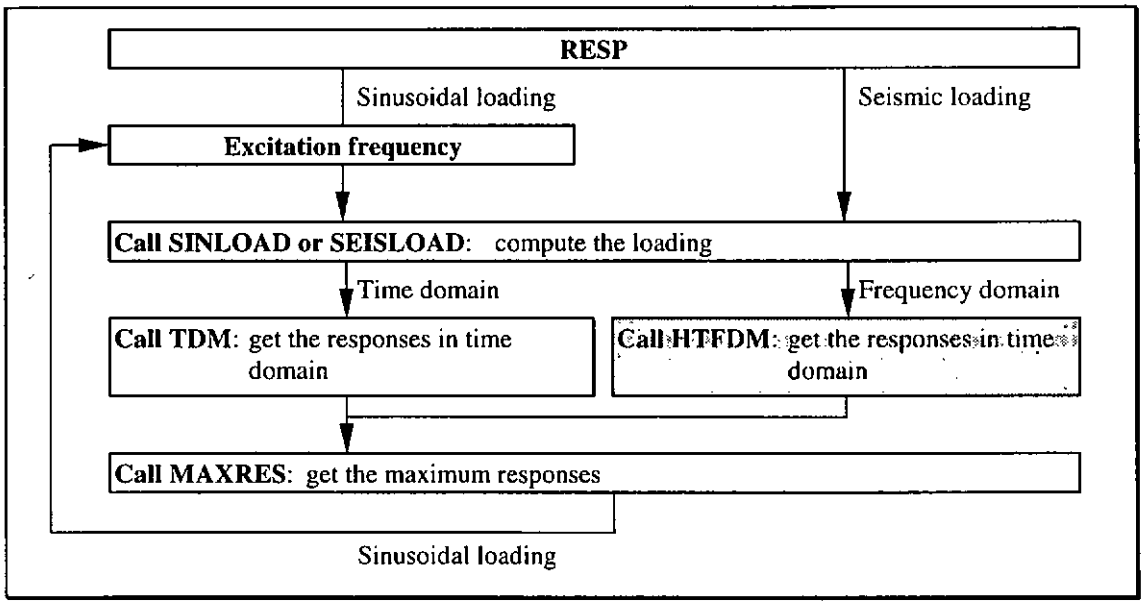

Figure 5.11 Diagram of the sub-program RESP

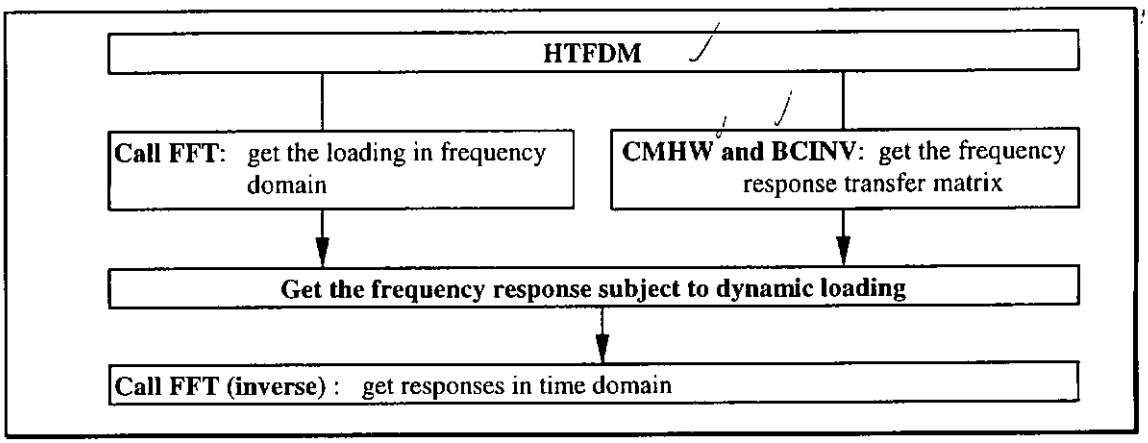

Figure 5.12 Diagram of the sub-program HTFDM

CHAPTER 6

CONTROL OF HORIZONTAL VIBRATION FOR FRAMED STRUCTURES

6.1 Introduction

Horizontal vibrations of building structures are always induced by wind or earthquake. It is the main problem to be solved for tall buildings, especially for those in seismic areas and seaside cities subject to typhoon attack (Davenport A.G., 1986; Davenport A.G., 1991). During past years, a lot of research work has been done on structures incorporated with viscoelastic damping devices to suppress such vibrations. When a building structure is excited by dynamic loading, story shifts will occur. Viscoelastic damping devices are mostly installed between neighboring stories to attenuate the story shifts of building structures. They can be incorporated in structures in different ways as shown in Figure 6.1. Dynamic behaviour of structures with viscoelastic damping devices connecting two members in one diagonal direction as shown in Figure 6.1(a) has been studied by Chang K. C. et al (1995) and Ito Yoshio et al (1995). Research work on structures with two inclined members incorporated with viscoelastic damping devices at each story as shown in Figure 6.1(b) has been done by Kasai Kazuhiko et al (1994). Studies on structures with high damping devices such as friction, yielding steel and fluid viscous dampers installed between the braced structure and the upper floor or installed in the bracing system as shown in Figure 6.1(c) and Figure 6.1(d) respectively have been carried out by Niwa Naoki et al (1995) and Constantinou M. C., (1994). Effectiveness in vibration control for structures with these kinds of damping devices has been evaluated.

It has been found by experimental work in Chapter Three that viscoelastic damper ZJD-1 has good energy dissipation ability. If this kind of damper is installed in structures, it is expected that it would be effective in controlling vibration. In the present study, a damping device has been designed and installed in a framed structure. The effectiveness in vibration control of a framed structure with such a damping device has been studied by dynamic tests. The structure has also been analyzed by the developed method in Chapter Five and the comparison of experimental and analytical results has been made.

Dynamic behaviour of structures incorporated with viscoelastic dampers vary with many factors such as properties of the structure, damper material, damper size, damper area and loading conditions, etc.. Constrained by the test conditions, dynamic tests can only be carried out with limited changes of parameters. Comprehensive parametric studies have been performed to give some guidelines on design of vibration control either for the retrofit of old buildings or for the design of new buildings (Maison Bruce F., 1994). With the proposed analytical method which has been proved to be accurate enough to predict the response of structures with viscoelastic dampers, a four-story building have been studied by varying the design parameters and some useful conclusions have been drawn.

6.2 Description of Test set-up

A viscoelastic damper ZJD-1 stuck by glue with metal plates on both sides is fixed by inner bolts to two 10mm thick steel plates whose mass is 5.706Kg each as shown in Figure 6.2 and then connected with a braced structure by bolts to form the damping device. The braced structure is made up of 102×51 Channels.

The damping device is installed in a single story frame. The frame is constructed by members of standard 102×64 JOISTS. All the column-bases and member connections are fully welded. The elevation of the frame with damping device can be seen in Figure 6.3. And the appearance of the frame can be seen in Photo 6.1.

An exciter is applied to excite the frame in horizontal direction through a force transducer. The excitation signal is supplied by a sine random generator via a power amplifier and then sent to the exciter, which harmonically drives the frame at beam level in the direction of beam axis. Eight accelerometers are located at positions (CH1 to CH8 in Figure 6.3) along the right column to measure their responses. When the dynamic test is performed, excitation force and responses can be gathered by the DTAS (Dynamic Test and Analysis System) developed by the Research Institute of Nanjing Aeronautical Institute (1992). The set-up of the whole test system can be seen in Figure 6.4.

6.3 Experimental Test

Firstly, the frame is knocked by a hammer or excited by random excitation with white-noise signal. The first natural frequency of the frame can be obtained from the response in frequency domain processed by the DTAS software. Then the frequency step for tests with sinusoidal loading at different frequency range can be determined according to the natural frequency. For frequency range far away from the natural frequency, step can be set very large such as 5Hz to 10Hz, and for frequency range near the natural frequency, step should be set very small like 0.05Hz. At each excitation frequency, while keeping the amplitude of the

sinusoidal loading at a certain value with the assistance of the digital oscilloscope, responses of the points along the column can be collected with proper parameter setting of the DTAS. To improve the resolution of the response spectrum, time length is set long enough for gathering large amount of data in each group. In order to keep the precision of test data, response range is auto-regulated before data being collected. The maximum responses of the frame under cyclic loading at each excitation frequency can be obtained by the DTAS system.

6.4 Effectiveness in Horizontal Vibration Control

From the hammer tests, it can be observed that the response of the frame can be suppressed greatly by adding a viscoelastic damper. And vibration of the frame with a damper decreases very quickly, while that of the frame without damper lasts for a long time. The first resonant frequency of the frame without damping device is 41.5Hz, and it changes to 39.28Hz when the damping device is installed in the frame system. The decreasing is due to the mass of the steel plates of the damping device.

The maximum accelerations at different positions on the column of the frame without damper under sinusoidal loading with amplitude of 10N at various frequencies are shown in Figure 6.5. And those of the frame with dampers are shown in Figure 6.6. Comparing these two figures, it can be found that great effectiveness in vibration control can be achieved by the designed damping device. The maximum response at node A of the frame with the damping device under excitation at the resonant frequency is 20.13m/s^2 and that of the frame

without a damper is 144.145m/s^2. The great difference in acceleration at node A is demonstrated in Figure 6.7. Obviously, the damper is effective in attenuating response of the whole structure. The maximum resonant accelerations of the eight positions along the column of the frame with and without damper are presented in Figure 6.8, which shows the first mode of the frame. Effectiveness can also be embodied by damping ratio. Damping ratios of the frame with and without damping device have been calculated by half-band method from test data to be 0.56% and 0.27%, respectively.

6.5 Comparison of Experimental and Analytical Results

The tested frame incorporated with and without a viscoelastic damper have both been analyzed by the methods TDM and HTFDM proposed in Chapter 5 under the same conditions as those of the tests. The damper in the frame is considered as a viscoelastic damper element for analysis by the TDM and as a viscoelastic support by the HTFDM.

Table 6.1 Discretization of the framed structure for FEM analysis

Nodes		Elements	
1 : Point D	6 : Point F	1 : DC	6 : GH
2 : Point C	7 : Point G	2 : CB	7 : HI
3 : Point B	8 : Point H	3 : BA	8 : IJ
4 : Point A	9 : Point I	4 : AE	9 : BH*
5 : Point E	10: Point J	5 : FG	

Atten: when the damper is considered as a support, the 9th element does not exist.

Responses at any point of the frame can be obtained by finite element analysis with proper discretization of the structure. To determine the responses at point A

at the beam level of the frame, discretization of the structure is made as shown in Table 6.1. Maximum accelerations at the beam level of the frame without damper under different excitation frequencies by the TDM and the HTFDM are compared with the experimental values in Figure 6.9. Maximum accelerations at the beam level of the frame with damper under different excitation frequency by both analytical methods are compared with those of the experimental values in Figure 6.10. It can be seen that both the two analytical methods can well predict the dynamic response of the frame with and without viscoelastic damper. However, discrepancy exists between the experimental results and the analytical results. The causes for the discrepancy are two folds, firstly, the damping ratio of the tested structure is not exactly proportional, which leads to the error in the analytical results, secondly, the precision of the instruments and environmental disturbance results in the error of the experimental results.

From the figures, it can be found that the analytical curve by the HTFDM is closer to the experimental curve than that determined by the TDM no matter whether the viscoelastic damper is incorporated in the framed structure or not. The difference between the two analytical methods can also be expressed by damping ratio. The damping ratio of the frame without and with a damper calculated by the TDM are 0.275% and 0.586%, respectively while those calculated by the HTFDM are 0.273% and 0.572%. The experimental results are 0.27% and 0.56%, respectively. It can be seen that damping ratios calculated by the HTFDM are closer to the experimental results than those calculated by the TDM. Computing time of the TDM and the HTFDM for the same task has also been compared. For the frame incorporated with damper, to get the stable responses of the structure under excitation frequency which is close to the

resonant frequency, responses in more than one period should be computed by the TDM and the time step should be small enough. However, responses of the structure could be obtained by HTFDM in one period only. To calculate the response of the frame with damper for each excitation frequency by Pentium 100MHz/16M, only about 1.82 seconds are needed by the HTFDM while nearly 63.99 seconds are needed by the TDM. Therefore, to analyze a structure with viscoelastic dampers, great amount of computing time will be saved if the HTFDM is applied.

6.6 Parametric Studies on Framed Structures

Experimental and analytical results of the framed structure have given us the idea that the viscoelastic damping device is capable of reducing vibration of the tested frame in horizontal direction and enhance the damping ratio of the framed structure. The effectiveness in vibration control is affected by many factors, such as the properties of the braced structure, damper material, damper dimensions, damper location and loading conditions, etc.. Comparisons of experimental and analytical results have proved that the analytical methods can well predict responses of structures with the designed damping devices. The influence caused by various factors can be evaluated by the HTFDM. Parametric studies on the tested frame have been performed. Since the proposed damping device is intended to be designed for full-scaled framed building structures, whose characteristics such as stiffness and mass are different from the tested frame, parametric studies have also been carried out on a four-story real building structure. Because both the results obtained from the studies by changing

parameters like damper material, damper dimension, loading condition and temperature give the same trends, it is believed that the proposed method is accurate enough to predict the dynamic behaviours of the full-scaled structures and the parametric studies based on the four-story building structure would be useful for developing some guidelines for practical design in vibration control. The work introduced in the following sub-sections are based on the studies on the latter one.

The four-story building structure model is built based on the information provided by the book "Design of Structural Steelwork" (Bates W., 1975). Properties of the structure are listed briefly in Table 6.2. The resonant frequencies of the structure are 5.80Hz, 17.18Hz, and 36.37Hz. Referred to "Vibration of Building Structures" (Wang G. Y., 1978), damping ratio of the structure before dampers being incorporated in is assumed to be 1.0%. Dampers are installed in the same way as illustrated in the experimental test.

Table 6.2 Properties of the building structure

Story	Story height (m)	Mass (kg)	Shear stiffness (N/m)
1	4.5	700000	4905283424.0.
2	4.0	650000	6984280500.0
3	4.0	650000	6984280500.0
4	3.5	350000	10425514915.0

For parametric studies in the following sub-sections, parameters except those to be studied are set as follows. For the wind effect, a sinusoidal force with amplitude of 5000N is assumed to act at the roof level of the building. In practical application, different kinds of damper can be chosen for controlling the vibration of structures. Referring to the dampers supplied by 3M corporation (Soong T. T., 1997), a kind of viscoelastic dampers with parameters $G_0 = 0.6$,

$G_1 = 0.07$ and $\alpha = 1.02$ is assumed to be applied in the building at the environmental temperature of 25°C, the thickness of the damper is 4mm and the area of the damper for each story is $80A_0$ ($A_0 = 10800\,\text{mm}^2$).

Responses such as acceleration, velocity and displacement have all been calculated for the parametric studies. Although the scales of them may be different, their changing trends are similar, in the following sections, studies are concentrated on acceleration.

6.6.1 Variation of brace stiffness

The ratio (R_{bd}) of shear stiffness of the brace to equivalent shear stiffness of the damper is one of the main factors affecting the capability of energy dissipation. When dampers are installed between two neighboring stories of a building structure with the support of braces, if the braced structure is too flexible, much of the relative displacement between stories will be attributed to the braced structure, which results in little deformation in the damper. Thus the damper can not function effectively. But making the brace too rigid will be more costly. In this sub-section, the effect of R_{bd} is studied. Since the equivalent stiffness of a damper changes with the excitation frequency and the environmental temperature, the value of the equivalent stiffness under excitation at the first resonant frequency of the structure and at temperature of 25°C is applied to determine the ratio R_{bd} in the present study. When R_{bd} is changed from 0.0 to ∞, responses at the roof level of the building structure under different excitation frequencies have been calculated. The maximum acceleration curves are shown in Figure 6.11. And the maximum resonant accelerations are shown in Figure

6.12. It is not difficult to find that the maximum resonant acceleration decreases with the stiffness ratio. When R_{bd} is small, the damper does not function effectively and change of the stiffness ratio will affect the effectiveness greatly. However, when the ratio is large enough, the effectiveness will gradually tend to the maximum and any increase in the brace stiffness will no longer have much effect on the effectiveness. It is also found that the resonant frequency of the structure increases with the stiffness ratio, which can be seen in Figure 6.13. Since equivalent stiffness of the dampers is much less than the stiffness of the building structure, the change of resonant frequency caused by the change of R_{bd} is very small.

Table 6.3 Damping ratios of the building structure with brace of different stiffness

Stiffness ratio R_{bd}	Damping ratio (%)	Stiffness ratio R_{bd}	Damping ratio (%)
0.00	1.002	8.00	2.065
0.50	1.397	16.00	2.132
1.00	1.590	32.00	2.168
2.00	1.791	∞	2.208
4.00	1.960		

The damping ratio of the structure can also demonstrate the influence of the stiffness ratio on the effectiveness in vibration control. The damping ratios of the building structure with brace of different stiffness ratio have been calculated and are listed in Table 6.3. The trend of change of the damping ratio with R_{bd} is shown in Figure 6.14. It can be seen that when the stiffness ratio is small, the damping ratio increases rapidly with the stiffness ratio. When R_{bd} is large

enough, however, the damping ratio of the structure increases very slightly with the stiffness ratio.

The stiffness ratios of the similar damping devices were set to values larger than 10.0 in the examples given in the papers written by some former researchers (Kirekawa A. et al, 1992; Kasai Kazuhiko et al, 1995), for the present study, it can be seen that they are large enough for the dampers to function effectively. In practical design, when a certain kind of damper is chosen to be installed in a structure, the structural properties of the brace should be chosen carefully to make the stiffness suitable for the dampers to take effect. In the following parametric studies, R_{bd} is assumed to be large enough to facilitate the damping device to function in its maximum capacity.

6.6.2 Variation of damper material

Different kinds of damper have different energy dissipation ability and equivalent stiffness. In applying dampers to a structure, the objective is to increase the damping ratio of the structure as much as possible while keeping the change of the natural frequency as small as possible. Therefore, in this section, loss modulus of a damper at a certain condition is varied from 0.25~2.0 of that of the selected damper by changing the parameter G_1 of the IFDM.

Responses of the building with dampers of different parameter G_1 under cyclic loading at different excitation frequencies have been calculated. Maximum accelerations at the roof level of the building structure with dampers of different kinds under dynamic loading at different excitation frequencies are shown in Figure 6.15. The maximum resonant accelerations at the roof level of the building

are shown in Figure 6.16. It is obvious that when the loss modulus of the dampers increases, the maximum resonant acceleration decreases and the damping ratio increases. Damping ratios of the building structure with dampers of different kinds have been calculated and listed in Table 6.4. It can be seen obviously from Figure 6.17 that the damping ratio at the first natural frequency increases with the loss modulus of the dampers.

Table 6.4 Damping ratios of the building with dampers of different parameter G_1

$G_1/G_{1\,(Original)}$	Damping ratio (%)	$G_1/G_{1\,(Original)}$	Damping ratio (%)
0.25	1.299	1.25	2.539
0.50	1.591	1.50	2.89
0.75	1.893	1.75	3.257
1.00	2.208	2.00	3.648

6.6.3 Variation of damper dimension

6.6.3.1 Variation of damper area

Damper area is a main factor for vibration control of a structure with viscoelastic dampers. Dampers with area of $20A_0$, $40A_0$, $60A_0$, $80A_0$ and $100A_0$ are assumed to be incorporated in each story of the building respectively for the purpose of investigating the effect of damper area on the dynamic response. With loading at the roof level, responses of the building structure have been calculated. Curves for maximum acceleration at the roof level of the building with dampers of different areas and subject to cyclic loading of different excitation frequencies are plotted in Figure 6.18. The maximum resonant accelerations are shown in Figure 6.19. It can be seen that when damper area increases, resonant acceleration of the frame decreases greatly. The maximum resonant acceleration decreases

nonlinearly with the damper area. The equivalent stiffness of dampers also changes with the damper area, the resonant frequency of the structure would be affected by the damper area. However, as the variation of equivalent stiffness of the damper is much less than the stiffness of the main structure, the effect is insignificant.

Damping ratios of the structure with dampers of different area have been calculated and listed in Table 6.5. The damping ratio increases nonlinearly with the damper area, which can be seen from Figure 6.20.

Table 6.5 Damping ratios of the building with dampers of different areas

Damper area ($\times A_0$)	Damping ratio (%)	Damper area ($\times A_0$)	Damping ratio (%)
0	1.022	60	1.896
20	1.301	80	2.219
40	1.594	100	2.537

Actually, when damper area increases, storage stiffness and loss stiffness will increase, thus stiffness and damping of the structure will increase as well. Therefore the resonant frequency of the structure and the damping ratio will increase, and the resonant response will decrease. The damping ratio of the structure can be considered as the ratio of the loss stiffness to the storage stiffness of the structure. When the loss stiffness changes, the storage stiffness including the stiffness of the structure will change also. From Equation (4.45), it is clear that the damping ratio of a structure will change with the damper area in a nonlinear relation. As the restoring force is concerned with the damper area and the damper deformation, it will also change nonlinearly with the damper area, and the response will be in nonlinear relation with the damper area as well. When the

damping ratio is very large, the forced structure will still vibrate (Long Y. Q. et al, 1988), but the response will be close to zero.

6.6.3.2 Variation of damper thickness

Damper thickness is concerned with shear strain of the damper, it is also an important factor for vibration control of a structure with viscoelastic dampers. In the present study, the damper thickness is set to 5mm, 10mm, 15mm, 20mm, 25mm and 30mm, respectively. The responses of the building structure with dampers of different thickness have been calculated. The maximum accelerations at the roof level of the building at different excitation frequencies are shown in Figure 6.21. It can be seen that thinner dampers are more appropriate for vibration control. The maximum resonant acceleration at the roof level increase nonlinearly with the damper thickness as shown in Figure 6.22. The effect on the resonant frequency of the structure by the variation of the damper thickness is also not noticeable obvious since the changing of the equivalent stiffness of the damper is much less than the stiffness of the main structure.

Table 6.6 Damping ratios of the building with dampers of different thickness

Damper thickness (mm)	Damping ratio (%)	Damper height (mm)	Damping ratio (%)
5	7.777	20	2.209
10	3.835	25	1.961
15	2.653	30	1.791

Damping ratios of the building with dampers of different thickness have been calculated and listed in Table 6.6. The damping ratio will decrease nonlinearly when the damper thickness increases, which can be seen in Figure 6.23.

In fact, when the damper thickness decreases, with the same shear displacement, the shear strain will become larger. The storage stiffness and loss stiffness of the damper will increase, which will result in decreasing of the maximum resonant response and increasing of the damping ratio. The nonlinearity embodied by the curves has been explained in section 6.6.3.2, and is not to be repeated here.

6.6.4 Variation of damper location

For a building structure, dampers can be incorporated in different positions. Dampers should be designed and installed in proper positions according to the characteristics of the structure. The characteristics of the building are mainly determined by the distribution of stiffness and mass. Mode shapes of the building structure are plotted in Figure 6.24. Five schemes, which are listed in Table 6.7, have been adopted for the damper installation. Dampers with total area of $80A_0$ are used for each scheme. Responses of the building structure incorporated with the same damper in different stories have been calculated. Maximum accelerations at the roof level of the structure at the four resonant frequency regions are shown in Figure 6.25 (a), (b), (c), (d), respectively. It can be seen that although the structure is incorporated with the same dampers, the effect is quite different when dampers are installed in different stories. For the building structure under consideration, it would be most effective if dampers are all incorporated in the story with the largest story shift. The damping ratios of the structure with dampers set in different stories in the four resonant regions have been calculated respectively. For example, the damping ratios of the building at the first resonant frequency are listed in Table 6.7. With reference to Figure 6.24, it can be found that difference in damping ratio between different schemes is

mainly due to the difference of story shift. When the dampers are installed in the story with larger story shift, the damping ratio of the structure will be larger also.

Table 6.7 Damping ratios of the building with the same dampers incorporated in different positions

Damper position	Damping ratio (%)	Damper postion	Damping ratio (%)
All dampers in the 1st story	1.804	All dampers in the 4th story	1.029
All dampers in the 2nd story	1.265	Dampers even distributed	1.301
All dampers in the 3rd story	1.131		

6.6.5 Variation of loading

Horizontal vibration of a building is mainly induced by wind or earthquake. For wind effect, responses of the structure subject to sinusoidal loading acting at different levels and loading with different amplitudes but acting at the roof level only have been studied. For earthquake effect, two kinds of seismic wave have been chosen to investigate the effectiveness in vibration control with the proposed damping devices.

6.6.5.1 Variation of loading position

The sinusoidal loading is assumed to act at each floor level of the building with and without dampers. Responses of the structure have been calculated. The maximum accelerations at the roof level of the building without dampers subject to cyclic loading with different excitation frequencies are shown in Figure 6.26 and those at the roof level of the building with dampers are shown in Figure 6.27. The ratio of the maximum resonant acceleration of the building with dampers to that without dampers is 0.49 for all cases. The damping ratios of the structure

with dampers subject to sinusoidal loading acting at different floor levels have been calculated and found to be the same for all cases also, which are equal to 2.208%.

6.6.5.2 Variation of loading amplitude

For this case study, sinusoidal loading with amplitudes of 1kN, 2kN, 3kN, 4kN, 5kN and 6kN are applied respectively on the structure. Maximum accelerations at the roof level of the structure without damper under various loading at different excitation frequencies are drawn in Figure 6.28 and those of the frame with damper are presented in Figure 6.29. The maximum resonant accelerations at the roof level of the building with and without damper are compared in Figure 6.30. Although the amplitude of the response can be reduced greatly while the loading amplitude is large, the response attenuation ratio is nearly the same, the maximum resonant acceleration of the structure with dampers is about 49% of that of the structure without dampers.

Damping ratios of the structure with dampers have been calculated and found to be 2.208% for all cases. In practice, the damping ratio of a structure without dampers increases with the loading amplitude. Since the damping ratio of the structure is assumed to be proportional, which does not change with loading amplitude in the analysis, and damping ratio of a damper does not change with shear displacement, the damping ratio of a structure with viscoelastic dampers does not change with loading amplitude.

6.6.5.3 Effectiveness in vibration control under seismic loading

Ground motions are generated by seismic wave and then transferred to structures through their basements, therefore vertical and horizontal vibration will occur in building structures. Normally, structures are damaged by horizontal vibration caused by ground motion. Thus only the horizontal effect is considered in design except for structures in neighbouring district of the earthquake epicenter or those in which serious consequence will be caused by vertical vibration.

Effect of earthquake is concerned with not only the characteristics of the ground motion, but also the properties of the site and the building structure themselves. Ground motion caused by earthquake is a kind of random vibration, the most important characteristics are magnitude, frequency spectrum and duration time. Whether a structure will be damaged or not is determined not only by the peak value of acceleration or velocity, but also the seismic wave spectrum and the duration time. Site properties have great effect on the ground motion. As the seismic wave being absorbed and filtered by the soil of the site, the ground motion will have different dominant periods for different kinds of soil (Weng Yijun et al, 1990). For hard rock area, the dominant periods are short, normally between 0.1s and 0.3s but for soft soil, the dominant periods can reach 1.5s~2.0s, which is harmful for high-rise buildings with longer periods in vibration, for example, earthquake in Mexico in 1985 which has long duration time with a dominant period of about 2.0s, caused many buildings of 9~16 stories, which has a natural period of around 2.0s damaged seriously. (Bao Shihua et al, 1989). Based on the above discussion, two typical seismic records are assumed to act on the building structure to check the effectiveness in vibration control with viscoelastic dampers under seismic loading.

6.6.5.3.1 Seismic records

Taft Wave was recorded from the Taft Lincoln School Tunnel of Kern County in California Earthquake with magnitude of 7.7 under the depth of 18km at 04:53 on July 21, 1952. Duration of the record in N-21-E direction was 54.36s and the peak acceleration was 152.70cm/s^2. Figure 6.31 shows the acceleration record of Taft Earthquake in N-21-E direction in time domain with 2719 data points.

El Centro earthquake record was obtained from the earthquake taken place at 8:37 of May 18, 1940 in El Centro site of Imperial Valley irrigation district with magnitude of 6.7 at the depth of 11km. Duration of the record in N-S direction was 53.73s and the peak acceleration was 341.70cm/s^2. The acceleration record in N-S direction with 2688 data points is presented in Figure 6.32.

6.6.5.3.2 Data processing of seismic records

To analyze a structure with viscoelastic dampers under seismic loading in frequency domain, acceleration records of typical earthquakes are transferred by FFT method. As for the requirements of the FFT, total data points number should be $N = 2^M$, where N and M are integers and the value of first point and last point should be equal. Therefore, the original seismic data should be pre-processed first to satisfy the requirements.

Assuming that the total number of points of the seismic record is K, values of the points are $a(i), i = 1, \cdots, K$ and the time step of the original data is t_a. The objective points number is N, values of which are $b(i), i = 1, \cdots, N$ and the time step of the pre-processed data is t_b. As the first data value and last data value of a whole seismic record are very small, let $b(1) = 0$, $b(2) = a(1)$, $b(N) = 0$,

$b(N-1)=a(K)$, values of other points should be interpolated according to the original data. Value of a new point i, where i is equal to 3 to $(N-2)$, is to be determined by the values of the two neighbouring old points i_{old} and $i_{old}+1$. And i_{old} can be obtained by

$$i_{old} = Int\left((i-2)\frac{K-1}{N-3}\right) \tag{6.1}$$

Then value of the new point is

$$b(i) = a(i_{old}) + \{a(i_{old}+1) - a(i_{old})\}\left\{(i-2)\frac{K-1}{N-3} - i_{old}\right\}. \tag{6.2}$$

It is obvious that the time step for new data series is,

$$t_b = \frac{t_a(K-1)}{N-3} \tag{6.3}$$

And the total time is,

$$T = \frac{t_a(K-1)(N-1)}{N-3} \tag{6.4}$$

To avoid leakage of the original data, normally the new data number is larger than that of the old one. After the seismic records being dealt with by the above method, the new data series can be transferred to frequency domain by FFT and the values obtained by FFT are corresponding to the frequencies as given by

$$f_i = \frac{(i-1)}{T},\ i = 1, \cdots, N. \tag{6.5}$$

Acceleration components of the seismic waves have been calculated by the above method. The dominant frequencies of the above two records were between 0~10Hz as shown in Figure 6.33 and Figure 6.34, respectively

6.6.5.3.3 Analysis of the structure under seismic loading

Dynamic equilibrium equation of a multi-degree-of-freedom system under ground motion can be written in frequency domain as

$$-\omega^2\mathbf{M}\mathbf{X}(\omega)+j\omega\mathbf{C}\mathbf{X}(\omega)+\mathbf{K}\mathbf{X}(\omega)+\mathbf{R}(\omega)=-\mathbf{M}\ddot{\mathbf{X}}_g(\omega) \tag{6.6}$$

Then displacement in frequency domain can be calculated by

$$\mathbf{X}(\omega)=-\bar{\mathbf{I}}(\omega)^{-1}\left[\mathbf{M}\ddot{\mathbf{X}}_g(\omega)\right] \tag{6.7}$$

The response of the building structure under seismic loading has been calculated by the HTFDM. The accelerations at the roof level of the structure under Taft N-21-E are shown in Figure 6.35, the maximum accelerations are 2.967m/s^2 and 4.121m/s^2 for the structure with and without dampers respectively. The accelerations at the roof level of the structure under El Centro-Ns are shown in Figure 6.36. The maximum accelerations are 5.51m/s^2 and 5.97 m/s^2 for the structure with and without dampers respectively. It can be seen that the effectiveness in vibration control of the structure with the same dampers subject to different earthquakes is different. Although the accelerations of the structure without dampers subject to El Centro-NS are larger than those of the structure with dampers, the ratio of the largest acceleration at the roof level of the building with dampers to that of the building without damper is 0.92, however the ratio is 0.72 for the building subject to Taft N-21-E. The difference is caused by the properties of different seismic waves, such as the energy distribution of the excitation in frequency domain.

If the effectiveness in vibration control can not satisfy the designer's requirement, it can be improved by changing the damper material or the damper dimensions.

For example, when the damper area in the building increases to $240A_0$, the maximum acceleration at the roof level of the building subject to the Taft N-21-E will be 2.070m/s^2 and that at the roof level of the building subject to the El Centro NS will be 4.431m/s^2. The corresponding acceleration ratios are 0.50 and 0.74, respectively. The effectiveness in vibration control increases significantly which can be observed clearly from the acceleration curves at the roof level of the building subject to these two seismic waves as presented in Figure 6.37 and Figure 6.38, respectively.

6.6.6 Variation of temperature

At different temperature, energy dissipation ability of a damper is different. Damping ratio and equivalent stiffness of a damper will decrease when temperature increases. Assuming that the IFDM with consideration of temperature for dampers is adopted $\tau(t) = e^{-0.056(T-25)}\left[0.6(t) + 0.07D^{1.02}\gamma(t)\right]$. The responses of the building at temperature of 20°C, 25°C, 30°C, 35°C and 40°C have been calculated. The maximum accelerations at the roof level of the structure at different excitation frequencies are shown in Figure 6.39. The maximum resonant accelerations are shown in Figure 6.40. It can be seen that when temperature increases, resonant acceleration will increase.

The damping ratios of the building at different temperature have been listed in Table 6.8 and the changing trail is shown in Figure 6.41. It can be seen when the temperature increases, the damping ratio will decrease. It is because when the temperature increases, the loss modulus and storage modulus of a damper will decrease, which leads to decreasing of the damping ratio and the equivalent

stiffness of the damper. Therefore, for a structure incorporated with viscoelastic dampers, when the temperature increases, the damping ratio and stiffness of the structure will decrease.

Table 6.8 Damping ratios of the building with dampers at different temperatures

Temperature (^{0}C)	Damping ratio (%)	Temperature (^{0}C)	Damping ratio (%)
20	2.64	35	1.675
25	2.208	40	1.513
30	1.902		

6.7 Discussions and Conclusions

- Proposed damping device for horizontal vibration control

A damping device has been designed for horizontal vibration control of framed structures. Dynamic tests on a framed structure with such damping device made of damper ZJD-1 has verified the effectiveness in vibration control of the structure as the response suppressed significantly and the damping ratio increased greatly. Since response is attenuated, internal forces of the structure would be consequently reduced, which will result in a much better design. Therefore, to design a structure with such damping devices, usually smaller section for members can be chosen and the cost of the whole structure would be cut down.

Because the installation of such a damping device is simple and convenient, it can be applied either to existing structures for enhancing its capability of energy dissipation or to new structures for economical design. In practical design, with some special treatments, such damping devices will not only act as an energy

dissipation element, but can also take some of the dead loads. For example, steel balls or bearings can be set in between steel plates in which the damper is incorporated, thus forces can be transferred through the damping device in the axial direction of the damper. Moreover, although diagonal brace damping device can give the damper larger deformation than the proposed damping device, the damper size installed in the device is limited and this type of device is usually not in harmony with architectural requirements such as the setting for windows or doors. These disadvantages may offset the advantages given by the diagonal brace damping device system.

- Verification of the analytical methods

Comparisons of the test results and analytical results have been made and it has proved that both the analytical methods TDM and HTFDM are able to predict accurately the response of a structure with such damping devices. It has also been found that the analysis by the HTFDM is better than that by the TDM. The TDM is an approximate method and the accumulated error would affect the accuracy of the analytical results. Furthermore, the analysis by the HTFDM also costs less time than that by the TDM.

- Guidelines for design with such damping devices

Vibration control of structures with viscoelastic dampers came about from the need first to suppress wind induced vibration in tall buildings. For example, 10,000 viscoelastic dampers were employed in each tower of the World Trade Centre to assist the tubular steel frame in limiting wind induced building oscillation to levels below human perception. With dampers installed, critical damping can be increased about 3 % at design wind. Subsequently, viscoelastic

damping devices were utilized to deal with seismic motions. Unlike frictional damping systems which do not operate below a threshold level of excitation, viscoelastic damping devices are effective all levels of seismic loading.

Although such damping devices are both effective for vibration control of structures due to wind and seismic loading, considerations in design are different for various loading conditions. Temperature increases in the viscoelastic material of the dampers during earthquake shaking are small and are not looked as such a significant factor as for wind loading. Dominant frequencies of wind loading is always very low, which are less than 1.0 Hz, while that of seismic loading is among the range of 1.0~8.0Hz. Since viscoelastic damping is concerned with excitation frequencies, different kinds of material should be chosen for different loading conditions. For a building structure, the deformation style due to wind loading is different from that due to seismic loading. Therefore, dampers should be placed at different positions for various excitations. Furthermore, strain levels are different for different forms of excitation. In general, the strain level by wind loading is less than that by seismic loading. To keep the dampers within working range, dampers with large strain ability such as maximum of 200%~300% should be applied for seismic resistance.

Based on the parametric studies on a full-scaled building structure, some useful design guidelines for structures incorporated with the proposed damping devices are listed as follows.

1. In order to allow the damper takes sufficient effect, ratio of the brace stiffness to the equivalent stiffness of the damper under normal conditions should be larger than a certain value, which is suggested to be larger than 8.0.

2. Damper material type is the essential factor. Dampers with high damping and small storage modulus, which are available in the market, should be chosen. Thus, when such dampers are incorporated in a structure, the damping ratio of the structure would increase significantly and the stiffness of the structure would be affected slightly by the dampers.

3. Dampers with larger area would normally provide more effective. Small damper thickness is also beneficial for effectiveness, but if a damper is too thin, it is easy to be destroyed by violent vibration. The maximum displacement of the damper should be estimated before choosing the damper thickness.

4. Damping device location is very important for the effectiveness, the location should be determined by the dynamic characteristics of the structure and the loading conditions. For building structures, the devices should be installed between stories where large relative displacement may occur.

5. Dynamic behaviours of viscoelastic dampers are concerned with temperature. For structures in areas where temperature variation in a year is significant, dampers whose properties are less sensitive to temperature should be chosen. And for structures in areas where temperature variation in a year is mild, dampers with good loss modulus should be utilized. In addition, enough clear space should be provided for heat dissipating.

6. Loading conditions such as loading amplitude and loading positions are the factors to be considered in vibration control. For earthquake effect, the effectiveness in vibration control for a structure with the proposed damping devices is concerned with the characteristics of the seismic wave. For vibration

control of a building under seismic loading, the properties of seismic waves which may be occur and those of the structure should be considered together.

7. In practical design, all parameters as well as the additional cost of the damping devices and installation requirements should be considered together. When the required effectiveness can be achieved by different ways, the cost would be the final determining factor.

6.8 References

Bao Shihua and Fang Ehua (1989), High-rise building structural design (Second Edition), Tsinghua University Press, Beijing. (In Chinese)

Bates W. (1975), Design of Structural Steelwork--Medium Rise Building--, Constrado, Constructional Steel Research and Development Organisation, Croydon.

Chang K. C., Soong T. T., Oh S. T. and Lai M. L. (1995), Seismic Behaviour of Steel Frame with Added Viscoelastic Dampers, Journal of Structural Engineering, Vol.121, No. 10, pp1418-1426.

Constantinou M. C. (1994), Principles of Friction, Viscoelastic, Yielding Steel and Fluid Viscous Dampers: Properties and Design, International Center for Mechanical Sciences: Passive and Active Structural Vibration Control in Civil Engineering, pp209-240.

Davenport A. G. (1991), Safety and Uncertainties in Wind Engineering for Construction, pp.1-11, International Workshop on Technology for Hong Kong's Infrastructure Development.

Davenport A. G. (1986), Damping in talling Buildings: Its Variability and Treatment in Design, ASCE Spring Convention, Seattle.

Hsu Sheng-Yung and Fafitis Apostolos (1992), Seismic Analysis Design of Frames with Viscoelastic Connections, Journal of Structural Engineering, Vol.118, No. 9, pp 2459-2473, September.

Ito Yoshio, Kirekawa Akio and Asano Kiyoaki (1995), Vibration Control Utilizing Viscoelastic Material-Chiba Portside Tower Building-, A New Direction in Seismic Design, pp319-322, Tokyo.

Kasai Kazuhiko, Munshi Javeed A., Lai Ming-Lai and Maison Bruce F. (1994), Viscoelastic Damper Hysteretic Model: Theory, Experiment, and Application, Technical Papers on Passive Energy Dissipation, ATC-17-1, pp521-532.

Kirekawa A., Ito Y. and Asano K. (1992), A Study of Structural Control Using Viscoelastic Material, Proceeding of The Tenth World Conference, pp2047-2054.

Kasai Kazuhiko and Fu Yaomin (1995), Seismic Analysis and Design Using Viscoelastic Dampers, A New Direction in Seismic Design, Tokyo, pp113-140.

Long Y. Q. and Bao S. H. (1988), Structure Mechanics, High Education Press, Beijing. (In Chinese)

Maison Bruce F. and Kasai Kazuhiko (1994), Case Study of Building Retrofit Using Viscoelastic Dampers, Fifth U. S. National Conference on Earthquake Engineering, Vol. 1, pp 597-606.

Niwa Naoki, Kobori Takuji, Takahashi Motoichi, Hatada Tomohko, Kurino Haruhiko and Tagami Jun (1995), Passive Seismic Response Controlled, High-rise Building with High Damping Device, Earthquake Engineering and Structural Dynamics, Vol. 24, pp665-671.

Research Institute of Nanjing Aeronautical Institute (1992), Dynamic Test and Analysis System User Guide, Vibration Engineering.

Soong T. T. and Dargush G. F. (1997), Passive Energy Dissipation Systems in Structural Engineering, John Wiley & Sons.

Wang G. Y. (1978), Vibration of building structures, Science Press, P. R. C. (In Chinese)

Weng Yijun and Feng Shiping (1990), Seismic resistance design of building structure, Earthquake Press, Beijing (In Chinese)

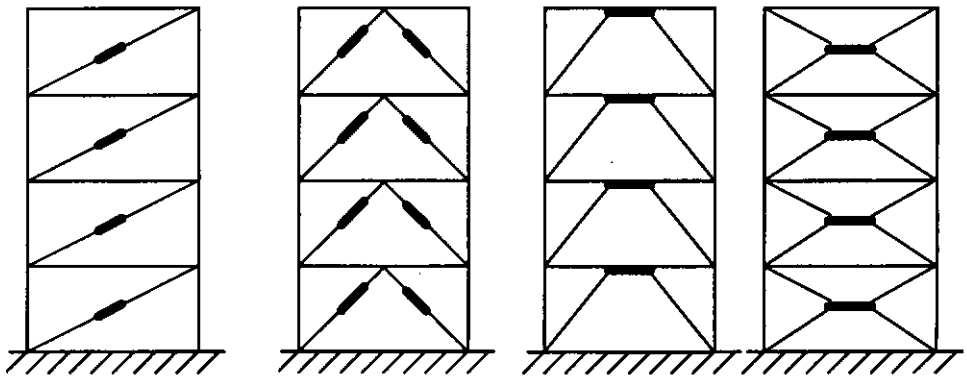

Figure 6.1 Damper installation methods in framed structures

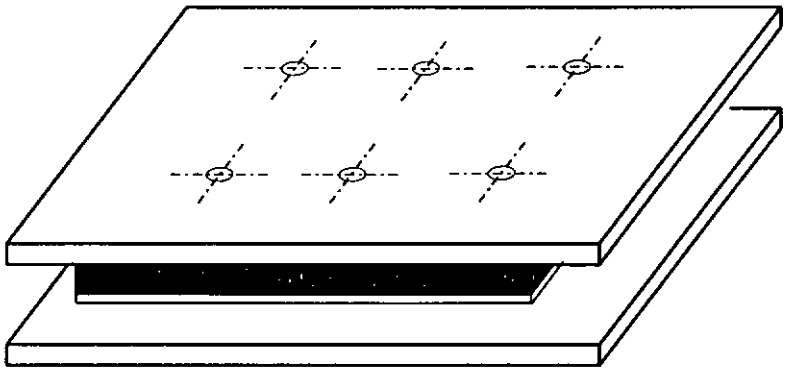

Figure 6.2 Damper installed between two steel plates

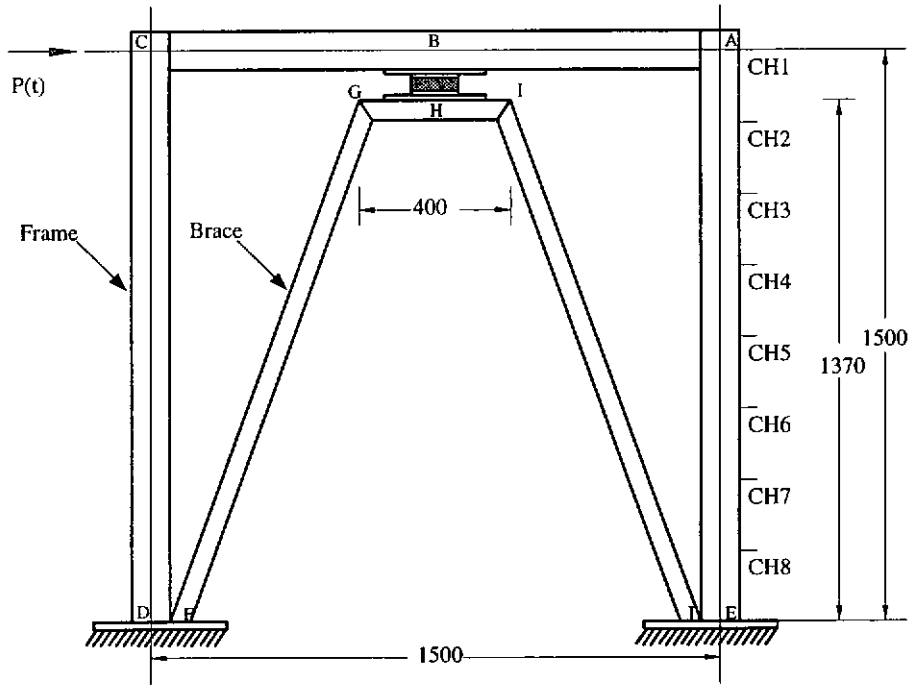

(Unit of length: mm)

Figure 6.3 Elevation of the steel frame under horizontal excitation

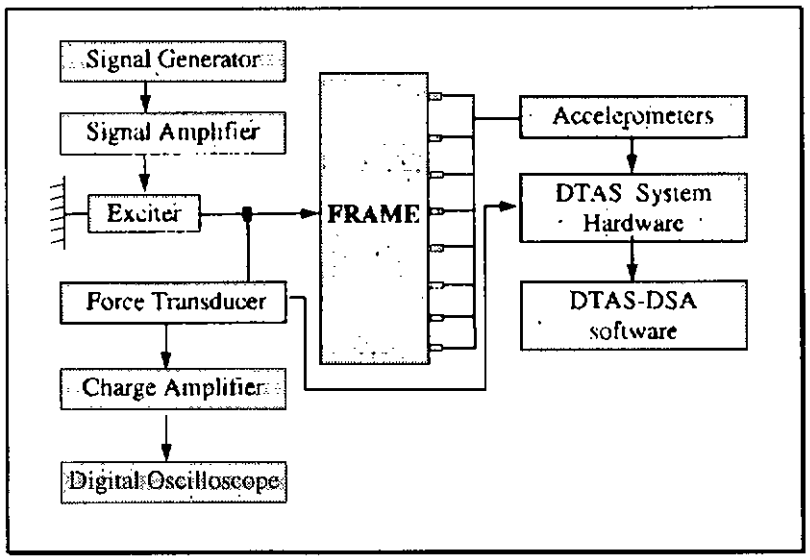

Figure 6.4 Set-up of test system

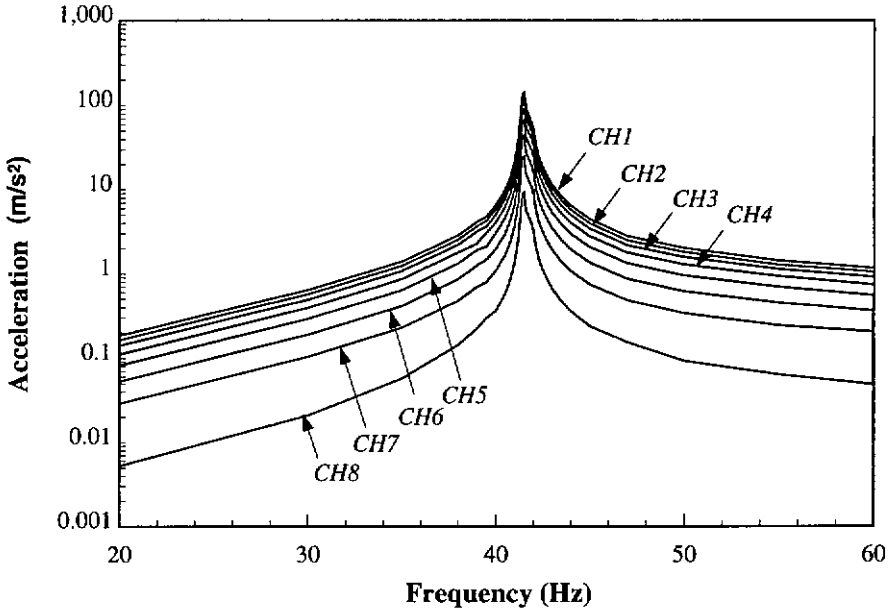

Figure 6.5 Maximum accelerations at different positions of the frame without damper

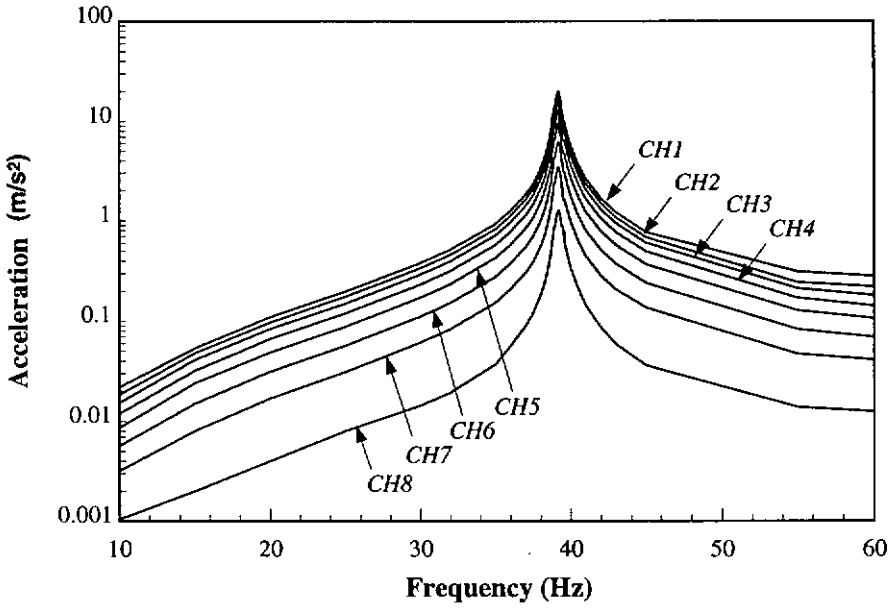

Figure 6.6 Maximum accelerations at different positions of the frame with a damper

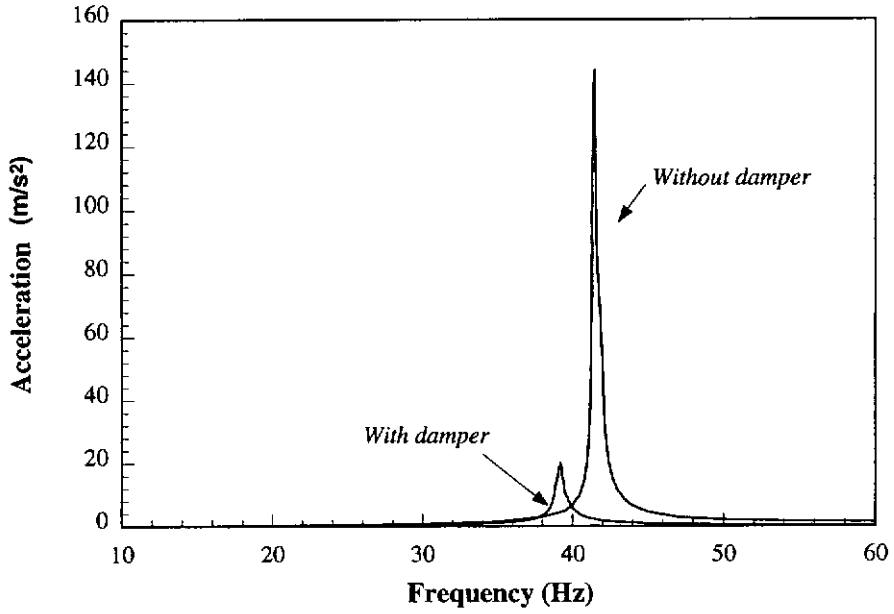

Figure 6.7 Maximum accelerations at node A of the frame with and without damper

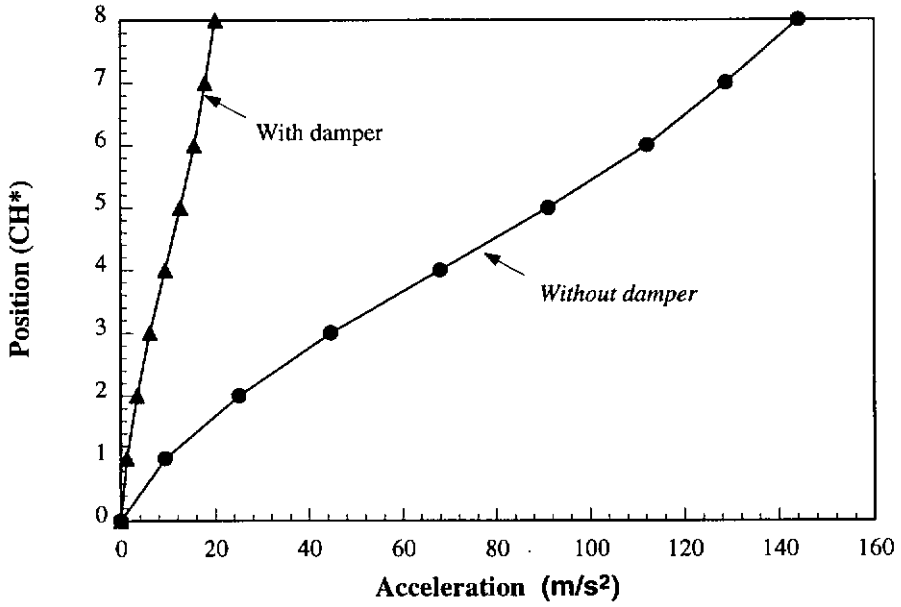

Figure 6.8 The maximum resonant accelerations of the frame with and without damper

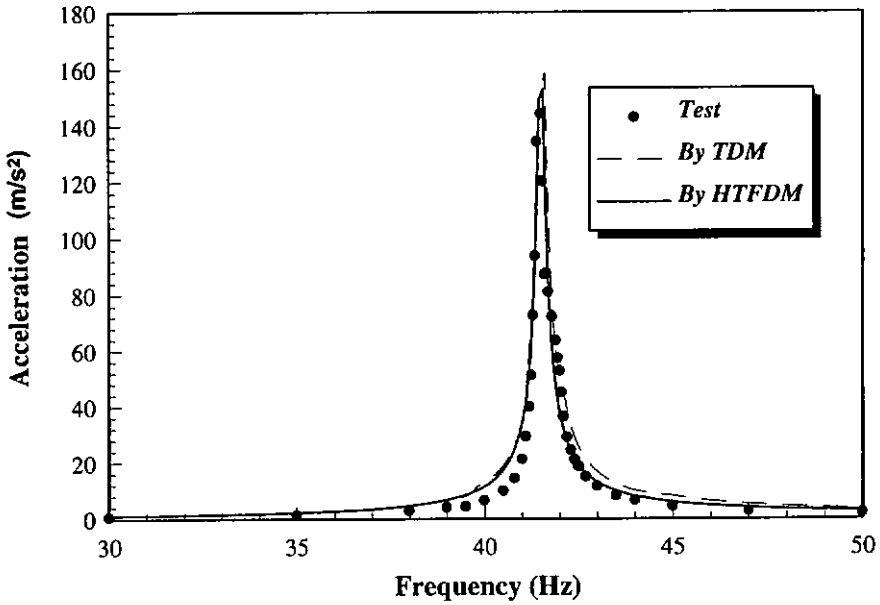

Figure 6.9 Maximum acceleration curve at node A of the frame without damper

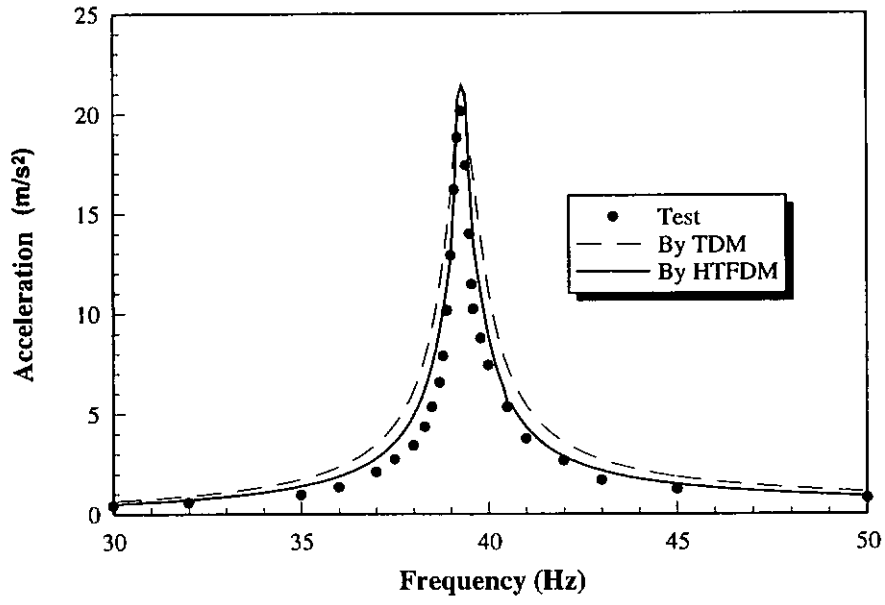

Figure 6.10 Maximum acceleration curve at node A of the frame with a damper

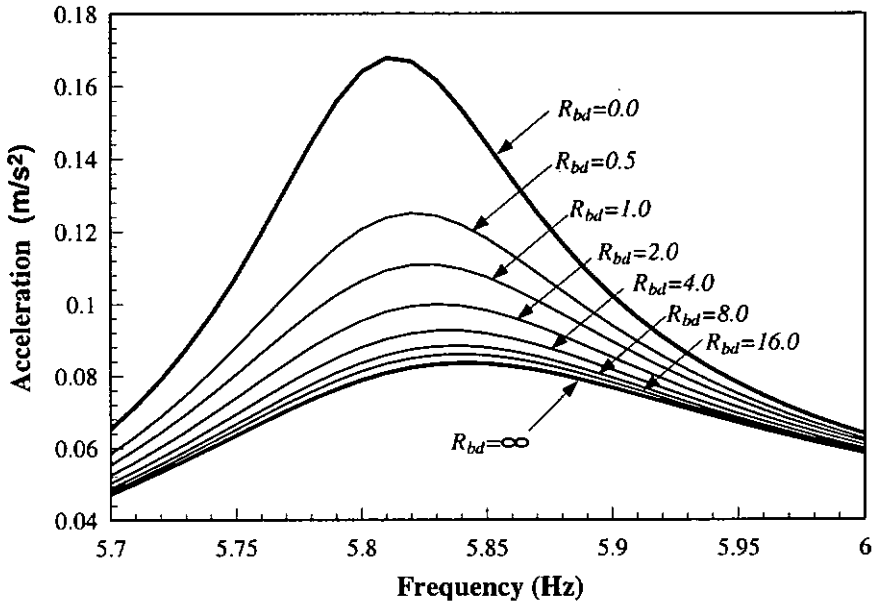

Figure 6.11 Maximum accelerations at the roof level of the building with brace of different stiffness

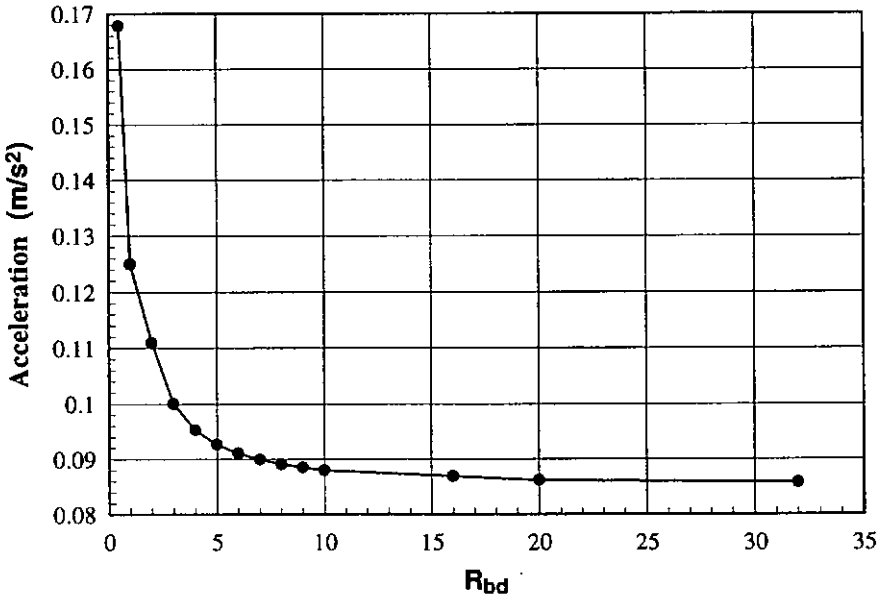

Figure 6.12 Maximum resonant accelerations at the roof level of the building with brace of different stiffness

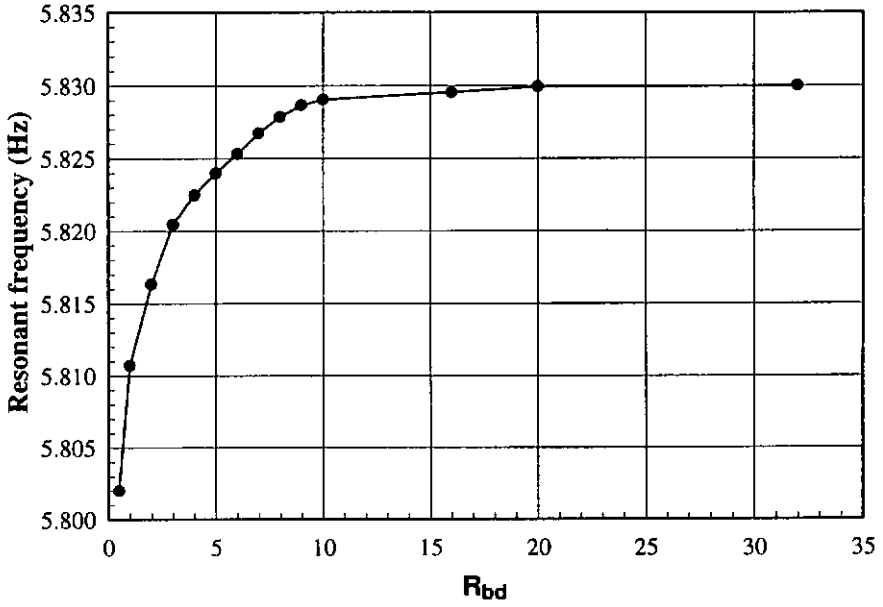

Figure 6.13 Resonant frequencies of the building structure with brace of different stiffness

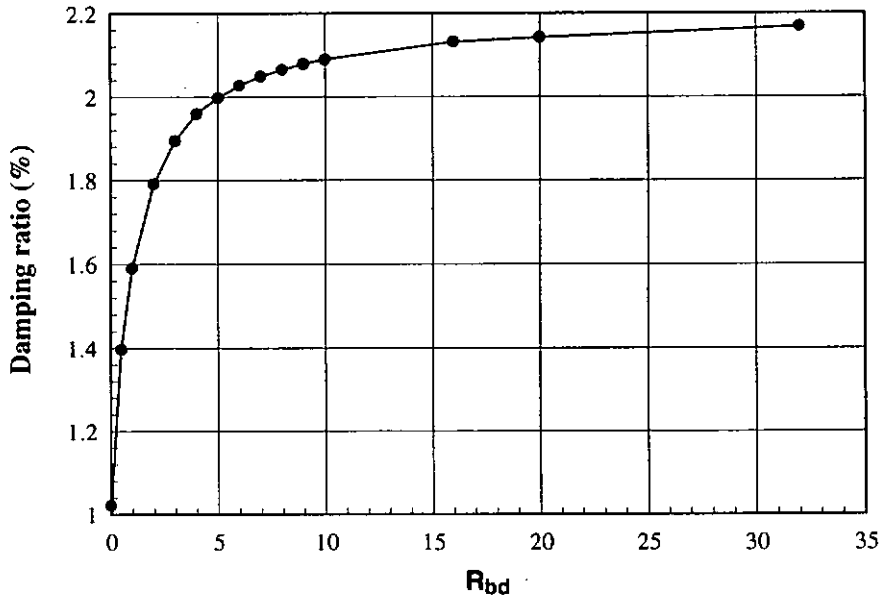

Figure 6.14 Damping ratios of the building structure with brace of different stiffness

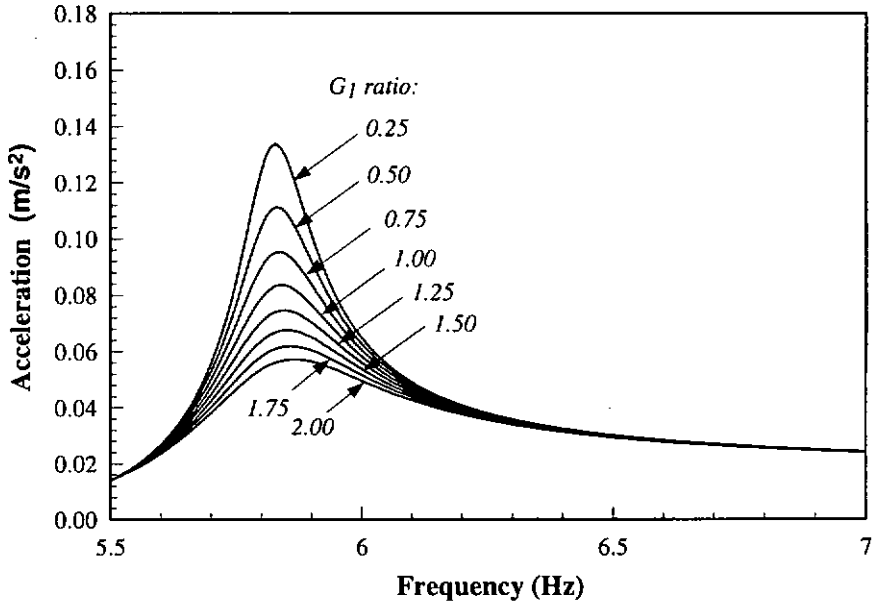

Figure 6.15 Maximum accelerations at the roof level of the building incorporated with dampers of different kinds

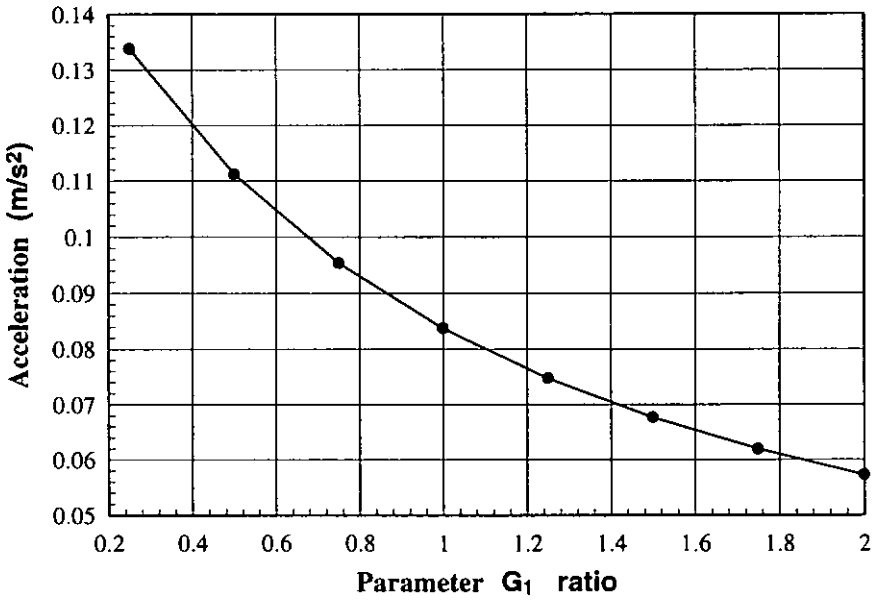

Figure 6.16 Maximum resonant accelerations at the roof level of the building incorporated with dampers of different kinds

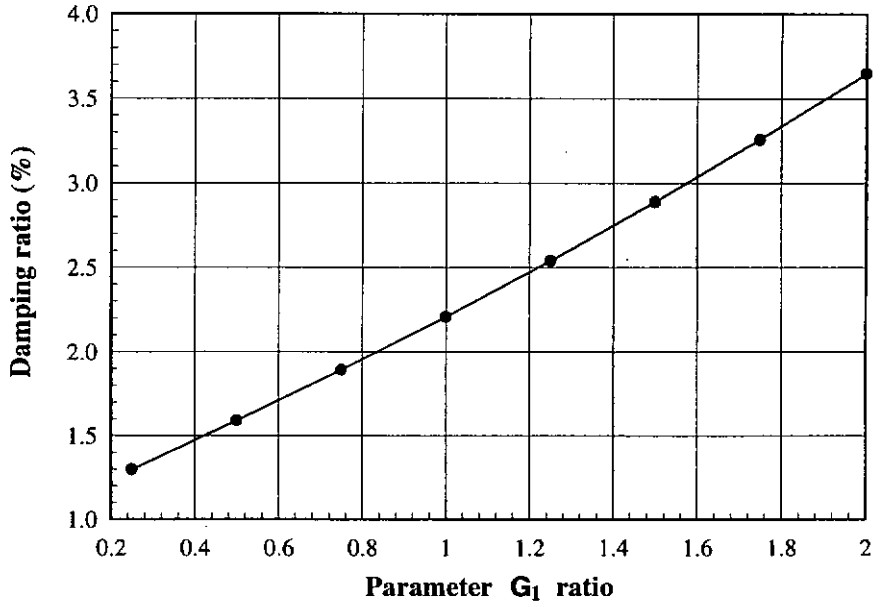

Figure 6.17 Damping ratios of the building with dampers of different kinds

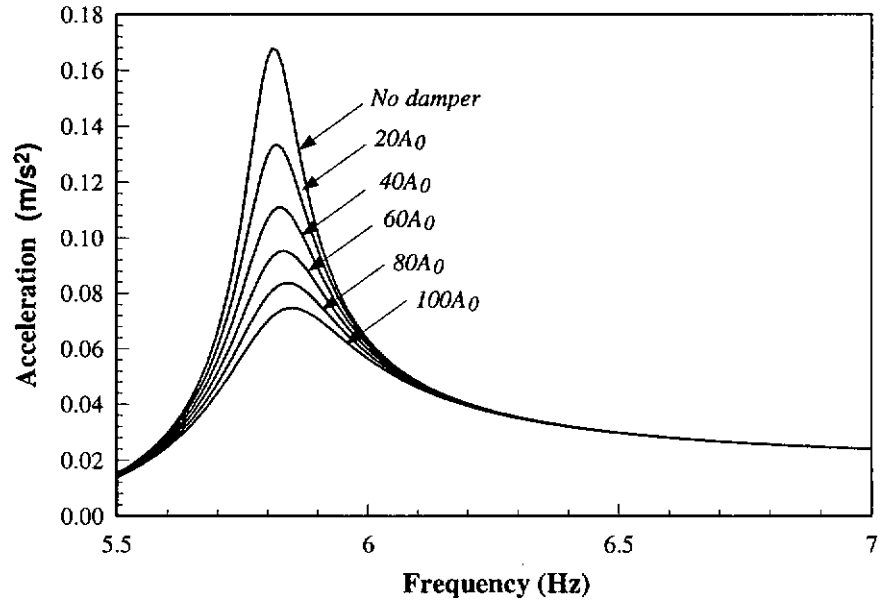

Figure 6.18 Maximum accelerations at the roof level of the building incorporated with dampers of different areas

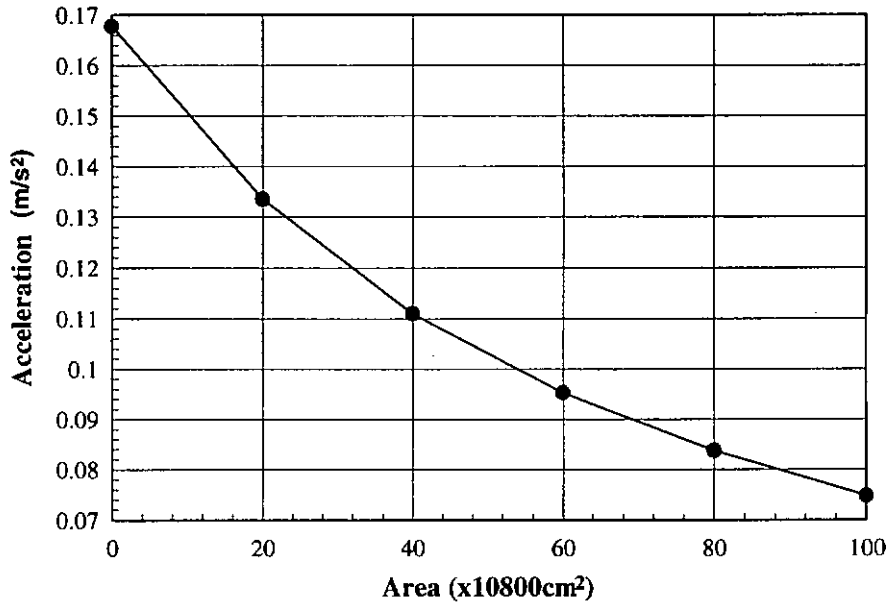

Figure 6.19 Maximum resonant accelerations at the roof level of the building incorporated with dampers of different areas

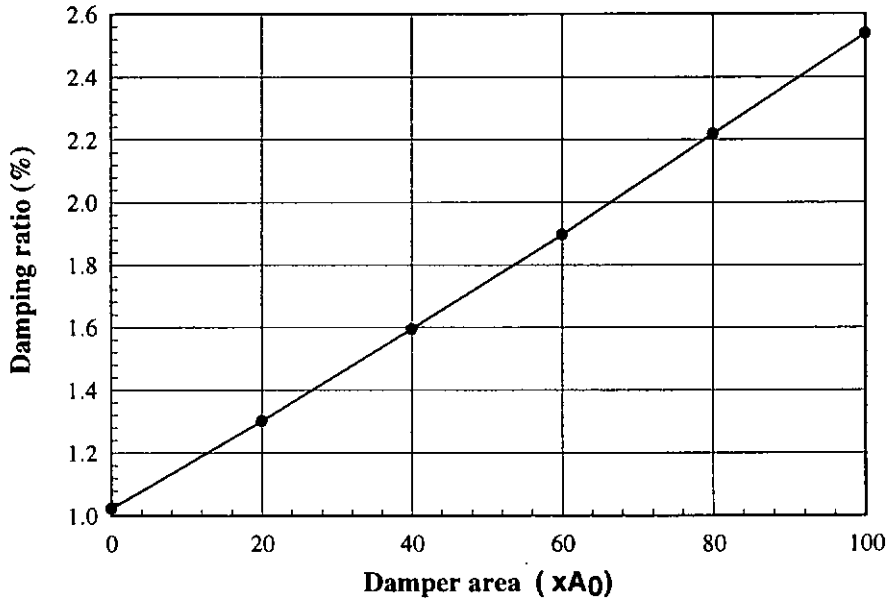

Figure 6.20 Damping ratios of the building with dampers of different areas

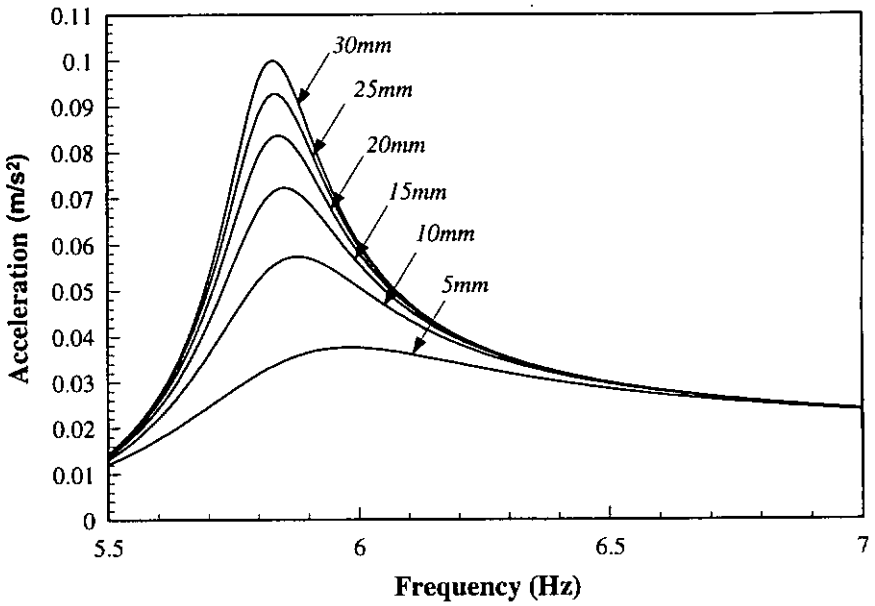

Figure 6.21 Maximum accelerations at the roof level of the building incorporated with dampers of different thickness

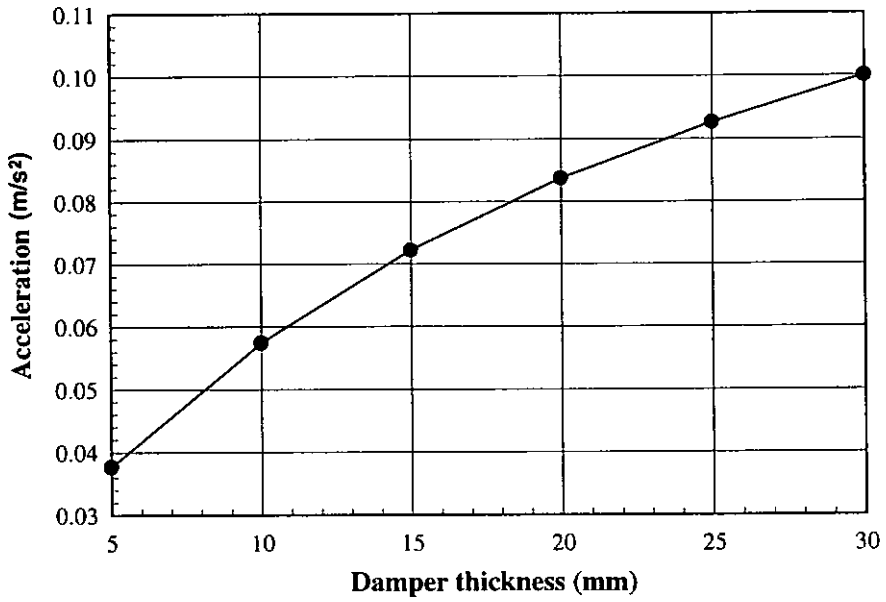

Figure 6.22 Maximum resonant accelerations at the roof level of the building incorporated with dampers of different thickness

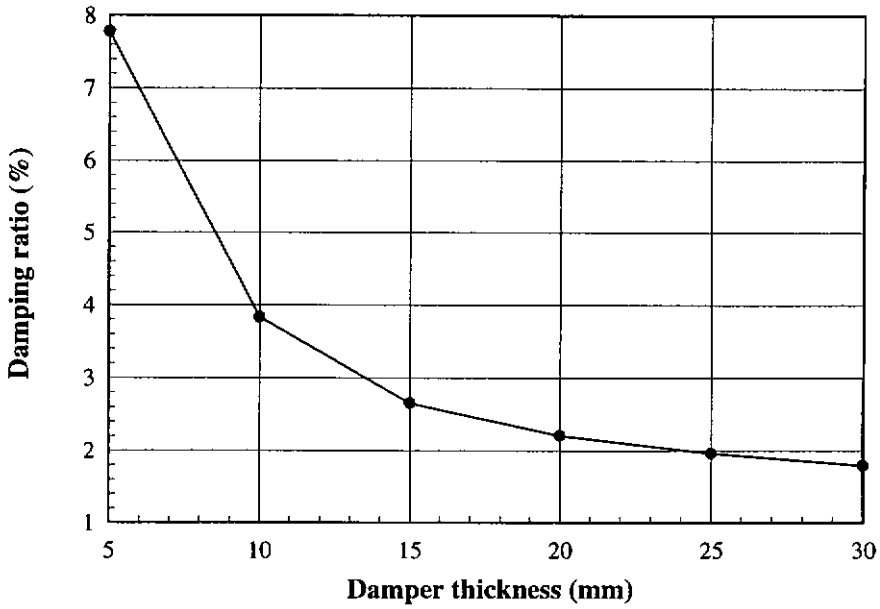

Figure 6.23 Damping ratios of the building with dampers of different thickness

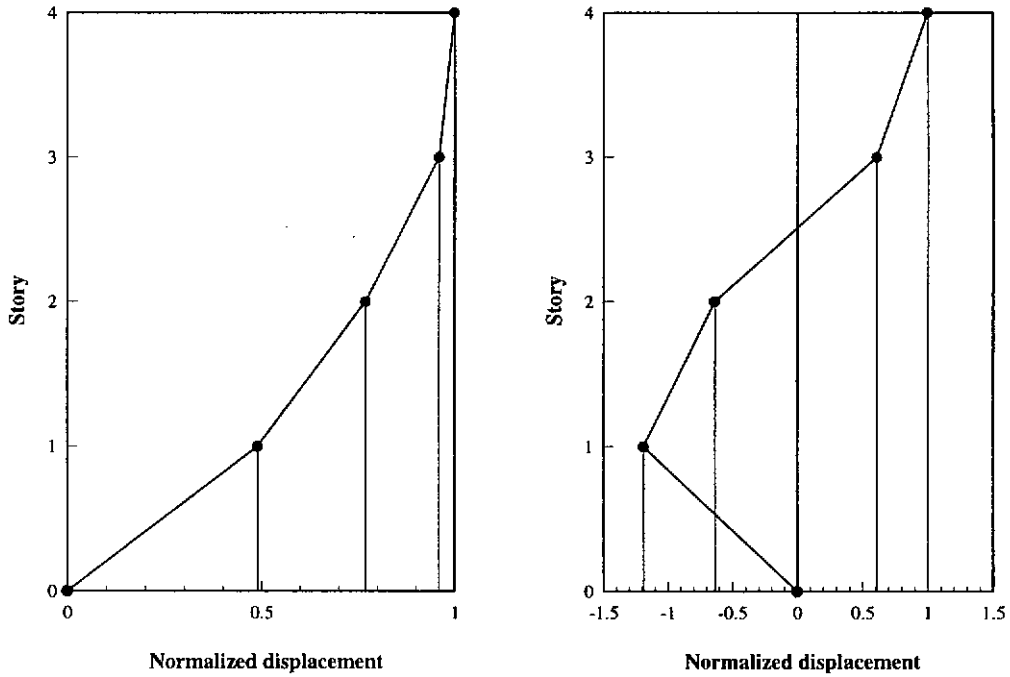

(a) The 1st mode (b) The 2nd mode

Figure 6.24 Mode shapes of the building structure

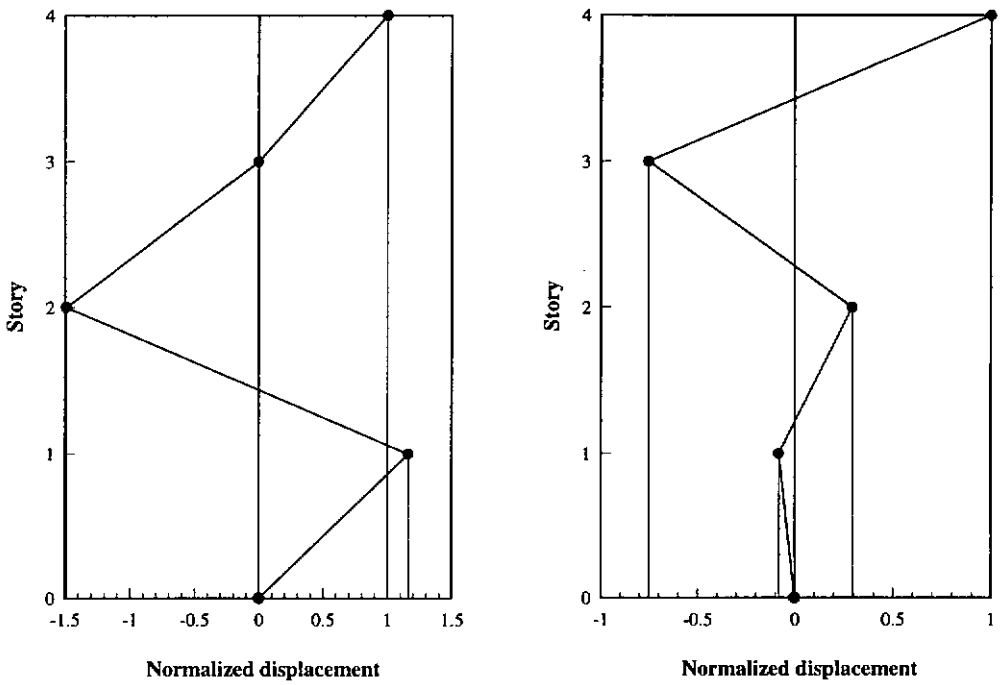

(c) The 3rd mode (d) The 4th mode

Figure 6.24 Mode shapes of the building structure (Continued)

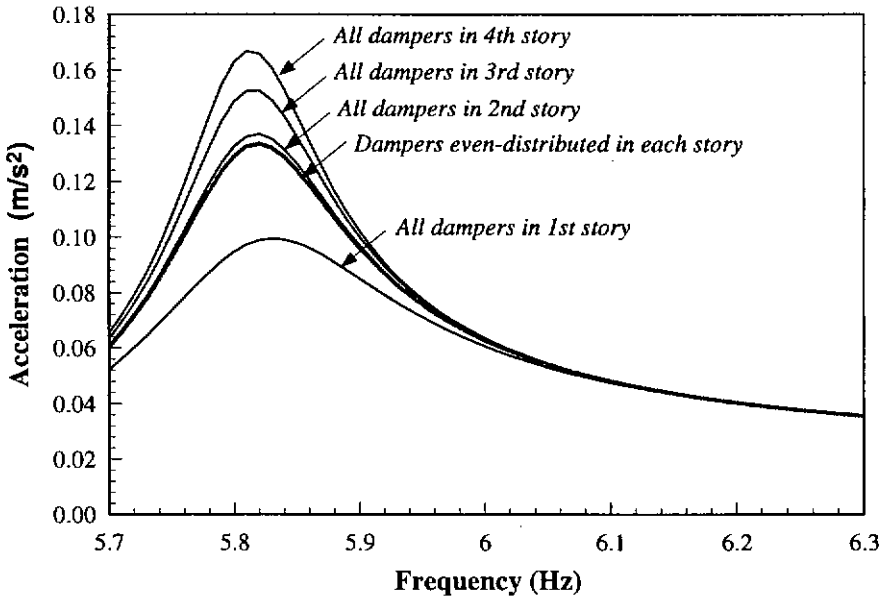

(a) In the 1st resonant frequency range

Figure 6.25 Maximum accelerations at the roof level of the building with dampers incorporated in different positions

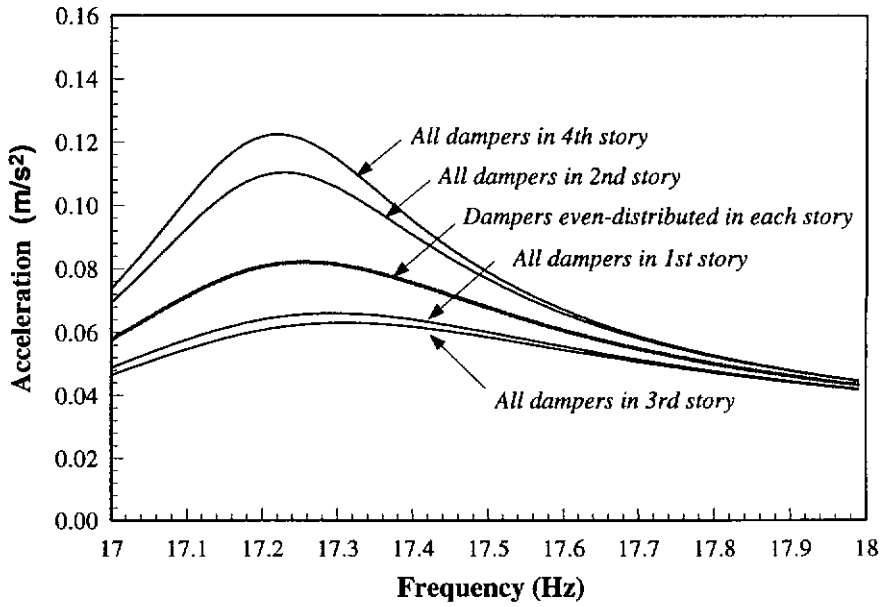

(b) In the 2nd resonant frequency range

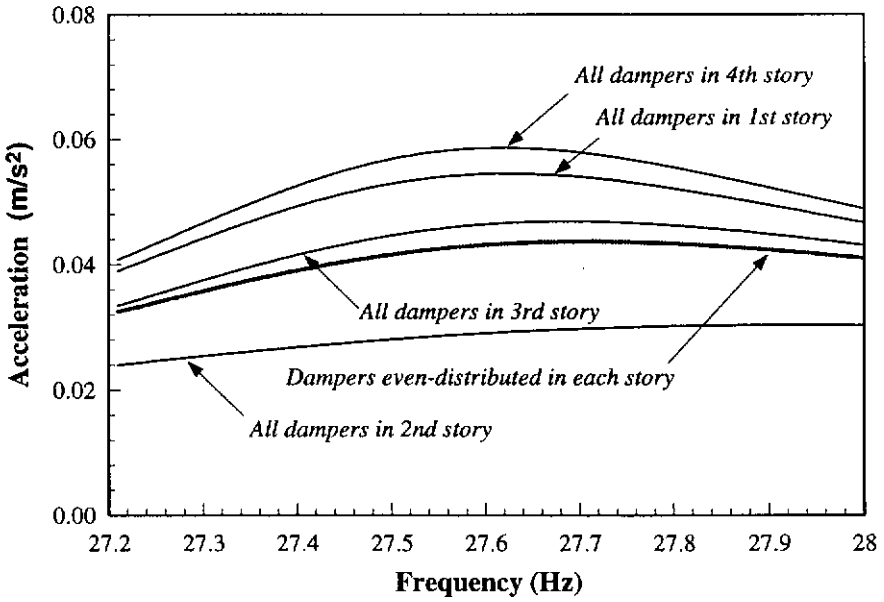

(c) In the 3rd resonant frequency range

Figure 6.25 Maximum accelerations at the roof level of the building with dampers incorporated in different positions

(Continued)

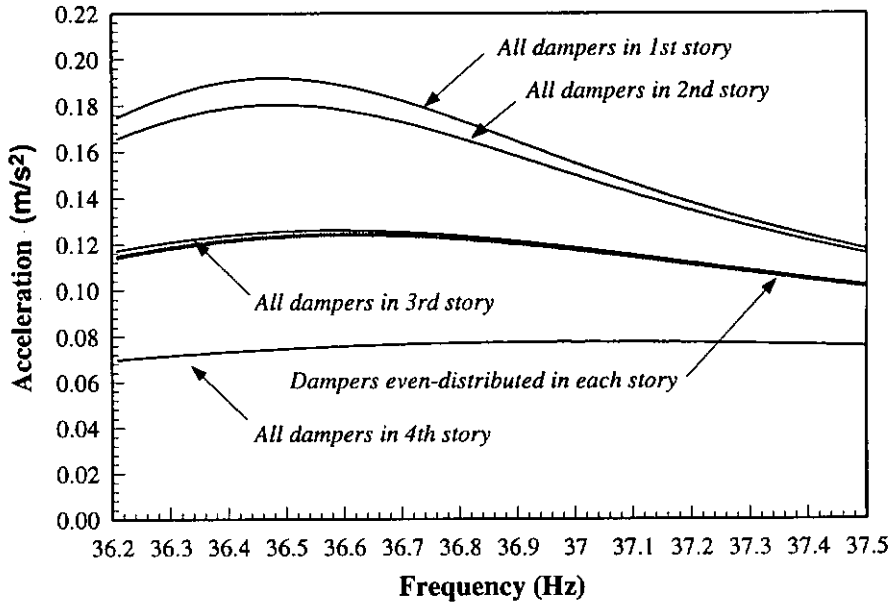

(d) In the 4rd resonant frequency range

Figure 6.25 Maximum accelerations at the roof level of the building with dampers incorporated in different positions

(Continued)

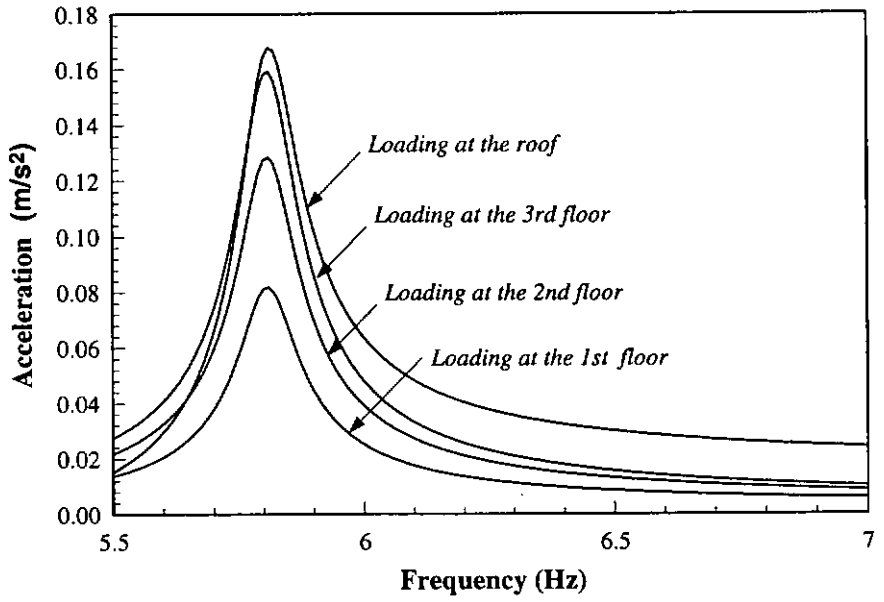

Figure 6.26 Maximum accelerations at the roof level of the building without damper under loading acting at floor levels

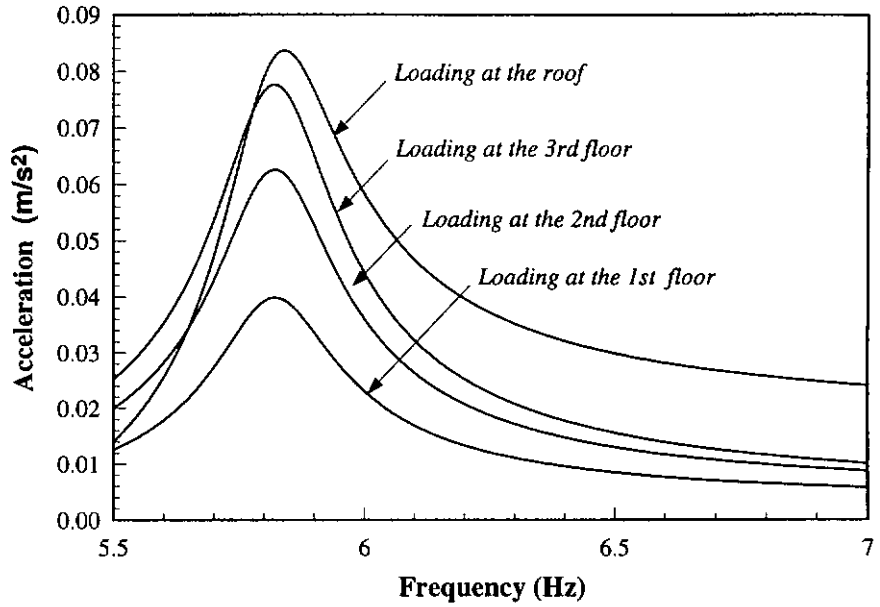

Figure 6.27 Maximum accelerations at the roof level of the building incorporated with dampers under loading acting at different positions

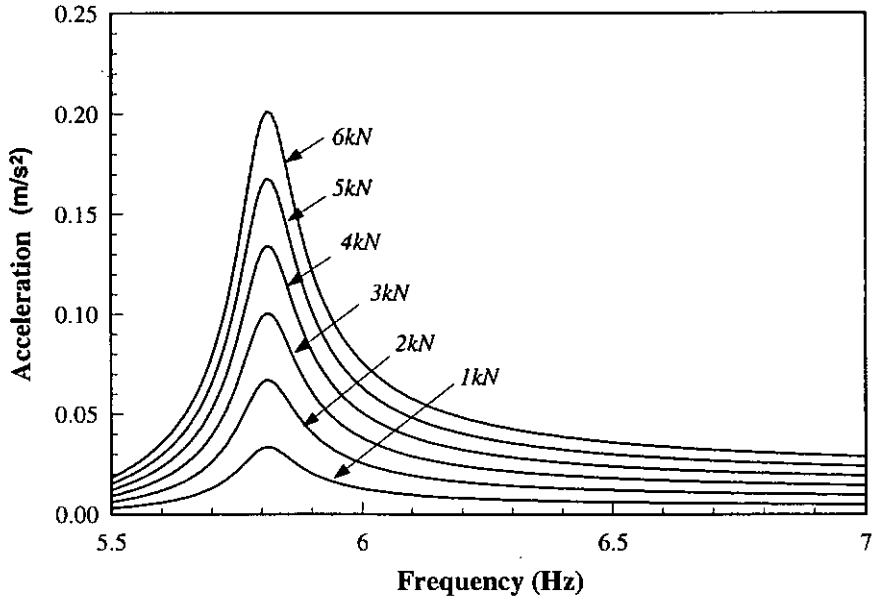

Figure 6.28 Maximum accelerations at the roof level of the building without damper under loading of different amplitudes

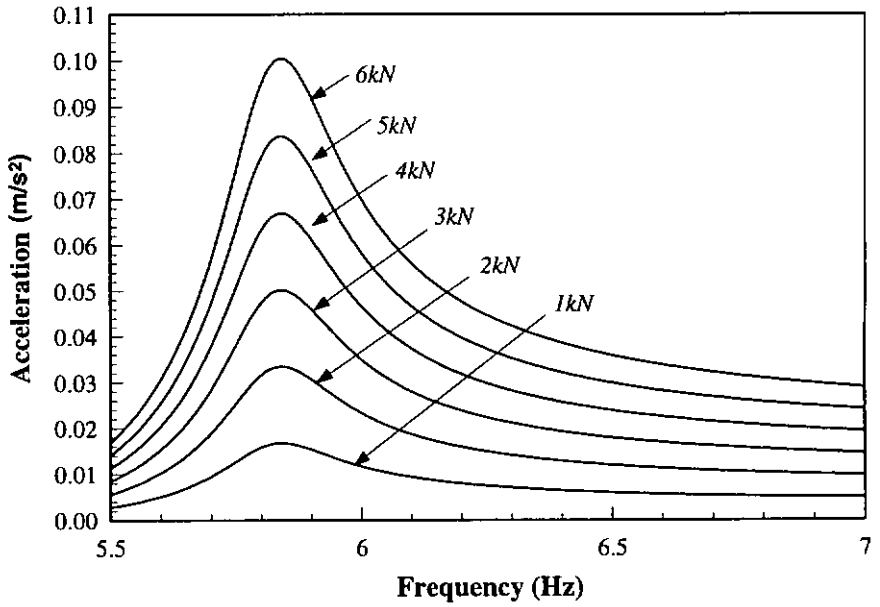

Figure 6.29 Maximum accelerations at the roof level of the building with dampers under loading of different amplitudes

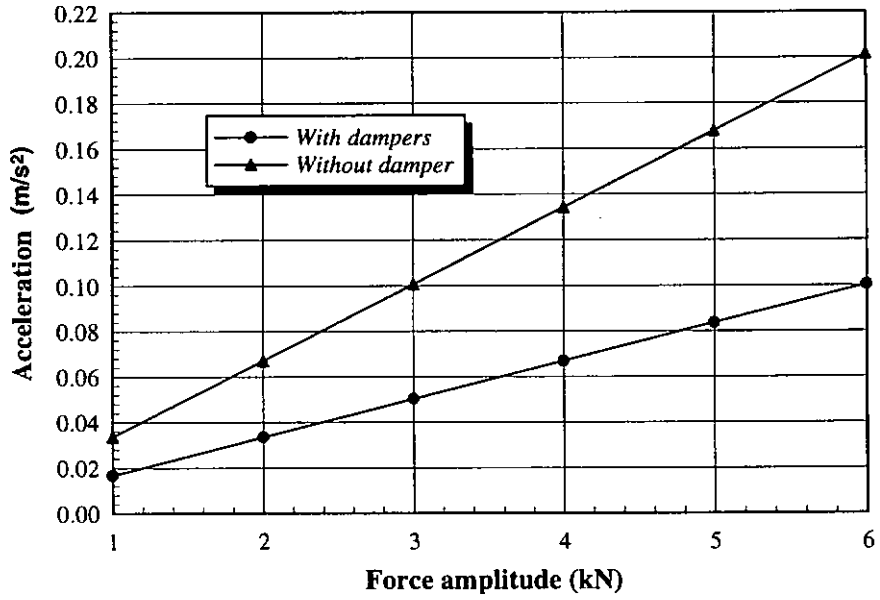

Figure 6.30 Maximum resonant accelerations at the roof level of the building under loading of different amplitudes

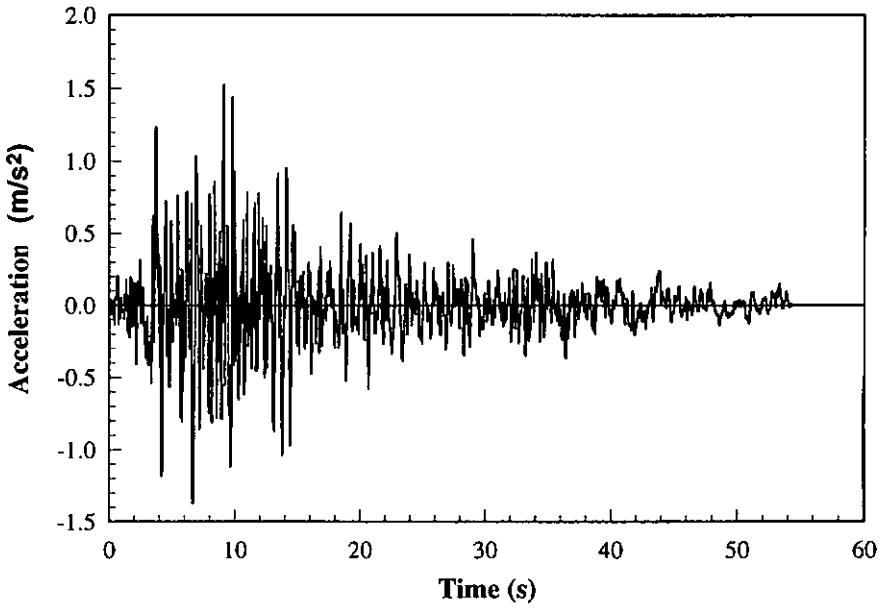

Figure 6.31 Seismic record of Taft (N-21-E)

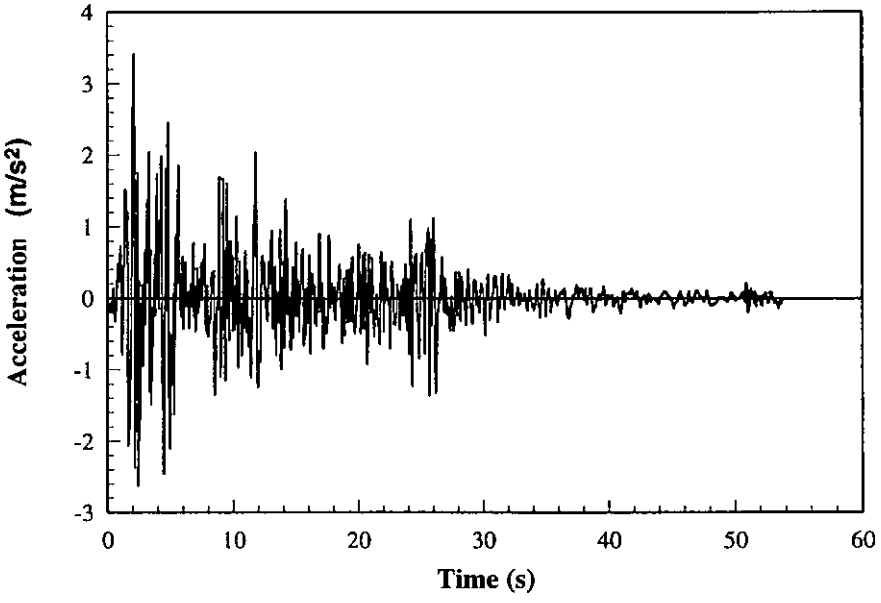

Figure 6.32 Seismic record of El Centro (N-S)

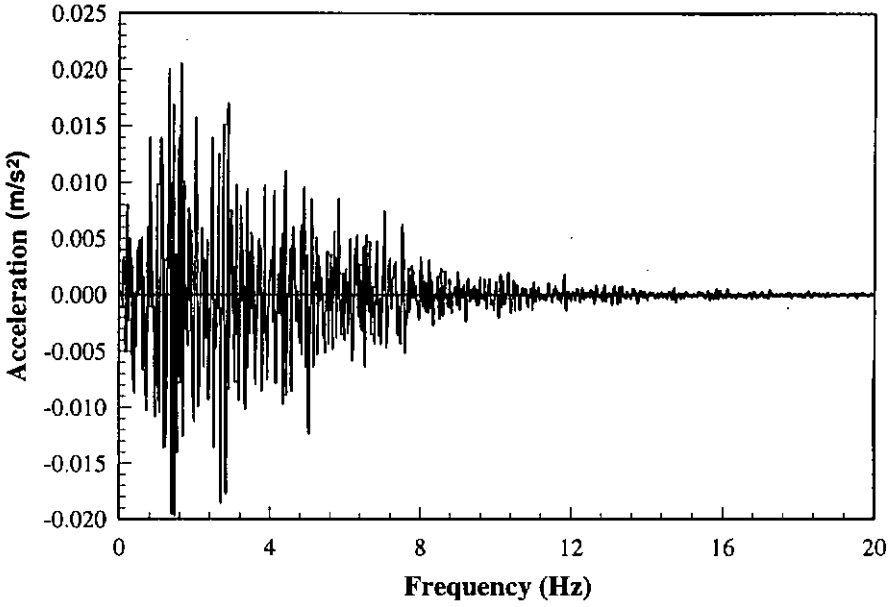

Figure 6.33 Acceleration components at different frequencies of Taft (N-21-E)

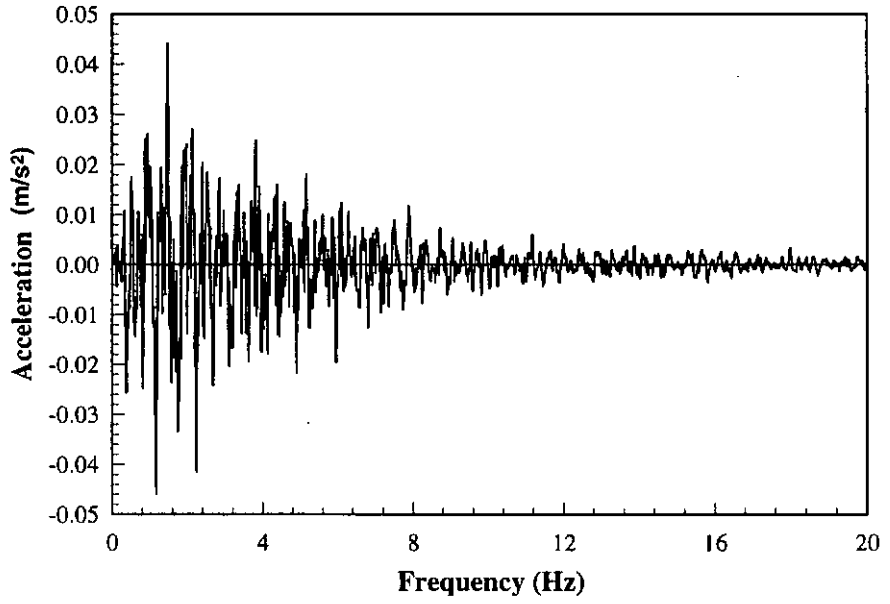

Figure 6.34 Acceleration components at different frequencies of El Centro (N-S)

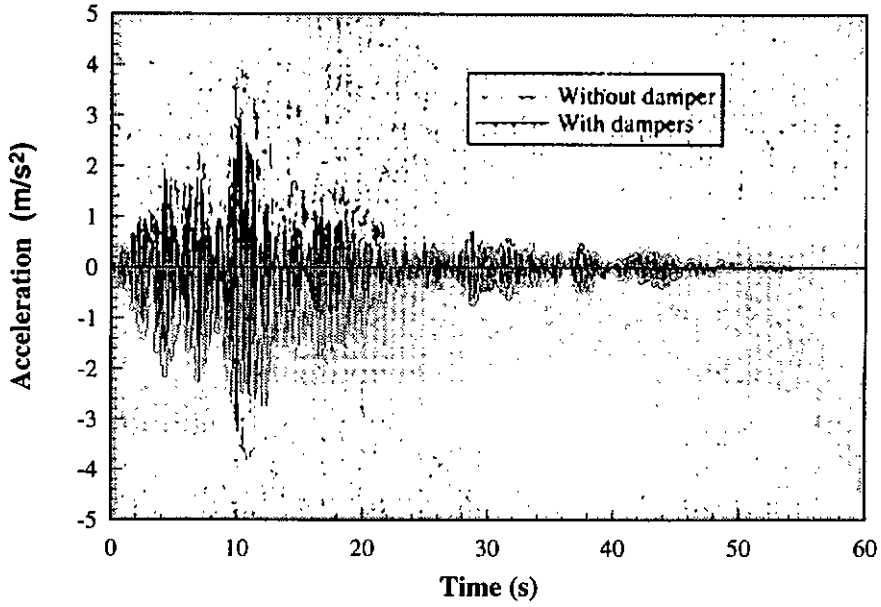

Figure 6.35 Accelerations at the roof level of the building with and without dampers ($80\,A_0$) subject to Taft (N-21-E)

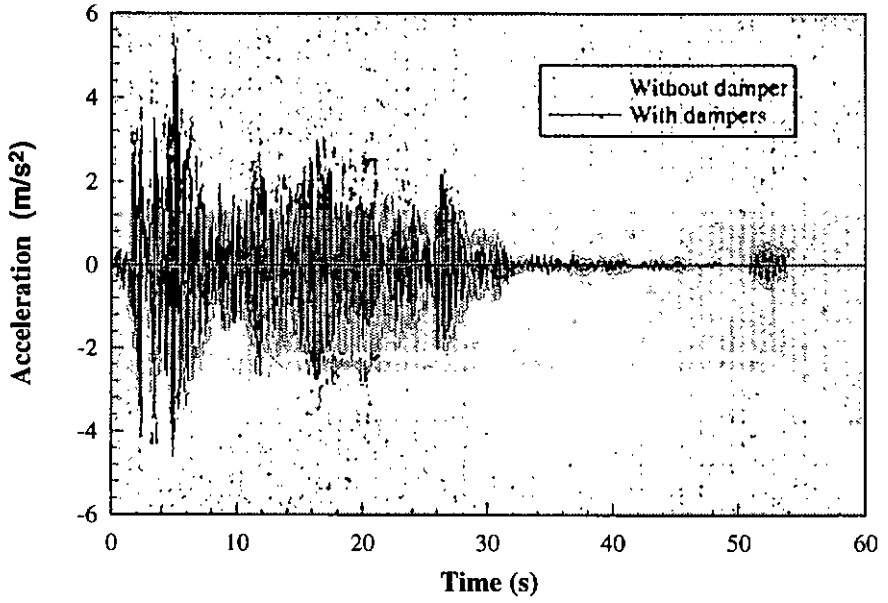

Figure 6.36 Accelerations at the roof level of the building with and without dampers ($80\,A_0$) subject to El Centro (N-S)

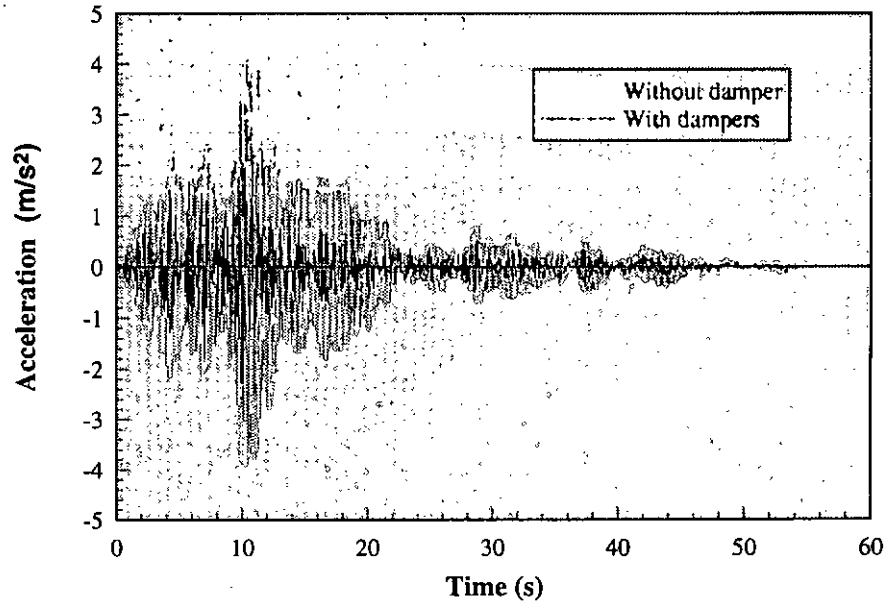

Figure 6.37 Acceleration at the roof level of the building with and without dampers ($240\,A_0$) subject to Taft (N-21-E)

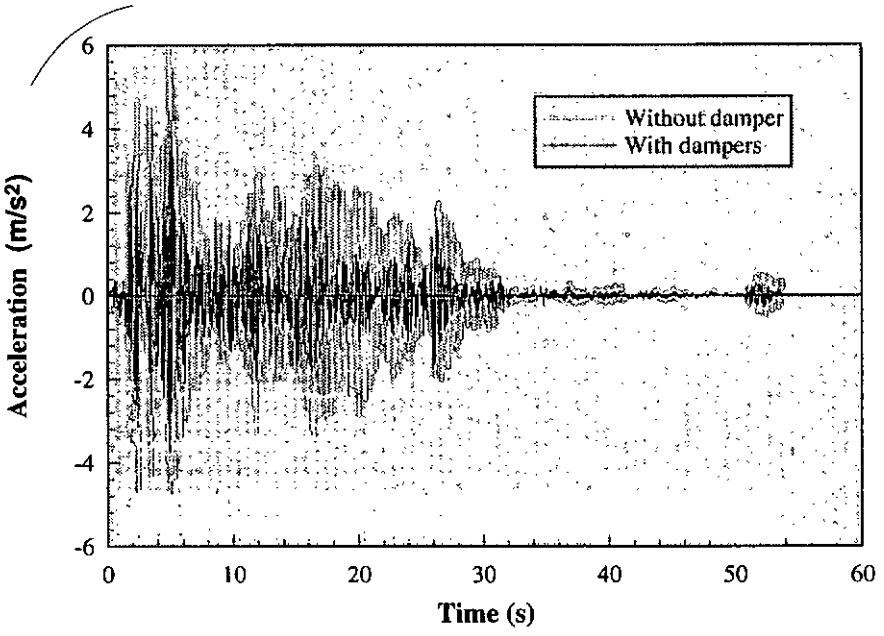

Figure 6.38 Acceleration at the roof level of the building with and without dampers ($240\,A_0$) subject to El Centro (N-S)

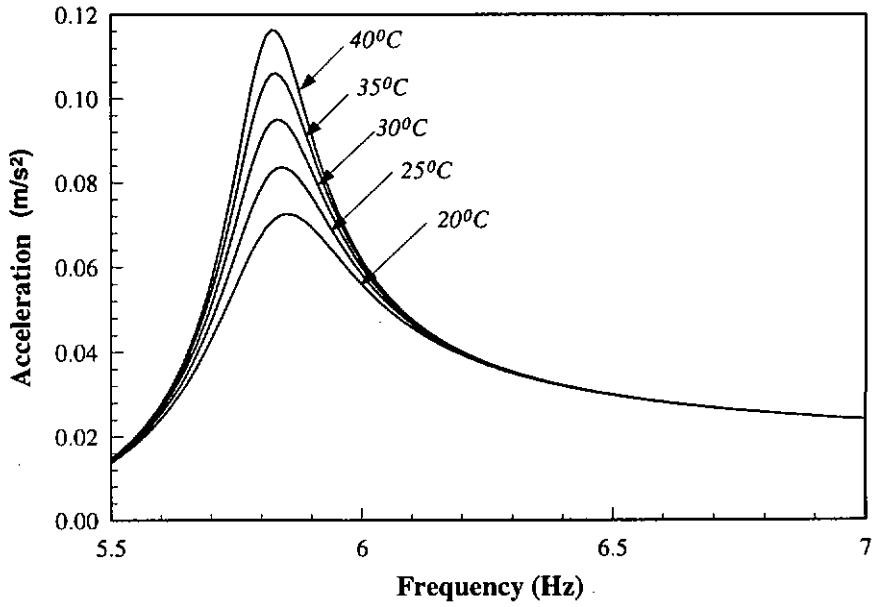

Figure 6.39 Maximum accelerations at the roof level of the building with dampers at different temperatures

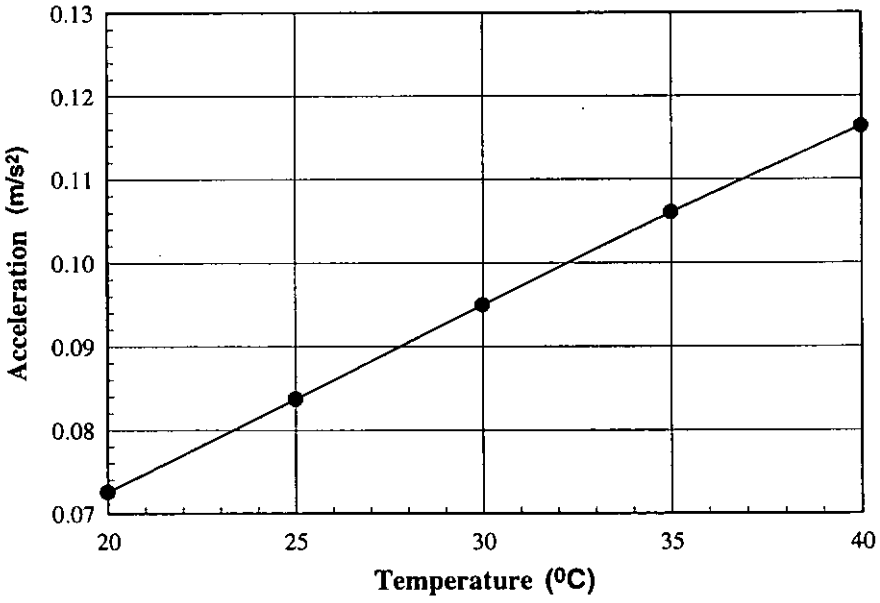

Figure 6.40 Maximum resonant accelerations at the roof level of the building incorporated with dampers at different temperatures

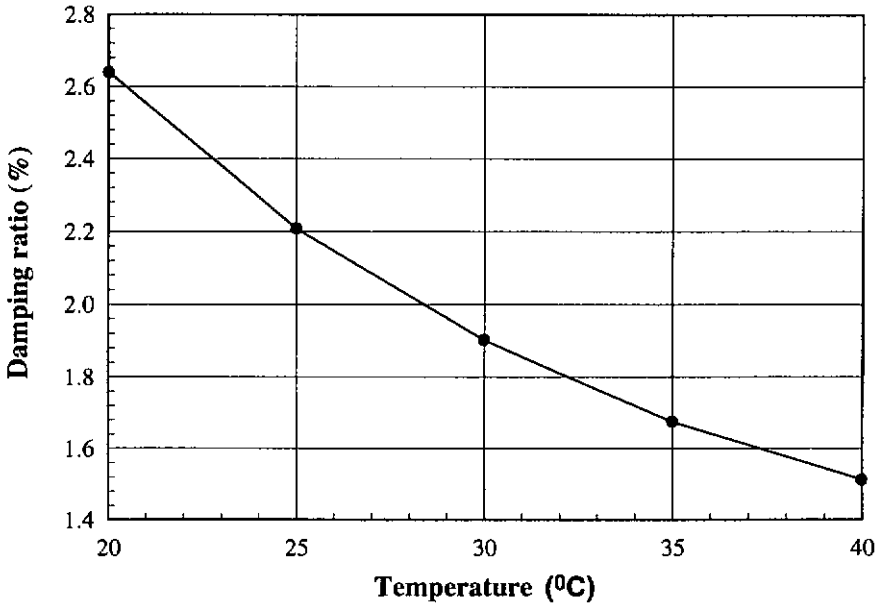

Figure 6.41 Damping ratios of the building with dampers at different temperatures

Photo 6.1 Appearance of the tested frame

CHAPTER 7

CONTROL OF VERTICAL VIBRATION FOR LONG SPAN STRUCTURES

7.1 Introduction

Vertical vibrations are always generated by a variety of human activities and undefined office machinery in buildings that have large column-free areas for general use. Wyatt T. A. (1985) studied the vibration problem of floor system induced by rhythmic vertical jumping like dance of a crowd and developed the design guide for floor systems subject to vibration (1989). Excessive floor vibrations have become a major serviceability consideration in modern building design with the increasing use of high-strength, light-weight structural materials. Moreover, the demand for open-space areas in office and commercial retail buildings has led to the use of floor systems that have longer spans and are thus more flexible than those used in the past. A lot of long span structures such as gymnasiums, dance halls and concert halls etc. built in the last few decades have experienced excessive vibrations due to human activity (Bachmann H., 1992, Sarah E. Mouring, et al, 1994). Vibration tests and analysis of such a floor system were accomplished by Osborne K. P. and Ellis B. R. (1990) and it was found that considerable vibration which was over human perception occurred in such long span structures under human activities. Unfavourable consequences will be brought by vibration of such long span structures due to environmental excitation of daily life. It is therefore important to find ways to control such vibration in order to achieve satisfactory dynamic performance. Although sometimes vibration of a structure can be reduced by adding supports or damping devices

along the span of the structure, it is nonetheless not practical for structures with special architectural requirements. Therefore, consideration of vibration control of such structures in the present study is mainly concentrated on the design of a special beam-column connection.

Applications of dampers at the ends of structural members to suppress vibration have been found in the past years. In general, dampers can be installed in various ways according to the deformation behaviour of the horizontal member. For instance, viscoelastic dampers are located between the lower chords of the horizontal trusses and the columns of the outside wall in the Twin Towers of the World Trade Center in 1969 (Mahmoodi P. et al), which is shown in Figure 7.1. Upon oscillation of the building there is a relative motion between the lower chord of the truss and a column on the building perimeter. This motion generates shear deformation in the viscoelastic part of the damper thereby dissipating a part of the oscillation energy. An energy dissipating connection, in which the elastometric pads are under compression, is shown in Figure 7.2. It was designed and installed in braced and unbraced frames to resist earthquake excitation by Hsu Sheng-Yung et al (1992) and the result of the study showed that the connection could well reduce the response of the structure. No matter what kind of damping connection is used, relative rotation of the beam (truss) to the column is the original source of generating displacement in the dampers.

In the present study, in order to reduce vertical vibration of long span structures where relative rotation between the beam and its neighbouring column exists, a special beam-column connection incorporated with viscoelastic dampers has been designed and experimental study on this kind of beam-column connections

incorporated with viscoelastic dampers has been carried out. The beam with and without dampers incorporated in the beam-column connections have been analyzed by the TDM and the HTFDM. Comparisons of the experimental and analytical results have been made to verify the proposed analytical methods. Thereby, a large amount of numerical simulation work has been done on a full-scaled long span beam with the designed beam-column connections. Based on the parametric studies, some useful guidelines have been obtained for the design of long span structures with beam-column connections incorporated with viscoelastic dampers.

7.2 Description of Beam-column Connection

A long-span beam with its two ends connected with two rigid columns has been designed for dynamic tests. With span-to-depth ratio of 22.7, the length of the I-section beam is 4.54m and the cross section of the beam is shown in Figure 7.3. The beam is connected with columns by web angles bolted in the middle of the beam web. The elevation of the beam-column connection without damper is shown in Figure 7.4(a). Dampers HD91 are used in the beam-column connections. Area of each damper is chosen as 12.5cm×12.5cm according to the beam section. The dampers are set at the upper and lower flanges of the beam. One side of each damper is stuck on the beam flange by Araldite Rapid glue. A cleat angle that is bolted to the column is stuck on the other side of each damper. Appearance of this kind of connection is shown in Figure 7.4(b). When the beam vibrates, it will rotate slightly around the beam end, and the damper on the flanges can be assumed to mainly undergo shear deformation.

7.3 Experimental Test

When dynamic tests are performed on the beam, seven accelerometers are deployed along the beam to measure responses at different positions. The distance between neighbouring accelerometers is 1/8 span of the beam. Before tests being performed on the beam, the accelerometers used for measuring responses and forces have all been calibrated. When the beam is excited, response signals can be picked up by the accelerometers and then transferred to the DTAS (Research Institute of Nanjing Aeronautical Institute, 1992). After that, the test data can be input to a computer operated by the software for DTAS.

In addition to hammer tests, a sinusoidal loading generated by an exciter is acting at the middle point and other positions of the beam. Before the tests, the exciter has been adjusted carefully to align the force acting on the beam vertically. The exciter is controlled by the signal generator via the signal amplifier. The amplitude of the force can be monitored with the support of a digital oscilloscope. The set-up of the dynamic test system is displayed in Figure 7.5 and the elevation of the long span beam under dynamic loading is shown in Figure 7.6. And the appearance of the beam can be seen from Photo 7.1.

Dynamic tests have been done on the beam under three different situations: beam without damper (case I), beam with dampers stuck between beam flanges and angles (case II) and without dampers but cleat angles bolted on the flanges (case III). For each case, firstly, hammer tests are performed on the beam. The first three natural frequencies are captured. They are 35.16Hz, 147.0Hz and 281.5Hz for case I, 42.3Hz, 153.5Hz and 288Hz for case II and 58.5Hz, 169Hz and 310Hz

for case III, respectively. Secondly, based on the natural frequencies obtained at stage one, sinusoidal tests are performed on the beam with small frequency steps near the resonant frequencies. In order to compare the results of different cases conveniently, the force amplitude of each case is set to 10N. The frequency range for measurement is set between 5Hz and 340Hz which contains all the first three natural frequencies of the beam under different situations.

For loading acting at the mid-span of the beam, responses of the beam at the first and the third resonant frequencies are large, the effectiveness in vibration control are studied based on these responses. However, responses at the second resonant frequency are very small, thus responses at point of 3/4 span of the beam while applied loading is also at 3/4 span are collected for studying the effectiveness in vibration control.

7.4 Effectiveness in Vertical Vibration Control

The maximum accelerations at different positions of the beam under case I conditions and subject to sinusoidal loading acting at the mid-span with excitation frequencies falling within the first resonant frequency region are presented in Figure 7.7. Those of the beam under case II conditions are shown in Figure 7.8 and those of the beam under case III conditions are shown in Figure 7.9. It is obvious from these figures that the responses at the middle point are larger than those of other positions for all the cases. Resonant responses of case II are less than those of case I and case III. It can be seen more clearly from Figure 7.10, in which maximum acceleration curves at the middle point of the beam for the three cases are compared. The maximum resonant acceleration at the middle

point of the beam for case I is 48.33m/s^2, that for case II is 7.93m/s^2 and that for case III is 36.26m/s^2. It means that the maximum resonant acceleration at the middle point for case II is only 16.4% of that for case I and 21.9% of that for case III. Damping ratios are also calculated to illustrate the effectiveness in vibration control. Those for case I, II and III are 0.224%, 1.11% and 0.245%, respectively. The maximum resonant responses at different points of the beam for the three cases are drawn in Figure 7.11 and the values in between are interpolated to simulate the mode shapes. Effectiveness in vibration control at different positions can be seen clearly from this figure.

The study of the effectiveness in vibration control with viscoelastic dampers for the second resonant frequency has been carried out by collecting responses when the sinusoidal loading is applied at the point of 3/4 span of the beam. The maximum accelerations at the point of 3/4 span for case I, II and III with exciting frequencies falling within the second resonant frequency region are shown in Figure 7.12. The maximum resonant accelerations for the three cases are 8.05m/s^2, 1.84 m/s^2 and 7.43 m/s^2, respectively. The corresponding damping ratios of the beam are 0.540%, 1.102% and 0.459%, respectively. The resonant responses at different positions are drawn in Figure 7.13 and the values in between are interpolated to simulate the second mode shape of the beam with different beam-column connections. From the above comparisons, it can be seen that the effectiveness in vibration control can still be achieved for the second resonant frequency by the proposed beam-column connections incorporated with viscoelastic dampers.

The effectiveness in vibration control for the third resonant frequency is studied based on the responses of the beam with applied loading at the mid-span. The maximum accelerations at the middle point of the beam for case I, II and III at different excitation frequencies within the third resonant frequency region are shown in Figure 7.14. The maximum resonant accelerations of these three cases are 8.93m/s^2, 4.06m/s^2 and 5.70m/s^2, respectively. The corresponding damping ratios of these three cases are 0.547%, 1.053% and 0.778%, respectively. The maximum resonant accelerations at different positions are drawn in Figure 7.15 and the values in between are interpolated to simulate the third mode shape of the beam for the three different cases. From these comparisons, it can be found that the effectiveness in vibration control is also achieved for the beam with the proposed damping connections.

7.5 Comparison of Experimental and Analytical Results

Although the bending stiffness of the beam-column connection for case I is very small, it still has a certain value. Thus, during analysis, the beam ends for case I are considered as being simply supported but with an additional rotational stiffness. The rotational stiffness of the beam-column connection with and without angles has been determined according to the natural frequencies and modal shapes of the beam. The simulation work has been done for case I, II and III, to make the illustration forthright, the following presentation is concentrated on the beam of case I and case II.

The analytical study has been mainly concentrated on the first natural frequency since the second and third resonant frequencies are beyond the tested frequency range for the shear test of damper HD91.

The long span beam with and without dampers incorporated at the beam-column connections have been analyzed by both the TDM and the HTFDM. Restoring forces of the dampers are calculated by Equation (5.20). The discretization of the beam for FEM is very simple as shown in Table 7.1.

Table 7.1 Discretization of the beam for FEM analysis

Nodes		Elements	
1 : Point A	6 : Point F	1 : AB	6 : FG
2 : Point B	7 : Point G	2 : BC	7 : GH
3 : Point C	8 : Point H	3 : CD	8 : HI
4 : Point D	9 : Point I	4 : DE	
5 : Point E		5 : EF	

The responses of the beam at different positions along the beam which is subjected to sinusoidal loading at different excitation frequencies have been calculated and comparisons of experimental and analytical results have been made. The maximum accelerations at the middle point of the beam for case I are shown in Figure 7.16. And those at the middle point of the beam for case II are shown in Figure 7.17. From both these two figures, it can be seen that both the TDM and the HTFDM can well predict the responses of the beam with and without dampers under dynamic loading. It has also been found from these figures that the results obtained by the HTFDM are better than those by the TDM. The maximum acceleration curve obtained by the HTFDM is much closer to the test data points than those obtained by the TDM. The damping ratios of the beam

with and without dampers calculated by the TDM are 0.245% and 1.16%, respectively, while they are 0.245% and 1.13% obtained by the HTFDM. The damping ratios also indicate that the HTFDM is better than the TDM. Computing time of the TDM and the HTFDM for beam analysis has also been compared. The computing time for calculating the response of the beam with dampers for each excitation frequency with the HTFDM by Pentium 100MHz/16M is only about 0.61s while it is nearly 22.52s if calculated by the TDM, which shows that the HTFDM is better than the TDM in terms of saving computing time.

7.6 Parametric Studies on a Long Span Beam

Experimental and analytical studies have shown that the response of the tested beam in vertical direction can be attenuated greatly by the proposed beam-column connections incorporated with viscoelastic dampers HD91. The effectiveness in vibration control should be concerned with factors such as damper material, damper dimensions, damper location, damper number, characteristics of the beam and loading conditions, etc. Parametric studies have been performed on the tested beam. Comparing with the tested beam, the main beam used for large column-free floor system is always much longer and the mass of the floor slab and other additional elements should be considered in carrying out dynamic analysis. The frequencies of human activities are normally less than 20Hz, which usually covers the first natural frequency of the floor-beam system. The effectiveness in vibration control with the proposed beam-column connections for a long span beam, which is similar to the main beam of the floor studied by Osborne K. P. (1990), has been investigated by numerical simulation. The results show the same trends as given by the tested beam. It is believed that the proposed analytical

method is accurate enough to predict the dynamic response of the full-scaled floor system. Parametric studies on the effectiveness in vertical vibration control with the proposed beam-column connections based on the full-scaled long span beam have been carried out by the HTFDM, the results of which is useful for establishing some guidelines for practical design.

7.6.1 Response analysis of selected beam for parametric studies

The beam with section of 546×406×403kg/m is 16m long. The additional mass added on the beam by the secondary beams and the floor is 1400kg/m. Referring to the test results by K. P. Osborne, damping ratio of the beam without damper is 0.7%. To simulate the effect of the dynamic motion, a sinusoidal loading with amplitude of 600N is assumed to act at the mid-span of the beam. Dampers HD91 with dimensions of 400×400×4 are incorporated in the beam-column connections.

Responses of the beam with three types of beam-column connections as the tested three cases have all been obtained by the proposed analytical method. Maximum accelerations at the middle point of the beam at different excitation frequencies have been presented in Figure 7.18. The maximum accelerations at the resonant frequency are 2.9m/s^2, 1.97m/s^2 and 3.62m/s^2 for these three cases respectively. It can be seen that the response of the beam can also be attenuated greatly with the proposed beam-column connections. And when the dampers are incorporated in the beam-column connections, the damping ratio of the beam will increase to 1.05%.

In the following parametric studies, in order to illustrate the problem more clearly, all the parameter values except the variable to be studied are the same as those described in this sub-section. Responses such as acceleration, velocity and displacement have all been calculated for the parametric studies. Although the scales of them are different, their changing trends are similar, and for the beam-floor systems, what we care about most are acceleration and displacement, in the following sections, studies are concentrated on acceleration and associated with displacement in some parts.

7.6.2 Variation of damper material

When viscoelastic dampers are to be incorporated in a structure, choosing a suitable damper material, which is available in the market, is very important. To change the damper material, the loss modulus of a damper could be varied from 0.25~2.0 of that of the damper HD91 by changing the parameter G_1 of the IFDM. The responses at the middle point of the beam with dampers of different parameter G_1 subject to cyclic loading at different excitation frequencies have been calculated. The curves of the maximum accelerations at the middle point of the beam with respect to the parameter G_1 and the excitation frequency are plotted in Figure 7.19. The maximum resonant accelerations at the middle point of the beam with respect to the parameter G_1 are also plotted in Figure 7.20. It is obvious that when the loss modulus of the damper increases, the resonant acceleration decreases. The damping ratio of the structure with dampers of different kind have been calculated and listed in Table 7.2. It can be seen

apparently from Figure 7.21 that the damping ratio of the beam at the first natural frequency increases with the loss modulus of the damper.

Table 7.2 Damping ratios of the beam with dampers of different parameter G_1

$G_1/G_{1\,(HD91)}$	Damping ratio (%)	$G_1/G_{1\,(HD91)}$	Damping ratio (%)
0.25	0.808	1.25	1.127
0.50	0.886	1.50	1.204
0.75	0.967	1.75	1.285
1.00	1.051	2.00	1.368

From the above study, it can be seen that it would be more effective in vibration control if the material used for the viscoelastic dampers is of higher damping value. In order not to affect the stiffness of the beam too much, the material also with small equivalent stiffness should be chosen.

7.6.3 Variation of damper dimension

Restoring force provided by the dampers are concerned with damper area and shear strain of the damper. When the damper area increases, the restoring force will increase as well. The shear strain of a damper is determined by the shear displacement and the damper thickness. When the damper thickness increases while the other conditions remain unchanged, the maximum shear strain will decrease, the restoring force of the damper will decrease as well. Therefore, the damper area and the damper thickness are the two important factors for vibration control. In practical design, when the selected damper incorporated in the beam-column connection can still not satisfy the requirement for vibration control, damper dimensions can be changed to improve the effectiveness.

7.6.3.1 Variation of damper thickness

Responses at the middle point of the beam with damper thickness changed from 1mm to 10mm under cyclic loading at different excitation frequencies have been calculated, respectively. Maximum accelerations at the middle point of the beam at different excitation frequencies are shown in Figure 7.22. The maximum resonant accelerations at the middle point of the beam are shown in Figure 7.23. It can be seen that when the damper thickness increases, the resonant acceleration becomes larger. The maximum acceleration is not in linear relation with the damper thickness.

Table 7.3 Damping ratios of the beam with dampers of different thickness

Thickness (mm)	Damping ratio (%)	Thickness (mm)	Damping ratio (%)
1	2.564	6	0.924
2	1.457	7	0.891
3	1.175	8	0.867
4	1.051	9	0.849
5	0.977	10	0.832

Damping ratios of the beam with dampers of different thickness have been calculated and listed in Table 7.3. It can be seen obviously from Figure 7.24 that the damping ratio of the beam will increase when damper thickness decreases.

7.6.3.2 Variation of damper area

Responses of the beam, with damper area changed from 0.25 to 2.00 of that of the damper used in section 7.6.3.1 at different excitation frequencies have been

calculated. The maximum accelerations at the middle point of beam with dampers of different area are shown in Figure 7.25. And the maximum resonant acceleration responses are shown in Figure 7.26. It can be seen that the resonant acceleration increases nonlinearly with the damper area.

The damping ratios of the beam in different cases have been calculated and listed in Table 7.4. The damping ratio of the beam increases with the damper area as shown in Figure 7.27.

Table 7.4 Damping ratios of the beam with dampers of different areas

Damper area ($\times A_0$)	Damping ratio (%)	Damper area ($\times A_0$)	Damping ratio (%)
0.25	0.782	1.25	1.146
0.50	0.867	1.50	1.244
0.75	0.958	1.75	1.346
1.00	1.051	2.00	1.457

From the above studies, it can be seen that damper dimensions affect the effectiveness in vibration control of long span structures with the proposed beam-column connections significantly. In practical design, the effectiveness can be improved by selecting thinner dampers or increasing the damper area referring to the changing trends of the response or the damping ratio provided by the presented figures.

7.6.4 Variation of damper number

For a beam with the developed beam-column connections, totally four dampers can be incorporated in the two connections. In fact, limited by the circumstances,

four dampers in total can not always be used for a beam. For instance, to the utmost only two dampers can be stuck on the bottom flange of a beam on the roof of a building. In some special areas, dampers are not permitted to be installed at the beam-ends due to architectural requirements. The damper number should be determined by the actual conditions. The effectiveness in vibration control of a beam with different number dampers has been carried out as follows. Four cases have been considered: 1, one damper at one end of the beam; 2, one damper at one end and one damper at the other end; 3, two dampers at one end and one damper at the other end; 4, two dampers at each end.

The maximum accelerations and displacements at the middle point of the beam with different number of dampers at the first resonant frequency have been calculated and are shown in Figure 7.28 and Figure 7.29, respectively. And the maximum resonant accelerations and displacements of the beam with different number of dampers are presented in Figure 7.30 and Figure 7.31. It is obvious that the more the damper number is, the more the response of the beam can be attenuated. The resonant frequency also increases with the damper number not only due to the equivalent shear stiffness of the added dampers, but also the axial stiffness of dampers.

The damping ratios of the beam incorporated with different number of dampers have been calculated and listed in Table 7.5. The damping ratio of the beam increases with the damper number and the increasing trend is shown in Figure 7.32.

Table 7.5 Damping ratios of the beam with different number of damper

Damper number	Damping ratio (%)	Damper number	Damping ratio (%)
1	0.806	3	0.975
2	0.896	4	1.051

For a beam with the same damper number, influence of the damper arrangement pattern is studied. If two dampers are incorporated in the beam, one way is to set both dampers at one side (case A) and the other way is to set one damper at each side (case B). The responses of the beam with two kinds of damper setting subject to sinusoidal loading acting at the mid-span and the 1/4 span of the beam have both been calculated and the corresponding maximum accelerations at the middle point of the beam at different excitation frequencies are shown in Figure 7.33(a) and Figure 7.33(b), respectively. When the loading is acting at the 1/4 span, the loading position is near the beam-column connection if dampers are set at one side. It can be seen that the maximum resonant acceleration at the middle point of the beam for case A is larger than that of case B for different loading positions. The damping ratios of the beam are 0.881% and 0.896% for case A and case B, respectively. It can be seen that to set dampers at both ends is better than to set dampers at one side while leaving the other side without damper. It is because that the structure is symmetric when the dampers are installed at both two sides, while it is unsymmetrical when the dampers are installed at one side only.

7.6.5 Variation of loading

7.6.5.1 Variation of loading position

Loading can act at any place of a structure in practical use. For example, sometimes, dynamic loading like human activities would move along the beam, machines would be installed at different positions. The effectiveness in vibration control of the structure with loading acting at different positions have been carried out and are presented in this section. Four positions along the beam, which are at 1/8, 1/4, 3/8 and 1/2 span of the beam, are chosen as the loading positions. Maximum accelerations and displacements at the middle point of the beam without damper at different excitation frequencies have been calculated and are shown in Figure 7.34 and Figure 7.35, respectively. In order to distinguish the curves clearly, Log-scale is applied for the y-axis. The maximum accelerations and displacements at the middle point of the beam with dampers have also been calculated and are shown in Figure 7.36 and Figure 7.37. It can be seen that the maximum responses can be reduced greatly for all these four cases and the resonant frequency does not change with loading position. The damping ratios of the beam incorporated with dampers under loading at different positions have been calculated and it is found that the damping ratio remains unchanged when the loading position is changed. The damping ratio is equal to 1.051% for all cases. The attenuation ratios of the response under loading at different positions are compared in Figure 7.38, it can be seen that the effectiveness are nearly the same for loading at different positions. Usually, in practical application, the objective of vibration control of a structure is to keep the maximum response

below a certain value, if the loading position is near the mid-span, more dampers, dampers with larger area or thinner dampers should be adopted.

7.6.5.2 Variation of loading amplitude

Response of a structure is also determined for a variety of loading amplitudes. When the amplitude of sinusoidal force acting on the beam is small, the vibration is not obvious and even can not be perceived. While the amplitude increases, the vibration will become violent. Loading of amplitudes of 100N, 200N, 300N, 400N, 500N, 600N, 700N, 800N, 900N and 1000N are assumed to act on the beam, respectively. Maximum accelerations and displacements at the middle point of the beam without damper under loading of different amplitudes and at different excitation frequencies are shown in Figure 7.39 and Figure 7.40, respectively. The maximum accelerations and displacements at the middle point of the beam with dampers under loading of different amplitude are shown in Figure 7.41 and Figure 7.42. The maximum resonant accelerations and displacements of the beam with and without dampers under loading of different amplitudes are presented in Figure 7.43 and Figure 7.44. The maximum responses of a structure either with or without dampers change with the loading amplitude linearly. From these figures, it can be seen that no matter the force amplitude is small or large, the response can be reduced significantly and the resonant frequency remains unchanged. The damping ratios of the beam with dampers under different loading conditions have been calculated and it has been found that the values are all 1.051% for different loading amplitude. In another word, the damping ratio of a structure incorporated with dampers does not change

with loading amplitude. The reason is that the damping ratio of the structure without damper is assumed to be proportional and the damping ratio of a damper does not change with shear displacement amplitude.

Although the amplitude of response is reduced greatly when the loading force is large, the effectiveness in vibration control is nearly the same, which can be seen from Figure 7.45. Thus, in practical design, it is only required to work out the solution by assuming one loading amplitude.

7.6.6 Variation of temperature

Since energy dissipation ability of a damper changes with the temperature, the temperature of the environment should be an important factor for the effectiveness in vibration control. When the dynamic tests were performed on the damper HD91, the environmental temperature was about 25°C. According to the study in Chapter Four, the IFDM for HD91 with consideration of temperature can be expressed as $\tau(t) = e^{-0.056(T-25)}\left[0.795\gamma(t) + 0.0285D^{0.724}\gamma(t)\right]$. Responses of the beam at temperature of 20°C, 25°C, 30°C, 35°C and 40°C have been calculated. The maximum accelerations and displacements at the middle point of the beam at different excitation frequencies are shown in Figure 7.46 and Figure 7.47, respectively. It can be seen that when the temperature increases, the maximum responses increase greatly while the resonant frequency of the structure decreases. The damping ratios of the beam at different temperatures have been listed in Table 7.6 and the changing trail is shown in Figure 7.48. It can be seen that when the temperature increases, the damping ratio of the beam will decrease. It is because that when the temperature increases, the loss modulus

and the storage modulus of a damper will decrease, which leads to decreasing of the damping ratio and the equivalent stiffness of the damper. Therefore, for a structure incorporated with viscoelastic dampers, when the temperature increases, the damping ratio and the stiffness of the structure will decrease.

Table 7.6 Damping ratios of the beam with dampers at different temperatures

Temperature (^{0}C)	Damping ratio (%)	Temperature (^{0}C)	Damping ratio (%)
20	1.170	35	0.891
25	1.051	40	0.851
30	0.958		

7.7 Discussions and Conclusions

- The proposed beam-column connection

A special beam-column connection incorporated with viscoelastic dampers has been designed to control vertical vibration of long span beams, especially for long span beam-floor system. Great effectiveness in vertical vibration control of long span structures has been demonstrated by the experimental studies on a beam with and without the proposed viscoelastic beam-column connections. This kind of beam-column connection incorporated with viscoelastic dampers is an entirely new damping device. Such connection can make the damper undergo mainly shear deformation under dynamic loading. The thickness of the dampers incorporated in the connection is always very small. The damper is stuck between cleat angles and flanges of the beam. If possible, the damper can be stuck first between two thin steel plates whose area is a little larger than that of the damper

to make the damper incorporated more conveniently in the connections. This kind of connection can be applied not only for beam-column connections, but also for any connections of structural members, where relative rotation exists between them. Comparing with the damping devices shown in Figure 7.2 and Figure 7.3, this kind of beam-column connection can fabricated in a structure more conveniently and can be used widely for various kinds of structures.

This kind of damping device can be used in fact not only to suppress vertical vibration for long span structures, but also to control vibration of building structures in horizontal direction. When a building is excited by wind or earthquake, it will sway horizontally and relative rotation between the vertical and horizontal structural members will occur. If the designed damping devices are used between the horizontal members and the vertical members, energy will be dissipated and horizontal vibration of the framed structures will be attenuated.

- Verification of the analytical methods

Comparison of the experimental and analytical results for a long span beam have demonstrated that the developed HTFDM and TDM can well predict the response and the damping ratio of a structure with such connections incorporated with or without viscoelastic dampers.

Although this type of beam-column connection is also effective in attenuating vibration in the second and the third natural frequency region of the beam, no comparison of experimental and analytical results has been made since these two higher natural frequency regions are out of the frequency range used for the dynamic shear tests on the damper specimen.

- Guidelines from the parametric study

To design a long span structure with the proposed beam-column connections, both the deflection requirement under static loading and vibration requirement under dynamic loading should be satisfied. If the stiffness of a beam is too small due to the installation of dampers, a larger beam section may need to be used. In order to obtain good effectiveness in vibration control, factors like damper material, damper area, damper thickness, damper number and environment temperature should be considered. The guidelines for practical design obtained from the parametric studies are listed briefly as follows.

1. Better effectiveness in vibration control can be achieved by dampers with larger loss modulus, it is important to choose a suitable kind of damper which is available in the market.

2. The effectiveness can also be improved by increasing the damper area, but damper area is constrained by the structural member sizes such as the width of the beam flange. Since the largest damper width to be applied is limited by the width of the beam flange, in order to improve the effectiveness in vibration control, the length of the damper can be extended. However, if the damper length is too long, the outer most tension at the edge of damper may exceed the strength of the glue and make the damper separated from the beam or the angle. Moreover, the increase in tension and compression of the damper will further constrain the rotation of the beam, which will also increase the natural frequency of the beam further.

3. Thinner dampers are more effective in vibration control and can also reduce cost. Thicker dampers also occupy more space. However, if the thickness of a

damper is too small, the damper is easier to be damaged when it is subject to violent or large vibration. Therefore, in practical application, based on the estimation of the vibration of the beam and the acceptable level of vibration, the thickness of the damper should be designed as thin as possible.

4. Four dampers should be used at both ends of a long span structure as far as practical. If constrained by the real situation, not all the four dampers can be installed, it is better to spread the dampers at both two ends rather than to place them at one end.

5. Temperature will affect the effectiveness in vibration control of long span structures. In the design of the viscoelastic beam-column connection, the temperature effect should be taken into consideration. In other words, the right parameter values should be chosen for the damper in accordance with the temperature of the working environment.

6. Although loading condition does not affect the effectiveness in vibration control, it is the main factor for designing the viscoelastic beam-column connection for vibration control.

Since the properties of the beam such as beam sections and beam span are determined by the ultimate limit state design, they are always not practical to change to satisfy the requirements of the serviceability limit state such as the vibration level. Therefore, they are not considered in the parametric studies.

7.8 References

Bachmann H. (1992), Case Studies of Structures with Man-induced Vibrations, Journal of Structural Engineering, ASCE, Vol.118, No.3, pp. 631-647.

Hsu Sheng-Yung and Fafitis Apotolos (1992), Seismic Analysis Design of Frames with Viscoelastic Connections, Journal of Structural Engineering, Vol. 118, No. 9.

Mahmoodi P., Robertson L. E., Yontar M., Moy C. and Feld L., Performance of Viscoelastic Structural Dampers in World Trade Center Towers, Vibration Control Systems Construction Market, 3M Technology Report.

Osborne K. P. and Ellis B. R. (1995), Vibration Design and Testing of a Long-Span Lightweight floor, the Structure Engineer, Vol.68, No.10, pp181-186.

Research Institute of Nanjing Aeronautical Institute (1992), Dynamic Test and Analysis System User Guide, Vibration Engineering.

Sarah E. Mouring and Bruce R. Ellingwood (1994), Guidelines to Minimize Floor Vibrations from Building Occupants, Journal of Structural Engineering, ASCE, Vol. 120, No. 2, pp507-526.

Wyatt T. A. (1989), Design Guide on the Vibration of Floors, the Steel Construction Institute, ISBN: 1-870004-34-5.

Wyatt T. A. (1985), Floor Excitation by Rhythmic Vertical Jumping, Short Communication, Journal of Engineering Structure, Vol.7, pp208-210.

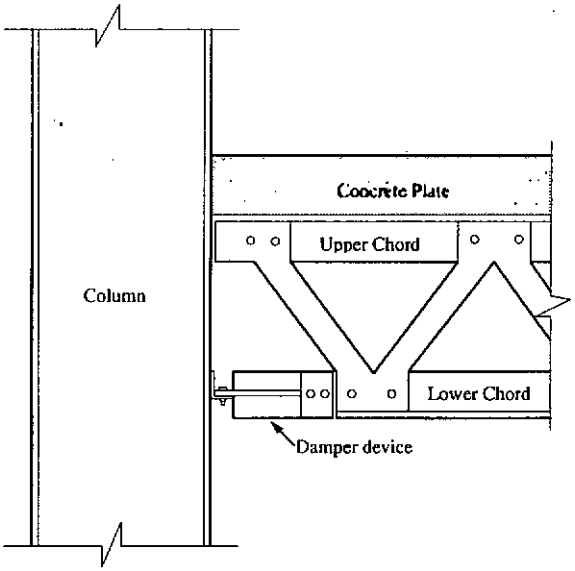

Figure 7.1 Damping device of Word Trade Centre

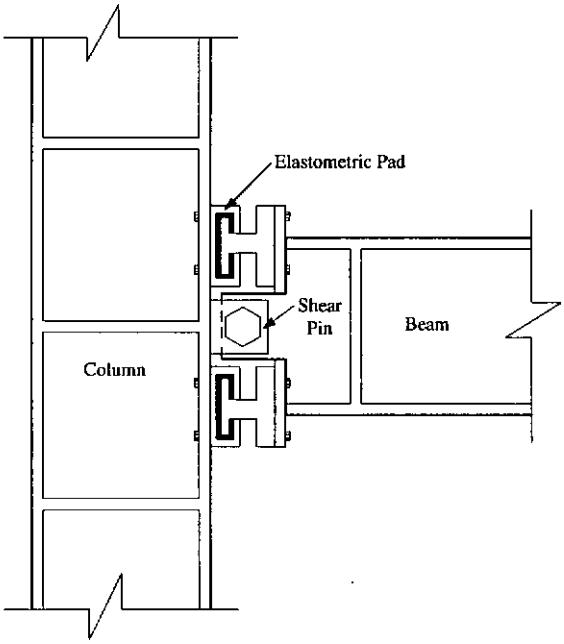

Figure 7.2 Beam-column connection designed by Sheng-Yung Hsu

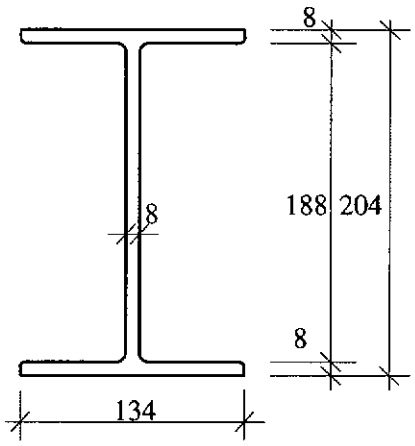

Figure 7.3 Section of the tested beam

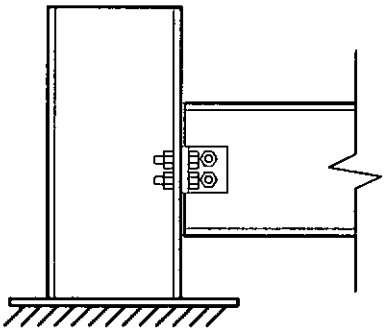

(a) Without viscoelastic dampers

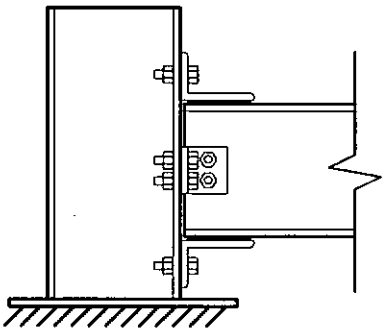

(b) With viscoelastic dampers

Figure 7.4 Elevation of the beam-column connection

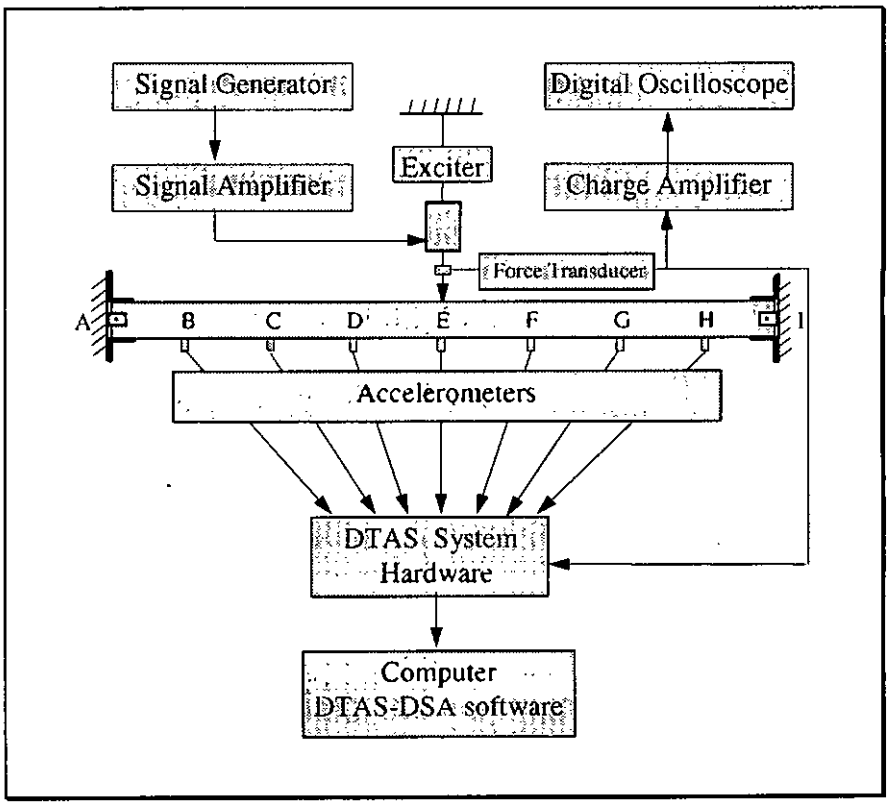

Figure 7.5 Set-up of the test system

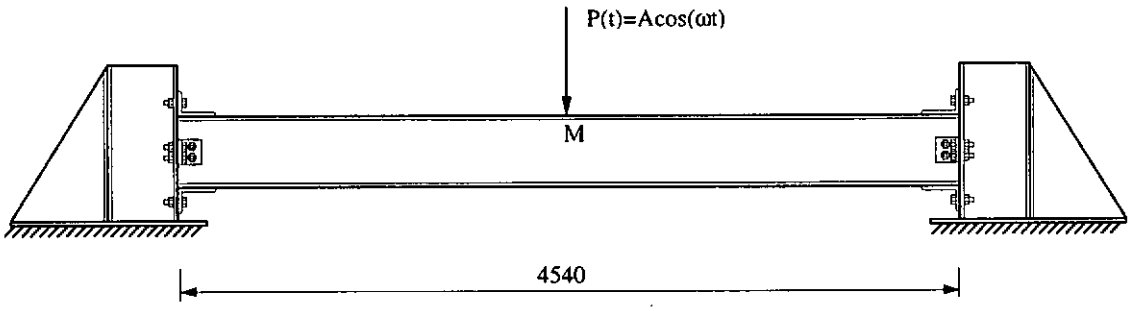

Figure 7.6 Elevation of the tested beam

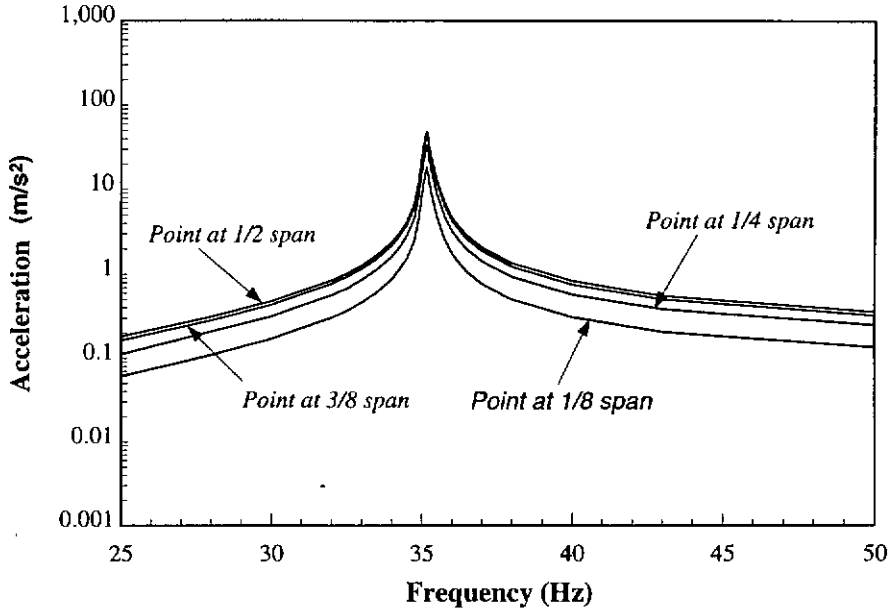

Figure 7.7 Maximum accelerations of case I in the first resonant frequency region

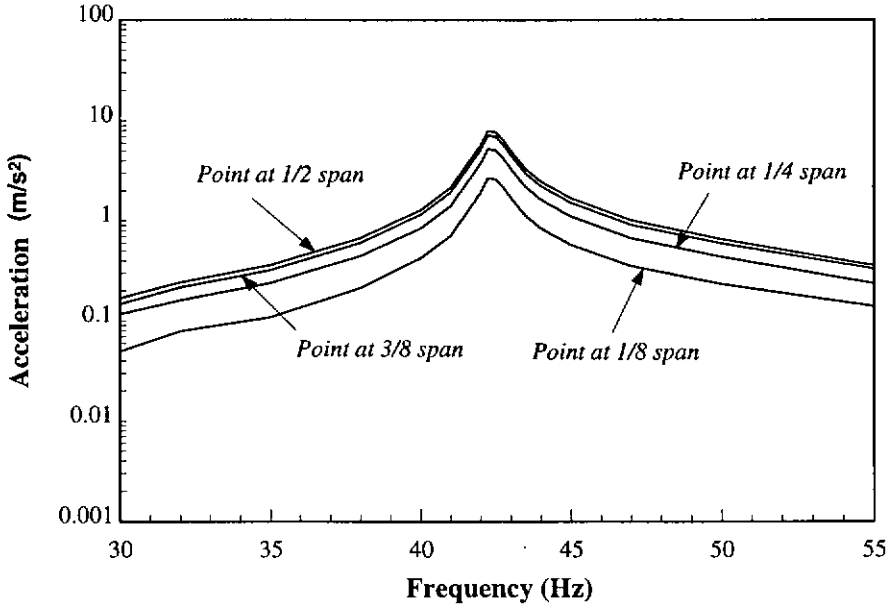

Figure 7.8 Maximum accelerations of case II in the first resonant frequency region

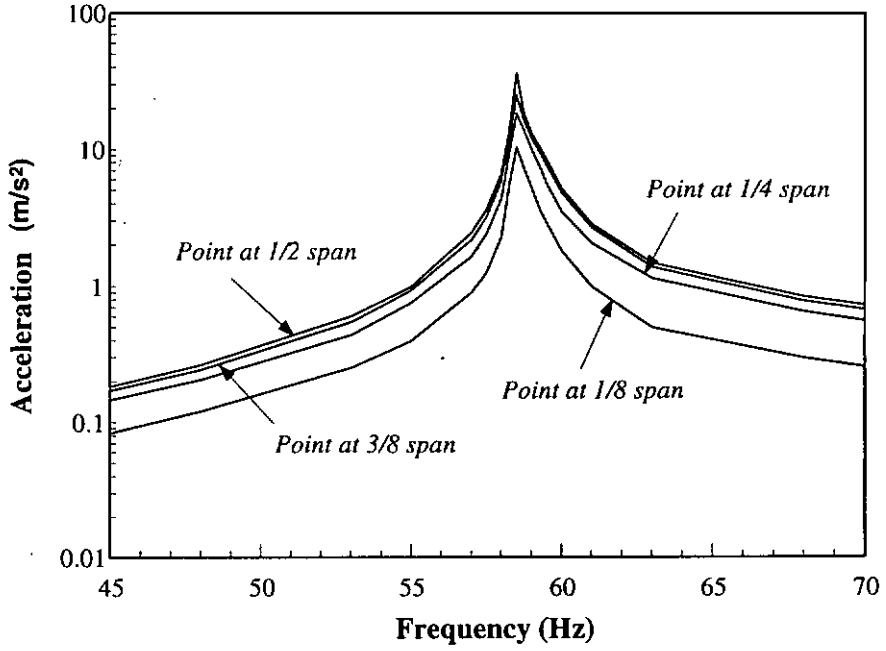

Figure 7.9 Maximum accelerations of case III in the first resonant frequency region

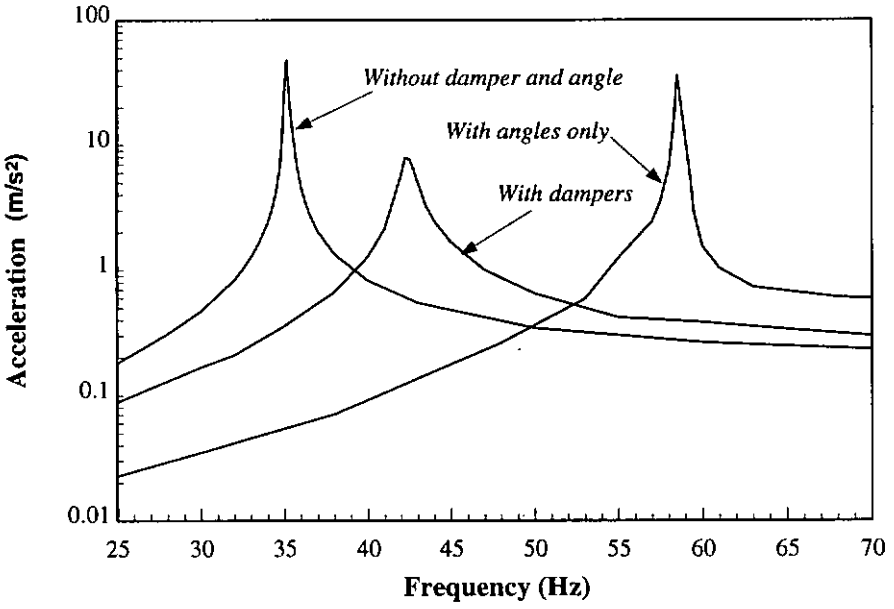

Figure 7.10 Maximum accelerations at the middle point of the beam in the first resonant region

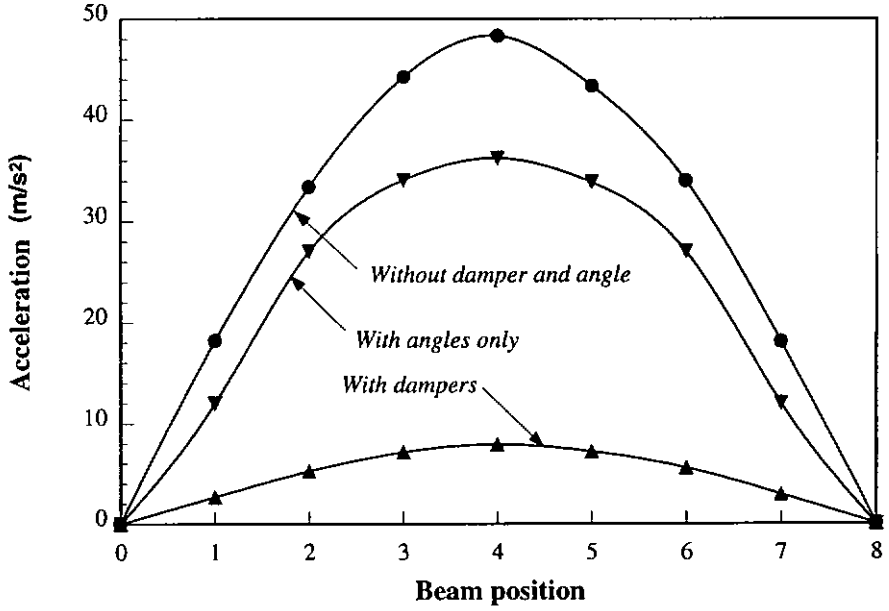

Figure 7.11 Maximum accelerations at different positions of the beam with and without dampers at the first resonant frequency

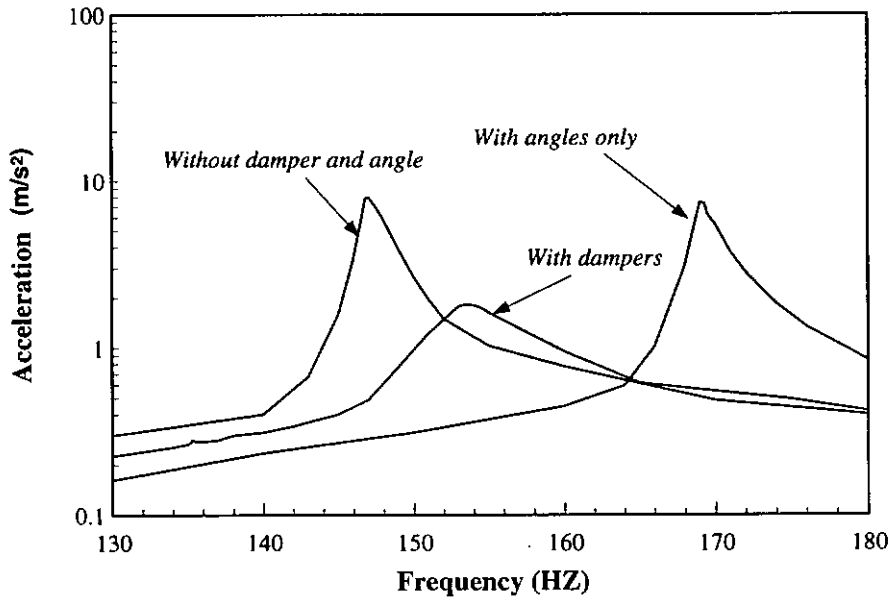

Figure 7.12 Maximum accelerations at point of 3/4 span of the beam with dampers in the second resonant frequency region under loading at 3/4 span

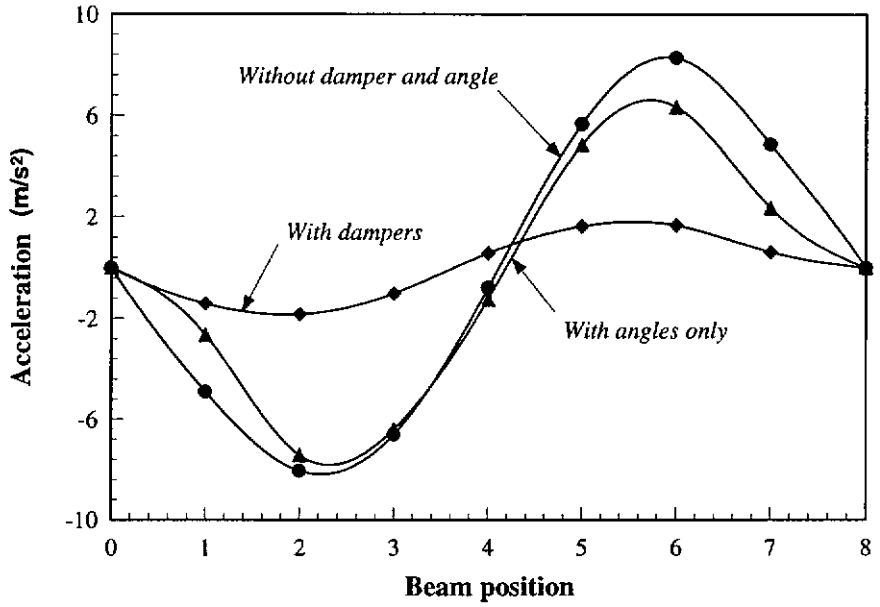

Figure 7. 13 Maximum accelerations at different positions of the beam with and without dampers at the second resonant frequency

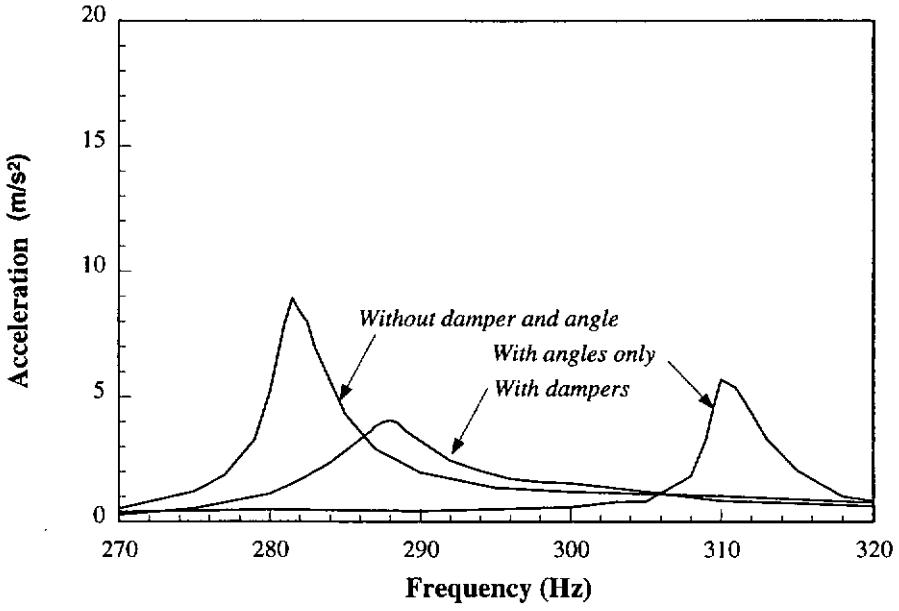

Figure 7.14 Maximum accelerations at the middle point of the beam in the third resonant frequency region

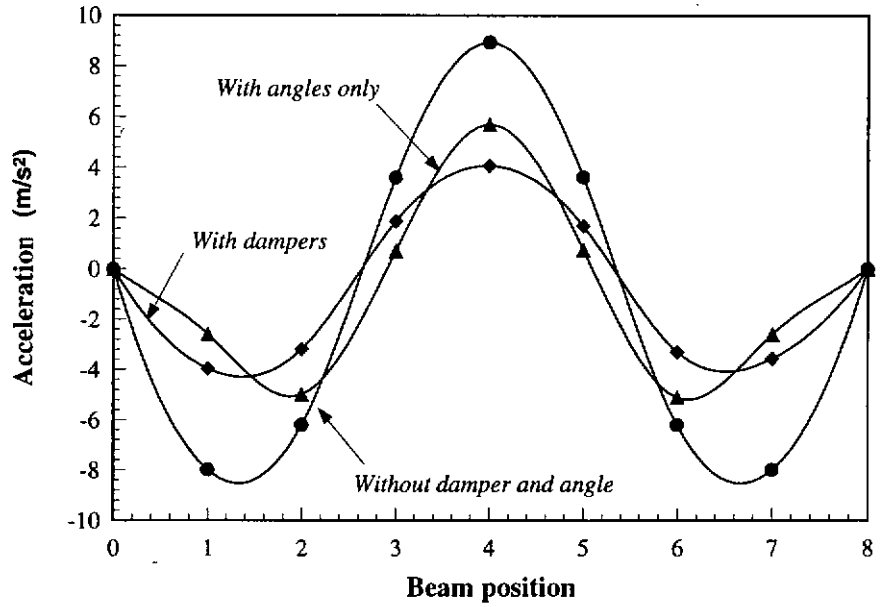

Figure 7.15 Maximum accelerations at different positions of the beam with and without dampers at the third resonant frequency region

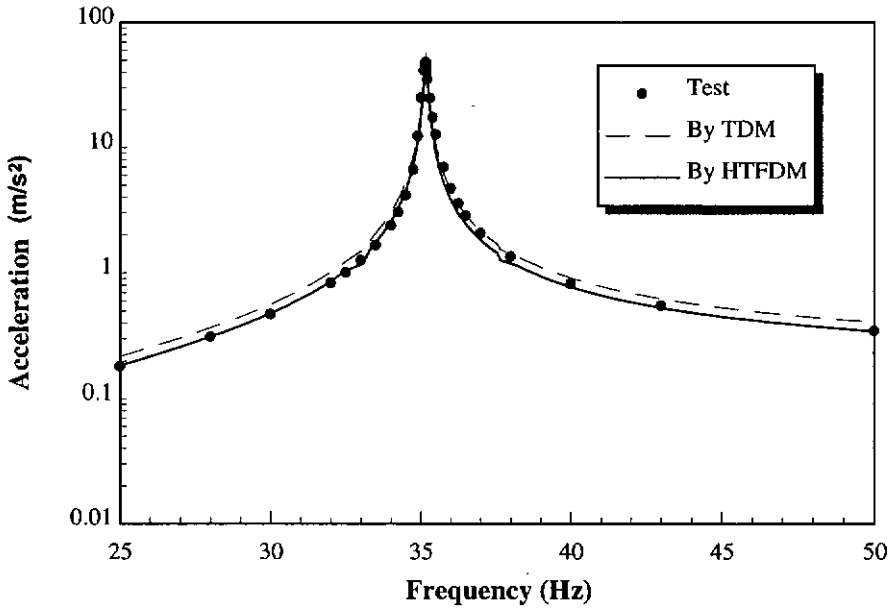

Figure 7.16 Maximum accelerations at the middle point of the beam without damper in the first resonant frequency region

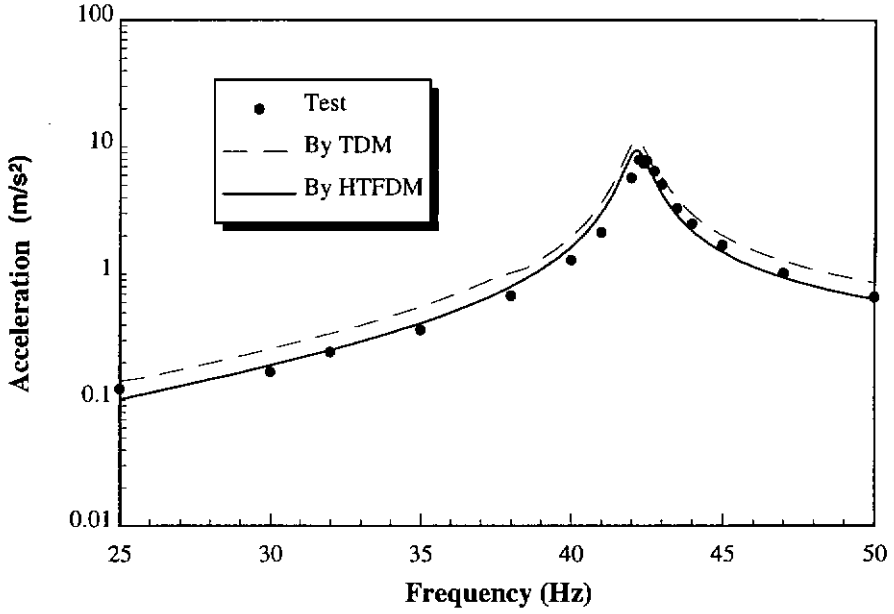

Figure 7.17 Maximum accelerations at the middle point of the beam with dampers in the first resonant frequency region

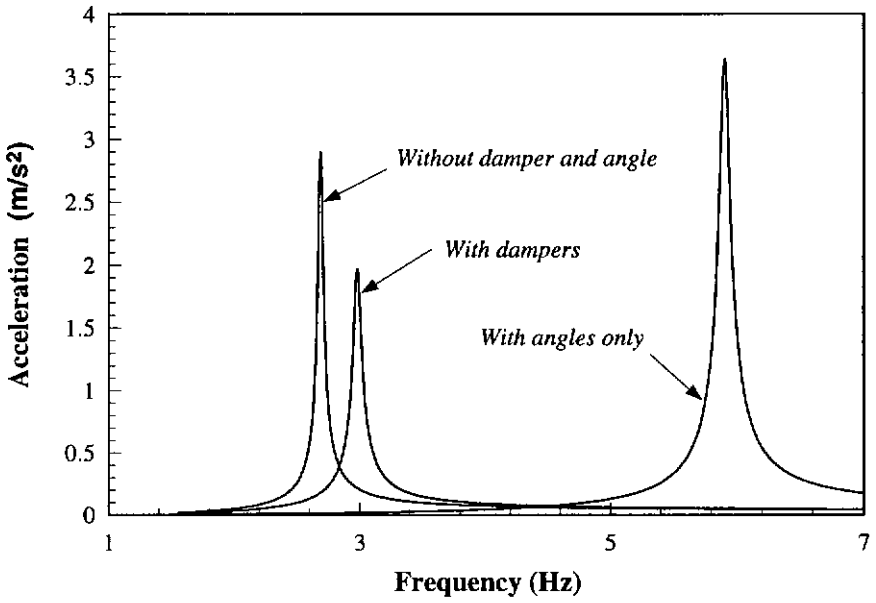

Figure 7.18 Maximum accelerations of the long span beam with and without dampers

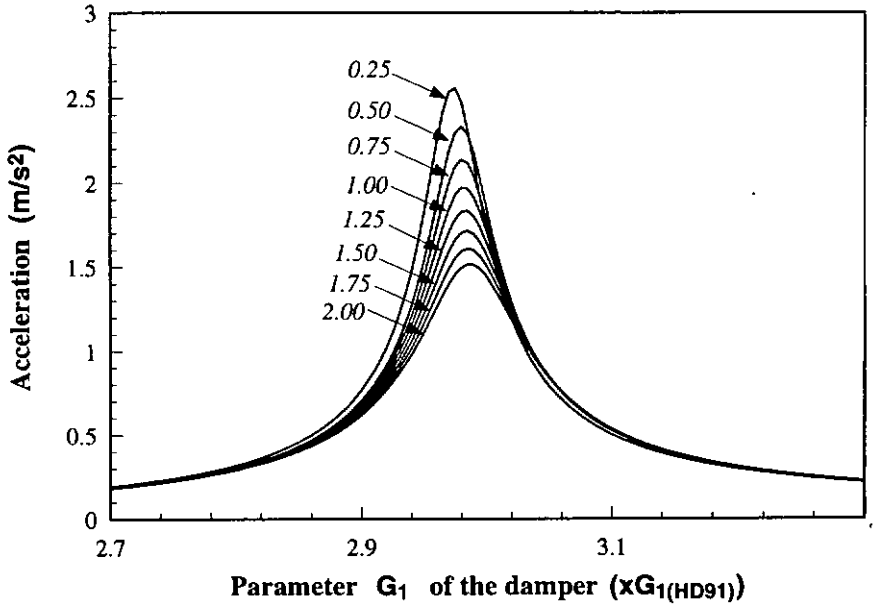

Figure 7.19 Maximum accelerations at the middle point of the beam with dampers of different parameter G_1

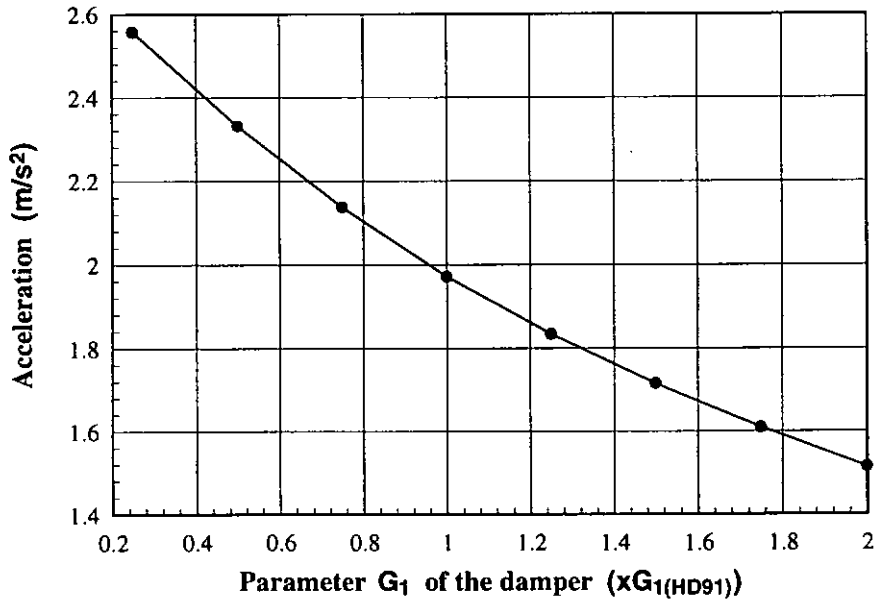

Figure 7.20 Maximum resonant accelerations at the middle point of the beam with dampers of different parameter G_1

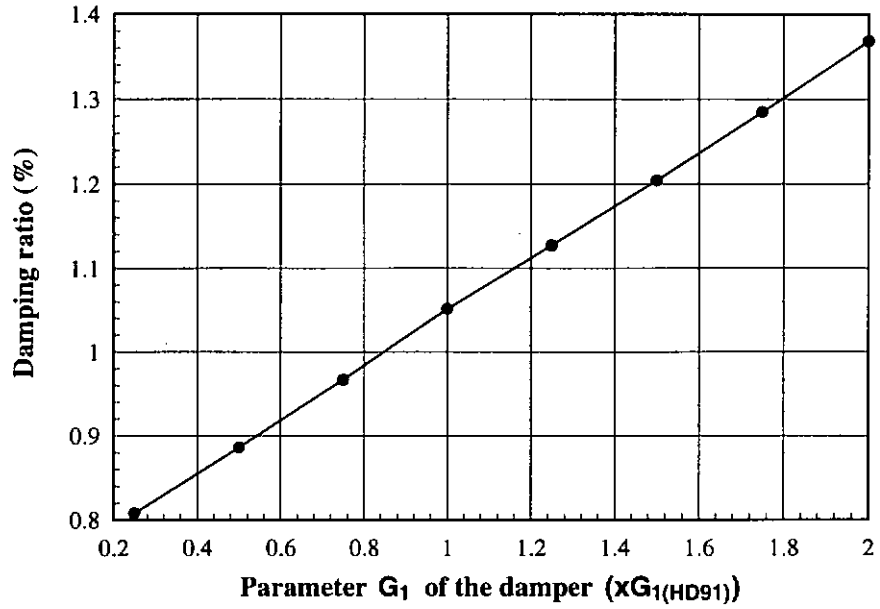

Figure 7.21 Damping ratios of the beam with dampers of different parameter G_1

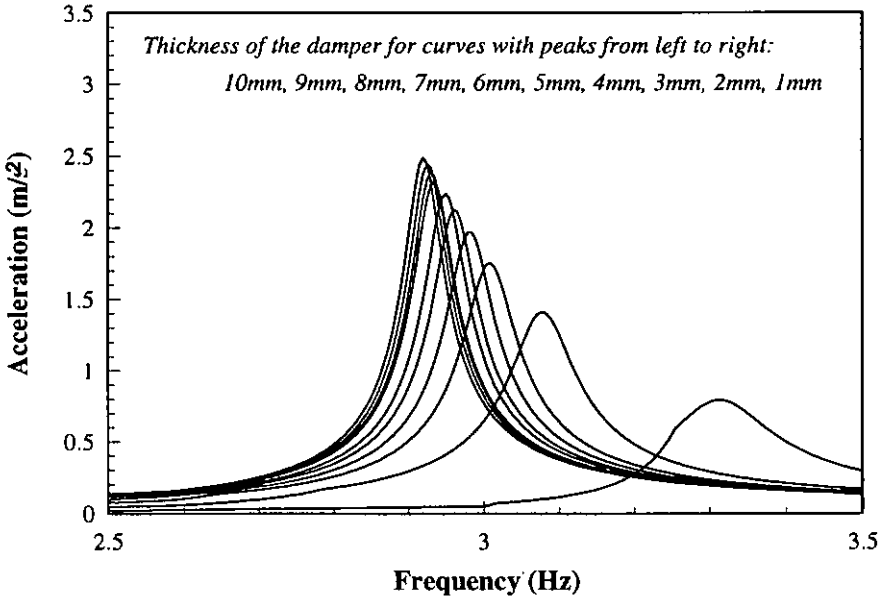

Figure 7.22 Maximum accelerations at the middle point of the beam with dampers of different thickness

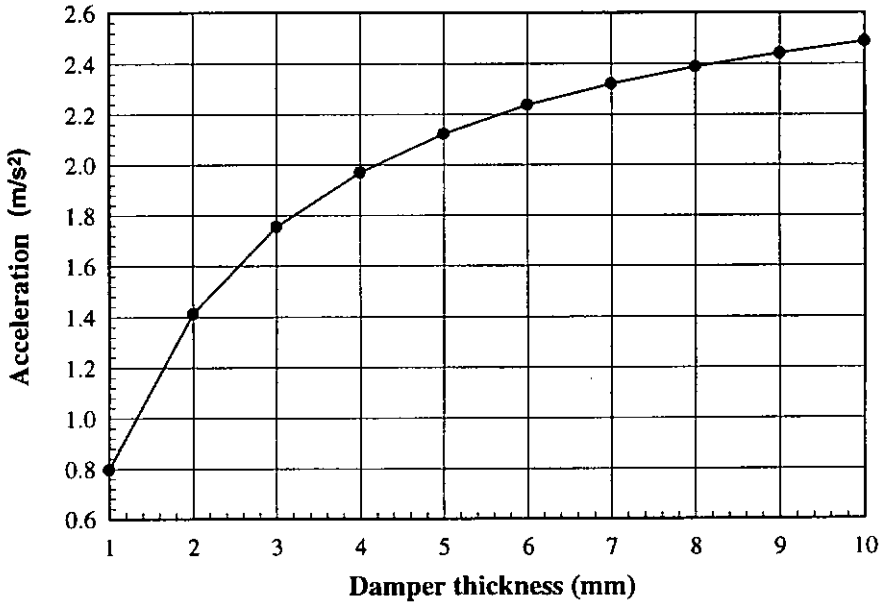

Figure 7.23 Maximum resonant accelerations at the middle point of the beam with dampers of different thickness

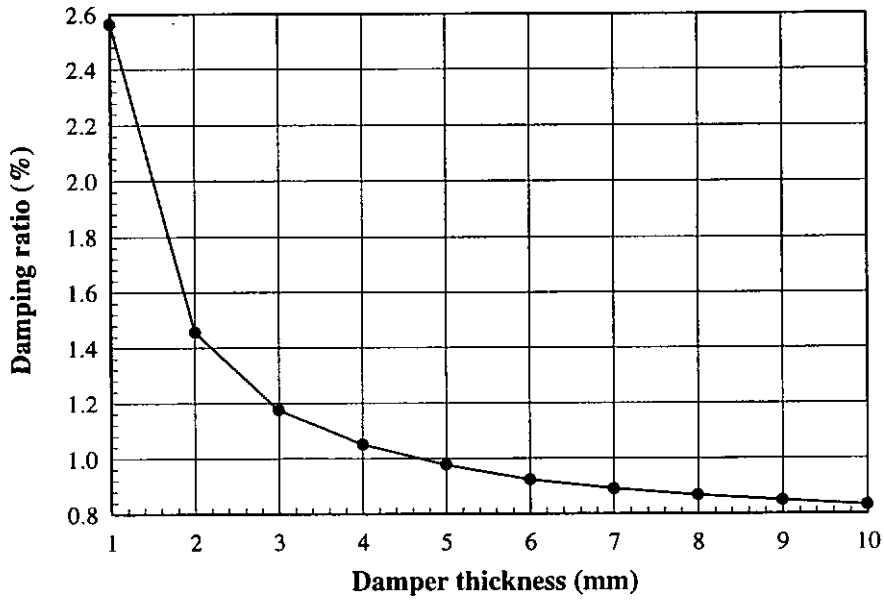

Figure 7.24 Damping ratios of the beam with dampers of different thickness

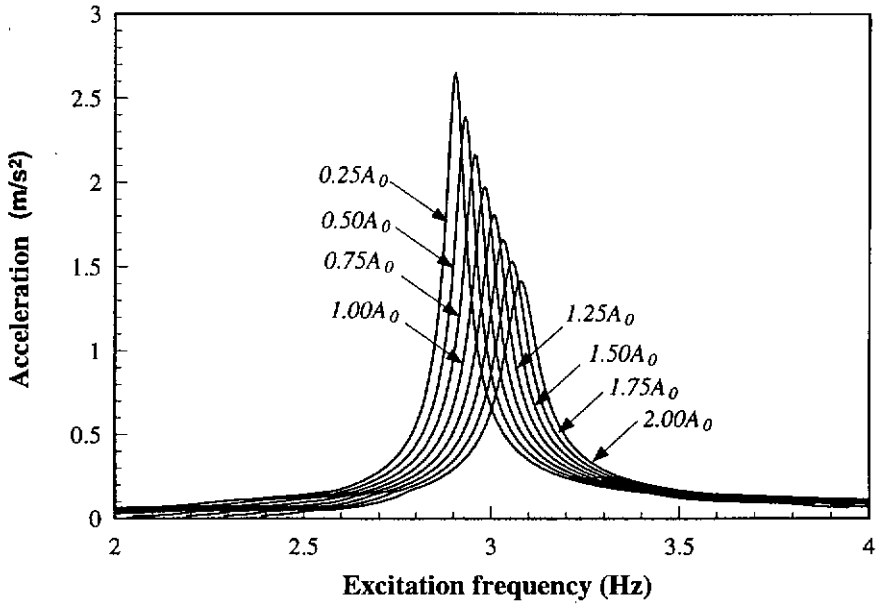

Figure 7.25 Maximum accelerations at the middle point of the beam with dampers of different areas

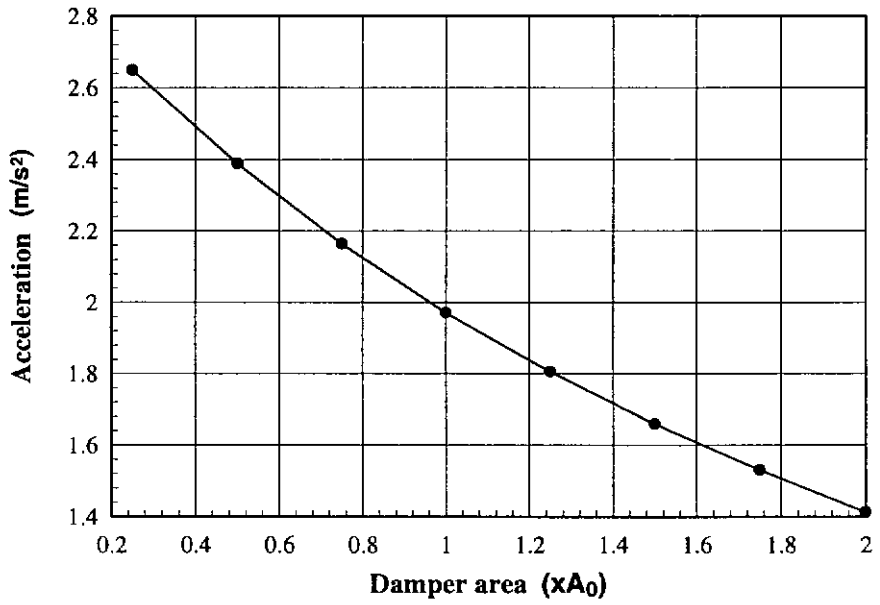

Figure 7.26 Maximum resonant accelerations at the middle point of the beam with dampers of different areas

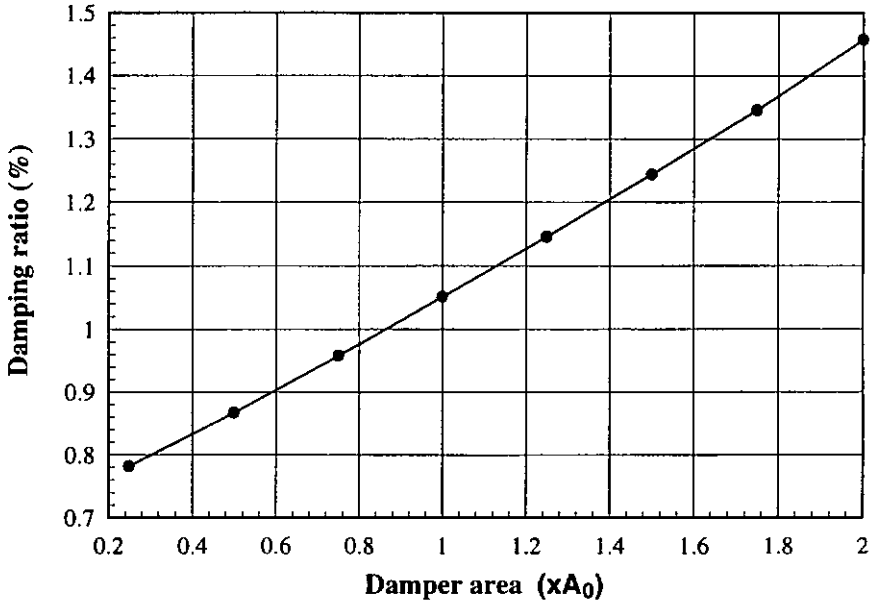

Figure 7.27 Damping ratios of the beam with dampers of different areas

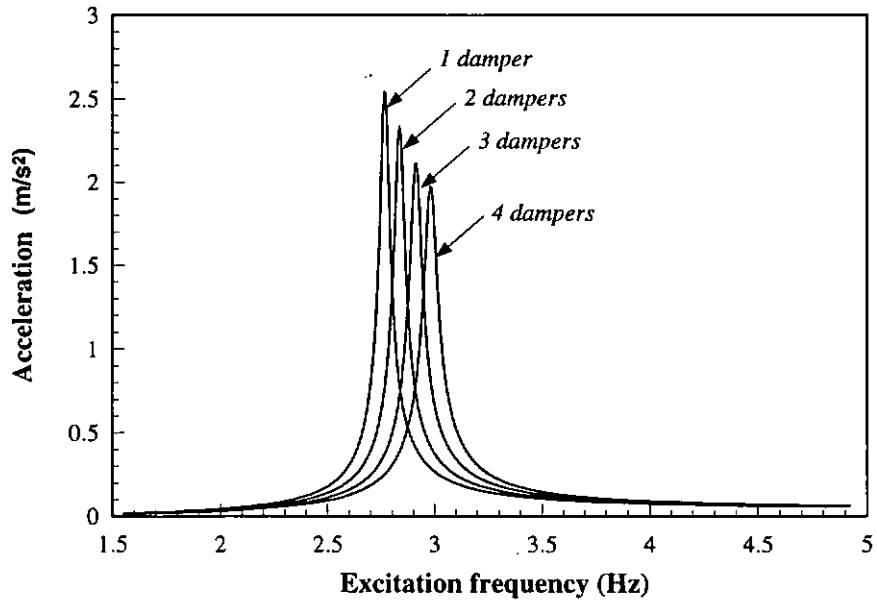

Figure 7.28 Maximum accelerations at the middle point of the beam with different number dampers

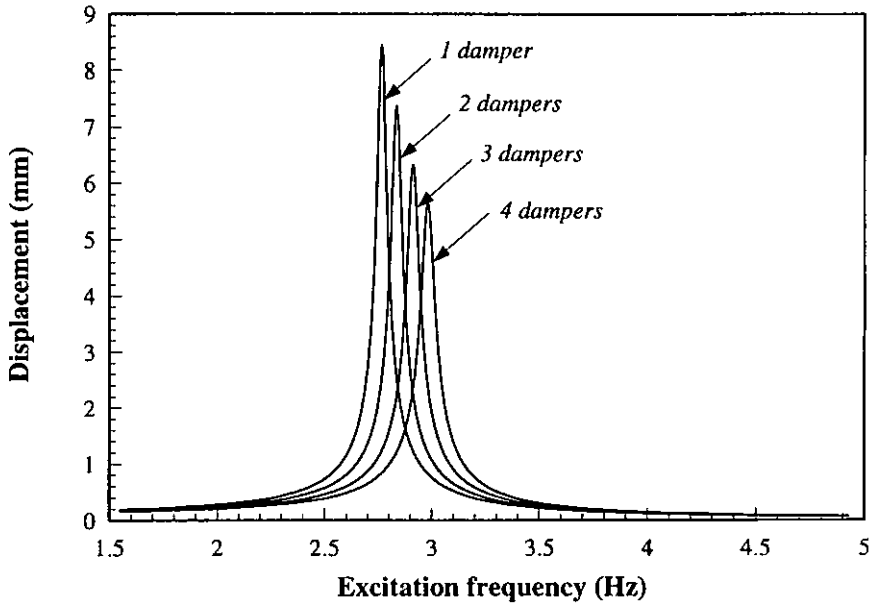

Figure 7.29 Maximum displacements at the middle point of the beam with different number dampers

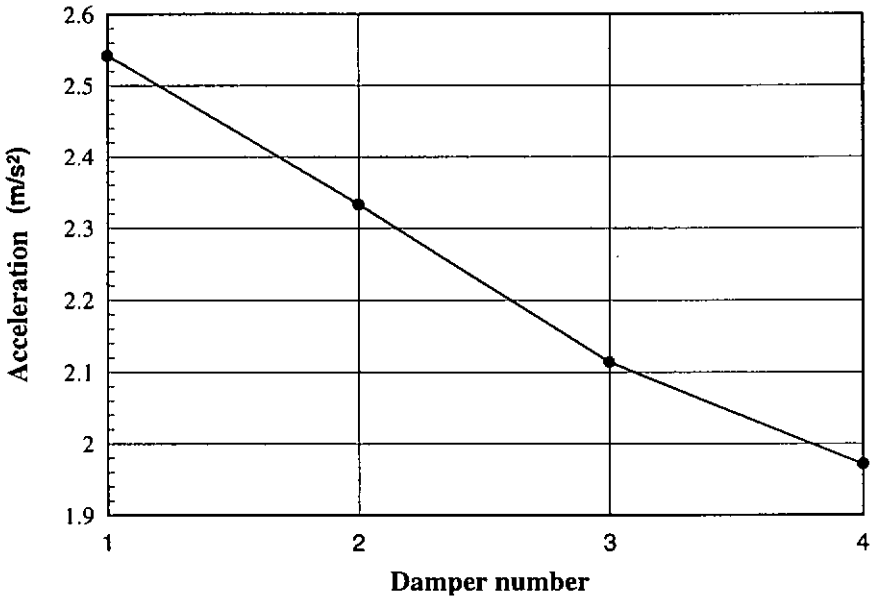

Figure 7.30 Maximum resonant accelerations at the middle point of the beam with different number dampers

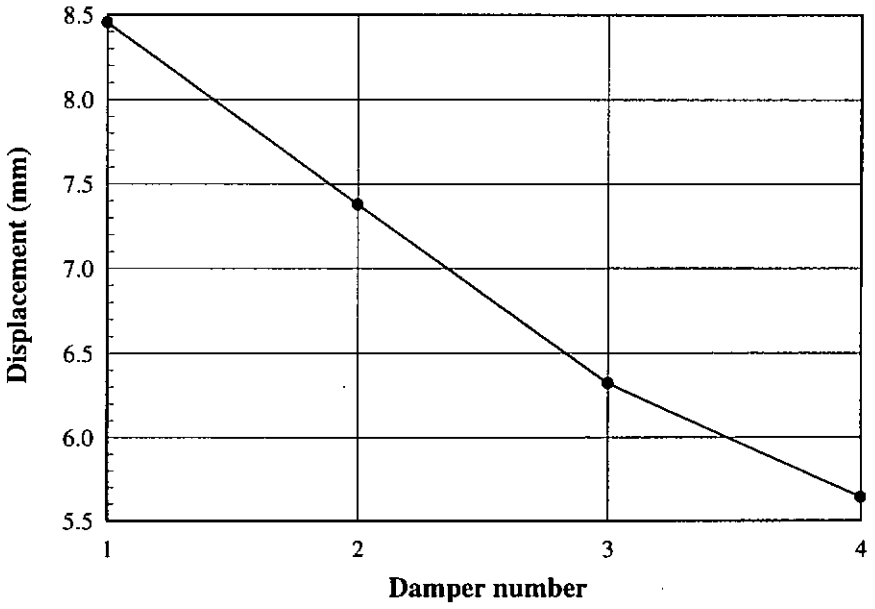

Figure 7.31 Maximum resonant displacements at the middle point of the beam with different number dampers

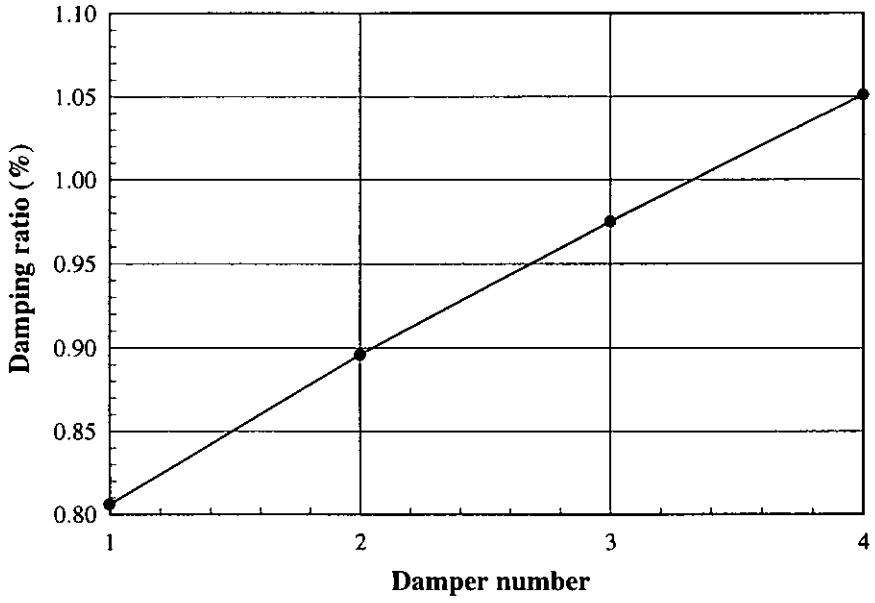

Figure 7.32 Damping ratios of the beam with different number dampers

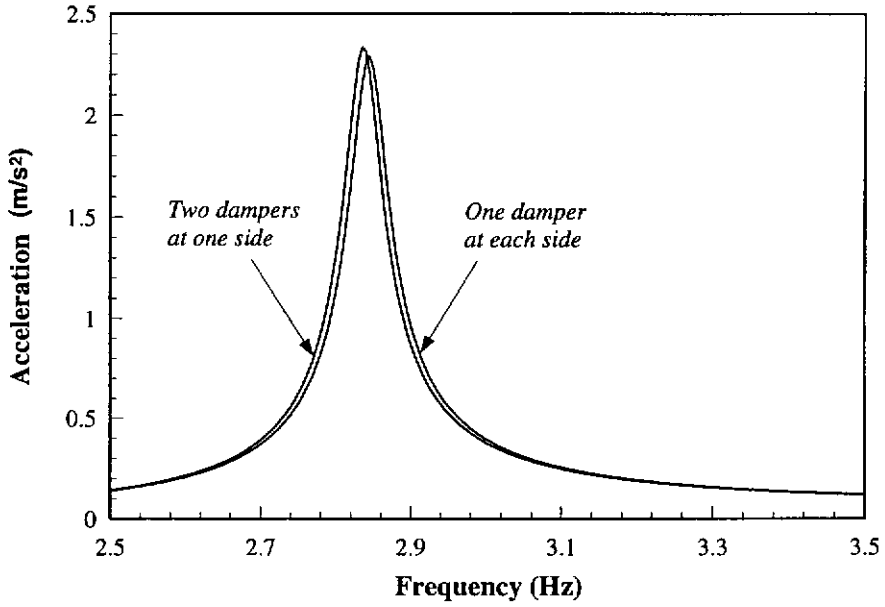

(a) Loading at the mid-span of the beam

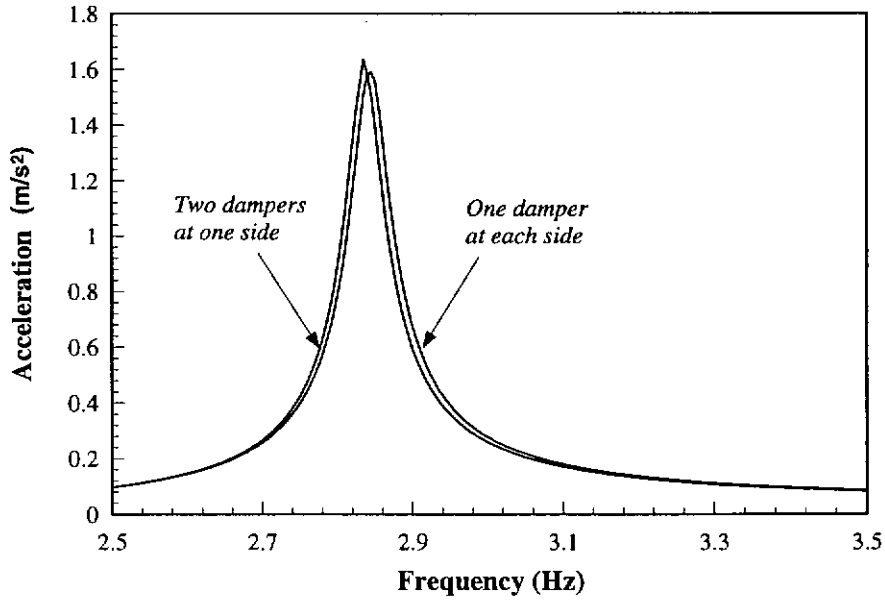

(b) Loading at the 1/4 span of the beam

Figure 7.33 Maximum accelerations at the middle point of the beam with dampers of different arrangement patterns

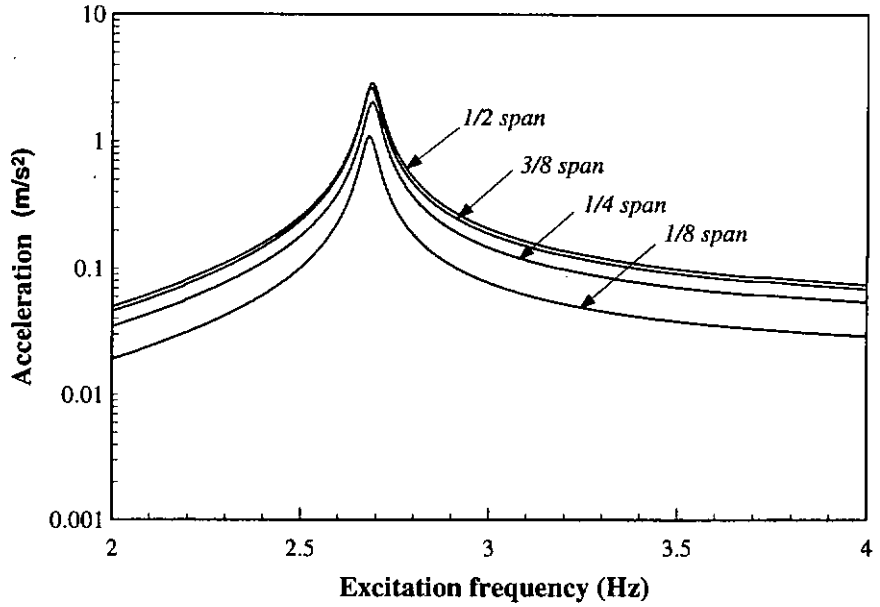

Figure 7.34 Maximum accelerations at the middle point of the beam without damper under loading at different positions

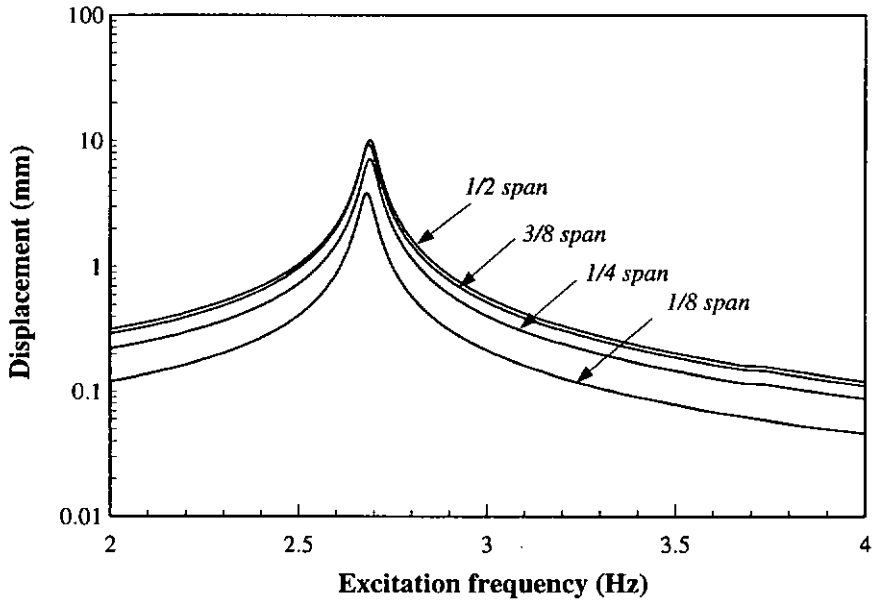

Figure 7.35 Maximum displacements at the middle point of the beam without damper under loading at different positions

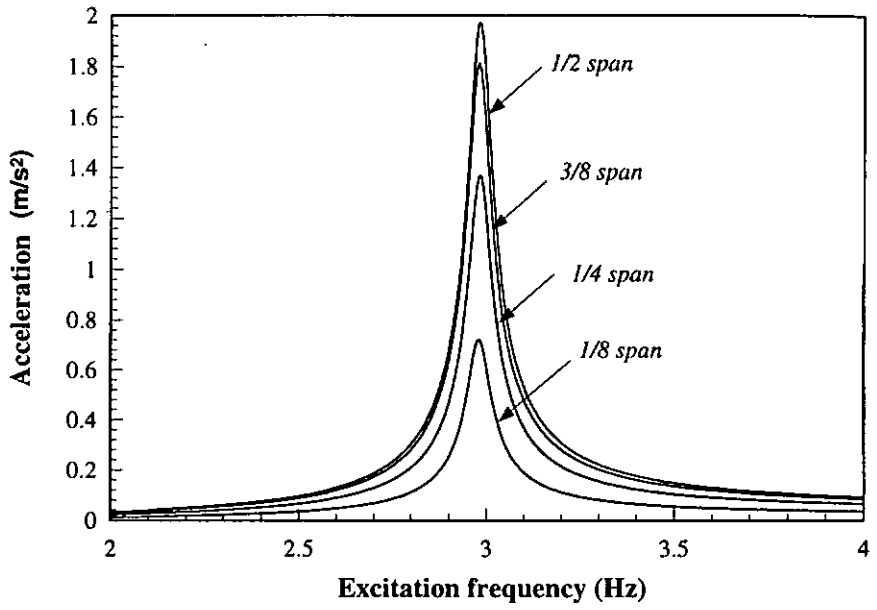

Figure 7.36 Maximum accelerations at the middle point of the beam with dampers under loading at different positions

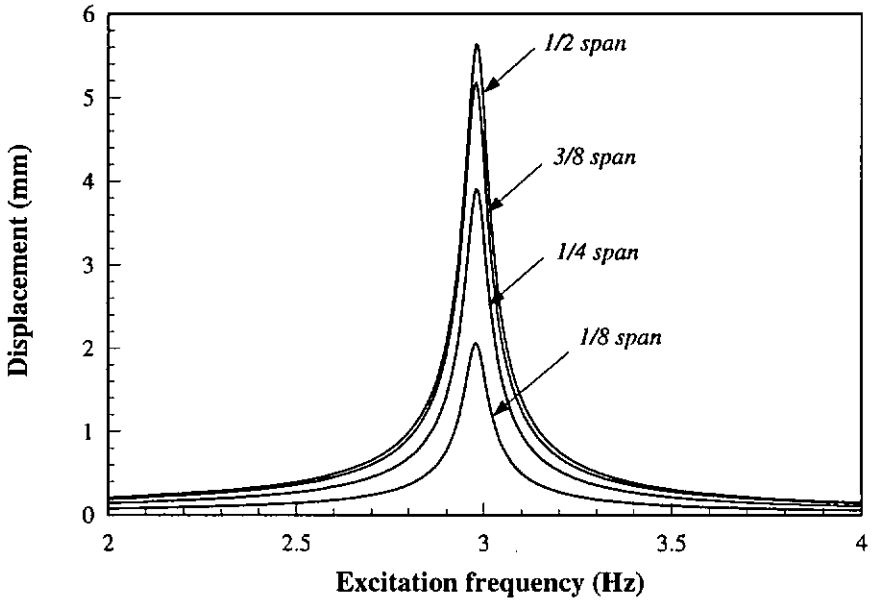

Figure 7.37 Maximum displacements at the middle point of the beam with dampers under loading at different positions

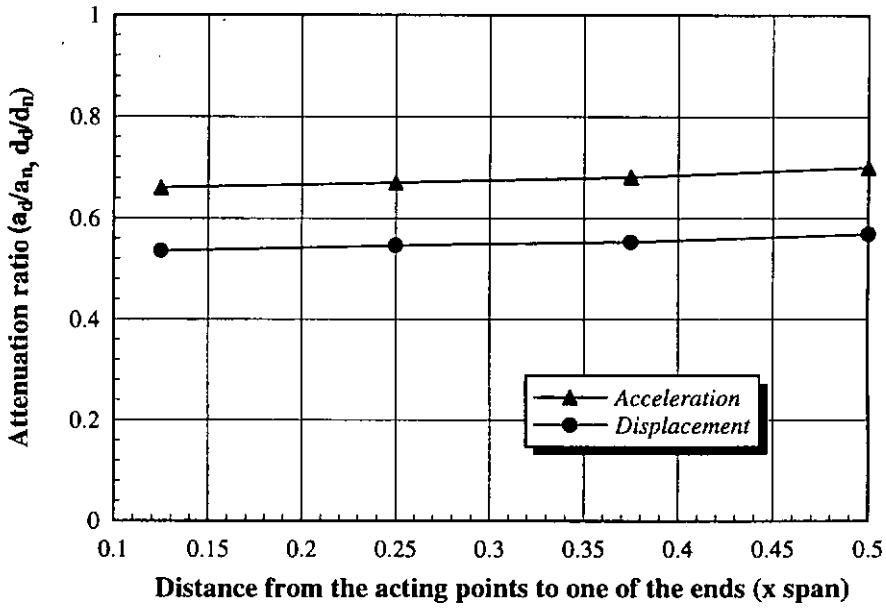

Figure 7.38 Attenuation ratios of responses of the beam with dampers to those without damper under loading at different positions

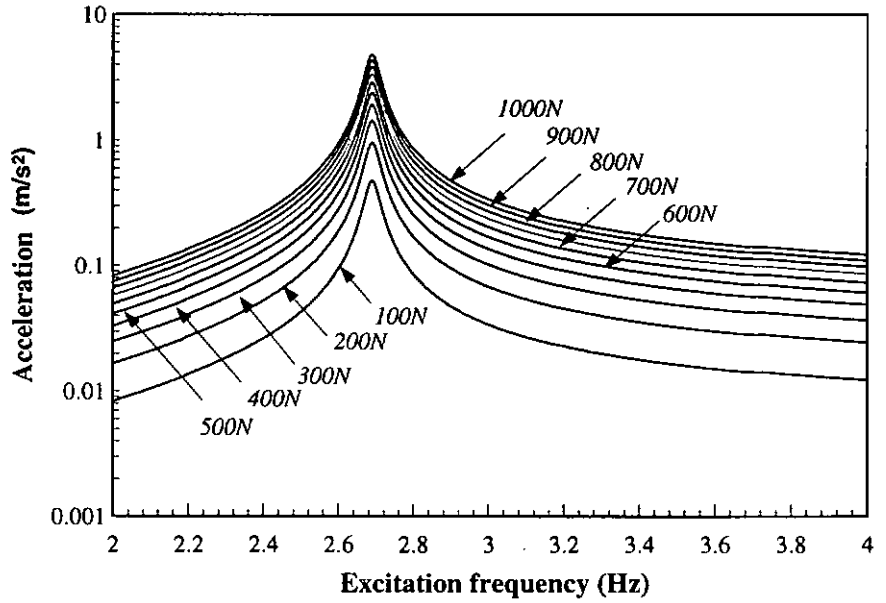

Figure 7.39 Maximum accelerations at the middle point of the beam without damper under loading of different amplitudes

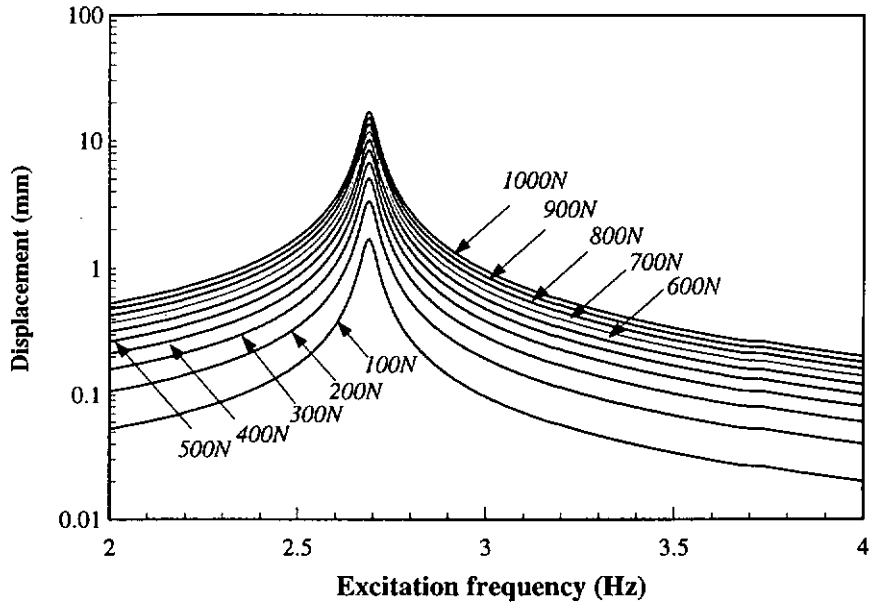

Figure 7.40 Maximum displacements at the middle point of the beam without damper under loading of different amplitudes

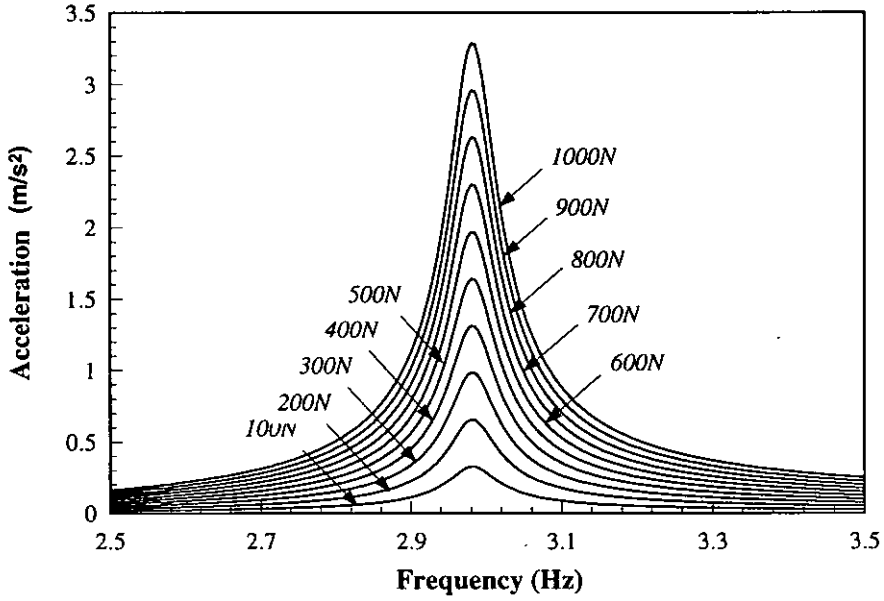

Figure 7.41 Maximum accelerations at the middle point of the beam with dampers under loading of different amplitudes

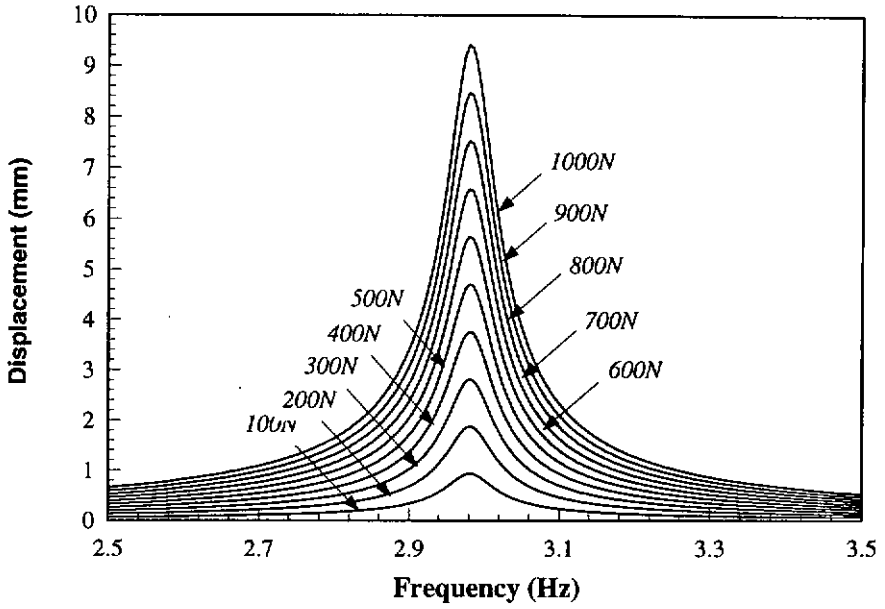

Figure 7.42 Maximum displacements at the middle point of the beam with dampers under loading of different amplitudes

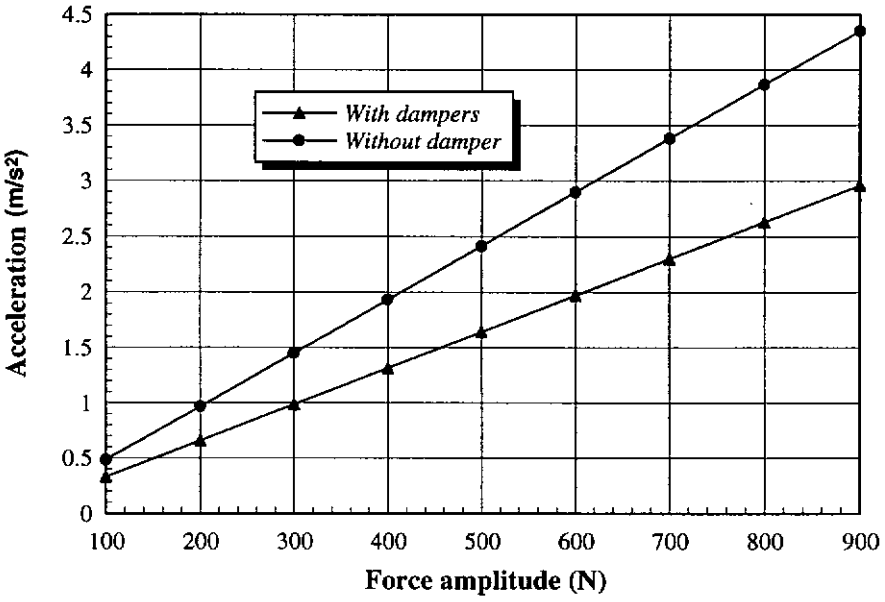

Figure 7.43 Maximum resonant accelerations of the beam with and without dampers

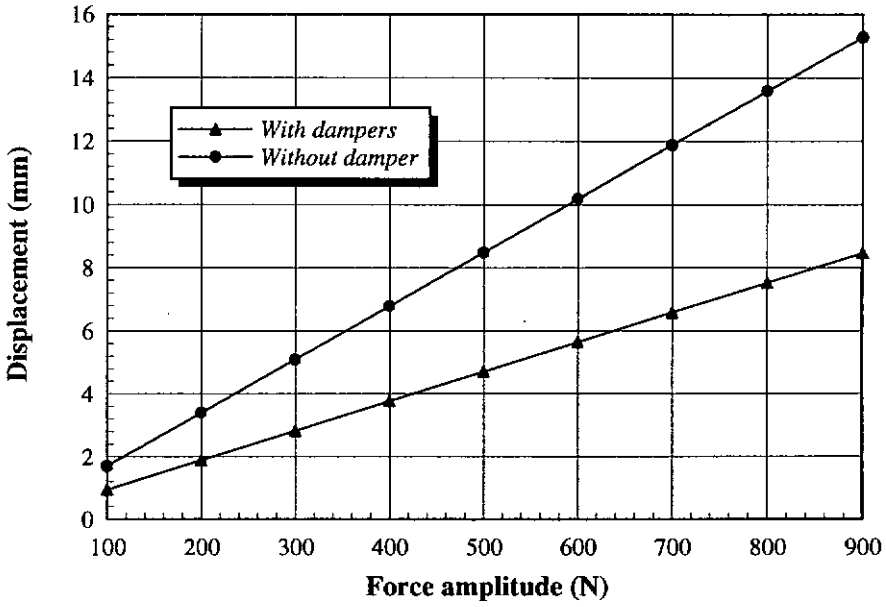

Figure 7.44 Maximum resonant displacements of the beam with and without dampers

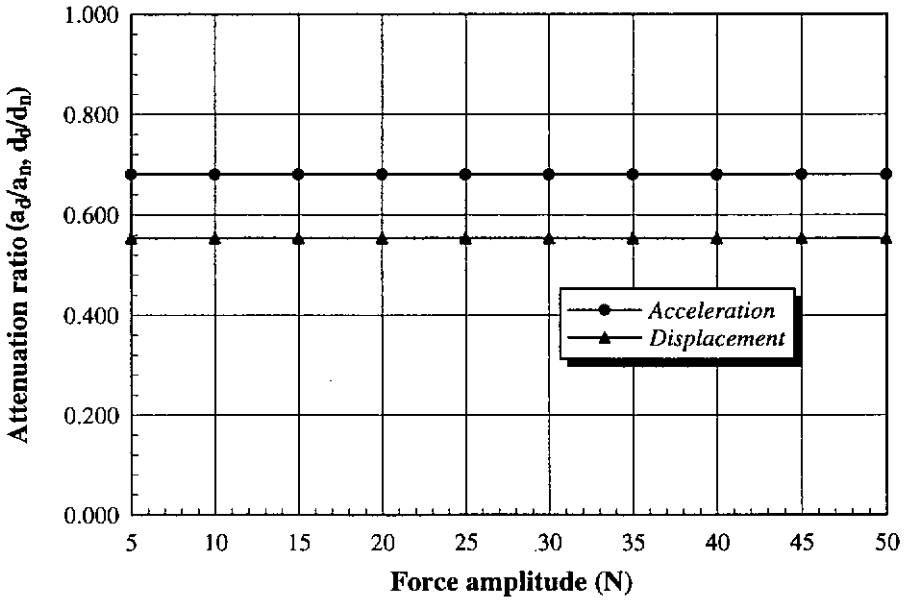

Figure 7.45 Attenuation ratios of responses of the beam with dampers to those without damper under loading of different amplitudes

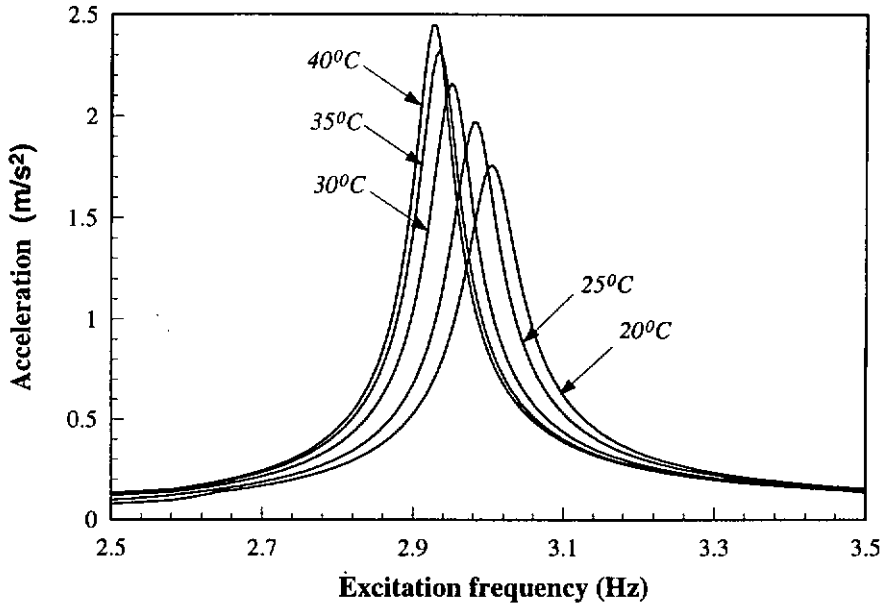

Figure 7.46 Maximum accelerations at the middle point of the beam with dampers at different temperature

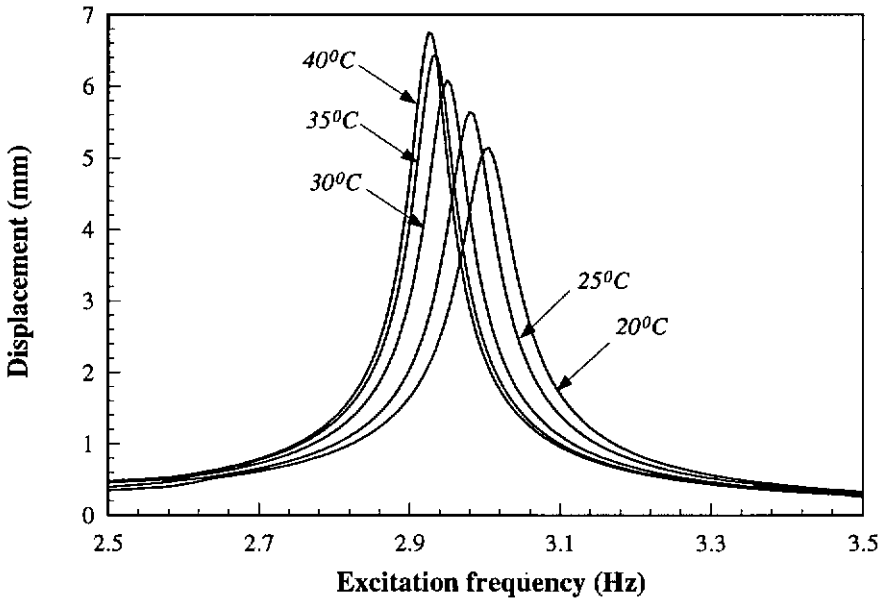

Figure 7.47 Maximum displacements at the middle point of the beam with dampers at different temperature

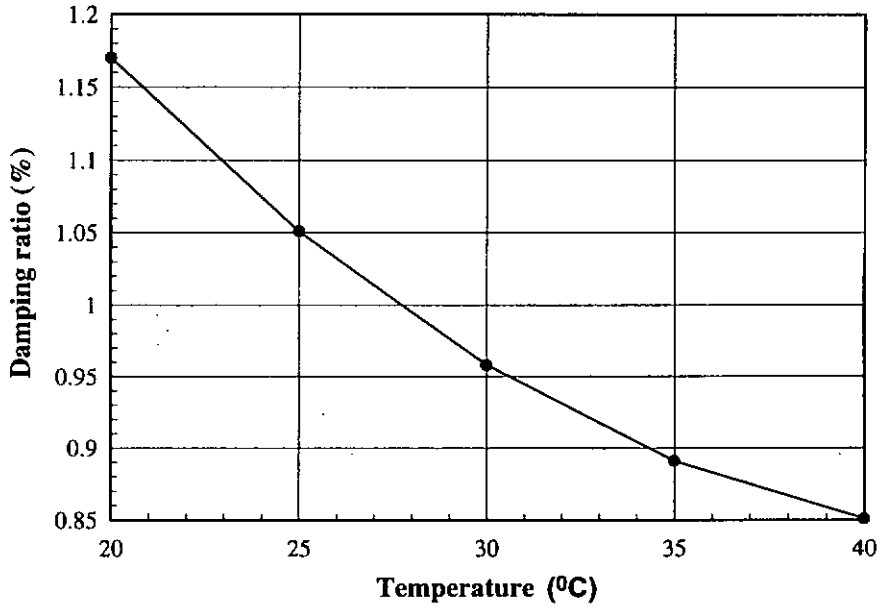

Figure 7.48 Damping ratios of the beam incorporated with dampers with dampers at different temperature

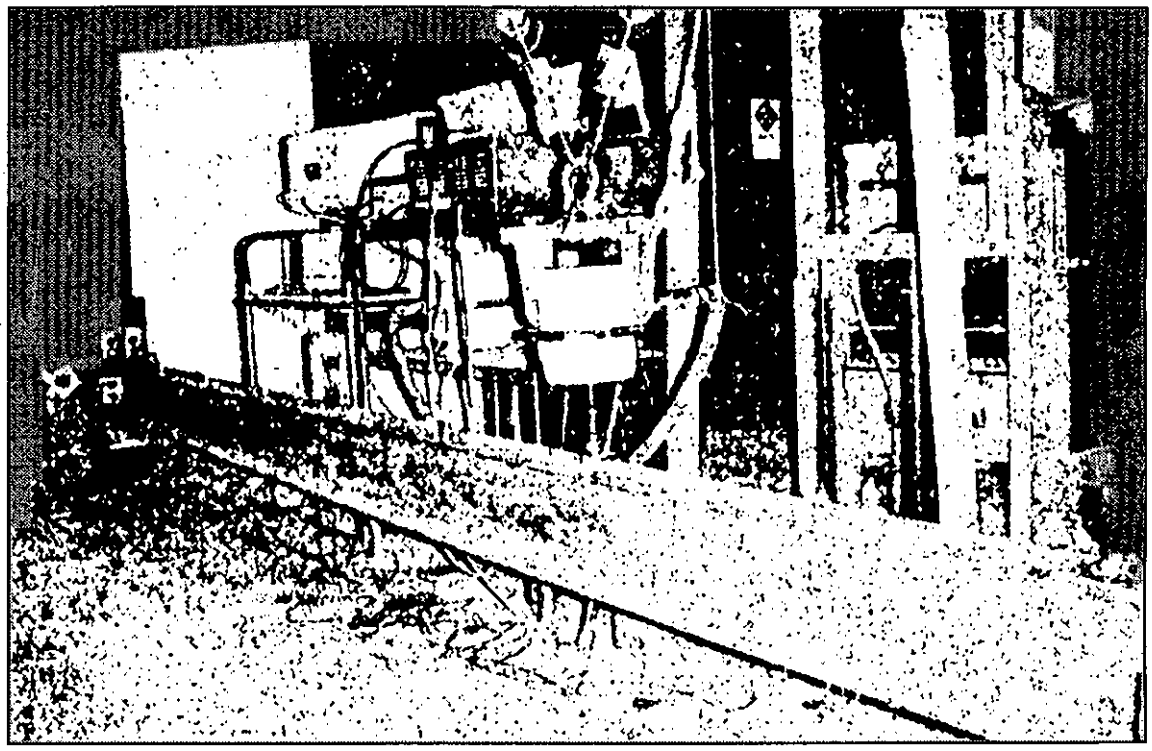

Photo 7.1 Appearance of the beam test

CHAPTER 8

CONCLUDING REMARKS AND FUTURE WORK

8.1 Concluding Remarks

The experimental work, modelling, analysis and parametric studies presented in the previous chapters can be summarized as follows.

Characteristics of viscoelastic dampers

1. Dynamic behaviours of viscoelastic dampers have been studied based on the experimental work carried out on two kinds of viscoelastic damper ZJD-1 and HD91. The area enclosed by the hysteresis loops of such dampers, which embody energy dissipation ability, increases with the excitation conditions such as the displacement amplitude and the excitation frequency. Equivalent stiffness and damping ratio of the dampers do not change with the shear displacement while they change with the excitation frequency. The difference between the two kinds of damper has been found that the equivalent stiffness of damper ZJD-1 changes slightly with the excitation frequency, while that of damper HD91 changes significantly and the damping ratio of damper ZJD-1 increases linearly with the excitation frequency while that of damper HD91 increases nonlinearly.

Modelling and identification of mathematical model

2. According to the experimental results of the viscoelastic dampers and the characteristics of the commonly used mathematical models for such dampers, the fractional derivative model has been chosen and improved to describe the dynamic behaviours of the viscoelastic dampers. To cover the properties of various viscoelastic dampers, the parameter α of the original model has been redefined in the improved model (IFDM). Temperature

factor has also been incorporated in the IFDM based on the experimental results obtained by other researchers.

3. The dynamic properties of the viscoelastic dampers are embodied in the test data collected under various conditions. To evaluate the parameters of the improved model accurately, two kinds of method, LFIM and NFIM have been developed for considering all the test data obtained in different test conditions simultaneously in the identification process. The parameter values of damper ZJD-1 and damper HD 91 have been identified by both LFIM and NFIM.

4. By comparison between the hysteresis loops derived from the IFDM and those of the test results for the two kinds of damper, it has been found that the IFDM can well describe the dynamic behaviour of different viscoelastic dampers. Furthermore, by comparison of the hysteresis loops derived from the commonly used Kelvin-Voigt model with those of the experimental results, it has been proved that the fractional derivative model is more versatile and can be used more widely for various kinds of viscoelastic damper than the Kelvin-Voigt model.

5. The properties such as storage modulus, loss modulus, phase-lag of stress to strain, damping ratio and energy dissipation ability of the IFDM with different parameters and under different loading and temperature conditions have been studied in detail. It has been verified that the IFDM can well describe the dynamic behaviours of various viscoelastic dampers.

Modelling and analytical methods for structures with viscoelastic dampers

6. Two kinds of modelling scheme, namely viscoelastic elements and viscoelastic supports, have been proposed for viscoelastic dampers incorporated in structures in the dynamic analysis according to the location of dampers with respect to the finite element model. An analytical method

TDM in association with the modelling schemes has been developed and the IFDM is adopted in the analysis to represent the viscoelastic dampers. Because of the complexity of finding the solution for IFDM, analysis in time domain is very time consuming. Since the IFDM has simple expression in frequency domain, an analytical method for structures with viscoelastic dampers in hybrid time-frequency domain (HTFDM) has been developed. With the FFT technique, this method can be used for structures subject to not only sinusoidal excitation, but also random excitation like seismic loading. Moreover, the damping matrix of the structure incorporated with viscoelastic dampers can be obtained by the analytical method, which is useful for carrying out dynamic analysis with other software packages.

Horizontal vibration control of building structures with viscoelastic dampers

7. Horizontal vibrations occur in building structures under dynamic loading. A practical damping device (frame-damper-brace system) has been designed for horizontal vibration control. It has been proved from the experimental tests that such damping device is very effective in horizontal vibration control. By comparisons of the experimental and analytical results, the proposed analytical methods TDM and HTFDM for predicting the response of structures incorporated with viscoelastic dampers under dynamic loading have been verified.

8. A large amount of numerical simulation work has been performed on a multi-story building structure for the parametric study of damper design. Parameters such as the ratio of shear stiffness between brace and damper, damper material, damper dimension, loading condition and temperature condition have been studied. The effectiveness in vibration control with respect to the change of parameters have been obtained, based on which

some useful guidelines have been drawn for the design of horizontal vibration control with the proposed damping device.

Vertical vibration control of building structures with viscoelastic dampers

9. Vertical vibrations of long span structures caused by human activities or machinery will bring unfavourable consequences for human's daily life. To control such vibrations, a beam-column connection incorporated with viscoelastic dampers has been designed. Experimental work has been carried out on a long span beam with such beam-column connections. Great effectiveness in vibration control with such damping device has been demonstrated by the test results.

10. By comparisons of the analytical results given by TDM and HTFDM with the experimental results, it has been found that these two methods can well predict the responses of long span structures with the proposed viscoelastic beam-column connections. The HTFDM is also found to be better than the TDM.

11. Numerical simulation has been carried out on a real long span beam with and without the proposed beam-column connections. Parameters such as damper material, damper dimension, loading condition and temperature condition have been studied. The effectiveness in vibration control with respect to the change of parameters have been obtained, based on which some useful guidelines have been drawn for the design of vertical vibration control with the proposed damping device.

8.2 Future Work

Vibration control of flexible structures with viscoelastic dampers is of great significance in practical application. For practical design, the work carried out in this thesis is not enough and a lot of work still need to be done in the future.

Further experimental study on viscoelastic dampers

1. Temperature effect is an important factor which would affect the dynamic characteristics of viscoelastic dampers. Limited by the test conditions, temperature effect has not been considered in the experimental work carried out on the two selected dampers in the present study. For further study, testing equipment should be developed to facilitate the investigation of viscoelastic dampers with respect to temperature.

2. In practical application, dampers are always under dead or dynamic pre-load in their axial direction. The effect of the axial loading on the shear properties of the dampers has not been studied in the experimental work. To obtain the coupling relation of dynamic behaviour of viscoelastic dampers between axial and shear directions, experimental work has to be carried out by a specially designed dynamic test system.

Further development of mathematical model

3. Based on the experimental work to be carried out at different temperatures and those consideration of the coupling effect between axial and shear direction, the mathematical model can be further developed to predict more accurately the dynamic behaviours of viscoelastic dampers under various conditions.

Experimental study on structures with dampers under stochastic loading

4. It has been proved by numerical simulation that viscoelastic dampers are effective for vibration control of structures under random excitation like

seismic loading. In order to verify experimentally the effectiveness, it is worthy to perform dynamic tests on such structures under stochastic loading with a shaking table.

To build damping device gallery

5. For practical application, design of viscoelastic damping devices varies with the complex design requirements for different types of structures. To make the design convenient, damping device gallery is worthwhile to be established based on what have been developed so far by researchers. The gallery should include different kinds of viscoelastic damping device with introduction of their advantages and disadvantages and also practical notes of application.

To link up with other structural analysis softwares

6. Many commercial softwares for the analysis of structures such as ETABS and SUB series have been developed and widely used by designers and researchers. To develop an interface for linking up the current developed analytical methods for structures incorporated with viscoelastic dampers with such softwares is of much practical value for structure design.

APPENDIX

Appendix 1 Experimental Results of Damper ZJD-1 in Shear Direction

Excitation frequency (HZ)	Displacement Amplitude (mm)	Equivalent Stiffness (N/mm)	Energy Dissipated per cycle (N.mm)	Damping ratio
3Hz	0.05	871.591	0.60281	0.04424
	0.10	872.303	2.41132	0.04437
	0.15	873.221	5.42559	0.04389
	0.20	872.892	9.64567	0.04444
	0.25	871.442	15.0744	0.04395
	0.30	870.993	21.7328	0.04342
	0.35	872.437	29.5299	0.04478
	0.40	873.091	38.5227	0.04322
6Hz	0.05	870.722	1.22353	0.08854
	0.10	869.734	4.89353	0.08890
	0.15	870.251	11.0182	0.08905
	0.20	869.925	19.5721	0.08873
	0.25	870.228	30.5783	0.08924
	0.30	870.064	44.0398	0.08877
	0.35	869.739	59.9355	0.08927
	0.40	869.596	78.2834	0.08949
9Hz	0.05	868.438	1.84531	0.13453
	0.10	867.994	7.38006	0.13721
	0.15	868.513	16.6551	0.13845
	0.20	866.986	29.5205	0.13441
	0.25	868.762	46.1242	0.13889
	0.30	868.438	66.4283	0.13438
	0.35	869.312	90.4054	0.13475
	0.40	868.217	118.021	0.13736
12Hz	0.05	865.933	2.47491	0.18227
	0.10	866.279	9.89643	0.17922
	0.15	864.854	22.2659	0.18348
	0.20	865.665	39.5873	0.18556
	0.25	868.943	61.8582	0.18776
	0.30	865.976	89.0704	0.18334
	0.35	865.992	121.235	0.18212
	0.40	866.927	158.369	0.18589

Appendix 1 Experimental Results of Damper ZJD-1 in Shear Direction (Continued)

Excitation frequency (HZ)	Displacement Amplitude (mm)	Equivalent Stiffness (N/mm)	Energy Dissipated per cycle (N.mm)	Damping ratio
15Hz	0.05	863.937	3.10159	0.22934
	0.10	862.834	12.4234	0.22934
	0.15	863.355	27.9543	0.22934
	0.20	862.937	49.7085	0.22934
	0.25	862.536	77.6648	0.22934
	0.30	861.997	111.887	0.22934
	0.35	862.685	152.203	0.22934
	0.40	863.383	198.822	0.22934
18Hz	0.05	860.829	3.74154	0.27702
	0.10	860.833	14.9761	0.27702
	0.15	859.997	33.6788	0.27835
	0.20	860.589	59.8695	0.27564
	0.25	859.783	93.5342	0.27214
	0.30	859.829	134.685	0.28012
	0.35	860.059	183.355	0.27365
	0.40	859.179	239.478	0.27458
20Hz	0.05	859.134	4.16622	0.30821
	0.10	859.532	16.6621	0.30906
	0.15	858.693	37.4932	0.30847
	0.20	858.884	66.6514	0.30695
	0.25	858.238	104.161	0.30746
	0.30	857.991	149.977	0.30823
	0.35	858.438	204.185	0.30325
	0.40	859.746	266.645	0.30458
25Hz	0.05	855.287	5.23052	0.38819
	0.10	854.593	20.9273	0.38998
	0.15	853.952	47.0744	0.39045
	0.20	854.247	83.6982	0.39135
	0.25	853.883	130.741	0.39012
	0.30	853.774	188.331	0.38475
	0.35	853.837	256.312	0.38542
	0.40	854.373	334.773	0.38831

Appendix 1 Experimental Results of Damper ZJD-1 in Shear Direction (Continued)

Excitation frequency (HZ)	Displacement Amplitude (mm)	Equivalent Stiffness (N/mm)	Energy Dissipated per cycle (N.mm)	Damping ratio
30Hz	0.05	848.252	6.29992	0.47335
	0.10	849.592	25.1997	0.47207
	0.15	847.654	56.6993	0.47645
	0.20	848.671	100.799	0.47812
	0.25	849.147	157.498	0.47245
	0.30	849.632	226.797	0.47367
	0.35	849.359	308.696	0.47549
	0.40	849.571	403.195	0.47258
35Hz	0.05	845.241	7.37264	0.55154
	0.10	845.974	29.4904	0.55241
	0.15	846.014	66.3534	0.55362
	0.20	847.034	117.962	0.55259
	0.25	847.421	184.315	0.55574
	0.30	846.154	265.414	0.55564
	0.35	845.947	361.257	0.55127
	0.40	845.347	471.846	0.55657
40Hz	0.05	841.654	8.44836	0.63352
	0.10	841.238	33.7934	0.63851
	0.15	840.995	76.0352	0.63834
	0.20	841.035	135.174	0.63953
	0.25	840.224	211.209	0.63964
	0.30	840.847	304.141	0.63977
	0.35	840.694	413.972	0.64024
	0.40	841.582	540.695	0.63873
45Hz	0.05	837.346	9.52682	0.71965
	0.10	837.218	38.1073	0.72488
	0.15	837.164	85.7414	0.72349
	0.20	836.987	152.429	0.72367
	0.25	836.680	238.144	0.72369
	0.30	836.871	342.925	0.72549
	0.35	837.192	466.854	0.72214
	0.40	836.882	609.776	0.72873

Appendix 2 Experimental Results of Damper HD91 in Shear Direction

Excitation frequency (HZ)	Displacement Amplitude (mm)	Equivalent Stiffness (N/mm)	Energy Dissipated per cycle (N.mm)	Damping ratio
3Hz	0.05	1258.52	2.38561	0.12369
	0.10	1257.79	9.54153	0.12547
	0.15	1259.25	21.4627	0.12259
	0.20	1256.64	38.1641	0.12316
	0.25	1258.24	59.6352	0.12468
	0.30	1255.16	85.8787	0.12248
	0.35	1259.12	116.845	0.12165
	0.40	1256.57	152.626	0.12325
6Hz	0.05	1351.32	3.93748	0.18964
	0.10	1349.59	15.9495	0.18874
	0.15	1350.98	35.4664	0.18542
	0.20	1349.67	62.9281	0.18561
	0.25	1348.62	98.4845	0.18555
	0.30	1347.61	141.646	0.18842
	0.35	1349.09	192.945	0.18339
	0.40	1350.54	251.932	0.18566
9Hz	0.05	1427.96	5.27863	0.23452
	0.10	1428.97	21.1145	0.23825
	0.15	1429.32	47.5047	0.23565
	0.20	1429.87	84.4521	0.23544
	0.25	1427.64	131.936	0.23478
	0.30	1428.46	190.011	0.23241
	0.35	1429.09	258.653	0.23663
	0.40	1423.65	337.882	0.23799
12Hz	0.05	1502.31	6.49908	0.27518
	0.10	1501.85	25.9963	0.27642
	0.15	1502.31	58.4918	0.27872
	0.20	1504.09	103.985	0.27964
	0.25	1503.49	162.477	0.27754
	0.30	1502.44	233.967	0.27361
	0.35	1504.75	318.455	0.27881
	0.40	1505.13	415.941	0.27254

Appendix 2 Experimental Results of Damper HD91 in Shear Direction (Continued)

Excitation frequency (HZ)	Displacement Amplitude (mm)	Equivalent Stiffness (N/mm)	Energy Dissipated per cycle (N.mm)	Damping ratio
15Hz	0.05	1567.36	7.63692	0.30751
	0.10	1566.54	30.5477	0.30885
	0.15	1569.87	68.7322	0.30963
	0.20	1565.74	122.191	0.30994
	0.25	1568.58	190.923	0.30745
	0.30	1569.01	274.929	0.31057
	0.35	1568.88	374.209	0.31247
	0.40	1567.64	488.763	0.30875
18Hz	0.05	1633.45	8.71297	0.33754
	0.10	1632.78	34.8519	0.33986
	0.15	1631.47	78.4167	0.34278
	0.20	1633.66	139.407	0.34167
	0.25	1632.85	217.824	0.34062
	0.30	1632.97	313.667	0.33831
	0.35	1631.99	426.935	0.33904
	0.40	1632.74	557.637	0.34273
20Hz	0.05	1674.47	9.40262	0.36035
	0.10	1673.64	37.6105	0.36147
	0.15	1672.98	84.6236	0.35852
	0.20	1672.74	150.442	0.35914
	0.25	1673.75	235.065	0.35546
	0.30	1673.09	338.494	0.35354
	0.35	1673.64	460.728	0.35652
	0.40	1672.71	601.768	0.35875
25Hz	0.05	1771.78	11.0488	0.39694
	0.10	1770.99	44.1952	0.39256
	0.15	1770.57	99.4391	0.39782
	0.20	1772.04	176.786	0.40003
	0.25	1769.54	276.225	0.39745
	0.30	1770.46	397.766	0.39364
	0.35	1769.38	541.371	0.39434
	0.40	1771.75	707.142	0.39859

Appendix 2 Experimental Results of Damper HD91 in Shear Direction (Continued)

Excitation frequency (HZ)	Displacement Amplitude (mm)	Equivalent Stiffness (N/mm)	Energy Dissipated per cycle (N.mm)	Damping ratio
30Hz	0.05	1860.65	12.6056	0.42888
	0.10	1861.74	50.4223	0.43147
	0.15	1862.41	113.478	0.43154
	0.20	1863.54	201.689	0.43162
	0.25	1862.66	315.139	0.43113
	0.30	1861.74	453.801	0.43055
	0.35	1862.09	617.673	0.43043
	0.40	1860.98	806.757	0.43029
35Hz	0.05	1951.74	14.0918	0.46242
	0.10	1950.63	56.3671	0.45999
	0.15	1951.09	126.826	0.45546
	0.20	1951.87	225.468	0.45824
	0.25	1952.01	352.294	0.45614
	0.30	1951.64	507.303	0.45329
	0.35	1949.87	690.496	0.45754
	0.40	1950.24	901.873	0.45668
40Hz	0.05	2034.64	15.5201	0.4855
	0.10	2036.27	62.0803	0.48574
	0.15	2036.74	139.681	0.48924
	0.20	2035.58	248.321	0.48234
	0.25	2036.34	388.002	0.48145
	0.30	2035.22	558.722	0.48655
	0.35	2034.98	760.483	0.48825
	0.40	2036.47	993.284	0.48475
45Hz	0.05	2116.12	16.8996	0.50864
	0.10	2117.64	67.5984	0.50329
	0.15	2117.49	152.097	0.50462
	0.20	2116.40	270.394	0.50146
	0.25	2115.994	422.497	0.50754
	0.30	2115.837	608.386	0.51028
	0.35	2117.045	828.081	0.50442
	0.40	2114.698	1081.58	0.50952

Appendix 3 Experimental Results of Damper ZJD-1 in Axial Direction

Excitation frequency (HZ)	Displacement Amplitude (mm)	Equivalent Stiffness (N/mm)	Energy Dissipated per cycle (N.mm)	Damping ratio
3Hz	0.05	3010.32	1.20862	0.02557
	0.10	3008.92	4.83448	0.02557
	0.15	3009.54	10.8776	0.02557
	0.20	3009.47	19.3379	0.02557
	0.25	3010.14	30.2155	0.02557
	0.30	3009.65	43.5103	0.02566
	0.35	3009.57	59.2223	0.02574
	0.40	3008.22	77.3516	0.02534
6Hz	0.05	3005.77	2.43574	0.05195
	0.10	3006.52	9.74296	0.05142
	0.15	3007.65	21.9217	0.05155
	0.20	3007.62	38.9718	0.05149
	0.25	3006.88	60.8935	0.05153
	0.30	3007.25	87.6866	0.05164
	0.35	3005.33	119.351	0.05177
	0.40	3005.91	155.887	0.05180
9Hz	0.05	3003.25	3.66994	0.07724
	0.10	3002.48	14.6798	0.07794
	0.15	3003.52	33.0295	0.07725
	0.20	3002.31	58.7747	0.07775
	0.25	3002.99	91.7485	0.07764
	0.30	3002.74	132.118	0.07734
	0.35	3003.06	179.827	0.07751
	0.40	3002.85	234.876	0.07727
12Hz	0.05	3001.07	4.90876	0.10445
	0.10	3000.77	19.6351	0.10422
	0.15	3000.65	44.1789	0.10433
	0.20	3001.06	78.5402	0.10431
	0.25	3000.97	122.719	0.10409
	0.30	3000.74	176.715	0.10389
	0.35	3000.86	240.529	0.10427
	0.40	3001.17	314.161	0.10411

Appendix 3 Experimental Results of Damper ZJD-1 in Axial Direction (Continued)

Excitation frequency (HZ)	Displacement Amplitude (mm)	Equivalent Stiffness (N/mm)	Energy Dissipated per cycle (N.mm)	Damping ratio
15Hz	0.05	2998.65	6.15103	0.13102
	0.10	2998.28	24.6041	0.13088
	0.15	2998.47	55.3593	0.13074
	0.20	2998.57	98.4165	0.13034
	0.25	2997.89	153.776	0.13069
	0.30	2997.75	221.437	0.13072
	0.35	2998.75	301.401	0.13047
	0.40	2997.94	393.666	0.13088
18Hz	0.05	2995.47	7.39606	0.15733
	0.10	2995.24	29.5842	0.15847
	0.15	2995.67	66.5645	0.15695
	0.20	2994.85	118.337	0.15778
	0.25	2994.98	184.901	0.15902
	0.30	2995.22	266.258	0.15886
	0.35	2994.64	362.407	0.15798
	0.40	2995.55	473.348	0.15695
20Hz	0.05	2994.08	8.22737	0.17502
	0.10	2993.65	32.9095	0.17564
	0.15	2993.47	74.0464	0.17741
	0.20	2993.88	131.638	0.17556
	0.25	2993.34	205.684	0.17485
	0.30	2992.89	296.185	0.17621
	0.35	2993.47	403.141	0.17729
	0.40	2993.66	526.552	0.17565
25Hz	0.05	2987.74	10.3095	0.21888
	0.10	2988.84	41.2787	0.21947
	0.15	2987.64	92.7854	0.21969
	0.20	2988.84	164.952	0.21957
	0.25	2987.94	257.737	0.21889
	0.30	2988.54	371.142	0.21946
	0.35	2989.46	505.165	0.21979
	0.40	2988.27	659.807	0.21966

Appendix 3 Experimental Results of Damper ZJD-1 in Axial Direction (Continued)

Excitation frequency (HZ)	Displacement Amplitude (mm)	Equivalent Stiffness (N/mm)	Energy Dissipated per cycle (N.mm)	Damping ratio
30Hz	0.05	2983.96	12.3962	0.26444
	0.10	2984.22	49.5849	0.26444
	0.15	2984.39	111.566	0.26444
	0.20	2985.01	198.34	0.26444
	0.25	2984.65	309.906	0.26444
	0.30	2984.22	446.264	0.26444
	0.35	2983.97	607.415	0.26444
	0.40	2984.16	793.358	0.26444
35Hz	0.05	2980.22	14.4868	0.30951
	0.10	2980.36	57.9472	0.30951
	0.15	2979.77	130.381	0.30951
	0.20	2979.89	231.789	0.31014
	0.25	2979.65	362.174	0.30957
	0.30	2979.47	521.525	0.30999
	0.35	2980.47	709.853	0.31024
	0.40	2979.48	927.156	0.30887
40Hz	0.05	2974.83	16.5807	0.35485
	0.10	2974.94	66.3228	0.35356
	0.15	2975.33	149.226	0.35284
	0.20	2975.44	265.291	0.35296
	0.25	2975.67	414.517	0.35364
	0.30	2974.98	596.905	0.35454
	0.35	2974.87	812.454	0.35267
	0.40	2975.36	1061.16	0.35777
45Hz	0.05	2971.08	18.6775	0.39947
	0.10	2970.49	74.7098	0.40119
	0.15	2970.66	168.097	0.40352
	0.20	2970.57	298.839	0.40164
	0.25	2971.02	466.936	0.39856
	0.30	2971.26	672.388	0.40338
	0.35	2970.34	915.195	0.40174
	0.40	2970.47	1195.36	0.40669

Appendix 4 Experimental Results of Damper HD91 in Axial Direction

Excitation frequency (HZ)	Displacement Amplitude (mm)	Equivalent Stiffness (N/mm)	Energy Dissipated per cycle (N.mm)	Damping ratio
3Hz	0.05	4970.22	6.29684	0.08105
	0.10	4969.84	25.1874	0.08088
	0.15	4969.62	56.6716	0.08065
	0.20	4969.98	100.749	0.08087
	0.25	4969.74	157.421	0.08034
	0.30	4970.08	226.686	0.08029
	0.35	4969.58	308.545	0.08064
	0.40	4969.69	402.998	0.08021
6Hz	0.05	5232.65	10.1164	0.12318
	0.10	5232.89	40.4657	0.12346
	0.15	5233.08	91.0479	0.12286
	0.20	5233.34	161.863	0.12297
	0.25	5232.58	252.911	0.12338
	0.30	5232.47	364.192	0.12325
	0.35	5232.56	495.705	0.12355
	0.40	5232.77	647.452	0.12374
9Hz	0.05	5456.05	13.3498	0.15621
	0.10	5455.77	53.3991	0.15603
	0.15	5455.45	120.148	0.15588
	0.20	5454.98	213.596	0.15569
	0.25	5455.75	333.744	0.15613
	0.30	5455.63	480.592	0.15549
	0.35	5455.74	654.139	0.15551
	0.40	5454.36	854.385	0.15533
12Hz	0.05	5656.05	16.2529	0.18346
	0.10	5655.99	65.0118	0.18352
	0.15	5655.68	146.276	0.18285
	0.20	5655.43	260.047	0.18299
	0.25	5655.23	406.323	0.18316
	0.30	5655.89	585.106	0.18307
	0.35	5656.21	796.394	0.18354
	0.40	5655.66	1040.19	0.18235

Appendix 4 Experimental Results of Damper HD91 in Axial Direction (Continued)

Excitation frequency (HZ)	Displacement Amplitude (mm)	Equivalent Stiffness (N/mm)	Energy Dissipated per cycle (N.mm)	Damping ratio
15Hz	0.05	5841.24	18.9337	0.20647
	0.10	5840.55	75.7318	0.20655
	0.15	5840.27	170.397	0.20664
	0.20	5841.36	302.927	0.20628
	0.25	5840.69	473.324	0.20685
	0.30	5841.22	681.586	0.20622
	0.35	5840.88	927.715	0.20639
	0.40	5841.36	1211.71	0.20645
18Hz	0.05	6015.04	21.4476	0.22736
	0.10	6014.25	85.7903	0.22729
	0.15	6014.37	193.028	0.22774
	0.20	6013.95	343.161	0.22688
	0.25	6014.33	536.189	0.22692
	0.30	6013.84	772.113	0.22753
	0.35	6014.67	1050.93	0.22734
	0.40	6014.89	1372.65	0.22769
20Hz	0.05	6125.02	23.0503	0.23978
	0.10	6124.44	92.2012	0.23985
	0.15	6124.65	207.453	0.24024
	0.20	6125.03	368.805	0.23958
	0.25	6125.24	576.257	0.24038
	0.30	6124.67	829.811	0.23846
	0.35	6124.88	1129.46	0.23726
	0.40	6125.90	1475.22	0.23594
25Hz	0.05	6386.36	26.8512	0.26666
	0.10	6386.25	107.405	0.26586
	0.15	6386.68	241.667	0.26495
	0.20	6386.99	429.618	0.26875
	0.25	6386.87	671.279	0.26774
	0.30	6386.37	966.641	0.26659
	0.35	6387.22	1315.71	0.26513
	0.40	6387.36	1718.47	0.26802

Appendix 4 Experimental results of damper HD91 in axial direction (Continued)

Excitation frequency (HZ)	Displacement Amplitude (mm)	Equivalent Stiffness (N/mm)	Energy Dissipated per cycle (N.mm)	Damping ratio
30Hz	0.05	6632.57	30.4175	0.29288
	0.10	6632.34	121.622	0.29315
	0.15	6632.88	273.757	0.29089
	0.20	6631.99	486.679	0.29234
	0.25	6632.25	760.436	0.29472
	0.30	6632.65	1095.03	0.29264
	0.35	6632.87	1490.46	0.29333
	0.40	6633.01	1946.72	0.29258
35Hz	0.05	6865.95	33.7998	0.31478
	0.10	6866.35	135.199	0.31562
	0.15	6866.66	304.198	0.31661
	0.20	6865.88	540.797	0.31349
	0.25	6865.74	844.996	0.31246
	0.30	6865.69	1216.79	0.31754
	0.35	6865.99	1656.19	0.31264
	0.40	6866.07	2163.19	0.31440
40Hz	0.05	7089.25	37.0323	0.33452
	0.10	7089.14	148.129	0.33216
	0.15	7088.96	333.291	0.33342
	0.20	7087.65	592.517	0.33472
	0.25	7087.47	925.808	0.33122
	0.30	7089.06	1333.16	0.33642
	0.35	7088.87	1814.58	0.33432
	0.40	7087.97	2370.07	0.33209
45Hz	0.05	7303.58	40.1393	0.34876
	0.10	7303.24	160.557	0.35047
	0.15	7303.63	361.253	0.35321
	0.20	7302.87	642.228	0.34882
	0.25	7302.99	1003.48	0.34645
	0.30	7303.38	1445.01	0.35022
	0.35	7303.16	1966.82	0.34769
	0.40	7302.89	2568.91	0.34936

Appendix 5 Some Sub-programs for the HTFDM

```
c     This sub-program is for calculating the structural responses by the HTFDM
      subroutine htfdm(omigaf,n)
      implicit double precision (a-h,o-z)
      parameter (m1=128,m2=7)
c     Fw(m1,n) and Xw(m1,n) are the force and response in frequency domain
c     where n is the total node number
c     Mm,Cc and Kk are the matrices of mass, damping and stiffness of a structure.
c     VIv is the damper position matrix
c     ComHw is the transfer matrix of ComHw*.Xw=Fw and is also
c        the transfer matrix of Xw=ComHw*Fw at last.
c     wj is the imaginary unit.
c     Ar and h are the area and height of the damper.
c     G0, G1 and Aifa2 are parameters of Fractional Derivative Model.
c     Omiga is frequency.
      common /nn1/MM(65,65),KK(65,65),MMINV(65,65),KKINV(65,65)
      common /nn2/CC(65,65),KD(65,65)
      common /Dampp/VIv(65,65)
      common /ZJD/nvdamp
      common /ZJDPOS/ZIv(65,65)
      common /para/G0,G1,Aifa2,g0z,g1z,aifa2z
      common /damsize/Ar,h
      common /vsupport1/kvsinfo,jsup,njsup(30),nesup(30)
      common /vsupport2/vl(30),vd(30),height(30)
      common /time/Timet, Dtime
      common /Timedomain/ftr(m1),fti(m1),xtr(m1),xti(m1)
      common /Timed2/atr(m1),ati(m1)
      common /inout/nexcited,ndirec(5),nodep(5),ndireco,nodeo,nout
      common /a11/ampl(5),ww(5)
      common /a12/np(5),loadinfo,loaddire
      common /load/ftime(m1,5)
      common /cmhw/ comhw(65,65)
      dimension Omiga(m1),Fw(m1,65),Xw(m1,65)
      dimension ftime(m1,65)
      dimension AAr(65,65),AAi(65,65)
      dimension Xxw(65),Ffw(65)
      dimension is(65),js(65)
      double precision Mm,Kk,Cc,Kd,MMinv,KKinv
      double complex ComHw,Xw,Fw,wj,Xxw,Ffw
c     Xxw(n1) and Ffw(n1) if the internal variable for each frequency.
      P2=8*datan(1.0d0)
      wj=(0.0d0,1.0d0)
      Period=1.0d0/(omigaf)
      dtime=period/(2.0d0**m2)
      do 19 i=1,nexcited
         do 29 k=1,m1
            ftr(k)=ftime(k,np(i))
```

```
            fti(k)=0.0d0
29          continue
            call FFT(ftr,fti,m2,m1,1)
            do 15 k=1,m1
               omiga(k)=(k-1)*omigaf
               If(k.ne.1.or.k.ne.n/2) then
                  ftr(k)=2*ftr(k)
                  fti(k)=-2*fti(k)
               end if
               Fw(k,np(i))=cmplx(ftr(k),fti(k))
15          continue
19       continue
         do 99 k=1,m1
         omiga(k)=omiga(k)*p2
            omig=omiga(k)
            call cmhw(omig,n)
         do 50 i=1,n
            do 50 j=1,n
               AAr(i,j)=real(ComHw(i,j))
               AAi(i,j)=aimag(ComHw(i,j))
50          continue
            call bcinv(aar,aai,n,l,is,js)
            if(l.ne.0) then
               do 60 i=1,n
               do 60 j=1,n
                  ComHw(i,j)=cmplx(aar(i,j),aai(i,j))
60             continue
            else
               return
            end if
            do 70 i=1,n
               Ffw(i)=Fw(k,i)
70          continue
            call bcmul(ComHw,Ffw,n,Xxw)
            do 80 i=1,n
               Xw(k,i)=Xxw(i)
80          continue
            xtr(k)=real(Xxw(nout))
            xti(k)=aimag(Xxw(nout))
99       continue
         call tran(xtr,xti,m1)
         do 89 i=1,m1
            atr(i)=-omiga(i)**2*xtr(i)
            ati(i)=-omiga(i)**2*xti(i)
89       continue
c        calculate the response displacement in time domain
         call fft(xtr,xti,m2,m1,-1)
c        calculate the acceleration in time domain
```

```
      call fft(atr,ati,m2,m1,-1)
      call maxres(xtr,m1,xtrmax,xtrmin)
      call maxres(atr,m1,atrmax,atrmin)
131   format(1x,f10.5,2x,f15.8,2x,f15.8)
      return
      end

c     Sub-program to calculate the ComHw(i,j)
      subroutine cmhw(omig,n)
      common /nn1/MM(65,65),KK(65,65),MMINV(65,65),KKINV(65,65)
      common /nn2/CC(65,65),KD(65,65)
      common /Dampp/VIv(65,65)
      common /ZJD/nvdamp
      common /ZJDPOS/ZIv(65,65)
c     For KV model, aifa2 or aifa2z=1.0
      common /para/G0,G1,Aifa2,g0z,g1z,aifa2z
      common /cmhw/ comhw(65,65)
      double precision Mm,Kk,Cc,Kd,MMinv,KKinv
      double complex ComHw,wj
      wj=(0.0d0,1.0d0)
      do 10 i=1,n
         do 10 j=1,n
            ComHw(i,j)=-Omig**2*Mm(i,j)
10       continue
         do 20 i=1,n
         do 20 j=1,n
            ComHw(i,j)=ComHw(i,j)+wj*Omig*Cc(i,j)
20       continue
         do 30 i=1,n
         do 30 j=1,n
            ComHw(i,j)=ComHw(i,j)+Kk(i,j)
30       continue
         do 40 i=1,n
         do 40 j=1,n
c           Ar/h has been considered in VIv
            ComHw(i,j)=ComHw(i,j)+VIv(i,j)*g0
            if(nvdamp.ne.0) then
               ComHw(i,j)=ComHw(i,j)+ZIv(i,j)*g0z
            end if
40       continue
         do 45 i=1,n
         do 45 j=1,n
            ComHw(i,j)=ComHw(i,j)+VIv(i,j)*G1*(omig*wj)**aifa2
            if(nvdamp.ne.0) then
               ComHw(i,j)=ComHw(i,j)+ZIv(i,j)*G1z*(omig*wj)**aifa2z
            end if
45       continue
      end
```

```
c       Sub-program to get the inverse matrix of a complex matrix (n x n)
c       ar is the real part of the matrix and ai is the imagine part of the matrix
        subroutine bcinv(ar,ai,n,l,is,js)
        implicit double precision (a-h,o-z)
        dimension ar(65,65),ai(65,65),is(n),js(n)
        l=1
        do 100 k=1,n
           d=0.0
           do 10 i=k,n
           do 10 j=k,n
              p=ar(i,j)*ar(i,j)+ai(i,j)*ai(i,j)
              if (p.gt.d) then
                 d=p
                 is(k)=i
                 js(k)=j
              end if
10         continue
           if(d+1.0.eq.1.0) then
              l=0
              write(*,20)
              return
           end if
20         format(1x,'ERR * * NOT INV')
           do 30 j=1,n
              t=ar(k,j)
              ar(k,j)=ar(is(k),j)
              ar(is(k),j)=t
              t=ai(k,j)
              ai(k,j)=ai(is(k),j)
              ai(is(k),j)=t
30         continue
           do 40 i=1,n
              t=ar(i,k)
              ar(i,k)=ar(i,js(k))
              ar(i,js(k))=t
              t=ai(i,k)
              ai(i,k)=ai(i,js(k))
              ai(i,js(k))=t
40         continue
           ar(k,k)=ar(k,k)/d
           ai(k,k)=-ai(k,k)/d
           do 50 j=1,n
              if(j.ne.k) then
                 p=ar(k,j)*ar(k,k)
                 q=ai(k,j)*ai(k,k)
                 s=(ar(k,j)+ai(k,j))*(ar(k,k)+ai(k,k))
                 ar(k,j)=p-q
```

```
                ai(k,j)=s-p-q
            end if
50      continue
        do 70 i=1,n
            if(i.ne.k) then
                do 60 j=1,n
                    if(j.ne.k) then
                        p=ar(k,j)*ar(i,k)
                        q=ai(k,j)*ai(i,k)
                        s=(ar(k,j)+ai(k,j))*(ar(i,k)+ai(i,k))
                        t=p-q
                        b=s-p-q
                        ar(i,j)=ar(i,j)-t
                        ai(i,j)=ai(i,j)-b
                    end if
60                  continue
            end if
70      continue
        do 80 i=1,n
                if(i.ne.k) then
                p=ar(i,k)*ar(k,k)
                q=ai(i,k)*ai(k,k)
                s=(ar(i,k)+ai(i,k))*(ar(k,k)+ai(k,k))
                ar(i,k)=q-p
                ai(i,k)=p+q-s
            end if
80      continue
100   continue
      do 130 k=n,1,-1
        do 110 j=1,n
            t=ar(k,j)
            ar(k,j)=ar(js(k),j)
            ar(js(k),j)=t
            t=ai(k,j)
            ai(k,j)=ai(js(k),j)
            ai(js(k),j)=t
110      continue
        do 120 i=1,n
            t=ar(i,k)
            ar(i,k)=ar(i,is(k))
            ar(i,is(k))=t
            t=ai(i,k)
            ai(i,k)=ai(i,is(k))
            ai(i,is(k))=t
120     continue
130   continue
      return
      end
```